LIGHTWEIGHT FOAMED CONCRETE (LFC) THERMAL AND MECHANICAL PROPERTIES AT ELEVATED TEMPERATURES AND ITS APPLICATION TO COMPOSITE WALLING SYSTEM

A thesis submitted to the University of Manchester for the degree of

Doctor of Philosophy

in the Faculty of Engineering and Physical Sciences

2010

MD AZREE OTHUMAN MYDIN

School of Mechanical, Aerospace and Civil Engineering

CONTENTS

LIST OF TABLES

LIST OF FIGURES

NOMENCLATURE

ACRONYMS

DD	Dry Density
F/C	Fly ash-Cement ratio
F.E	Finite Element
F.E.M	Finite Element Modeling
HGP	Hot Guarded Plate
LFC	Lightweight Foamed Concrete
NSC	Normal weight concrete
NSE	No Stopping Edge
S/C	Sand-Cement ratio
S-F	Simply supported-Free
S-S	Simply supported-Simply supported
UBBL	Uniform Building By-Laws
W/C	Water-Cement ratio
WE	Welded Edge
WSE	With Stopping Edge

NOTATION

A_c	Area of concrete (mm^2)
A_{hs}	Main heater surface area (mm^2)
A_{vf}	Area of the profile voids on one face (mm^2)
b	Width of plate (mm)
b_{eff}	Effective width (mm)
c	Specific heat of material (J/kg°C)
c_{add}	Additional specific heat (J/kg°C)
c_p	Overall specific heat capacity (J/kg°C)
c_{pi}	Component specific heat (J/kg°C)
d	Specimen thickness (mm)
d_e	Pore (bubble) size (mm)
E	Modulus of elasticity (kN/mm^2)
E_c	Modulus of elasticity of concrete at ambient temperature (kN/mm^2)
$E_{c.0}$	Modulus of elasticity of concrete at zero porosity (kN/mm^2)
E_{cT}	Modulus of elasticity of concrete at elevated temperature (kN/mm^2)
E_s	Modulus of elasticity of the steel (kN/mm^2)
e	Effective emissivity
e_w	Dehydration water content (%)
F	Design load (kN/m)
F_i	Weight fraction of each component

f	Modification factor accounting for water movement
f_c	Concrete compressive strength at ambient temperature (N/mm^2)
f'_c	Concrete compressive stress at ambient temperature (N/mm^2)
$f_{c,0}$	Compressive strength of concrete at zero porosity (N/mm^2)
f_{cr}	Concrete tensile strength ambient temperature (N/mm^2)
f_{crT}	Concrete tensile strength at elevated temperature (N/mm^2)
f_{cT}	Concrete compressive strength at elevated temperature (N/mm^2)
f'_{cT}	Concrete compressive stress at elevated temperature (N/mm^2)
f_y	Yield stress (N/mm^2)
G_k	Characteristic dead load (kN/m)
h	Convection heat transfer coefficient (W/m^{2}K)
I_s	Second moment of area of steel (mm^4)
I_c	Second moment of area of concrete (mm^4)
k	Elastic buckling coefficient
k^*	Effective thermal conductivity (W/mK)
k_{amb}	Thermal conductivity at ambient temperature (W/mK)
k_{dry}	Thermal conductivity of dry LFC (W/mK)
k_g	Effective thermal conductivity of gas (W/mK)
k_s	Thermal conductivity of the solid (W/mK)
$k(T)$	Temperature dependent thermal conductivity (W/mK)
L	Thickness of the panel (mm)

L_p	Length of the composite panel (mm)
N_c	Resistance of the LFC core (kN)
N_s	Resistance of the steel sheeting (kN)
N_u	Ultimate resistance of panel (kN)
Q_k	Characteristic imposed load (kN/m)
P_{cr}	Critical buckling load (kN)
T	Temperature (^oC)
T_0	Initial temperature (^oC)
T_∞	Ambient temperature (°C)
t	Time (s)
t_p	Thickness of the plate (mm)
x, y, z	Cartesian coordinates
V_w	Volume percentage of water (%)
v	Poisson's ratio
W	Electrical power input to the main heater (watt)
W_{dry}	Weight of oven-dried sample (g)
W_{sat}	Weight in air of saturated sample (g)
W_{wat}	Weight in water of saturated sample (g)

GREEK SYMBOLS

α	Concrete reduction factor
Δc	Average additional specific heat (J/kg°C)
ΔT	Temperature difference (°C)
ε	Porosity (%)
ε_{cT}	Strain at elevated temperature
ε_{oT}	Strain at the maximum concrete stress
σ	Stefan-Boltzmann constant(W/m^2K^4)
σ_{cr}	Local buckling stress (N/mm^2)
ρ	Density (kg/m^3)
ρ_{dry}	Dry density (kg/m^3)
ρ_m	Casting density (kg/m^3)
ρ_{sc}	Solid density of cement paste (kg/m^3)
ϕ	Geometric view factor

ABSTRACT

LFC is cementatious material integrated with mechanically entrained foam in the mortar slurry which can produce a variety of densities ranging from 400 to 1600 kg/m^3. The application of LFC has been primarily as a filler material in civil engineering works. This research explores the potential of using LFC in building construction, as non-load-bearing partitions of lightweight load-bearing structural members. Experimental and analytical studies will be undertaken to develop quantification models to obtain thermal and mechanical properties of LFC at ambient and elevated temperatures.

In order to develop thermal property model, LFC is treated as a porous material and the effects of radiant heat transfer within the pores are included. The thermal conductivity model results are in very good agreement with the experimental results obtained from the guarded hot plate tests and with inverse analysis of LFC slabs heated from one side.

Extensive compression and bending tests at elevated temperatures were performed for LFC densities of 650 and 1000 kg/m^3 to obtain the mechanical properties of unstressed LFC. The test results indicate that the porosity of LFC is mainly a function of density and changes little at different temperatures. The reduction in strength and stiffness of LFC at high temperatures can be predicted using the mechanical property models for normal weight concrete provided that the LFC is based on ordinary Portland cement.

Although LFC mechanical properties are low in comparison to normal weight concrete, LFC may be used as partition or light load-bearing walls in a low rise residential construction. To confirm this, structural tests were performed on a composite walling system consisting of two outer skins of profiled thin-walled steel sheeting with LFC core under axial compression, for steel sheeting thicknesses of 0.4mm and 0.8mm correspondingly. Using these test results, analytical models are developed to calculate the maximum load-bearing capacity of the composite walling, taking into consideration the local buckling effect of the steel sheeting and profiled shape of the LFC core.

The results of a preliminary feasibility study indicate that LFC can achieve very good thermal insulation performance for fire resistance. A single layer of 650 kg/m^3 density LFC panel of about 21 mm would be able to attain 30 minutes of standard fire resistance rating, which is comparable to gypsum plasterboard. The results of a feasibility study on structural performance of a composite walling system indicates that the proposed panel system, using 100mm LFC core and 0.4mm steel sheeting, has sufficient load carrying capacity to be used in low-rise residential construction up to four-storeys.

DECLARATION

No portion of the work referred to in the thesis has been submitted in support of an application for another degree or qualification of this or any other university or other institute of learning

COPYRIGHT STATEMENT

i. The author of this thesis (including any appendices and/or schedules to this thesis) owns certain copyright or related rights in it (the "Copyright") and he has given The University of Manchester certain rights to use such Copyright, including for administrative purposes.

ii. Copies of this thesis, either in full or in extracts and whether in hard or electronic copy, may be made only in accordance with the Copyright, Designs and Patents Act 1988 (as amended) and regulations issued under it or, where appropriate, in accordance with licensing agreements which the University has from time to time. This page must form part of any such copies made.

iii. The ownership of certain Copyright, patents, designs, trade marks and other intellectual property (the "Intellectual Property") and any reproductions of copyright works in the thesis, for example graphs and tables ("Reproductions"), which may be described in this thesis, may not be owned by the author and may be owned by third parties. Such Intellectual Property and Reproductions cannot and must not be made available for use without the prior written permission of the owner(s) of the relevant Intellectual Property and/or Reproductions.

iv. Further information on the conditions under which disclosure, publication and commercialisation of this thesis, the Copyright and any Intellectual Property and/or Reproductions described in it may take place is available in the University IP Policy (see http://www.campus.manchester.ac.uk/medialibrary/policies/intellectual-property.pdf), in any relevant Thesis restriction declarations deposited in the University Library, The University Library's regulations (see http://www.manchester.ac.uk/library/aboutus/regulations) and in The University's policy on presentation of Theses

ACKNOWLEDGEMENTS

There are many individuals I wish to acknowledge, without their support the completion of this project would have been impossible. First and foremost I offer my sincerest gratitude to my supervisor, Prof. Yong C. Wang, who has supported me throughout my thesis with his patience, constant inspiration and encouragement whilst allowing me the room to work in my own way.

Acknowledgement is also made to the funding bodies of my PhD studies, University of Science Malaysia and Ministry of Higher Education Malaysia.

I gratefully acknowledge the assistance rendered to me by academic members and staff of the School of Mechanical, Aerospace and Civil Engineering. My particular thanks go to the technical staff members Mr. Jim Gee, Mr. John Mason, Mr. Bill Storey, Mr. Paul Townsend and Mr. Paul Nedwell for their invaluable assistance and experience when conducting the experimental portion of the research.

Special thanks are expressed to my colleagues, past and present, in the fire and structures research group especially to Ima Rahmanian and Dr. Jifeng Yuan for their care and advice.

I would greatly like to express my sincere appreciation to my loving parents Mr. Othuman Mydin Abdul Rahman and Mrs. Salmah Majid and my sisters Noor Azleen and Noor Hafeezah for their boundless love and encouragement. Finally, I wish to express my greatest gratitude to my beloved wife Shafizanur Osman for her love and support all through these years.

CHAPTER 1

INTRODUCTION

1.1 BACKGROUND

In recent years, the construction industry has shown significant interest in the use of lightweight foamed concrete (LFC) as a building material due to its many favourable characteristics such as lighter weight, easy to fabricate, durable and cost effective. LFC is a material consisting of Portland cement paste or cement filler matrix (mortar) with a homogeneous pore structure created by introducing air in the form of small bubbles. With a proper control in dosage of foam and methods of production, a wide range of densities (400 – 1600 kg/m^3) of LFC can be produced thus providing flexibility for application such as structural elements, partition, insulating materials and filling grades. LFC has so far been applied primarily as a filler material in civil engineering works. However, its good thermal and acoustic performance indicates its strong potential as a material in building construction. In fact, there has been widespread reported use of LFC as structural elements in building schools, apartments and housing in countries such as Libya, Russia, Brazil, Malaysia, Mexico, Saudi Arabia, Indonesia, Egypt and Singapore (Kearsley and Mostert, 2005). Figures 1.1 to 1.4 show some examples of the application of LFC in real project.

Figure 1.1 LFC blocks being used in a housing project in Malaysia (www.portafoam.com)

Figure 1.2 Large scale LFC infilling of an old mine in Combe Down, United Kingdom (www.bathnes.gov.uk)

Figure 1.3 Cast in-situ LFC wall in Surabaya, Indonesia (www.portafoam.com)

Figure 1.4 LFC being employed in a high rise building floor screed in Penang, Malaysia (www.portafoam.com)

This project is concerned with exploring the potential of using LFC as a building material. Although LFC mechanical properties are low compared to normal weight concrete, LFC may be used as partition or light load-bearing walls in low rise residential construction. The first stage to realize the potential of LFC for application as a load-bearing material in building construction is to obtain reliable thermal and mechanical properties at elevated temperatures for quantification of its fire resistance performance and some indication of whether it has adequate load-bearing performance. In order to gain a clearer understanding of the properties of LFC so as to develop a method to dependably predict its performance under ambient and elevated temperatures, this research will involve both experimental and theoretical investigations to ensure that the analytical model is generically applicable and validated.

This research is divided into four main stages. The first stage is to develop a theoretical model for temperature dependant thermal properties (thermal conductivity and specific heat) and to conduct transient heating tests in an electric kiln on LFC slabs to establish the through depth temperature profiles for validation of its thermal properties. In the second stage, compression and bending tests are performed at elevated temperatures to establish the mechanical properties of unstressed LFC. Thirdly, experiments are performed to observe the compressive structural behaviour of LFC based composite walling system and to investigate methods of calculating their strength at ambient temperature. Finally, a feasibility study will be executed to assess the applicability and limits of this LFC based system in building construction in terms of its fire resistance and structural performance.

1.2 OBJECTIVES AND SIGNIFICANCE OF RESEARCH

LFC is a relatively new construction material compared to normal weight concrete. The major factor limiting the use of LFC in applications is insufficient knowledge of the material performance at elevated temperatures.

In building application, load carrying capacity and fire resistance are the most important safety requirements. In order to comprehend and eventually predict the performance of LFC based systems, the material properties at ambient temperature and elevated temperatures must be known at first stage. To be able to predict the fire resistance of a building structure, the temperatures in the structure must be determined.

For such calculations, knowledge of the thermal properties, at elevated temperatures of the material is essential. In this research, the important thermal properties of LFC at elevated temperatures will be investigated. These properties include thermal conductivity, specific heat, porosity and density change of LFC. For quantification of structural performance, LFC mechanical properties will be established, including compressive strength, compressive modulus, strain at maximum compressive strength, compressive stress-strain relationship, failure modes, flexural tensile strength and flexural tensile modulus. To indicate feasibility of using LFC in building construction, it is necessary to carry out investigation of structural performance of LFC based building components. In this research, a composite walling system will be investigated.

The main objectives of this study are:

- To experimentally study and quantify the thermal properties of LFC at high temperatures so as to obtain material property data for prediction of fire resistance of LFC based systems through transient heating tests.
- To develop and validate proposed thermal property models for LFC.
- To experimentally examine and characterize the mechanical properties of LFC at ambient and elevated temperatures.
- To assess and propose mechanical properties prediction equations of LFC, based on comparison of the experimental results with existing models for normal weight concrete.
- To experimentally investigate the compressive behaviour of composite wall panels consisting of two outer skins of profiled thin-walled steel sheeting with LFC core and to analytically develop a model to calculate the maximum load-bearing capacity of the composite walling system.
- To carry out feasibility study on fire resistance and structural performance of using LFC in low-rise residential construction.

1.3 OBJECTIVIES OF RESEARCH METHODOLOGY

In order to fill some of the gaps identified by the literature review (Chapter 2), this research aims to achieve the following objectives:

(i) Studying in depth the thermal properties of LFC at ambient and high temperatures;

(ii) Studying in depth the mechanical properties of LFC at ambient and high temperatures;

(iii) Investigating the feasibility of using LFC in lightweight load-bearing construction as panel walls.

The following section will present a detailed description of the methodology for this research.

1.3.1 Temperature-dependent thermal properties of LFC

The specific heat of LFC can be accurately quantified based on proportions of components in LFC. Nevertheless, quantifying thermal conductivity requires more effort. Considering the porous nature of LFC, the thermal conductivity model should take into consideration not only heat conduction through the solid and void components of LFC, but also convection and radiation within the pores. Although thermal conductivity can be measured, it is a time consuming and expensive process, particularly if high temperature properties are required. Also a lot of experimental measurements will be necessary to enable a detailed temperature – thermal conductivity curve to be drawn. A theoretical based approach would enable the most important parameters to be identified and where measurement is necessary, only a few key points will be measured. This project will take a combined of theoretical and experimental approach.

As will be shown in sections 3.4.2 and 3.4.3 (Chapter 3), given the initial thermal conductivity of LFC at ambient temperature, its moisture content and porosity, the thermal conductivity of LFC depends primarily on the pore size and distribution. In the combined theoretical-experimental approach, a thermal conductivity – temperature model will be constructed assuming an effective pore size. This model will then be used

as input data into a one-dimensional finite difference heat conduction program developed by Rahmanian (2008) to predict temperature development through the thickness of LFC panel. High temperature tests will concurrently be carried out to measure temperature distributions through the LFC thickness. The effective pore size will be varied until good agreement between the numerical prediction and experimental results is obtained. To independently verify the proposed theoretical model for thermal conductivity – temperature relationship, limited thermal conductivity measurements using the guarded hot plate test will be obtained. Figure 1.5 summarizes the methodology to extract the effective thermal conductivity of LFC.

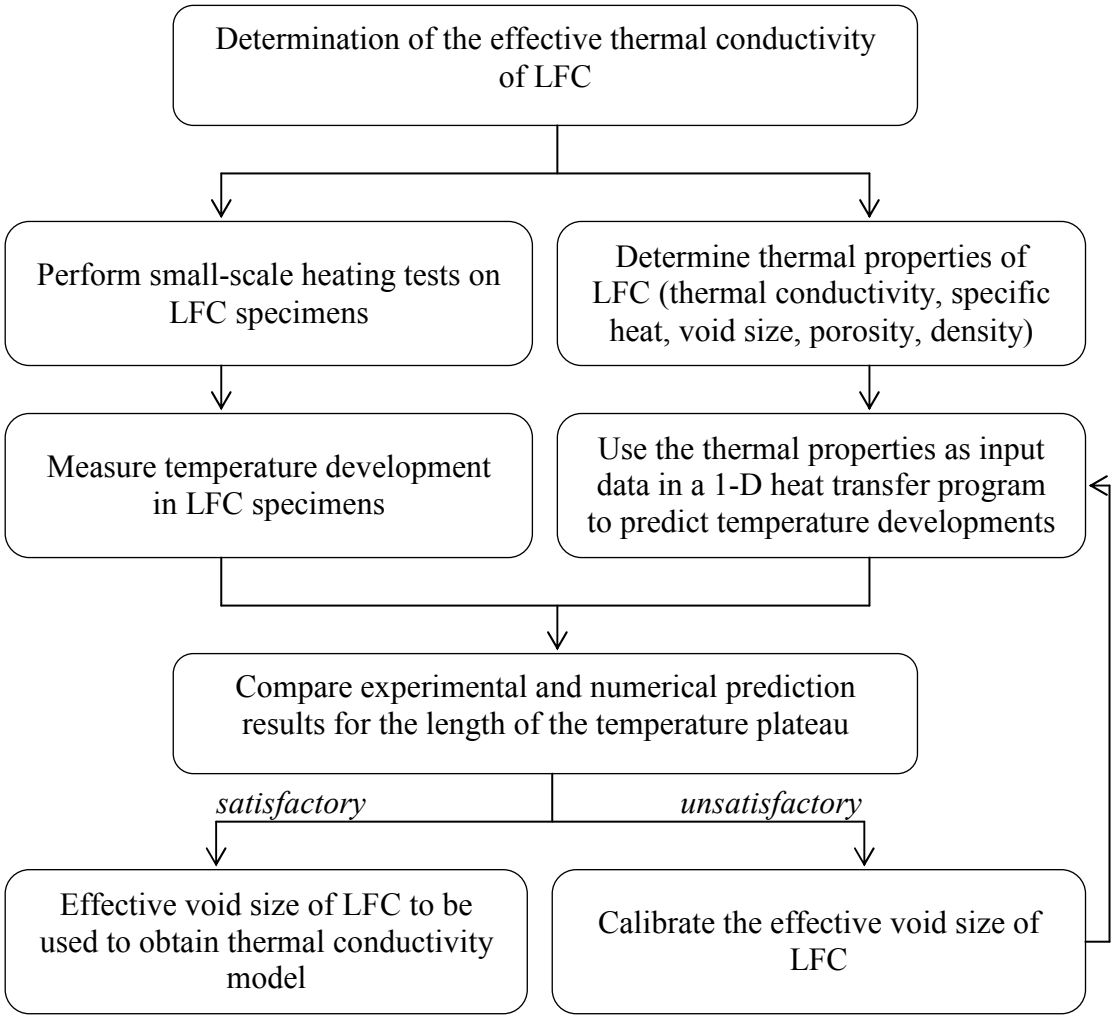

Figure 1.5 Methodology to determine the effective thermal conductivity of LFC

1.3.2 Temperature-dependent mechanical properties of LFC

The degradation mechanisms for cement-based material like LFC upon exposure to high temperatures comprise of mechanical damage as well as chemical degradation;

where each mechanism is dominant within a specific temperature range. As a two phase material with solid cement and air voids, the degradation mechanisms of LFC are mainly caused by deprivation of the cement paste. Although both mechanical and chemical degradation result in degradation of mechanical properties, the mechanisms occur at significantly different temperature ranges. To experimentally examine and characterize the mechanical properties of LFC at elevated temperatures, high temperature test will be performed at different temperature levels up to 600°C. Compression and bending strength tests will be carried out for LFC samples.

Afterwards several predictive models, based on studies on normal weight concrete, will be assessed to identify models that are suitable for predicting mechanical property degradation of LFC at high temperatures. Figure 1.6 demonstrates the methodology to examine and characterize the mechanical properties of LFC at elevated temperatures.

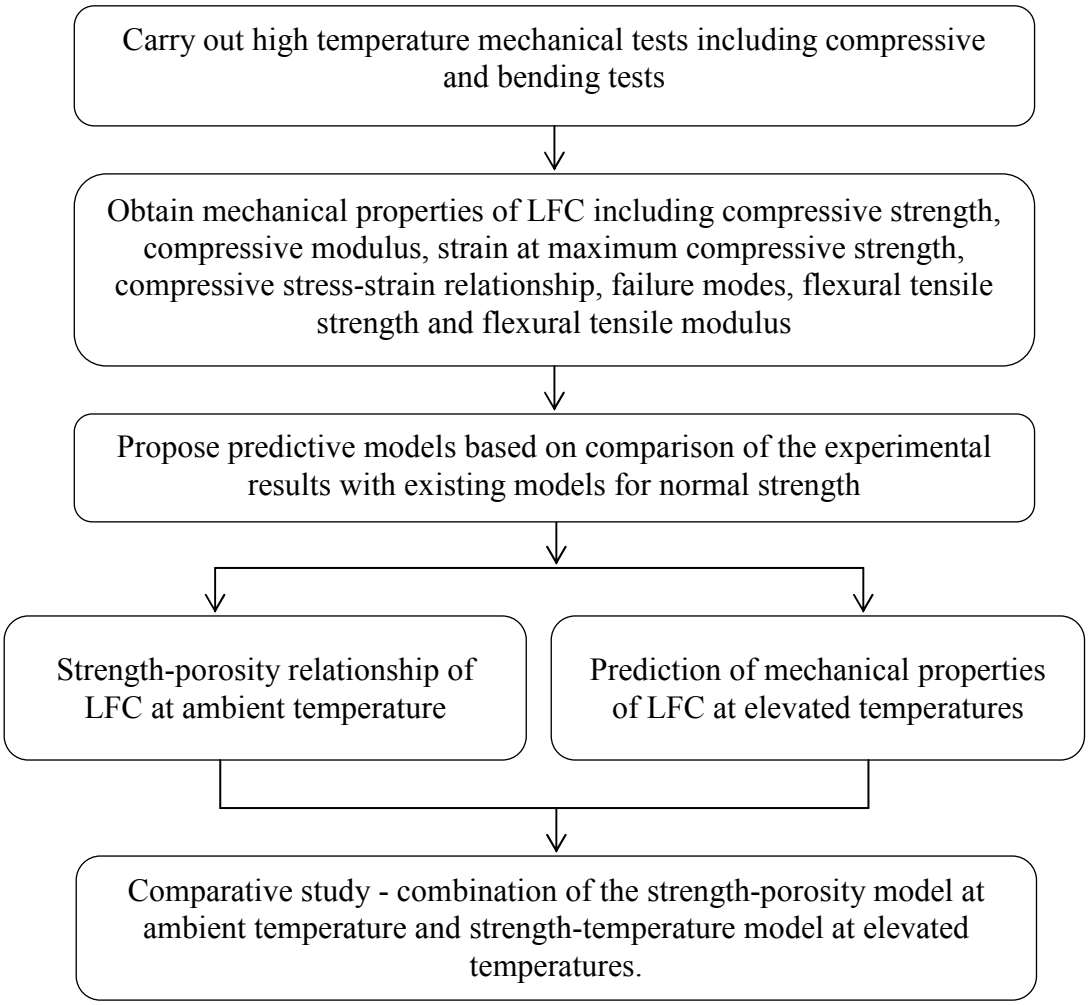

Figure 1.6 Methodology to examine and characterize the mechanical properties of LFC at elevated temperatures

1.3.3 Feasibility study of LFC composite walling system

This study will be carried out in two steps. In the first step, experimental and analytical studies of axial compressive behaviour of composite panels will be carried out to develop a model for composite behaviour between LFC core and steel sheeting, in particular, to quantify local buckling strength of the steel sheeting and LFC core strength. Due to limitation in resources, only a few samples will be tested at ambient temperature. Figure 1.7 summarizes the methodology to investigate the axial compressive behavior of composite panel system.

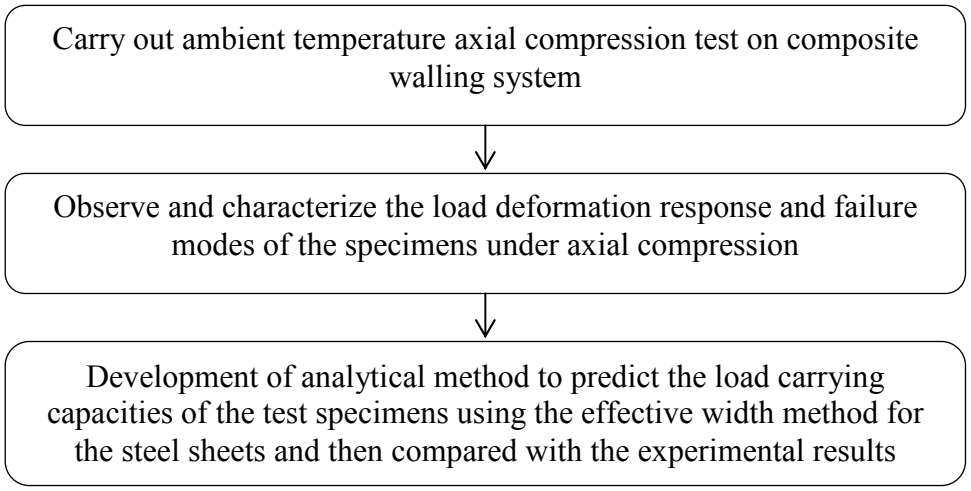

Figure 2.17 Methodology to examine the structural behavior of composite walling system under axial compression

In the second step, the information gained from this research, including thermal and mechanical properties as well as ambient temperature structural behaviour under axial compression, will be used to assess the feasibility of using LFC to construct low storey buildings, based on thermal insulation for fire resistance consideration and ambient temperature load carrying capacity for structural resistance. Figure 2.18 summarizes the methodology.

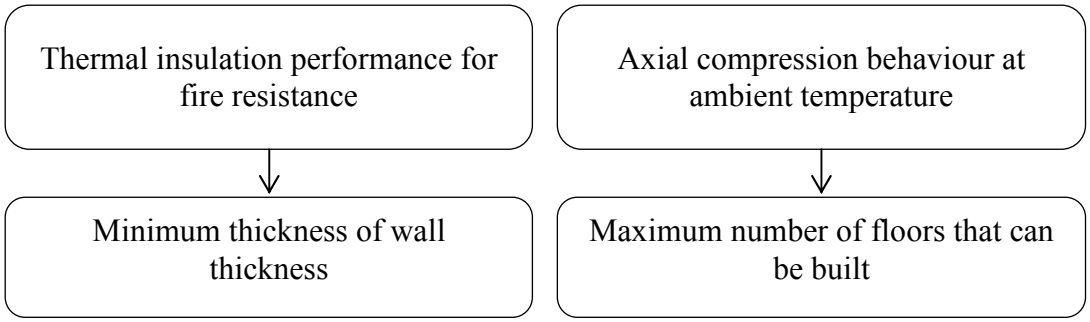

Figure 2.18 Methodology to assess the feasibility using LFC based wall panels in realistic construction.

1.4 THESIS ORGANISATION

This thesis does not contain a single chapter describing the experimental methods instead these are described separately in relevant chapter. This thesis is organized in the following nine chapters:

Chapter 1 provides general introduction to the project and the thesis.

Chapter 2 acknowledges a relevant literature review to LFC, including its application and design procedure, properties of LFC and cement-based material at ambient and elevated temperatures. Additionally, this chapter identifies the gaps in current knowledge to demonstrate the originality of this project.

Chapter 3 presents the results of a detailed experimental investigation to quantify the thermal properties of LFC at high temperatures, including thermal conductivity tests using the guarded hot plate method and transient high temperature tests on LFC slabs exposed to electrical heating from one side.

Chapter 4 develops theoretical models for thermal properties of LFC at elevated temperatures and presents validation of the models using the experimental results from Chapter 3. In addition, this chapter also presents the results of a sensitivity study to assess the consistence of the proposed thermal property models for LFC.

Chapter 5 display the results of an experimental programme to determine the mechanical properties of LFC at ambient and elevated temperatures. The mechanical properties include compressive strength, compressive modulus, strain at maximum

compressive strength, compressive stress-strain relationship, failure modes, flexural tensile strength and flexural tensile modulus at temperatures ranging from ambient to 600°C.

Chapter 6 reviews ambient and elevated temperatures mechanical property prediction equations for normal weight concrete and assess their applicability to LFC. A two-stage comparison will be made: assessment of models at ambient temperature and retention factors at elevated temperatures, based on ambient temperature results. The aim of this investigation is to propose a procedure to predict the mechanical properties of LFC, based on existing mechanical property predictive models.

Chapter 7 exhibits the results of an experimental and analytical study of the structural behaviour of a composite panel system consisting of two outer skins of profiled thin-walled steel sheeting and LFC core under axial compression. The objective of this investigation is to validate an analytical model to calculate the maximum load-bearing capacity of such composite panels.

Chapter 8 explores the feasibility of using LFC in lightweight residential construction, based on insulation performance for fire resistance and ambient temperature load carrying capacity under compression. The specific aim of the fire resistance study is to determine the minimum LFC thickness for providing different standard fire resistance ratings based on limiting the temperature rise on the unexposed surface of LFC panels. The specific aim of the structural analysis is to indicate the maximum scale of residential construction that may be realistically built using LFC based systems.

Chapter 9 summarizes the main findings of this research and recommends some further research studies to gain fuller understanding of LFC properties and performance of LFC based building systems.

CHAPTER 2

LITERATURE REVIEW

The aim of this project is to exploit the feasibility of using lightweight foamed concrete (LFC) in building construction. For this investigation, it will be necessary to obtain thermal and mechanical properties of LFC, both at ambient and elevated temperatures. The intended LFC construction type is composite walling system. This literature reviews covers material properties only and previous research on modeling and structural applications is described within the chapters where results on these are discussed. As conclusions to this chapter, gaps in current knowledge will be identified to demonstrate originality of this research.

2.1 INTRODUCTION TO LIGHWEIGHT FOAMED CONCRETE (LFC)

Since LFC is not a main stream construction material, a brief introduction to LFC will first be provided. LFC is defined as a cementitious material having a minimum of 20 per cent by volume of mechanically entrained foam in the mortar slurry (Van Deijk, 1992) in which air-pores are entrapped in the matrix by means of a suitable foaming agent. The air-pores are initiated by agitating air with a foaming agent diluted with water; the foam then carefully mixes together with the cement slurry to form LFC. Integrating the air-pores into the base matrix gives a low self-weight, high workability, excellent insulating values, but lower strength in contrast to normal weight concrete. LFC can be fabricated anywhere in any shape or building unit size.

LFC is not a new material in the construction industry. It was first patented in 1923 (Valore, 1954) and a limited scale of production was instigated in 1923. The use of LFC was very limited until the late 1970s**,** when it was started to be consumed in Netherlands for ground engineering applications and voids filling works. In 1987 a full-scale assessment on the application of LFC as a trench reinstatement was carried out in

the United Kingdom and the achievement of this trial led to the extensive application of LFC for trench reinstatement and other applications followed (Brady et al., 2001). Since then, LFC as a building material has become more widespread with expanding production and range of applications.

Over the past 20 years, LFC has primarily been used around the world for bulk filling, trench reinstatements, backfill to retaining walls and bridge abutments, insulation to foundations and roof tiles, sound insulation, stabilising soils (especially in the construction of embankment slopes), grouting for tunnel works, sandwich fill for precast units and pipeline infill. However, in the last few years, there is developing interest in using LFC as a lightweight non-structural and semi-structural material in buildings to take advantage its lightweight and good insulation properties (www.portafoam.com). LFC can have a wide range of densities and each density is produced for a particular type of application. Table 2.1 shows the range of densities suitable for different applications.

Table 2.1 Applications of LFC with different densities (www.litebuilt.com)

Density (kg/m^3)	Applications
300 - 600	Used for roof and floor insulation against heat and sound and also for interspaces filling between brickwork leaves in underground walls, insulation in hollow blocks and any other filling situation where high insulating properties are required.
600 - 900	Used for the production of precast blocks and panels for curtain and partition walls, slabs for false ceilings, thermal insulation and soundproofing screeds in multi-level residential buildings. LFC of this density range is also ideal for bulk fill application.
900 - 1200	Used in concrete blocks and panels for outer leaves of buildings, architectural ornamentation as well as partition walls, concrete slabs for roofing and floor screeds.
1200 - 1800	Used in precast panels of any dimension for commercial and industrial use, garden ornaments and other uses where structural concrete of light weight is an advantage

2.1.1 Constituents material of LFC

LFC with low density, i.e. having a dry density of up to about 600 kg/m^3, is frequently formed from cement (to which other binders could be added), water and stable foam whilst denser LFC will incorporate fine sand in the mix. The requirements of each constituent of LFC are explained below:

2.1.1.1 Cement

Portland cement SEM1 is typically used as the main binder for LFC. Additionally, rapid hardening Portland cement (Kearsley and Wainwright, 2001), calcium sulfoaluminate and high alumina cement (Turner, 2001) have also been used to reduce the setting time and to obtain better early strength of LFC. There was also an attempt to decrease the cost of production by using fly ash (Kearsley and Wainwright, 2001) as cement replacement to enhance consistency of the mix and to reduce heat of hydration while contributing for long term strength. The effect of using fly ash as cement replacement on compressive strength of LFC will be further discussed in Section 2.2.3.

2.1.1.2 Fillers (sand)

Sach and Seifert (1999) suggested that only fine sands having particle sizes up to about 4mm and with an even distribution of sizes should be used for LFC. This is primarily because coarser aggregate might lead to collapse of the foam during the mixing process. Coarse pulverised fuel ash (PFA) also can be used as a partial or total replacement for sand to make LFC with a dry density below about 1400 kg/m^3.

2.1.1.3 Water

The amount of water to be added to the mix depends on the composition of the mix design. Generally for lighter densities, when the amount of foam is increased, the amount of water can be decreased. The water-cement ratio must be kept as low as possible in order to avoid unnecessary shrinkage in the moulds. However, if the amount of water added to cement and sand is too low, the necessary moisture to make a workable mix will have to be extracted from the foam after it is added, thereby destroying some of the foam in the mix. The range of water-cement ratio used in LFC is between 0.4 to 1.25 (Kearsley, 1996), the appropriate value will be depending on the

amount of cement in the mix, use of chemical admixtures and consistence requirement. Plasticizers are not normally necessary to make LFC because of LFC has intrinsic high workability.

2.1.1.4 Surfactants (foaming agent)

There is an extensive choice of surfactants (foaming agent) available in the market. Generally two types of surfactants can be used to produce foam: protein and synthetic based surfactants. Protein based surfactants are produced from refined animal products such as hoof, horn and skin whilst synthetic based surfactants are produced using man made chemicals such as the ones used in shampoos, soap powders and soaps (Md Azree, 2004). The surfactant solution typically consists of one part of surfactant and between 5 and 40 parts of water but the optimum value is a function of the type of surfactant and the technique of production. It is very important to store all surfactants accordingly because they are inclined to deterioration at low temperatures.

According to McGovern (2000), foams formed from protein based surfactants have smaller bubble size, are more stable and have a stronger closed bubble structure compared to the foam produced using synthetic surfactants. Therefore, protein based surfactants would be best suited for the production of LFC of comparatively high density and high strength.The stability of foam is a function of its density and the type of surfactant. The foam has to endure its inclusion into the mortar mix and the chemical environment of the concrete until it has attained a reasonable set. A number of external environmental factors can exert influence on the stability of the foam such as vibration, evaporation, wind and temperature. Some or all of these may be present on a site and may lead to the breakdown in the foam structure.

Currently two methods can be used to produce LFC, either by pre-foaming method or mixed foaming method. Pre-foaming involves preparation of the base mix and the stable foam individually and then is added together. In the mixed foaming method, the foaming agent is mixed together with the base matrix. The properties of LFC are significantly reliant upon the quality of the foam; therefore, the foam should be firm and stable so that it resists the pressure of the mortar until the cement takes its initial set to allow a strong skeleton of concrete to be built up around the void filled with air (Koudriashoff, 1949).

2.1.2 Design procedure of LFC

At the moment, there is no standard method for designing LFC mix. For normal weight concrete, the user would signify a certain compressive strength and the water-cement ratio would be adjusted to meet the requirement. As far as LFC is concerned, not only the strength is specified, but also the density. Since the compressive strength of LFC is a function of density, the density can be used to modify the strength but this does not give any indication of the water requirement in the mix. It is not an easy task to achieve an accurate measurement of the density of LFC on site because of the hardened density of LFC depends on the saturation intensity in its pores.

According to Jones and McCarthy (2005), it is difficult to achieve the design density of LFC because it has a tendency to lose between 50 and 200 kg/m^3 of the total mix water because it depends on the concrete fresh density, early curing regime and exposure conditions.

2.2 RELEVANT STUDIES ON PROPERTIES OF LFC

There is a lack of published information on LFC. Among the LFC related literature collected by the author so far (around 60 in total), majority of these were published within the last 10 years and most of these previous studies on LFC were aimed at characterizing the ambient temperature properties of LFC. This section will review previous studies on properties of hardened LFC, including physical properties (density, air-void system and porosity), mechanical properties (compressive strength, tensile strength and modulus of elasticity), thermal properties and fire resistance performance.

2.2.1 Density of LFC

The relationship between dry density and casting density between 600 kg/m^3 and 1200 kg/m^3 can be calculated using the following linear equation (Kearsley and Mostert, 2005):

$$\rho_m = 1.034\rho_{dry} + 101.96 \ldots. (2.1)$$

where ρ_m is the target casting density (kg/m^3) and ρ_{dry} is the dry density (kg/m^3)

2.2.2 Air-void system and porosity of LFC

As will be explained in sections 3.4.2, 3.4.3 and 5.2, porosity and the pore structure will have significant effects on thermal conductivity and mechanical properties of LFC. High porosity is highly detrimental to the strength of LFC, particularly if the pores are of large diameter. Large pores also result in high thermal conductivity. As a cement-based material, LFC consists of gel-pores (dimensions from 0.0005μm up to 0.01μm), capillary-pores (0.01μm to 10μm) and air-pores (air entrained and entrapped pores) (Visagie and Kearsely, 2002). The gel-pores occupy between 40 to 55% of total pore volume but they are not active in permeating water through cement paste and they do not influence the strength (Brandt, 1995). However, the water in the gel-pores is physically bonded to cement and directly controls shrinkage and creep properties of LFC.

Air-pores in hardened LFC can be entrained or entrapped. Entrapped air-pores occur inadvertently during the mixing and placing of concrete. As LFC is a self-flowing and self-compacting concrete and exclusive of any coarse aggregate, the possibility of entrapped air is insignificant. In contrast, entrained air-pores are introduced intentionally during production of LFC by using an air-entraining chemical admixture (surfactants). Entrained air-pores are discrete and individual bubbles of spherical shape. They are uniformly distributed throughout the cement paste and are not interconnected with each other and therefore do not affect the permeability of LFC (Kalliopi, 2006). The total volume of capillary-pores and air-pores affects the strength of LFC.

Kearsley and Wainwright (2001) carried out research to investigate the relationship between porosity and dry density of LFC. In this study, they utilized a large amount of both classified and unclassified fly ash (pulverised and pozz-fill) as a cement replacement up to 75% by weight. Figure 2.1 shows the relationship between porosity and dry density of LFC obtained from their research. It can be seen from Figure 2.1 that there is a strong relationship between porosity and dry density of LFC. They found that the porosity of LFC is the combination of entrained air-pores and the pores within the paste and the porosity was found to be dependant primarily on dry density of LFC and

not on fly ash type and content. Kearsley and Wainwright proposed an equation to link the porosity and dry density of LFC (based on Figure 2.1) as follows:

$$\varepsilon = 18700\rho_{dry}^{-0.85} \quad \ldots\ldots(2.2)$$

where ε is the porosity (%) and ρ_{dry} is the dry density (kg/m^3)

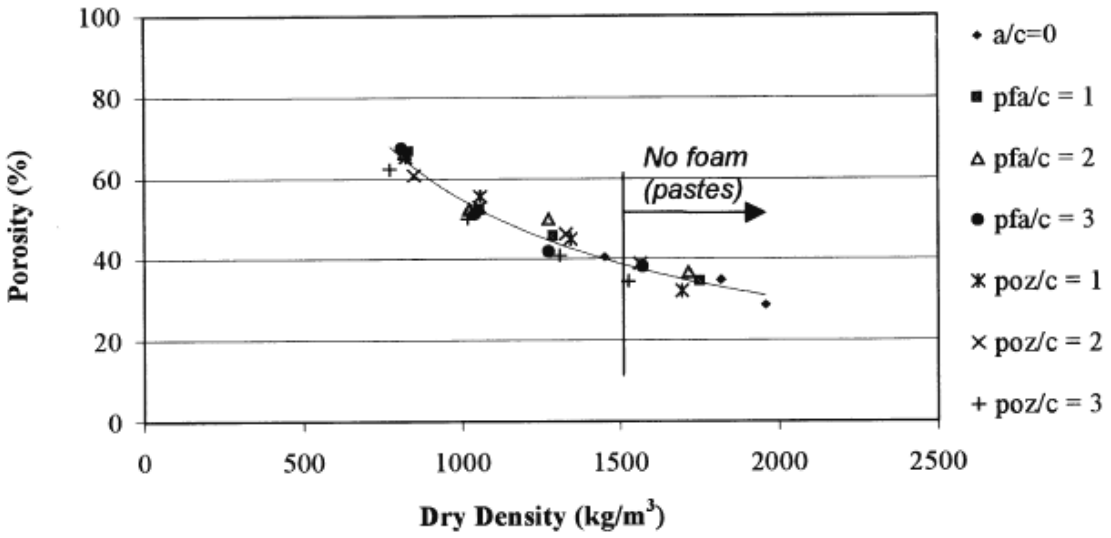

Figure 2.1 Porosity of LFC as a function of dry density (Kearsley and Wainwright, 2001)

Nambiar and Ramamurthy (2007) performed a study to distinguish the air-pore structure of LFC by identifying a few parameters that influence the density and strength of LFC. They used a camera connected to an optical microscope and computer with image analysis software to develop a quantification technique for these parameters. The LFC mixes used in their investigation included cement-sand and cement-fly ash mixes with a filler-cement ratio of 2 and varying foam volume (10% to 50%). The dimensions of the specimens for image analysis were 50 × 50 × 25 mm. Upon completing the image processing and air pore identification, the total area, perimeter, equivalent diameter of every defined area (air pore) in the images were analysed to obtain the percentage of pores, air-pore size distribution, shape of the pores in terms of shape factor and spacing factor for each mixes. Figures 2.2 and 2.3 show typical binary images for cement-sand mix and cement-fly ash mix respectively obtained from their research. It can be seen that the use of fly ash as a filler in LFC mix helped in achieving more uniform distribution of air voids than fine sand. Fly ash, being finer, helped to

achieve uniform distribution of air-pores by providing a well and uniform coating on each bubble and thereby preventing it from merging and overlapping. They also concluded that the air-pore shape had no influence on the properties of LFC as all air pores were of roughly the same shape and independent of foam volume.

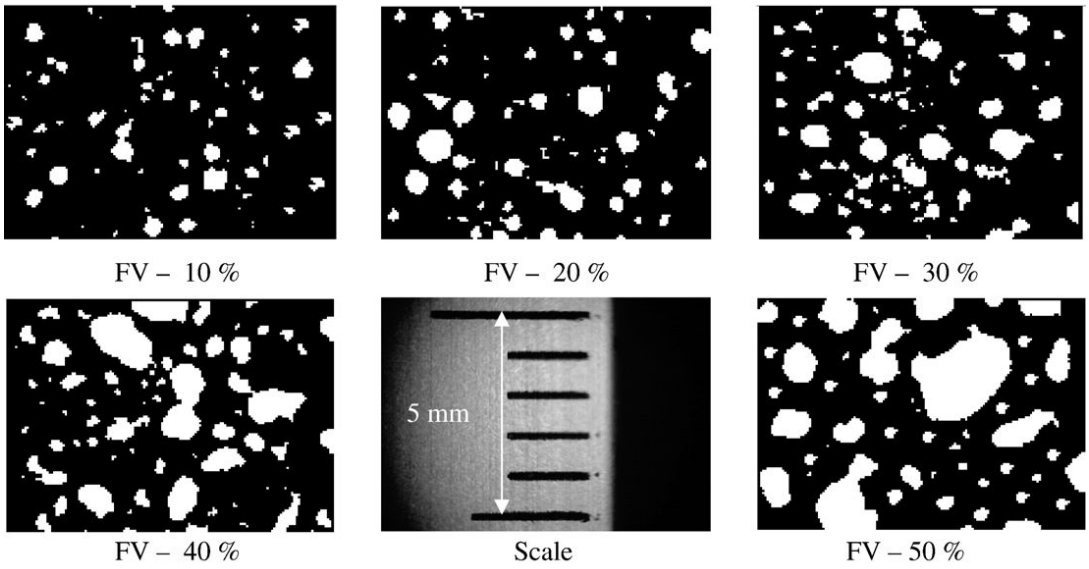

Figure 2.2 Typical binary images for cement-sand mixes (Nambiar and Ramamurthy, 2007)

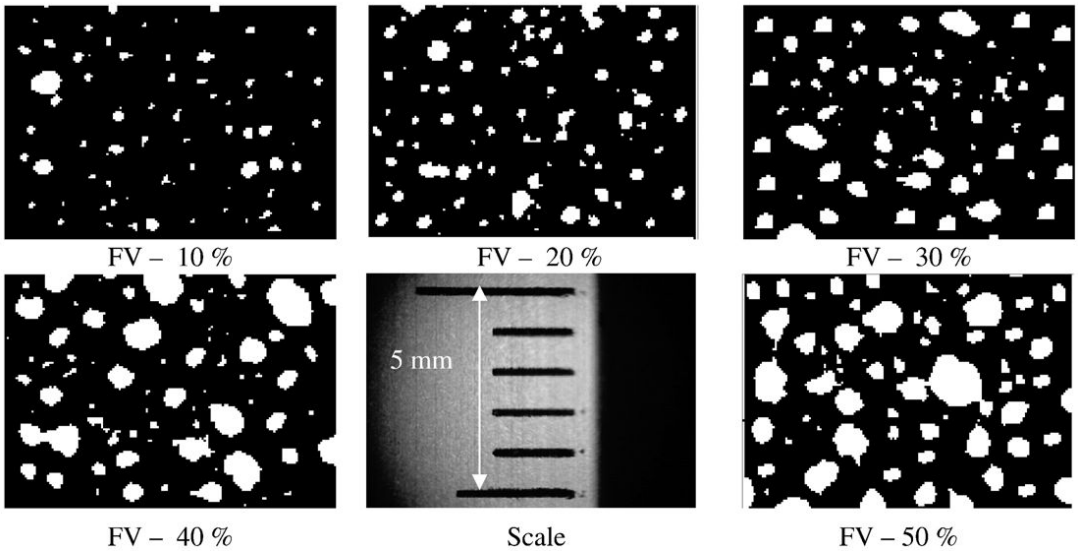

Figure 2.3 Typical binary images for cement-fly ash mixes (Nambiar and Ramamurthy, 2007)

2.2.3 Compressive strength of LFC

The compressive strength of LFC reduces with decreasing density. Table 2.2 shows a summary of the range of compressive strength of LFC for various mixture composition and densities reported in literature. For mixes with similar constituents, the density-strength relations should be reasonably comparable. But, because the constituents in LFC mixtures can differ widely, density is not necessarily a dependable indicator of the compressive strength of LFC. The other main factors that influence the strength of LFC are cement-sand ratio, water-cement ratio, type of cement and content, pore size and distribution, type of surfactants (foaming agents) and curing regime (Aldridge, 2005), (Hamidah et al., 2005). Higher sand-cement ratios result in LFC with lower compressive strength. The strength of lower density LFC can be increased to equal that of higher density LFC by increasing the amount of cement content in the mix.

The effect of water-cement ratio on compressive strength of LFC is imprecise. Dransfield (2000) reported that the strength of LFC decreases with reduction in water-cement ratio. Whilst an other report indicates that the compressive strength of LFC reduces with increasing water-cement ratio up to 0.45, an opposite trend is noted above this value (between 0.5 and 1.0) (De Rose and Morris, 1999).

Table 2.2 A review of LFC mixes, compressive strengths and density ranges (Ramamurthy et al., 2009)

Authors	Proportion of cement (kg/m^3) or composition	Ratios			Density range kg/m^3	Compressive strength (28 days) N/mm^2
		S/C	W/C	F/C		
Van Deijk (1991)	Cement-sand/ fly ash	-	-	-	280-1200	0.6 -10.0 (91 days)
Durack and Weiqing (1998)	270–398	1.23-2.5	0.61-0.82	-	982-1185 (DD)	1.0-6.0
	137-380	-	0.48-0.70	1.48-2.50	541-1003 (DD)	3.0-15.0 (77 days)
Kearsley and Wainwright (2001)	Cement-fly ash replacement 193-577	-	0.6-1.17	-	1000-1500	2.0-18.0
Jones and McCarthy (2005)	500	1.5-2.3	0.3	-	1400-1800	10.0-26.0
	500	-	0.65-0.83	1.15-1.77	1400-1800	20.0-43.0
Nambiar and Ramamurthy (2006)	Cement-sand mix (coarse)	With filler-cement ratio varied from 1 to 3 and fly ash replacement for sand varied from 0% to 100%			800-1350 (DD)	1.0-7.0
	Cement-sand mix (fine)					2.0-11.0
	Cement-sand-fly ash mix				650-1200 (DD)	4.0-19.0

** S/C: sand–cement ratio; F/C: fly ash–cement ratio; W/C: water–cement ratio; DD: dry density*

When cement is combined with silica fume (Kearsley, 1996) and fly ash (De Rose and Morris, 1999), higher compressive strength is achieved in the long term, owing to their pozzolanic reaction and filler characteristics, with a more marked effect at high LFC densities. Kearsley and Wainwright (2001) carried out a study on the effect of replacing large volumes of cement (up to 75% by weight) by both classified and unclassified fly ash on strength of LFC. They found that up to 67% of the cement could be replaced with ungraded and graded fly ash without any significant reduction in compressive

strength. The results signify that the compressive strength of LFC is principally a function of dry density, and LFC mixes with high fly ash content needed a longer time to reach their maximum strength which was observed to be higher than that attained using only cement.

In terms of the influence of fillers on strength of LFC, better strength is obtained when finer sand is used. For a given density, the mix with fine sand results in higher strength than the mix with coarse sand and the variation is higher at higher density. This higher strength-density ratio is credited to the moderately uniform distribution of pore in LFC with fine sand, while the pores were larger and irregular for mixes with coarse sand (Nambiar and Ramamurthy, 2006). Similar behaviour was observed when sand was replaced by fine fly ash.

Jones and McCarthy (2005) performed an extensive experimental exploration into the effect of utilization of unprocessed, run-of-station, low-lime fly ash in LFC, as a substitution for sand on the rheological, strength development and permeation/durability properties for LFC with plastic densities ranging between 1000 and 1400 kg/m^3. They found that the use of fly ash in LFC considerably benefited the compressive strength growth, predominantly after 28 days. At a given age, the fly ash coarse concretes were up to 6 times stronger than those of equivalent sand concretes.

The enhancement of strength with fly ash as filler is not pronounced at lower density range (higher percentage of foam volume) especially at earlier ages. This is due to the fact that at lower density range, the foam volume controls the strength rather than the material properties (Nambiar and Ramamurthy, 2006). The utilization of lime, demolition fines, recycled glass as fine aggregate has slight or no effect on compressive strength of LFC, while some decrease in strength was reported when crumb rubber, used foundry sand, china clay sand and quarry fines were used (De Rose and Morris, 1999), (Jones et al., 2005).

The compressive strength of LFC decreases with an increase in pore diameter for dry density of LFC between 500 and 1000 kg/m^3. Nevertheless for densities higher than 1000 kg/m^3, as the air-pores are far apart to have an influence on the compressive strength, the composition of the paste determines the compressive strength (Visagie and Kearsely, 2002). The type of surfactant (foaming agent) also has major effect on the

compressive strength of LFC. An increased of strength up to 70% was found with the used of protein based foaming agent rather than synthetic foaming agent (Dransfield, 2000).

In terms of curing regime, autoclaving increases the compressive strength. Hamidah et al. (2005) carried out an investigation to produce cost-effective mix for LFC by optimising the amount of sand in LFC mix by using different sand-cement ratio and curing conditions. In this study, a series of LFC of four different densities ranging from 1300 to 1600 kg/m^3 was fabricated using the appropriate mix proportions and a series of sand-cement ratios varying from zero to 2.0 for each series of density was attempted. Hamidah et al. found that water cured samples of LFC attained higher strength than those cured in air. For cement based material, the presence of water could promote the hydration process of cement for strength development, nevertheless the existence of foam in cement would delay the hydration and thus it is expected that LFC could only achieve maximum strength at later ages compared to that of normal weight concrete.

Kearsley and Mostert (2005) appears to be the only ones to have carried out an investigation to look into the effect of cement composition on the compressive strength of LFC exposed to high temperatures. From their background study, they found that Portland cement SEM1 was not suitable to fabricate LFC based firewalls for temperatures above 400°C. Above this temperature point, the calcium hydroxide in Portland cement SEM1 dehydrates forming calcium oxide. When calcium oxide reacts with water, damage will happen in the form of swelling and cracking. Montgomery (2003) used calcium aluminate cements to manufacture concrete that needs to withstand temperatures in excess of 300-400°C. The use of aluminate cement was found to increase the service temperature limit and enhance the ability of the material to withstand high temperatures which is due to the present of compounds with lower melting points in calcium aluminate. Therefore high alumina cement was used in the investigation carried out by Kearsley and Mostert (2005). Dolomite sand and fly ash were used in the mix to determine the effect of filler type on the properties of LFC. Table 2.3 shows the chemical composition of the materials used in their study where three types of cement composition were used, with increasing aluminate and decreasing calcium contents. From the experimental results, they found that compressive strength of LFC containing dolomite was noticeably reduced upon exposure to high

temperatures as shown in Figure 2.4. From Figure 2.4, it can be seen that the compressive strength of LFC containing dolomite is significantly lower than the strength of samples containing fly ash. The compressive strength of samples containing fly ash mixed with the cement with lower aluminate content (cement Type 2 in Table 2.3) increased significantly at high temperatures up to 800°C (refer Figure 2.5). The increase in strength can be attributed to the high strength ceramic bonds that developed as a result of thermo-chemical reactions at high temperatures. Figure 2.6 demonstrates the compressive strength of LFC containing Cement Type 3. The variation of compressive strength as a function of testing density shown in Figure 2.6 was found to be the same as that observed in LFC samples containing Cement Type 2 (Figure 2.5). Nevertheless the variation in compressive strength of LFC after heating seems to be less for the LFC containing cement with higher alumina content. LFC samples containing Cement Type 3 seem to result in slightly higher compressive strengths.

Table 2.3 Chemical composition of cement used in Kearsley and Mostert study

Oxides	Portland Cement	Fly Ash (%)	Cement Type 1 (%)	Cement Type 2 (%)	Cement Type 3 (%)
CaO	65.0	0.05	≤ 39.8	≤ 39.5	28.5 - 30.5
SiO_2	20.7	39.5	≤ 6.0	≤ 6.0	0.2 - 0.6
Al_2O_3	4.47	57.8	≥ 37.0	≥ 50.0	68.7 - 70.5
Fe_2O_3	2.87	0.79	≤ 18.5	≤ 3.0	0.1 - 0..3
TiO_2	0.43	0.21	< 4.0	< 4.0	< 0.4
Na_2O	0.09	0.05	< 0.4	< 4.0	< 0.5
K_2O	0.04	0.29			
MgO	2.13	0.31	< 1.5	< 1.0	< 0.5
SO_3	2.89	280 ppm	< 0.4	< 0.4	< 0.3
Al_2O_3/ CaO ratio	0.07	-	±0.9	±1.3	±2.4

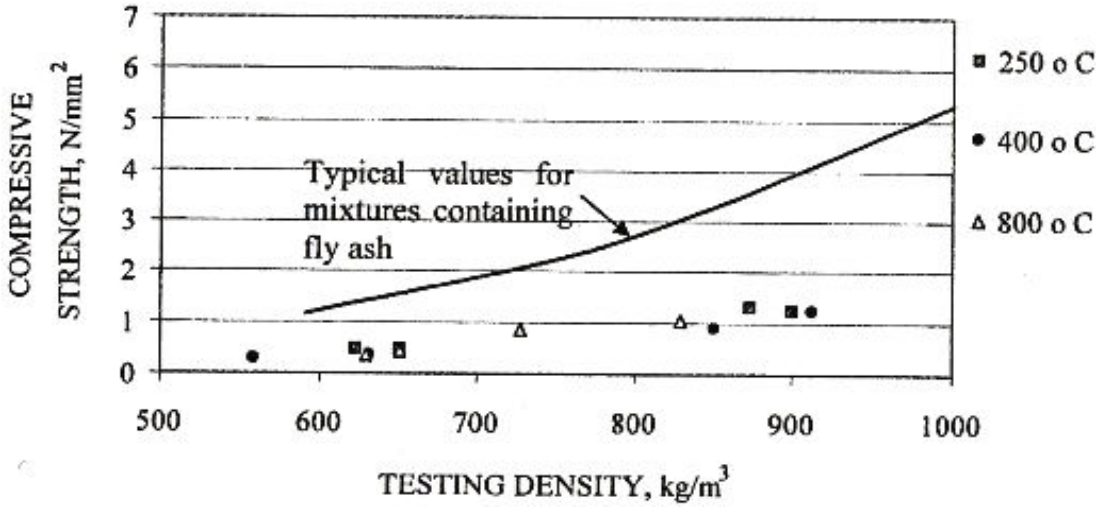

Figure 2.4 Compressive strength of LFC samples containing dolomite (Kearsley and Mostert, 2005)

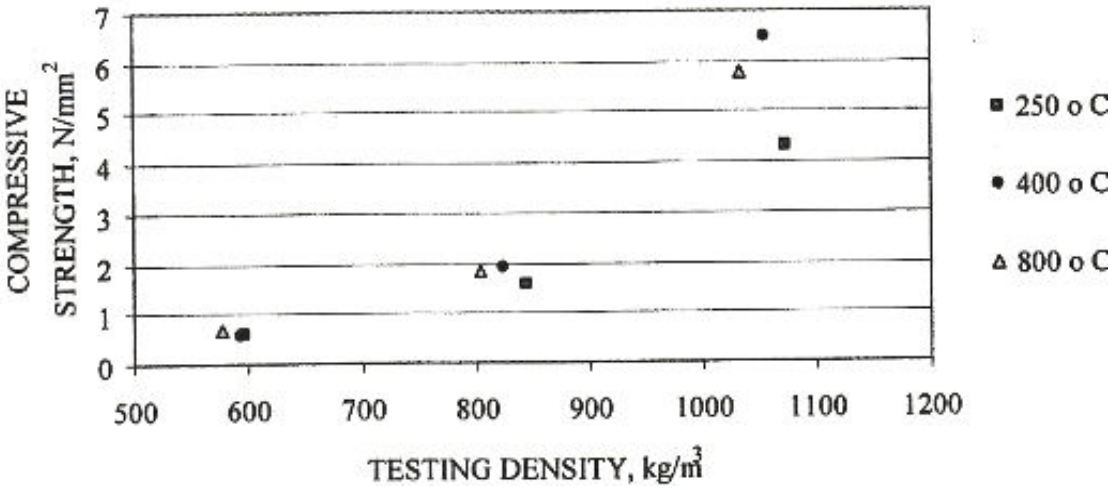

Figure 2.5 Compressive strength of LFC samples containing Cement Type 2 (Kearsley and Mostert, 2005)

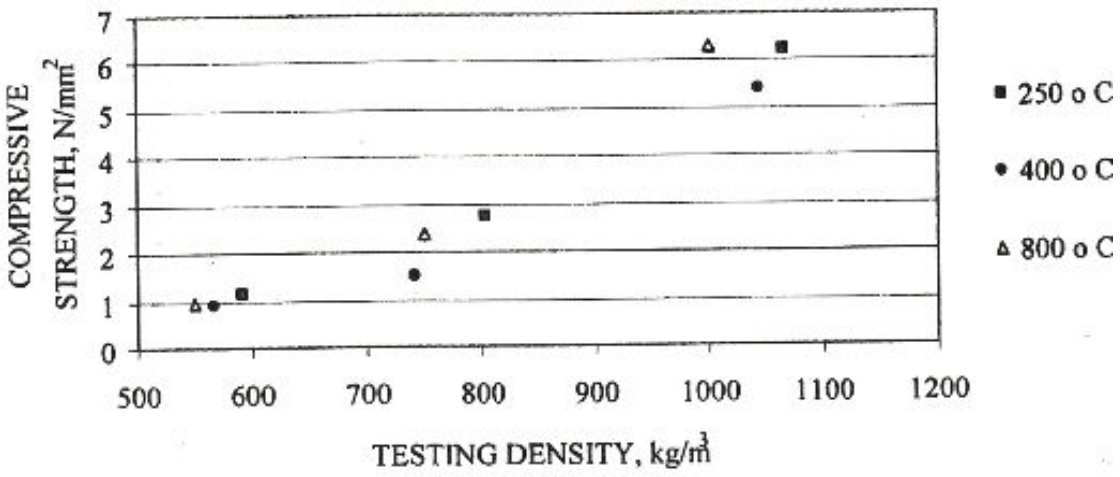

Figure 2.6 Compressive strength of LFC samples containing Cement Type 3 (Kearsley and Mostert, 2005)

Table 2.4 summarizes the effect of different parameters on compressive strength of LFC.

Table 2.4 Summary of the effect of different parameters on compressive strength of LFC

Parameters	Descriptions
Density	Compressive strength reduces with decreasing density.
Cement-sand ratio	Higher cement-sand ratios result in better strength. The strength of lower density mixes can be improved to equal that of higher density by increasing the amount of cement content in the mix.
Water-cement ratio	Effect of water-cement ratio on strength is imprecise. Dransfield (2000) found that the strength decreased with reduction in water-cement ratio whereas De Rose and Morris, 1999 reported that the strength reduced with increasing water-cement ratio up to 0.45 and opposite trend was observed for water-cement ratio between 0.5 and 1.0
Type of cement and content	Better strength is attained in the long term when cement is combined with silica fume (Kearsley, 1996) and fly ash (De Rose and Morris, 1999). The strength of LFC is principally a function of dry density (Kearsley and Wainwright, 2001)
Fillers	Mix with fine sand results in better strength than coarse sand and the disparity is higher at higher density. The use of fly ash significantly helped the growth of strength, primarily after 28 days
Pore size and distribution	For LFC dry density between 500 and 1000 kg/m^3, the compressive strength decreases with an increase in pore diameter. For densities above 1000 kg/m^3, the composition of the paste determines the compressive strength whilst the air-pores are far apart to have an influence on compressive strength (Visagie and Kearsely, 2002).
Type of surfactants	Protein based surfactant was found to increase the strength of LFC up to 70% compared to synthetic surfactant (Dransfield, 2000).
Curing regime	Autoclaving increases the compressive strength of LFC. Water cured samples of LFC attained higher strength than those cured in air (Hamidah et al., 2005)

2.2.4 Flexural and tensile strength of LFC

The ratio of flexural strength to compressive strength of LFC is in the range of 0.06–0.10 and this ratio was also found to reduce with increasing water-cement ratios and decreasing densities (Van Deijk, 1991). The splitting tensile strengths of LFC mixes are higher for mixes with sand than those with fly ash. This is attributed to the improved shear capacity between sand particles and the paste phase (Jones and McCarthy, 2005). The introduction of polypropylene fibers in LFC mix has been reported to improve the tensile and flexural strength of LFC, provided this does not affect the fresh concrete behavior and self-compaction (Kearsely and Mostert, 1997).

2.2.5 Modulus of elasticity of LFC

As a porous material, the static modulus of elasticity of LFC is expected to be considerably lower than that of normal weight concrete for dry densities between 500 and 1500 kg/m^3 with values typically varying from 1.0 to 8.0 kN/mm^2, respectively (Jones and McCarthy, 2005). LFC mix containing fly ash as fine aggregate is reported to show lower modulus of elasticity value than that of LFC with sand. Jones and McCarthy (2005) reported that the utilization of polypropylene fibers in LFC mix could enhance the value of modulus of elasticity of LFC between two and four times. They proposed two relationships to predict the modulus of elasticity of LFC as follows:

Sand as fine aggregate $$E_c = 0.42 f_c^{1.18} \quad \ldots. (2.3)$$

Fly ash as fine aggregate $$E_c = 0.99 f_c^{0.67} \quad \ldots. (2.4)$$

where E_c is the modulus of elasticity (kN/mm^2) and f_c is the compressive strength (N/mm^2).

Figure 2.7 shows a plot of modulus of elasticity against compressive strength based on Equation 2.3 and Equation 2.4. From Figure 2.7, it can be seen that for the same compressive strength (f_c), sand as aggregate gives higher modulus of elasticity values compared to fly ash aggregate. This difference is attributed to the high amount of fine aggregate in sand mix compared to fly ash mix, which contains completely paste with no aggregate (Jones, 2001).

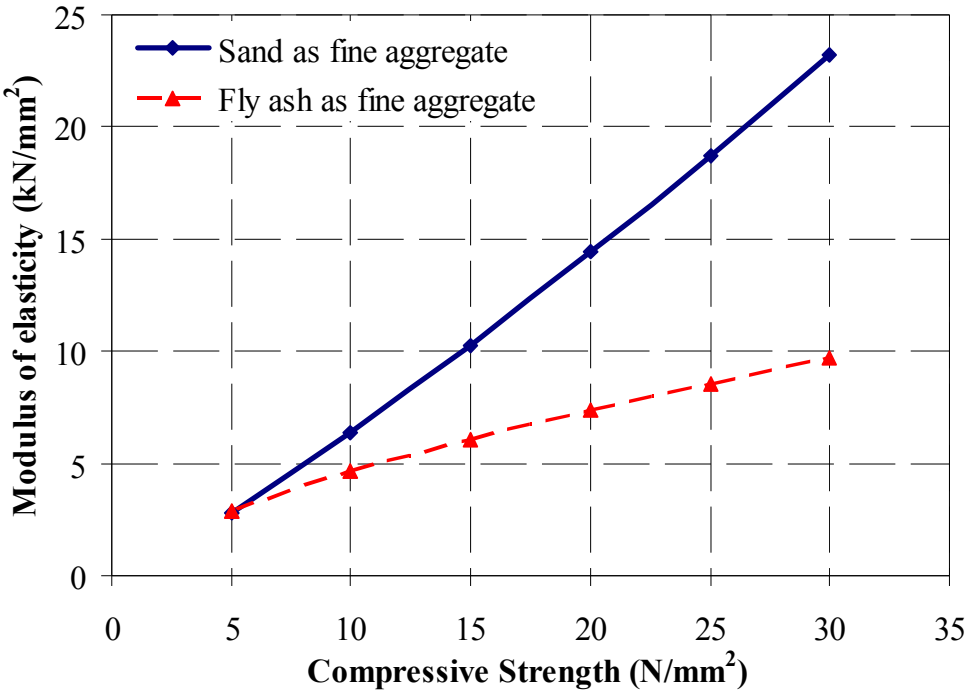

Figure 2.7 Relationship between modulus of elasticity and compressive strength of LFC

2.2.6 Thermal properties of LFC

Thermal properties are required in two design considerations: to provide thermal insulation at ambient temperature and to provide fire resistance. There is some data of LFC thermal properties at ambient temperature but little information is available for LFC thermal properties at elevated temperatures. One of the important objectives of this research is to obtain thermal properties of LFC at elevated temperatures for assessment of fire resistance.

2.2.6.1 Ambient temperature thermal properties

The cellular microstructure of LFC provides it with low thermal conductivity. According to BCA (1994) and Jones and McCarthy (2005), the thermal conductivity of LFC typically is 5 to 30% of that of normal weight concrete and range from between 0.1 and 0.7 W/mK for dry density values of 600 to 1600 kg/m^3 respectively. As pointed out by Kessler (1998), in practical terms normal weight concrete would have to be 5 times thicker than LFC ones to achieve similar thermal insulation. The thermal

conductivity of LFC with 1000 kg/m^3 density is reported to be one-sixth the value of typical cement-sand mortar (Aldridge and Ansell, 2001).

Since LFC is made by injecting air into a cement based mixture, the density of LFC is directly a function of the air inside LFC. Expectedly, the density of LFC should play an important role in determining its thermal properties. According to Weigler and Karl (1980), a reduction in LFC density by 100 kg/m^3 results in a lessening in its thermal conductivity by 0.04 W/mK.

In addition to use more air to reduce the thermal conductivity of LFC, it is possible to reduce the thermal conductivity of LFC by using pulverized fuel ash. For example, as reported by Giannakou and Jones (2002), a reduction in thermal conductivity by 12-38% was attained with the introduction of 30% pulverized fuel ash in the mix compared to the LFC with only Portland cement SEM1 as binder material. This was attributed to the lower density of fly ash particles. Figure 2.8 shows the ambient temperature thermal conductivity of LFC as a function of density.

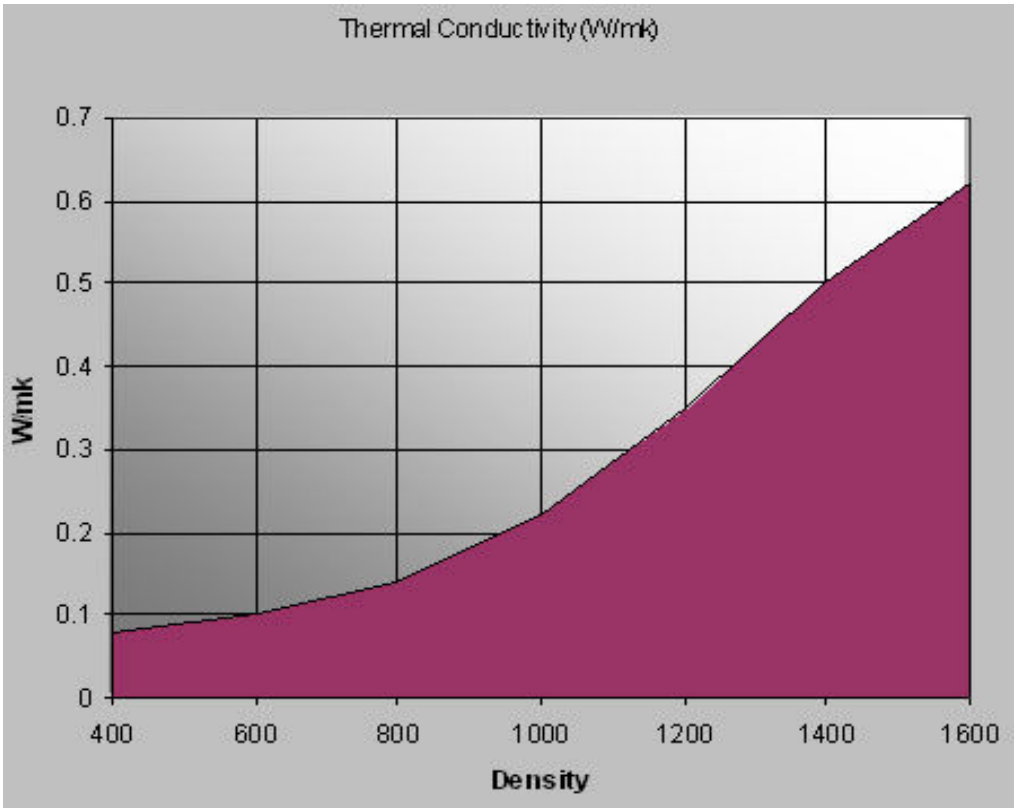

Figure 2.8 Thermal conductivity of LFC (www.foamedconcrete.co.uk)

2.2.6.2 Fire resistance and elevated temperature thermal properties

To evaluate fire resistance of a construction element, it is necessary to carry out heat transfer analysis to obtain temperature information and structural assessment. Temperature dependent thermal and mechanical properties are required. Compared to ambient temperature studies on LFC, there is little quantitative information available on elevated temperature thermal and mechanical properties of LFC. A major contribution of this study will be to help fill this significant knowledge gap.

According to Kessler (1998), the fire resistance of LFC is excellent; at low temperatures it is better than normal weight concrete in terms of the proportional loss in strength. But when exposed to high temperatures, it suffers from excessive drying shrinkage (Sach and Seifert, 1999). Study carried out by Kearsley and Mostert (2005) on the effect of cement composition on the properties of LFC exposed to high temperature indicated that LFC containing hydraulic cement with an Al_2O_3/CaO ratio higher than two could withstand temperatures as high as 1450°C without showing any sign of damage. According to Jones and McCarthy (2005), LFC has been found to be incombustible, and in a test on LFC concrete slabs with 100mm thickness, standard fire resistance of 2 ½ hours and 3 ¾ hours for 1250 kg/m^3 and 930 kg/m^3 oven dry densities respectively was established based on thermal insulation.

2.3 LIMITATION IN PREVIOUS STUDIES ON LFC PROPERTIES

The literature review presented in Section 2.2 clearly indicates that most of the investigations on LFC so far have focused on its ambient temperature properties only. Among these, the majority are about mechanical properties of LFC with only a very few on its thermal properties. Quantitative information on fire resistance performance is extremely sparse.

Nevertheless the reviewed literature does give some useful data of LFC mechanical and thermal properties at ambient temperature which can be used as the basis for further research. In particular, it is important to identify the most important parameters that influence the mechanical and thermal properties of cement-based LFC at elevated temperatures so that appropriate quantification models may be developed. Section 2.4 will further discuss the influential parameters.

2.4 PROPERTIES OF CEMENT-BASED MATERIAL AT ELEVATED TEMPERATURES

This section describes the thermal and mechanical properties of cement-based material at high temperatures. It will briefly explain the reasons for the changes in LFC properties during heating so as to provide references for further understanding of the changes. Chapter 3 and Chapter 6 will provide detailed explanations and development of thermal properties and mechanical properties models correspondingly.

2.4.1 Thermal properties of cement-based material

As mentioned earlier, LFC is a composite material made from a combination of filler (sand), cement binder and water. After mixing, the cement hydrates and hardens into a stone like material. Theoretically, combined mass and heat transfer should be carried out to obtain temperatures in LFC construction. However, modelling mass transfer (water movement) is complex. A common approximation is to conduct heat transfer only, but modifying the material thermal properties to reflect the effects of water movement. For heat transfer analysis, data on thermal conductivity, specific heat and density should be provided.

When cement-based material like LFC is exposed to high temperatures, the free water in the pores and some chemically bonded water in the hydrated cement paste are released, consuming a large amount of energy, just as happens in normal weight concrete. A few authors have described the reactions that take place in cement-based material at high temperatures. Vaporization of the free water takes place at around 100°C (Noumowe, 1995). It is generally considered that the evaporable water is completely eliminated at 120°C. Then between 180 to 300°C, loss of the chemically bond water happens through decomposition of the C-S-H and carboaluminate hydrates (Khoury, 1992). The high temperatures in the range of 400 to 600°C may then stimulate a series of reactions in the hardened LFC paste. These reactions originate with the complete desiccation of the pore system, followed by decomposition of the hydration products and the destruction of C-S-H gels (Rostasy, 1995). The conversion of calcium hydroxide into lime and water vapour during heating may lead to serious damage due to lime expansion (Lin et al., 1996). These changes will affect the thermal properties of LFC.

2.4.1.1 Thermal conductivity

Given that LFC is a porous material, its effective thermal conductivity will be affected by the air voids inside, and heat transfer through LFC should consider all three modes of heat transfer: conduction through the solid, and convection and radiation through the pores. Therefore the effective thermal conductivity of LFC should include these effects. Within each air-void, heat conduction will dominate at relatively low temperatures. At high temperatures, radiation will play a much more important role because the radiation coefficient is related to temperature raised to power three. The effective thermal conductivity of LFC at elevated temperatures depends not only on the thermal conductivities of the cement and the air, but also radiation effect inside the air voids.

2.4.1.2 Specific heat

The specific heat is the amount of heat energy per unit mass required to change the temperature of the material by one degree. Compared to thermal conductivity, this thermal property does not vary much with temperature. It has been found that filler type, mix proportion or age do not have great effect on the specific heat of ordinary cement-based material (Carman and Nelson, 1921). The main factor affecting the specific heat of LFC is the moisture content at the time of heating as water has relatively high specific heat. The specific heat of LFC consists of the base value of the dry components and the heat consumed heat due to water evaporation. During water evaporation, most of the heat supplied to the concrete is used for the removal of water and only a small amount is available for raising the temperature of the material. As a consequence, the specific heat increases considerably in these temperature intervals.

2.4.1.3 Density

The density of cement-based material like LFC is affected by the evaporation of water and reduces with increasing temperature.

2.4.2 Mechanical properties of cement-based material

Mechanical properties of concrete due to exposure to elevated temperatures have been studied since a long time ago. Table 2.5 provides a summary of investigations on normal weight concrete at elevated temperatures. Influence of these earlier studies have

provided data which formed the technical basis for the provisions and recommendations for determining concrete mechanical properties exposed to elevated temperatures in many existing codes.

Table 2.5 Summary of studies on normal weight concrete at elevated temperatures

Researchers	**Properties**	**Descriptions**
Li and Purkiss (2005)	Compressive strength, modulus of elasticity, strain at peak compressive stress	Performed a transient test on mechanical properties of concrete at high temperatures
Hertz (2005)	Compressive strength	Study on compressive strength of concrete that allowed for different types of aggregate at high temperatures
Lu (1989)	Modulus of elasticity	Investigation of fire response of reinforced concrete beams based on unstressed test procedure
Li and Guo (1993)	Modulus of elasticity, flexural tensile strength	Experimental investigation on strength and deformation of concrete under high temperature
Khennane and Baker (1993)	Modulus of elasticity, Strain at peak compressive stress	Investigation on concrete behavior under variable temperature and stress at high temperatures
Anderberg and Thelandersson (1976)	Strain at peak compressive stress, stress-strain relationship, flexural tensile strength	Study on mechanical properties of concrete based on transient tests at high temperatures
Bazant and Chern (1987)	Strain at peak compressive stress	Investigation of strain behavior of unstressed concrete at high temperatures
Lie and Lin model (1985)	Stress-strain relationship	Study on stress-strain relationship of concrete exposed to high temperatures
Terro (1998)	Flexural tensile strength	Carried out numerical modeling of the behavior of concrete structures under fire condition

There is no such extensive study of mechanical properties of LFC at elevated temperatures. Therefore Chapter 6 will assess the applicability of the different models suggested by various researchers presented in Table 2.5 for normal weight concrete to LFC.

Lin et al. (1996) conducted studies to investigate the microstructure of concrete exposed to elevated temperatures in both actual fire and laboratory conditions with the assistance of Scanning-Electron-Microscopy (SEM) and stereo microscopy. They found that the absorption of moisture from the surrounding medium provides a mechanism for the rehydration of calcium oxide and unhydrated cement grains that refilled the void spaces. They observed that long irregular fibers of C-S-H gel combined with ettringite and C-H crystals and formed as a result of rehydration.

In a study carried out by Schneider and Herbst (1989), chemical reactions and the behavior of calcium hydroxide, calcium carbonate, calcium silicate hydrate, non-evaporable water and micropores under various temperatures was examined. They found that the major increase of concrete permeability and porosity at high temperature was primarily produced by arising microcracks and by changes of material inner structure, as well as by crack opening due to high gas pressure values. As a result, the permeability of concrete depends not only on temperature levels, moisture content and gas pressure but also upon the degree of crack development.

It can be pointed out that the degradation mechanisms of cement-based material like LFC upon exposure to elevated temperatures include chemical degradation and mechanical deterioration where each mechanism is dominant within a specific temperature range. Chemical degradation occurs when the chemically bound water is released from the cement paste. The dehydration process in the cement paste becomes significant at temperatures above about 110 °C (Khoury et al., 2002) and diminishes the calcium silicate hydrate (C-S-H) links which provide the primary load-bearing formation in the hydrated cement. Furthermore, due to low permeability of the cement paste, internal water pressure built up during dehydration of the hydrated C-S-H, which increases internal stresses and induce microcracks in the material from about 300°C, resulting in decreased strength and stiffness of the material (Hertz, 2005), (Ai et al., 2001). At higher temperatures around 450°C, calcium hydroxide ($Ca(OH)_2$), which is one of the most vital compounds in cement paste, dissociates, resulting in the shrinkage

of LFC (Taylor, 1992). If the hot LFC is exposed to water, as in fire fighting, CaO in LFC turns into $Ca(OH)_2$ to cause cracking and destruction of LFC. It is still extremely difficult to accurately predict these mechanisms and experimental investigation remains essential.

2.4.3 Conclusions

Sections 2.4.1 and 2.4.2 have presented some brief explanations of thermal and mechanical properties of cement-based material at high temperatures. Cement-based material was found to be fundamentally a complex material and its properties can change dramatically when exposed to high temperatures thermally and mechanically. The principal effects of high temperatures on cement-based material are loss of compressive strength and stiffness, and increase in thermal conductivity. Though a lot of information has been gathered on both phenomena on cement-based material, there remains a need for more systematic studies of the effects of high temperatures on thermal and mechanical properties of LFC at high temperatures.

For thermal properties, all the key parameters such as density, specific heat and thermal conductivity has been identified and behaviour upon exposure to high temperatures has been discussed in brief. Particular attention will be given on these 3 main parameters and detailed explanations will be presented in Chapter 3 and Chapter 4.

On the other hand, for mechanical properties, the behavior of cement-based material has been discussed in terms of chemical degradation and mechanical deterioration when exposed to high temperatures. Summary of studies on normal weight concrete at elevated temperatures also have been identified which will be focused to develop conceptual models in order to establish a general methodology for use in finite element analysis of a concrete structure. These models will be further discussed in Chapter 6 to assess the applicability of these models to LFC.

2.5 POTENTIAL OF LFC FOR APPLICATION AS COMPOSITE STRUCTURAL LOAD-BEARING SYSTEM

As has become clear through this literature review, there is very little data and no systematic study of LFC thermal and mechanical properties at ambient and elevated temperatures. A major contribution of this research will be to fill this significant

knowledge gap. As part of this study investigating the use of LFC as a potential structural load-bearing material for building applications, this research will also investigate the performance of one type of structural element: lightweight composite panel under compression. This section provides a brief general review of the behaviour of this type of construction. Detailed models of calculation will be presented in Chapter 7.

This particular type of construction has been chosen because of its low thermal conductivity (leading to good insulation and high fire resistance) and usable amount of compressive resistance. It is considered feasible to construct lightweight LFC panels to be carried by manual workers on site without the use of machinery. However, since LFC is brittle, a suitable method of using LFC in load-bearing construction would be to use it in composite action with steel, which has high ductility. Should LFC be cast in-situ, the thin steel sheeting can be used as formwork during construction. The need for plywood formwork and the detailing of steel reinforcing bars is largely eliminated which significantly reduces the construction time and cost. Furthermore, because of the low density of LFC, the pressure on the steel sheeting during construction would be much lower than the case with normal weight concrete, allowing thin steel sheeting to be used.

When using thin-walled steel sheeting, the problem of local buckling under compression (Figure 2.9) should be considered. When using normal weight concrete in composite panel system, inward local buckling of the steel sheeting is prevented by the concrete inside (Figure 2.10). Because of low elastic stiffness of LFC, it is necessary to investigate whether LFC could still maintain this function.

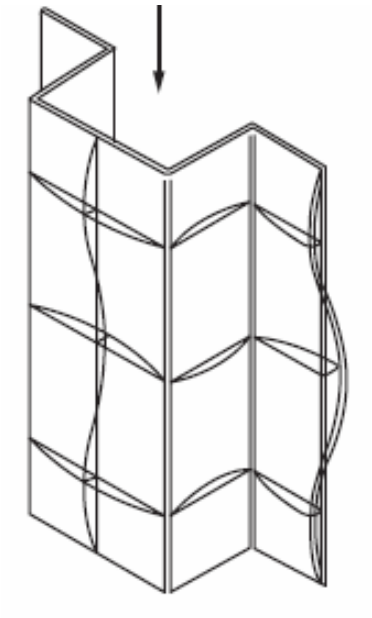

Figure 2.9 Local buckling in thin-walled steel section

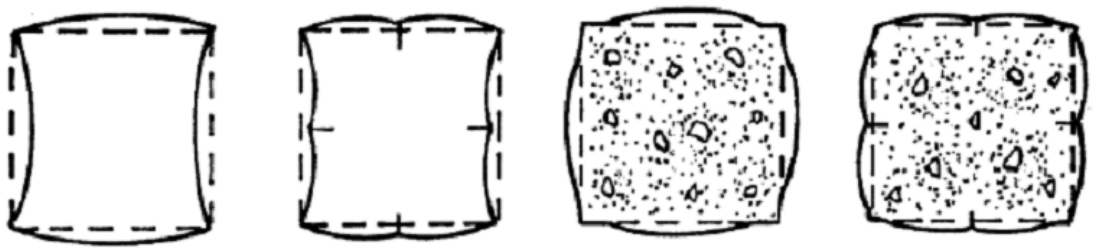

(a) steel section (b) composite section

Figure 2.10 Buckling modes of steel sections and composite sections (Shanmugam and Lakshmi, 2001)

The behaviour of steel-concrete composite structural elements under compression has been the subject of research of many researchers; majority of these researches are on composite columns. A few research studies, e.g. Wright and Gallocher (1995) and Wright (1998) mainly focused on composite walling. Application of the conclusions of these studies on composite walling to equivalent LFC systems will be explained in more detail in Chapter 7.

Central to determining the load carrying capacity of LFC composite walling system is quantification of local buckling of the steel sheeting acting in contact with concrete. A number of options are available and the applicability of these options to LFC panels will be assessed in Chapter 8.

2.6 SUMMARY

This chapter has comprehensively summarized the existing relevant studies on lightweight foamed concrete (LFC), including the method of production, mix design, mechanical properties, thermal properties and fire resistance performance. Key parameters that influence LFC thermal and mechanical parameters at ambient and elevated temperatures were identified. At ambient temperatures, the main parameters affecting the mechanical properties of LFC are the density, cement-sand ratio, water-cement ratio, type of cement and content, fillers, pore size and distribution, type of surfactants and curing regime. At high temperatures the mechanical properties of LFC are influenced by the chemical degradation and mechanical deterioration. Conversely, the key parameters affecting the thermal properties at ambient temperature are LFC density, porosity (amount of air inside) and the composition of the mix whilst at high temperatures. The important parameters are density, specific heat and thermal conductivity which is temperature dependent and highly influenced by water content. These key parameters will be used to guide development of experimentally based theoretical models to quantify LFC thermal and mechanical properties at ambient and elevated temperatures. This review has highlighted the potential application of LFC as a structural load-bearing element in low-rise residential construction.

CHAPTER 3

EXPERIMENTS FOR DETERMINING THERMAL PROPERTIES OF LFC AT ELEVATED TEMPERATURES

3.1 INTRODUCTION

As outlined in the previous chapter, this research includes investigation of thermal properties of LFC exposed to high temperatures. The thermal parameters investigated are thermal conductivity (k), specific heat (c) and density (ρ). This research will present experimental, analytical and numerical modelling results. This chapter will present the experimental results and Chapter 4 will present thermal property models and their validation using the experimental results of this chapter.

The density of LFC may be obtained by direct measurement and the results will be presented in this chapter. The specific heat of LFC may be calculated based on those of its constituent materials. LFC is lightweight but highly insulating. Therefore, among the three thermal properties considered, thermal conductivity is the most important factor. This will be further confirmed in Chapter 4 through the results of a sensitivity study in which the sensitivity of temperatures in LFC to changes in specific heat and thermal conductivity will be conducted. Therefore, the main emphasis of this research will be on thermal conductivity.

The thermal conductivity of LFC may be directly measured, as will be shown in this chapter. However, direct measurement of thermal conductivity requires expensive equipment and becomes very difficult at high temperatures. If only using direct measurement, it will be necessary to perform the experiments for LFC with any change in density. Another disadvantage with direct measurement is that it does not provide any understanding of how the material behaves. Therefore, this research has considered an alternative. In this method, a transient heat transfer test, exposing one side of an LFC

slab to high temperature and the other side to ambient temperature, is carried out. With the aid of a validated one-dimensional heat transfer analysis programme, the thermal conductivity of the LFC is obtained through trial and error. This trial and error process is not random and is based on theoretical consideration of thermal conductivity of LFC as a porous material. This chapter will present the experimental results, using both the alternative method of heating LFC slabs and the direct thermal conductivity measurement method, the guarded hot plate test. Chapter 4 will present the basics of the one-dimensional heat transfer programme and its validation, the thermal conductivity model for porous material, determination of LFC thermal conductivity-temperature relationships and comparison between these relationships with direct thermal conductivity test results.

3.2 HEAT TRANSFER TESTS ON LFC SLABS

3.2.1 Material constituents and design procedure of LFC

The LFC used in this study will be made from Portland cement SEM1, fine sand, water and stable foam in which the details of the constituent materials is shown in Table 3.1. The main objectives of this research are to determine the thermal and mechanical properties of LFC at high temperatures therefore only a constant cement-sand ratio of 2:1 and water-cement ratio of 0.5 will be used for all batches of LFC samples made for this research. A higher cement-sand ratio (2:1) was chosen to achieve better compressive strength and water-cement ratio of 0.5 was found acceptable to achieve adequate workability (Md Azree, 2004)

LFC samples of two densities of 650 and 1000 kg/m^3 will be cast and tested for thermal and mechanical properties test. The 650 kg/m^3 density was selected so as to enable comparison of thermal performance between LFC and that of other building materials of similar density, such as gypsum board; the 1000 kg/m^3 density will be used because LFC of this density would have a useful amount of mechanical properties to make it viable as a light load-bearing infill material, which may be combined with thin-walled steel in lightweight composite panel construction.

Table 3.1 Constituent materials used to produce LFC

Constituents	Type
Cement	Portland cement SEM1 (BS EN 197-1, 2000)
Sand	Fine sand with additional sieving to remove particles greater than 2.36 mm, to improve the LFC flow characteristics and stability. (BS EN 12620, 2002)
Stable foam	Noraite PA-1 (protein based) surfactant with weight of around 70 to 80 gram/litre produce from Portafoam TM2 System. The surfactant solution consists of one part of surfactant to 33 parts of water.

For this research, the design method recommended by the supplier of the foam making machine (Portafoam) from the University of Science Malaysia (www.portafoam.com) will be followed. It has the following 4 main steps:

(i) Decide the dry density and how much foamed concrete is required.

- For example target volume of foamed concrete required = 0.04 m^3
- Dry density = 700 kg/m^3
- Wet density = 700 + 100 = 800 kg/m^3 (based on density loss of 100 kg/m^3)

(ii) Calculate the weight of raw material needed.

- Total mass of raw materials = 0.04 x 800 = 32 kg
- This is made up of cement, sand, water and stable foam.
- Assuming foam weight is 5% of total mass
- Actual mass of solids (sand + cement + water) = 0.95 x 32 = 30.4 kg
- Assuming a cement-sand ratio of 2.0 and water-cement 0.5, the proportion of each material is as follows:
  - *Cement = 15.2 kg , Sand = 7.6 kg , Water = 7.6 kg*

(iii) Measure and calculate the mortar slurry density and slurry volume.

- Mix and measure the mortar slurry density and calculate its volume according to actual mix above.
- Slurry density = 2100 kg/m^3 (e.g. as measured)
- slurry volume = 30.4 / 2100 = 0.01447 m^3

(iv) Calculate the foam content in the mix from the foamed volume

- Foamed volume = 0.04 m^3
- Foam required in mix = 0.04 – 0.01447 = 0.02553 m^3
- Therefore estimated foam volume required = 25.53 litres

3.2.2 Methods of production and specimen preparation

All LFC samples were made in house. The stable foam was produced using foam generator Portafoam TM2 System (Figure 3.1), purchased from the Malaysian manufacturer (www.portafoam.com). This system runs from an air compressor and consists of a main generating unit, a foaming unit, and a lance unit. The foaming agent used was Noraite PA-1 (protein based) which is suitable for LFC densities ranging from 600 to 1600 kg/m^3. Noraite PA-1 comes from natural sources and has a weight of around 80 gram/litre and expands about 12.5 times when used with the Portafoam foam generator. Thermocouples were positioned during casting the LFC specimens. These thermocouples were found to be in the correct positions once the samples dried.

Figure 3.1 Portafoam TM2 foam generator system.

LFC was produced using a mixer by adding up the preformed foam to a base mortar mix. Any common type of mixer (tilt drum or pan mixer used for concrete or mortar) is suitable for LFC. The process of mixing consists of combining the cement and filler with water and mixing it until a homogeneous base mix is accomplished. The foam must be instantly added to the base mix and mixed until there is no physical sign of the foam on the surface and the foam is consistently dispersed and integrated in the mix. Figures 3.2-3.5 are provided to show how the production is carried out.

Three identical specimens were prepared for each density and were tested at 14 days after mixing. The slab tests were conducted in an electrically heated kiln. For these tests, LFC panels of densities 650 and 1000 kg/m^3 were cast and tested. All specimens had dimensions of 430 mm x 415 mm in plan and 150 mm in thickness. The high temperature tests were performed for two duplicate samples of each density.

Figure 3.2 Loading of water into the mixer

Figure 3.3 Loading of fine sand and cement into the mixer

Figure 3.4 Adding the foam into the mortar slurry

Figure 3.5 Checking the wet density of the mix

3.2.3 Experimental Set-up

Figure 3.6 shows the experimental set up. Each specimen was placed horizontally on top of an electric kiln as the source of heat, so that one side of the panel was subjected to kiln temperature and the other side faced up to the room temperature. The heating chamber has an internal diameter of 648 mm and 534 mm height. A cross section through the electric kiln and the test specimen is shown in Figure 3.7. There was a 280 mm x 265 mm opening on the top lid of the kiln, which allowed exposure of the lower side of the panel to elevated temperatures. A 30 mm thick layer of glass wool with the same opening size was laid under the specimen to insulate the contact surface of the top lid. The kiln temperature was increased to about 1200°C.

Figure 3.6 A typical set-up for the small-scale fire test

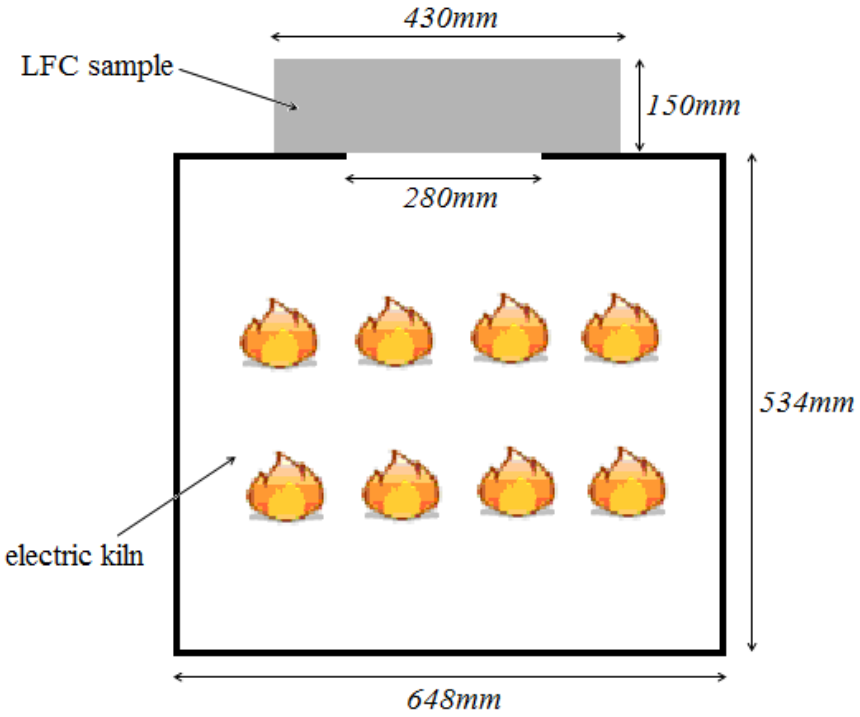

Figure 3.7 Cross section through the electric kiln and test specimen in elevation

3.2.4 Thermocouple arrangement

Heat transfer through each test LFC panel is assumed to be one dimensional. Therefore, to investigate temperature developments through each LFC panel, Type K thermocouples were placed throughout the thickness of the LFC specimen at the centre of the panel. Five thermocouples (T1-T5) were installed: on the exposed side, on the unexposed side and at quarter, half and three-quarter thickness, as shown in Figure 3.8, being 37.5mm, 75mm and 112.5mm from the heated surface.

To check the assumption of one-dimensional heat flow inside the LFC panel, four additional thermocouples (T6-T9) were positioned at two corners of a 150 x 150 mm square in the centre region of the specimen, as shown in Figure 3.8. One thermocouple was place inside the kiln, at an approximate distance of 50mm from the exposed surface of the panel, to record the kiln temperature.

.

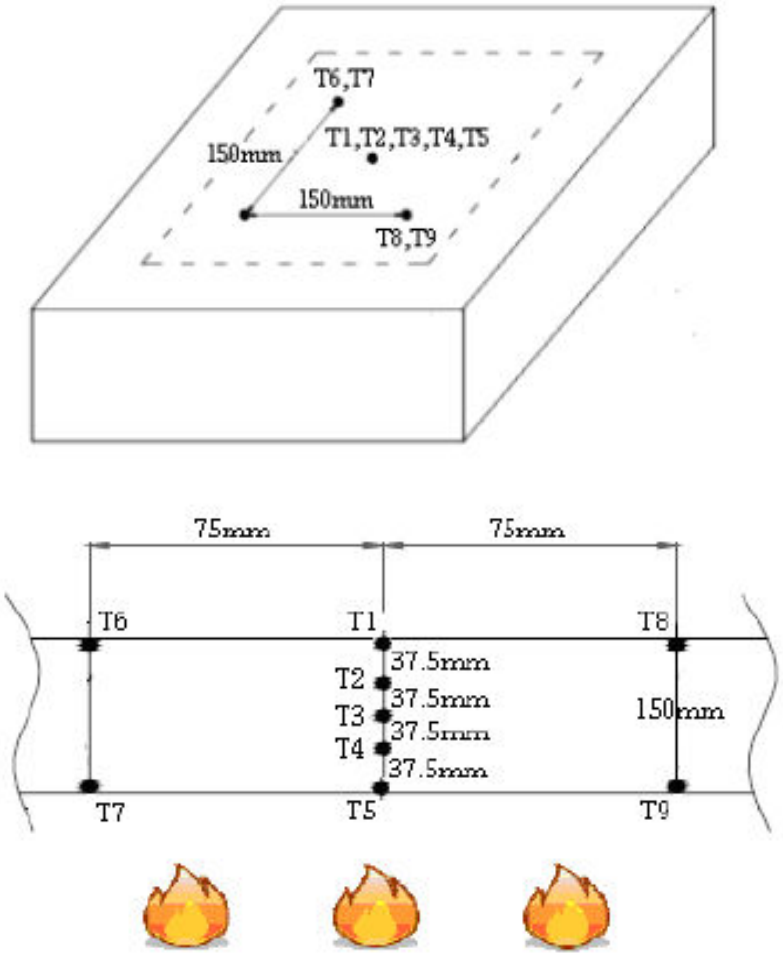

Figure 3.8 Thermocouple layout on LFC specimens on plan and throughout thickness

3.2.5 Kiln Temperature

LFC is considered to be non-reactive so its thermal properties are temperature dependent only. Therefore, at this stage of the study an electric kiln was deemed satisfactory as the source of heat and a Harrier Top Loading Electric Kiln was used for the experiments. The kiln temperature was controlled in such a way that its temperature-time relationship resembled that of the standard fire curve according to the British Standard for fire resistance testing (BS476, 1987). Figure 3.9 shows the heating curve achieved in the kiln, which is compared to a standard cellulosic fire curve (BS476).

There is some difference between the heating curve and the standard temperature – time curve. However, since this study relates the thermal properties of LFC to its temperature, rather than that of the air, and the recorded LFC slab surface temperatures

were used as input data, the kiln simply acted as a heating source. It was not important that its heating curve did not follow that of the standard fire curve exactly.

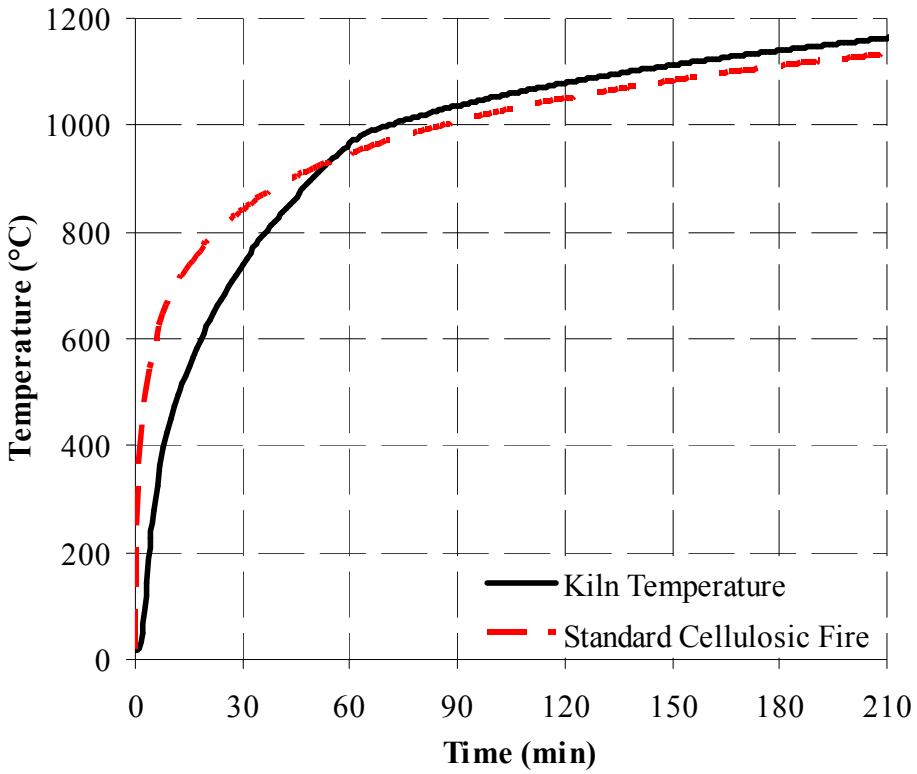

Figure 3.9 Time-temperature curve for the kiln against standard cellulosic fire curve

3.2.6 Recorded temperature results inside LFC

To confirm 1-Dimensional heat transfer in the LFC slabs, thermocouples were installed on the exposed and unexposed surfaces of the sample in the middle and near the four corners. Figures 3.10 and 3.11 compare these observations. The three thermocouples on each surface of the sample recorded very similar temperatures, thus confirming the one-dimensional heat transfer assumption.

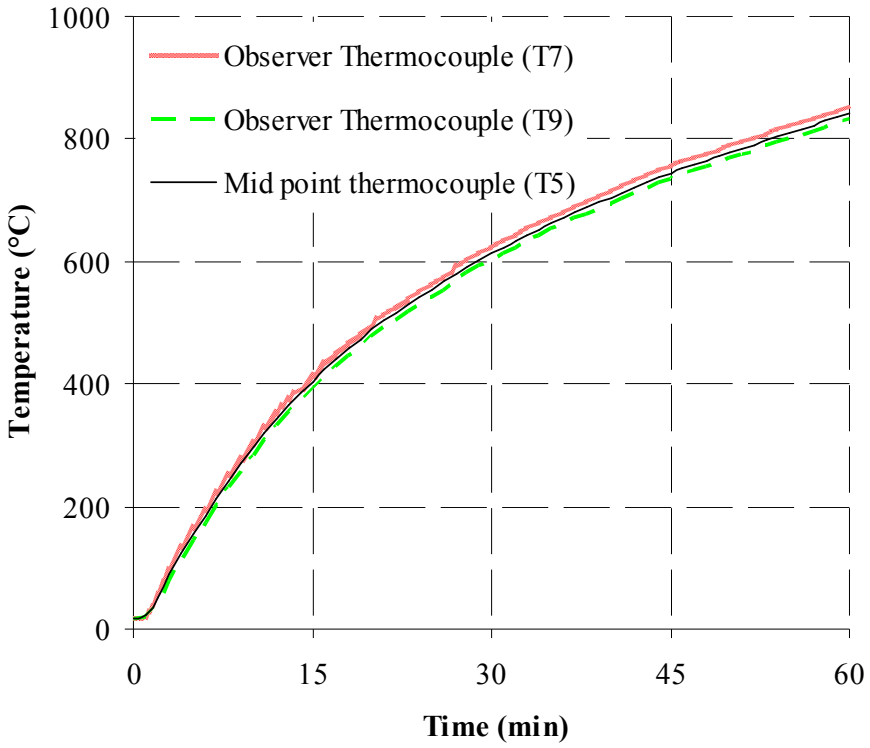

Figure 3.10 Temperature readings on top surface (exposed side) of one 650 kg/m^3 density test observer thermocouples in (Test 2)

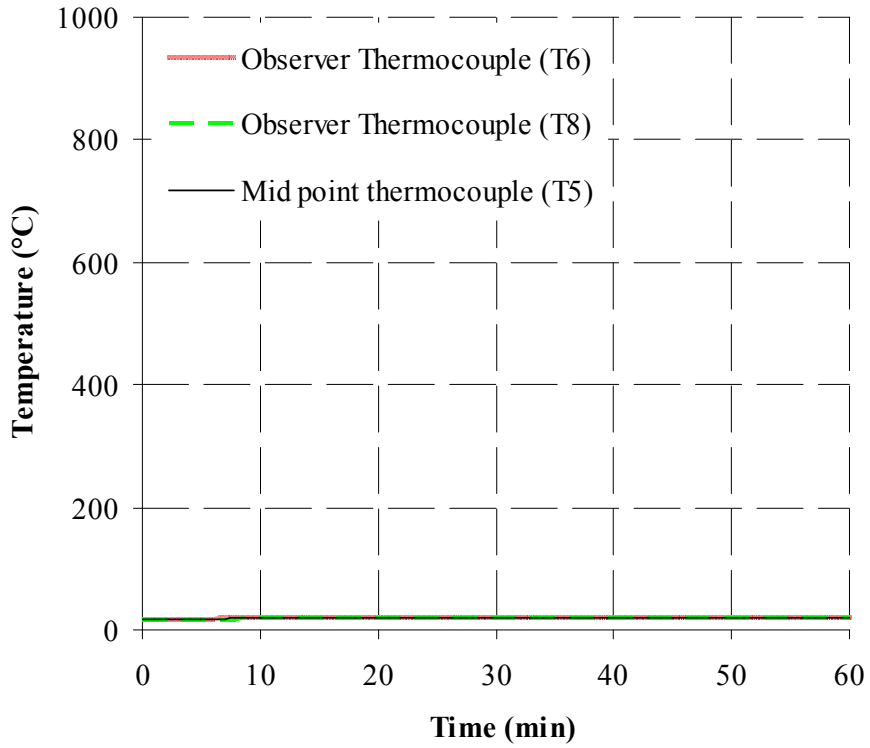

Figure 3.11 Temperature readings on bottom surface (unexposed side) of one 650 kg/m^3 density test observer thermocouples in (Test 2)

The LFC specimen temperatures were monitored through 5 thermocouples which were mounted at different thickness as been discussed in Section 3.2.3. For each density, 2 specimens were tested. Figure 3.12(a-d) and Figure 3.13(a-d) show the recorded temperatures for 650 kg/m^3 and 1000 kg/m^3 at different thickness respectively. Close agreement of test results were found for the two identical tests at different thickness for both densities.

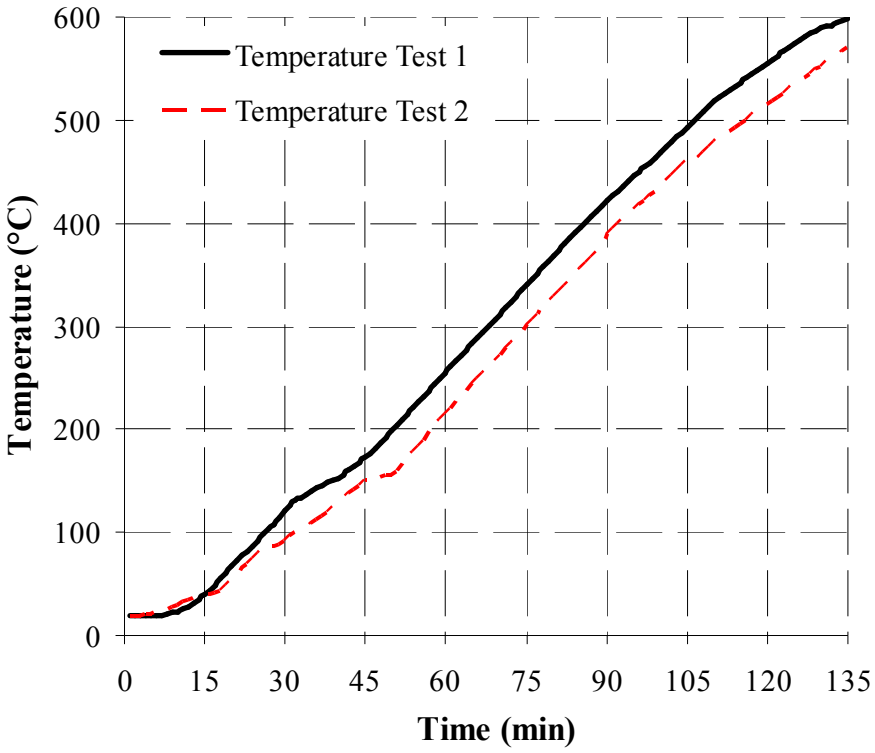

Figure 3.12(a) Recorded temperatures at different thickness for 650 kg/m^3 density at 37.5mm from exposed side

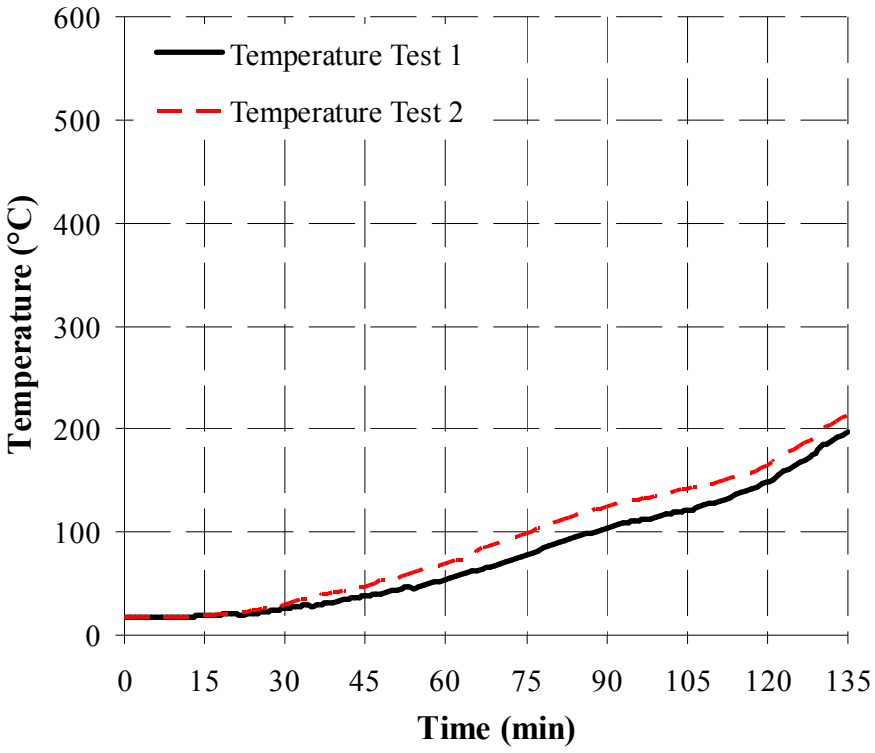

Figure 3.12(b) Recorded temperatures at different thickness for 650 kg/m^3 density at 70.0mm from exposed side

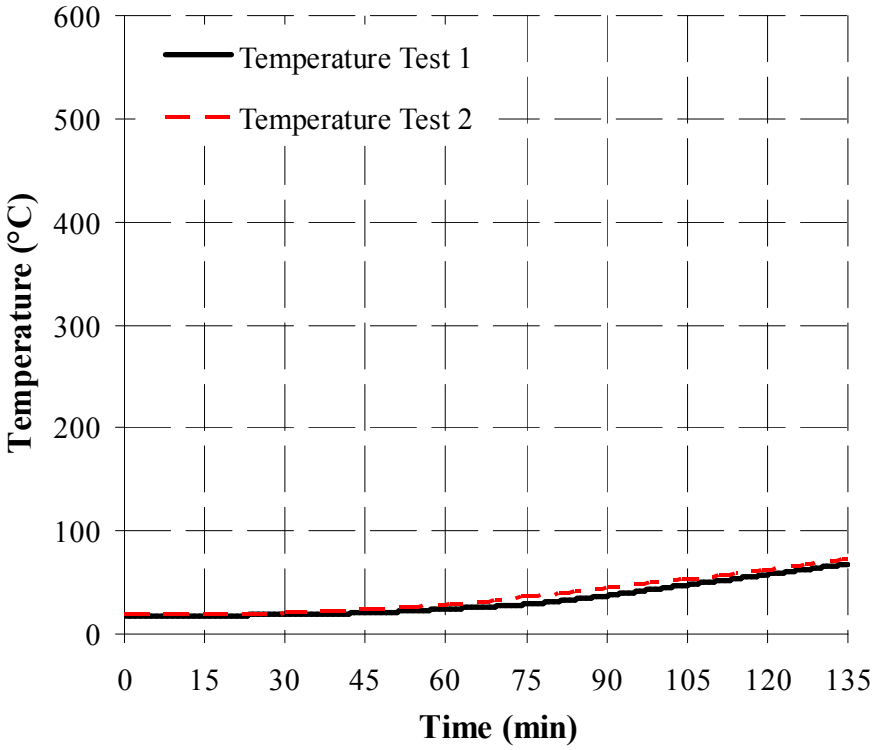

Figure 3.12(c) Recorded temperatures at different thickness for 650 kg/m^3 density at 112.5mm from exposed side

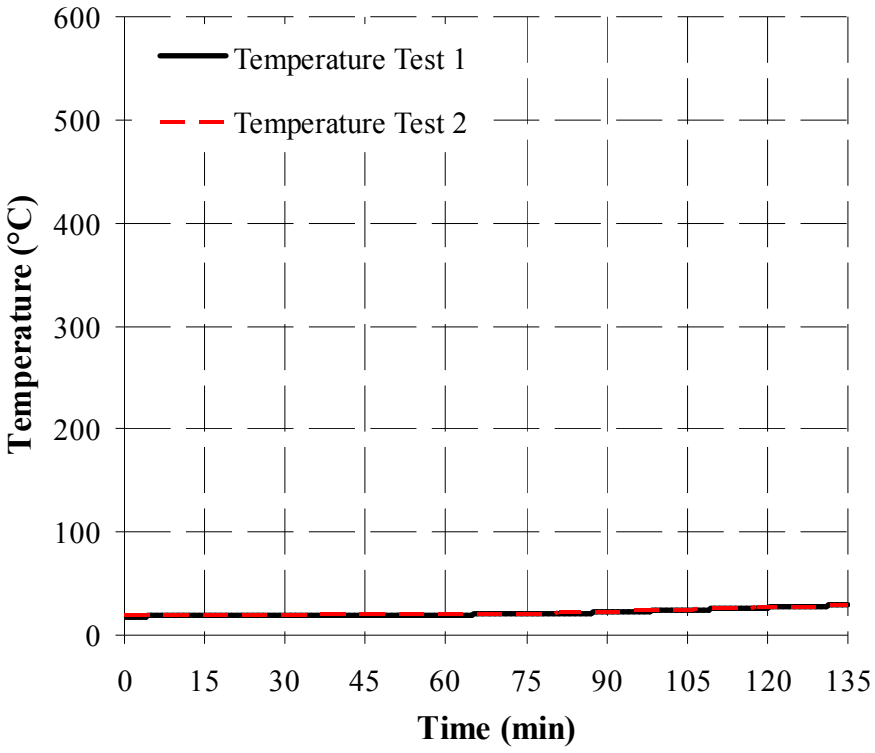

Figure 3.12(d) Recorded temperatures at different thickness for 650 kg/m^3 density at unexposed side

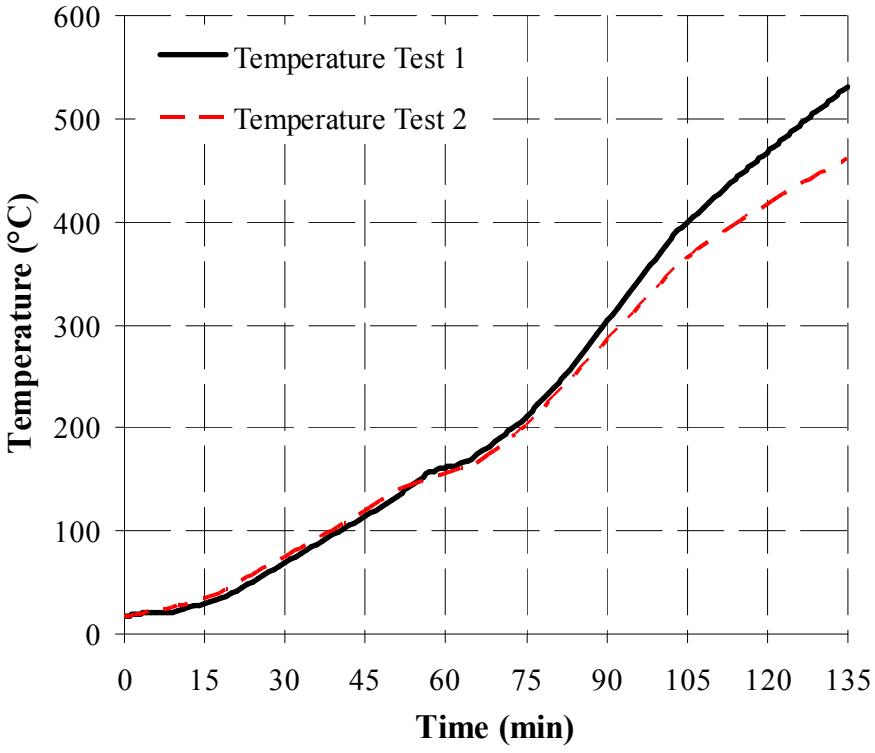

Figure 3.13(a) Recorded temperatures at different thickness for 1000 kg/m^3 density at 37.5mm from exposed side

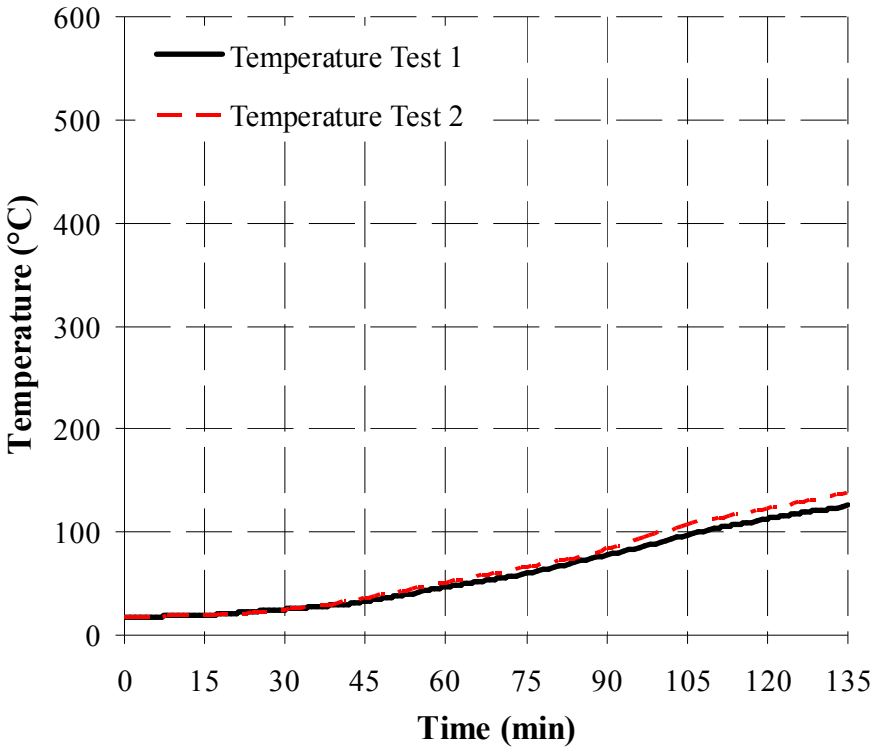

Figure 3.13(b) Recorded temperatures at different thickness for 1000 kg/m^3 density at 75.0mm from exposed side

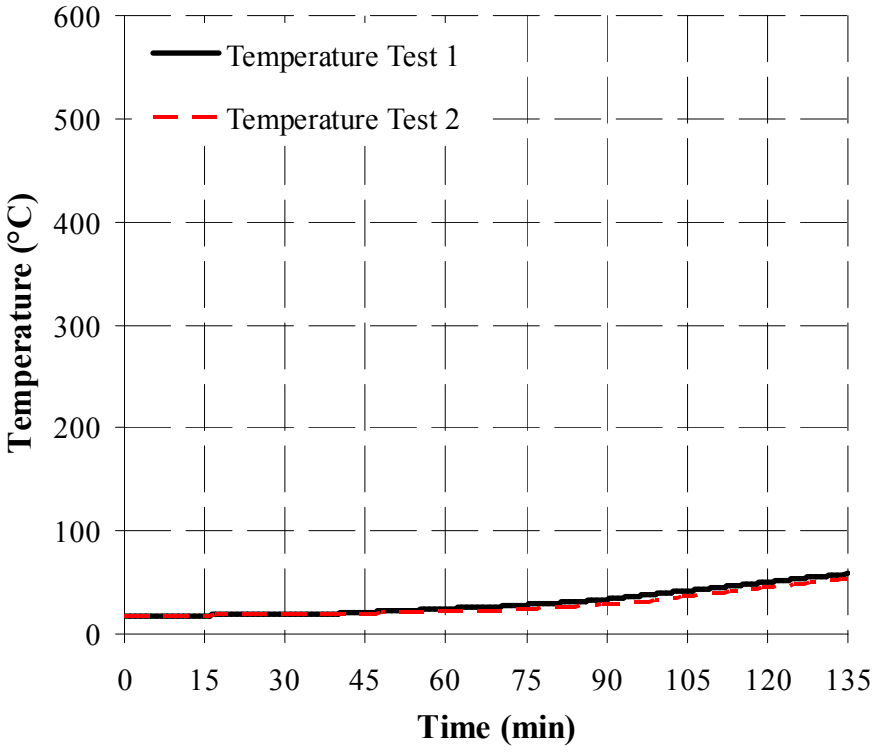

Figure 3.13(c) Recorded temperatures at different thickness for 1000 kg/m^3 density at 112.5mm from exposed side

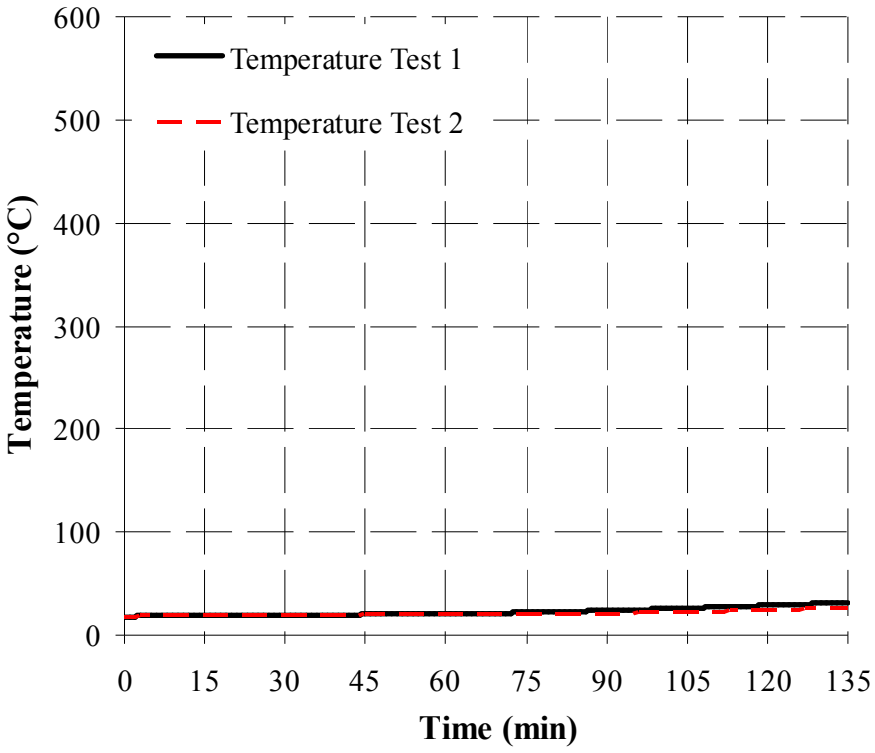

Figure 3.13(d) Recorded temperatures at different thickness for 1000 kg/m^3 density at unexposed side

Figure 3.14 show the comparison of the average temperature of the two LFC densities at all four different locations of measurements. It can be seen from Figure 3.14 that the recorded temperature growth at each location was less for LFC specimen of 1000 kg/m^3 density compared to LFC specimen of 650 kg/m^3 density. This is attributed to higher thermal capacitance value (density times specific heat) for LFC specimen of 1000 kg/m^3 density, which allow more heat to be absorbed thus slowing down the rate of temperature rise.

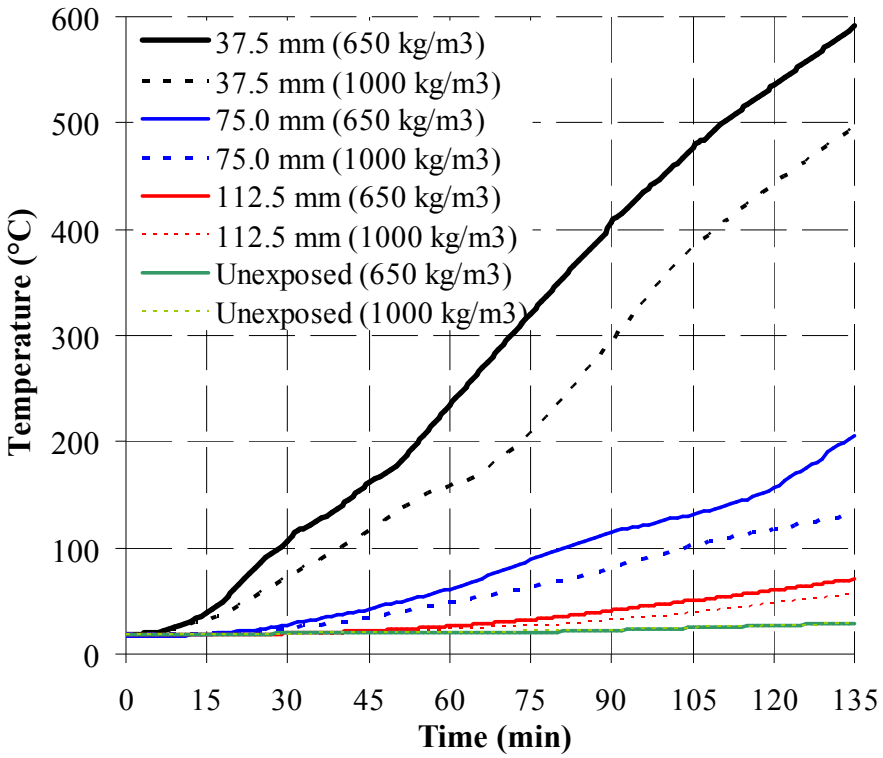

Figure 3.14 Comparison of the average temperature of the two LFC densities at all four locations of measurements

3.3 DENSITY AND SPECIFIC HEAT TESTS

3.3.1 Effects of moisture content and dehydration reactions on LFC density

Hydrated cement paste is composed from four major compounds of tricalcium silicate ($3CaO•SiO_2$), dicalcium silicate ($2CaO•SiO_2$), tricalcium aluminate ($3CaO•A1_20_3$) and tetracalcium aluminoferrite ($4CaO•A1_20_3•Fe_20_3$). The most significant products involved in hydration reactions are calcium silicate hydrate (C-S-H) and portlandite, also called calcium hydroxide ($Ca(OH)_2$).

LFC contains free water and chemically bond water. The free water content in LFC depends on the density (i.e., the free water content for the 650 kg/m^3 density is 1.7% by weight and for the 1000 kg/m^3 density is 3.2% by weight based on experiment data). Evaporation of the free and some of the chemically bond water will cause dehydration in LFC, which will affect all the three items of thermal properties of LFC (density, specific heat and thermal conductivity).

The dehydration process starts as early as 90°C. In the range of 90°C to 170°C, the evaporable free water and part of the chemically bond water escapes. The evaporable free water may be considered to have been completely eliminated by 170°C. Some chemically bond water is also lost through decomposition of the Calcium Silicate Hydrates (C-S-H) gel that takes place between 120°C and 140°C and decomposition of ettringite around 120°C (Taylor, 1992). In the temperature range between 200°C and 300°C, some of the chemically bond water is released from further decomposition of the C-S-H gel and the sulfoaluminate phases ($3CaO.Al_2O_3.CaSO_4.12H_2O$ and $3CaO.Al_2O_3.3CaSO_4.31H$) of the cement paste (Taylor, 1992). Further dehydration occurs at around 450°C, which corresponds to decomposition of $Ca(OH)_2 \rightarrow CaO + H_2O$ (Taylor, 1992) and it is completed at 530°C. At the second dehydration reaction, 75% of the chemically combined water is vaporised and the remaining 25% is then evaporated at the third dehydration reaction.

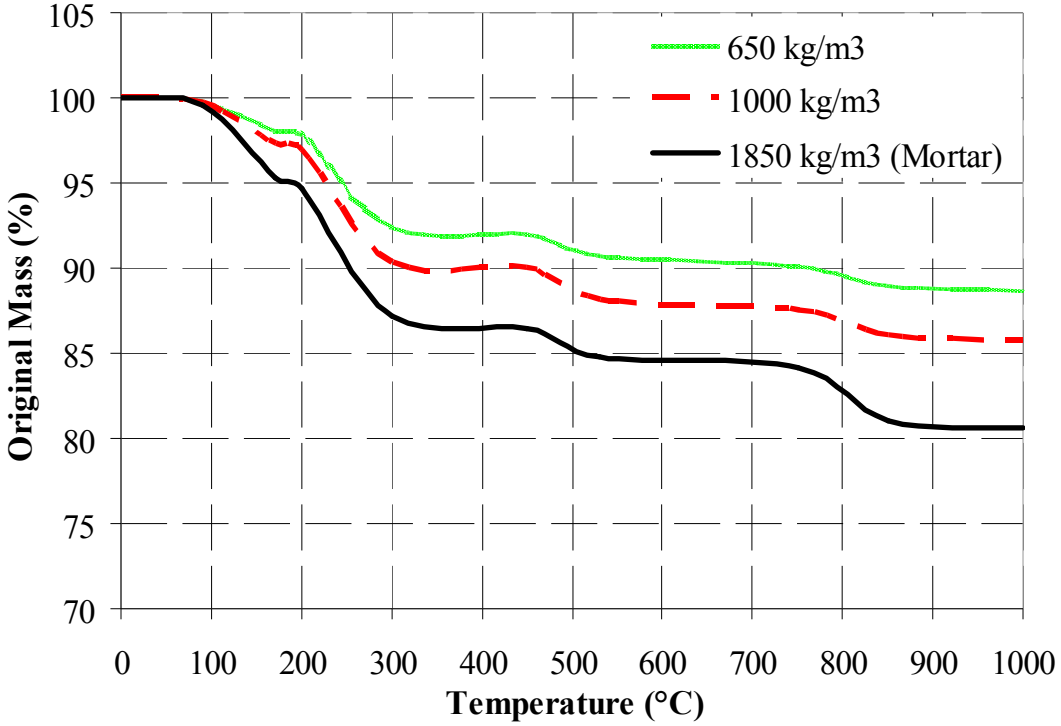

Figure 3.15 Percentage of original density at different temperatures

The previously described three stages of dehydration are accompanied by water loss or reduction in density of LFC. Figure 3.15 shows recorded densities of LFC at different temperatures, as ratio of the original density for two different initial density values, 650 kg/m^3 and 1000 kg/m^3. These values are also compared to the density change of mortar (density 1850 kg/m^3).

The results presented in Figure 3.15 were obtained by directly weighing samples after heating them to different temperatures. Usually thermo gravimetric analysis (TGA) may be performed to determine changes in weight at increasing temperatures. However, due to limitation in experimental facility, this study used manual recording according to the following procedure: three 100×100mm x 100mm LFC cubes of each density (650, 1000 and 1850 kg/m^3) were heated to different temperatures and then kept at the desired temperature for 24 hours. Their weight was recorded afterwards to obtain weight loss. The procedure was kept on until a maximum temperature of 1000°C.

The three curves are similar and the three dehydration phases can be clearly seen in Figure 3.15. This figure also shows a further weight loss phase, occurring between 750°C and 850°C, which can be assigned to the release of carbon dioxide (CO_2) from calcium carbonate ($CaCO_3$) (Taylor, 1992):

$CaCO_3 \rightarrow CaO + CO_2$

Table 3.2 summarises the density change values for the four phases (three phases of dehydration and final phase of CO_2 release) of weight loss.

Table 3.2 Density change values due to the dehydration process

Initial density (kg/m^3)	Remaining density at the end of each dehydration process (kg/m^3)			
	(1th) completed at 170°C	(2nd) completed at 300°C	(3rd) completed at 530°C	(Final) completed at 850°C
650	637	603	590	579
1000	973	903	881	860
1850	1763	1613	1569	1500

3.3.2 Specific heat for heat transfer analysis only

LFC can be considered as a non-reactive material and therefore its thermal properties can be considered to be temperature dependent only. Given that there is mass transfer involving water movement, precise treatment of thermal performance of LFC in fire should include combined heat and mass transfer. However, mass transfer can be rather complex to deal with and many of the mass transfer related material properties are

different to obtain. An alternative treatment is to carry out heat transfer analysis only, but taking into consideration the effects of mass transfer in heat transfer properties. The validity of such a treatment has been demonstrated by Ang and Wang (2004) on gypsum plaster, which has similar mass and heat transfer phenomena. The main effect of mass transfer, caused by moisture movement, is included in heat transfer analysis by modifying the specific heat of LFC. This will be explained in detail in Section 4.5.1.

The specific heat of LFC may be divided into two parts: the base value corresponding to a mixture of the dry components and the effect of water evaporation. The base value of the dry components may be calculated using Rule of mixtures as follows (Wang HB, 1995):

$$C_p = \sum_{i-1}^{n} F_i C_{pi} \quad \ldots (3.1)$$

where C_p is the overall specific heat capacity, C_{pi} is component specific heat, F_i is the volume fraction of each component and $\sum F_i = 1$.

According to the mixture law and bearing in mind the three phase of dehydration, the base value of specific heat of LFC should consist of four segments: from ambient temperature to the start of the first phase, from the end of the first phase to the start of the second phase, from the end of the second phase to the start of the third phase, and after the end of the third phase. However, existing literature, including fire resistant design codes for concrete structures such as EN 1992-1-2 (2004) and EN 1994-1-2 (2005), suggest that the base value which may be taken as a constant value is that at ambient temperature. Since LFC differs from normal concrete only in terms of density, the base value of LFC is also considered constant over the entire temperature range. Tables 3.3 and 3.4 give the weights of different components of the two densities of LFC (650 and 1000 kg/m^3) and the base value of specific heat at ambient temperature.

Table 3.3 Base value of specific heat for 650 kg/m^3 density

Material	Weight per 100 litre of LFC (kg)	Fractional weight (%)	Density (kg/m^3)	Fractional volume (%)	Specific heat of component (J/kg°C)	Contribution to specific heat of LFC (J/kg°C)
Cement	36.77	62.01	3130	47.59	920	571
Sand	18.38	31.01	2090	35.64	800	248
Water with foam	4.14	6.98	1000	16.77	4180	292
Total	57.97	100.00	-	100.00	-	1110

Table 3.4 Base value of specific heat for 1000 kg/m^3 density

Material	Weight per 100 litre of LFC (kg)	Fractional weight (%)	Density (kg/m^3)	Fractional volume (%)	Specific heat of component (J/kg°C)	Contribution to specific heat of LFC (J/kg°C)
Cement	53.96	58.89	3130	42.21	920	542
Sand	26.98	29.44	2090	31.60	800	236
Water with foam	10.69	11.67	1000	26.18	4180	488
Total	94.32	100.00	-	100.00	-	1265

In addition to the base value of specific heat, heat is also required to evaporate water from LFC. Therefore, the specific heat of LFC should be obtained from (Ang and Wang, 2004):

$$C_p = C_{p,dry} + C_{add} \quad \ldots (3.2)$$

where $C_{p,dry}$ is 1110 J/kg°C for LFC of 650 kg/m^3 and 1265 J/kg°C for LFC of 1000 kg/m^3 as calculated previously (Tables 3.3 and 3.4) and C_{add} is the additional heat

required to drive off water. C_{add} should be variable during the water evaporation temperature range to reflect that start and completion of water evaporation are gradual processes. A triangular distribution of specific heat over the water evaporation temperature range is typically assumed as shown in Figure 3.16. In this figure, Δc is the average additional specific heat.

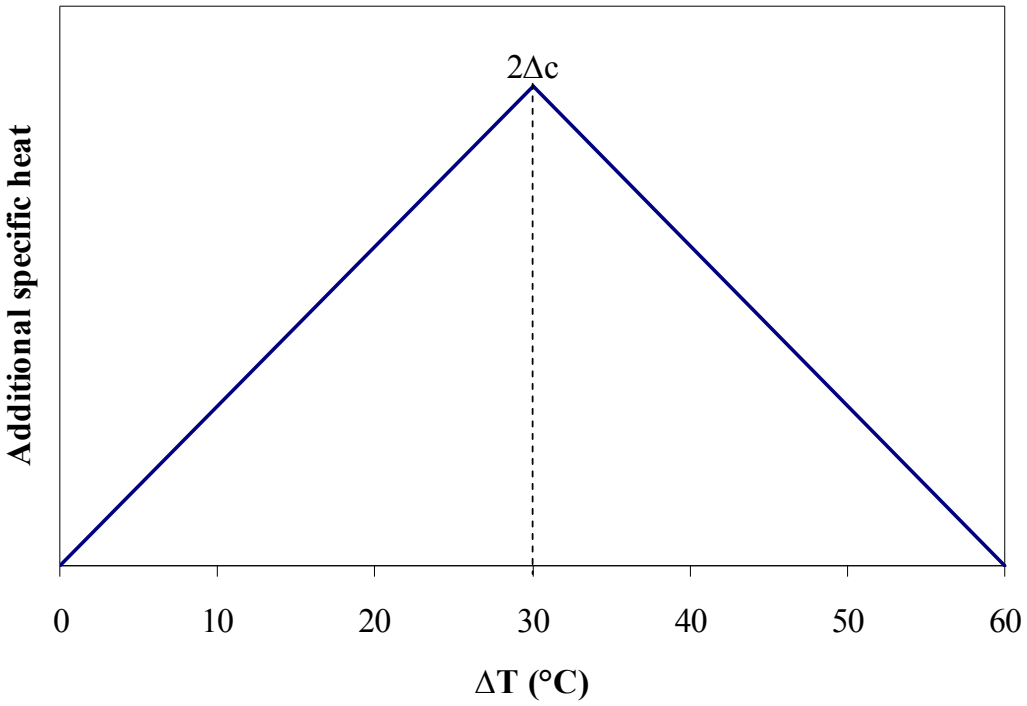

Figure 3.16 Additional specific heat for evaporation of free water (Ang and Wang, 2004).

Many previous studies (Noumowe, 1995), (Taylor, 1992) have assumed that water is simply evaporated at the evaporation temperature range. Consequently, the area within the triangle in Figure 3.16 is the latent heat of evaporation of water. However, Wang HB (1995) suggested that due to water movement, this was not sufficient and a higher value of specific heat should be applied. This has been confirmed by Ang and Wang (2004) who carried out a combined heat and mass analysis. In this study, the average additional specific heat for LFC was calculated as follows:

$$\Delta c = \frac{2.26 \times 10^6}{\Delta T} \times e \times f\,(J/kg°C) \quad \ldots (3.3)$$

in which the value of 2.26 x 10^6 J/kg is the latent heat of evaporation of water, Δc is the average additional specific heat, e is dehydration water content (percentage by total weight), ΔT is the magnitude of the temperature interval during which water is evaporated and f is a modification factor accounting for water movement. A value of f =1.4 was used. This value was established by Ang and Wang (2004) for gypsum. Ang and Wang who also found that this value to be relatively insensitive to different values of permeability provided the permeability is high. It was considered that both LFC and gypsum plaster are highly permeable materials so they should have a similar value of f. Since temperature rise in LFC is much more sensitive to changes in thermal conductivity than in specific heat, it was decided not worthwhile to refine the value of f. According to this procedure, the peak values of additional specific heat for LFC of 650 kg/m^3 and 1000 kg/m^3 densities are 2455 J/kg°C and 3796 J/kg°C respectively.

Since there are three phases of dehydration as explained previously, the above additional specific heat should be applied during each dehydration phase. Referring to the existing literature for the base value of specific heat, including fire resistance design codes for concrete, only the first phase of dehydration due to evaporation of the free water should be considered**.** Therefore, the specific heat – temperature relationship of concrete has only one peak, corresponding to the first phase. This appears to have been confirmed from the experimental results of this research. As can be seen from Figure 3.14, the temperature plateau between 90-170^{o}C is clearly noticeable, reflecting the first phase of dehydration. Afterwards, the temperature development is smooth and continuous without any plateau at the other two dehydration phases. Therefore, in this research, the additional specific heat will only be applied to the first phase of dehydration. As a summary, Figure 3.17 shows the temperature-dependent specific heat of LFC for both densities of 650 kg/m^3 and 1000 kg/m^3.

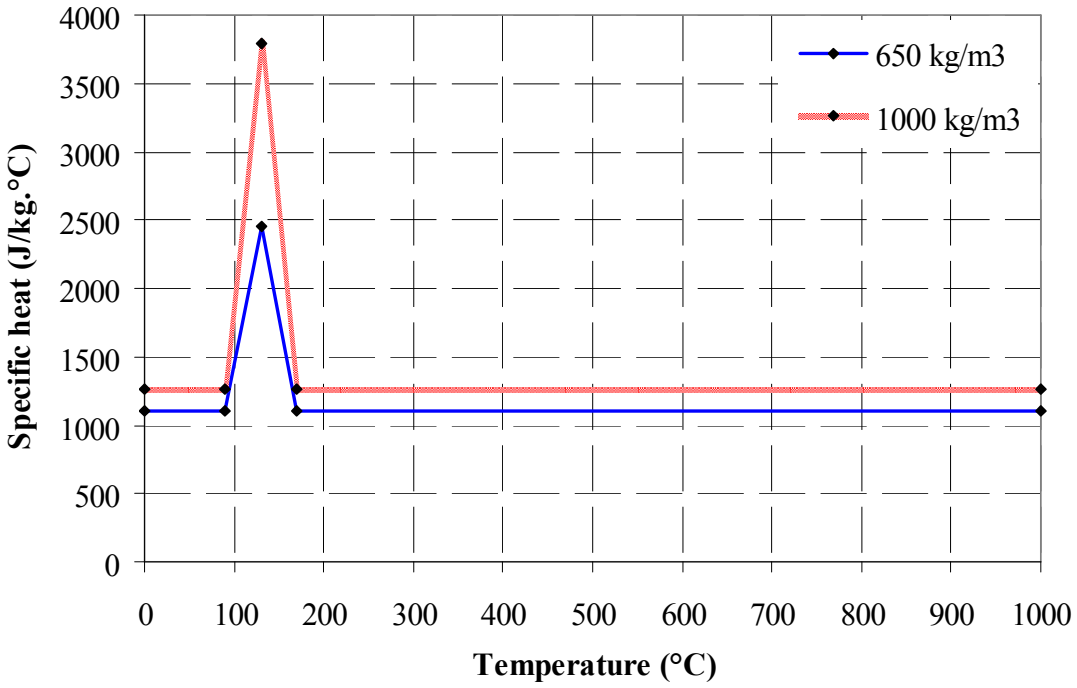

Figure 3.17 Specific heat of LFC (650 and 1000 kg/m^3 density) versus temperature

3.4 THERMAL CONDUCTIVITY RELATED TESTS

As mentioned in the introduction section, two methods will be used to obtain thermal conductivity of LFC. One is direct measurement method, using the Hot Guarded Plate test. The other one combines analytical modelling and transient heating test. For the latter, the analytical model treats LFC as a porous material and it is necessary to measure the porosity and pore size. These results are presented in this section.

3.4.1 Hot Guarded Plate Test

The HGP test followed the ASTM procedure in reference (ASTM, 1997). This particular test was conducted in concrete lab, University of Salford due to unavailability of such equipment in University of Manchester. The hot guarded plate test is generally recognized as the primary absolute method for measurement of the thermal transmission properties of homogeneous insulation materials in the form of flat slabs. This steady-state test method has been standardized by ASTM International as ASTM Standard Test Method C 177.

The basic HGP method consists principally of a hot plate and a cold plate. In a HGP test, the test specimen is placed on a flat plate heater assembly consisting of an electrically heated inner plate (main heater) surrounded by a guard heater. The guard

heater is carefully controlled to maintain the same temperature on both sides of the gap separating the main and the guard heaters. This prevents lateral heat flow from the main heater and ensures that heat from the electric heater flows in the direction of the specimen. On the opposite side of the specimen are additional flat plate heaters (cold plate) that are controlled at a fixed temperature selected by the operator. For a given heat input to the main heater, the hot plate assembly rises in temperature until the system reaches equilibrium.

The final hot plate temperature depends on the electrical power input, the thermal resistance of the specimen and the temperature of the cold plate. The average thermal conductivity, k, of the specimen is determined from the Fourier heat flow equation as follow:

$$k = \frac{W}{A}\left[1 \times \frac{d}{\Delta T}\right] \quad \ldots (3.4)$$

where W is the electrical power input to the main heater, A is the main heater surface area, ΔT is the temperature difference across the specimen, and d is the specimen thickness.

Table 3.5 presents the HGP test results.

Table 3.5 Thermal conductivity of LFC at different temperatures obtained through Hot Guarded Plate tests

Dry density (kg/m^3)	Thermal conductivity at different temperatures (W/mK)							
	20°C	90°C	105°C	150°C	170°C	180°C	200°C	250°C
650	0.23	0.23	0.21	0.16	0.13	0.13	0.14	0.15
1000	0.31	0.31	0.29	0.25	0.24	0.24	0.24	0.25
1850	0.48	0.48	0.47	0.45	0.43	0.43	0.43	0.44

3.4.2 Porosity and thermal conductivity of air

The porosity value of LFC was determined through the Vacuum Saturation Apparatus (Cabrera and Lynsdale, 1988). The measurements of LFC porosity were conducted on slices of 68mm diameter cores cut out from the centre of 100mm cubes. Two densities,

650kg/m^3 and 1000 kg/m^3, were considered. The specimens were dried at 105°C until constant weight had been attained and were then placed in a desiccator under vacuum for at least 3 hours, after which the desiccator was filled with de-aired, distilled water. The porosity was calculated using the following equation:

$$\varepsilon = \frac{(W_{sat} - W_{dry})}{(W_{sat} - W_{wat})} \times 100 \quad \ldots (3.5)$$

where ε is the porosity (%), W_{sat} is the weight in air of saturated sample, W_{wat} is the weight in water of saturated sample and W_{dry} is the weight of oven-dried sample. The measured results are given in Table 3.6.

Table 3.6 Porosity of LFC obtained through Vacuum Saturation for thermal properties test

Sample	Dry density (kg/m^3) W_{dry}	Saturated in air (kg/m^3) W_{sat}	Saturated in water (kg/m^3) W_{wat}	Porosity (%)
650/1	650	899	565	74.6
650/2	649	912	562	75.1
650/3	653	908	571	75.7
1000/1	1004	1294	719	50.4
1000/2	1007	1287	737	50.9
1000/3	1002	1278	725	49.9

For analysis purpose, the porosity values are taken as 75% and 50% for LFC of densities of 650 and 1000 kg/m^3 respectively.

To obtain the thermal conductivity of gas in the air pores, it is necessary to include the effects of radiation within the pores at high temperatures. Assuming the air pores may be represented by uniform distribution of spherical pores of diameter d_e, the effective thermal conductivity of the gas (λ_g) at elevated temperatures may be analytically derived to give the following equation (Yuan, 2009):

$$\lambda_g = 4.815 \times 10^{-4} T^{0.717} + \frac{2}{3} \times 4 d_e \sigma T^3 \quad \ldots (3.6)$$

where the first term is the gas thermal conductivity without the effect of thermal radiation and the second term represents the effect of radiation within the air pores. Although there is also convection with the air pores, due to the small size of the pores (never larger than 5mm), natural convection in the pores can be neglected (Burns and Tien, 1979).

3.4.3 Pore size measurements

In order to calculate the effective thermal conductivity of gas inside the air pores, it is necessary to establish the pore size. For the purpose of this study, the specimen preparation for the measurement of the pore size was slightly different then from recommended by ASTM C 457. ASTM C 457 specified the size and thickness of the specimen and length of travel in the linear traverse method (LTM), based on the size of aggregate. Mixtures from this study, however, do not contain any coarse aggregate but consist of high amounts of air (foam). To ensure the stability of the air pore walls during polishing, particularly in weaker specimens (lower density), all the specimens were vacuum-impregnated with slow-setting epoxy. To ensure consistency in results, all the specimens were prepared using similar techniques under the same environmental conditions, as follows.

Foremost, the specimens of 45 x 45 mm size with a minimum thickness of 15 mm were cut from the centre of two randomly selected 100 mm cubes using a diamond cutter. The face of the specimen was cut perpendicular to the casting direction. Sized specimens were saturated in acetone to stop further hydration reaction before drying at 105 °C. To ensure the stability of the air-pore walls during polishing, the dried and cooled specimens were vacuum impregnated with slow-setting epoxy. The impregnated specimens were polished as per ASTM C 457. After polishing and cleaning, the specimens were dried at room temperature for 1 day. Finally, an effective size 40 x 40 mm was considered for pore size measurement.

The pore size were measured according to ASTM C 457 under a microscope with a magnification of 60x on two specimens, prepared as per the procedure described previously, for each LFC specimen. Image analysis system consisted of an optical microscope and a computer with image analysis software. Figure 3.18 shows microscopic images of the internal pore structure of the 1000 and 650 kg/m^3 density

LFC. Clearly the pore sizes are not uniform. However, these two figures do clearly indicate that there is a dominant pore size and that the dominant pore size is primarily a function of the LFC density. The dominant pore size tends to increase as the LFC density reduces due to the higher quantity of foam used. From a microscopic analysis of the internal images of the two densities of LFC, the dominant pore size of the 650 and 1000 kg/m^3 density LFC has been determined as 0.72mm and 0.55mm respectively. Detailed investigation of the effects of pore size and distribution indicates that provided the total porosity is the same and there is a dominant pore size, the thermal conductivity of porous material may be calculated using the dominant pore size.

(a) 650 kg/m^3 density

(b) 1000 kg/m^3 density

Figure 3.18 Pore sizes of LFC for both densities

3.5 ADDITIONAL SPECIMENS FOR INDICATIVE STUDY ON FIRE RESISTANCE PERFORMANCE OF LFC PANEL

As mentioned in Chapter 1, one of the objectives of this research is to investigate feasibility of using LFC in lightweight residential construction, based on insulation performance for fire resistance. To execute this study, additional LFC specimens of 800, 1200 and 1400 kg/m^3 density were cast to determine the base input values such as density changes, moisture content, specific heat, porosity and pore size which are essential parameters to validate the one dimensional heat transfer analysis program. The thermal conductivity of LFC for all densities was obtained through Hot Guarded Plate test and the values are given in Table 3.7. The specific heat was in the same way as that for the 650 kg/m^3 and 1000 kg/m^3 density, described in Section 3.3.2, but with appropriate free moisture content. The porosities were also established through Vacuum Saturation and pore sizes were determined for each density through image analysis of the internal structure as discussed in Section 3.4.2.

Table 3.8 demonstrates the density change values for the four phases (three phases of dehydration and final phase of CO_2 release) of weight loss, Table 3.9 summarises the free water content, base specific heat and additional specific heat values for all LFC densities and finally Table 3.10 demonstrates the porosity for all LFC densities and variation of effective pore sizes.

Table 3.7 Thermal conductivity of LFC for different density

Density (kg/m^3)	Hot guarded plate test thermal conductivity (W/mK)		Calculated ambient temperature thermal Conductivity (W/mK)	
	Base value	Dry	Base value	Dry
800	0.272	0.193	0.269	0.182
1200	0.379	0.307	0.361	0.272
1400	0.429	0.362	0.402	0.323

Table 3.8 Density change values due to the dehydration process

Initial density (kg/m^3)	Remain density after first dehydration (kg/m^3)	Remain density after second dehydration (kg/m^3)	Remain density after third dehydration (kg/m^3)	Remain density after final dehydration (kg/m^3)
800	783	730	712	702
1200	1165	1069	1043	1010
1400	1351	1238	1208	1170

Table 3.9 Calculated free water content, chemically bound water, specific heat and additional specific heat values

Dry density (kg/m^3)	Free water (% by weight)	Specific heat (J/kg°C)	Additional specific heat at first dehydration process (J/kg°C)
800	2.4	1193	3091
1200	4.5	1313	4873
1400	5.3	1346	5538

Table 3.10 Porosity and effective pore size values

Dry density (kg/m^3)	Porosity (%)	Effective pore size (mm)
800	61	0.62
1200	37	0.49
1400	26	0.37

3.6 SUMMARY

This chapter has presented the experimental results necessary for determining thermal properties of LFC. In particular, in Chapter 4, an analytical model for thermal conductivity, based on treating LFC as porous material, will be acknowledged. In regards to use of this model, it is necessary to have information of porosity and pore

size. This chapter has laid out the experimental data. The thermal conductivity – temperature relationship of LFC will be obtained by calibrating the analytical model against 1-Dimensional transient heat conduction tests. The results of these heat conduction tests have also been discussed. For validation of the analytical model, Guarded Hot Plate tests were conducted to directly give thermal conductivity of LFC up to temperature 250°C.

CHAPTER 4

VALIDATION OF MODELS OF THERMAL PROPERTIES OF LFC

4.1 INTRODUCTION

One important objective of this research is to establish an analytical approach to obtain thermal properties, particularly thermal conductivity, of LFC. Chapter 3 has described the experiments and this chapter will explain how the analytical approach is developed and validated.

4.2 NUMERICAL ANALYSIS

Rahmanian (2008) has developed and implemented a computer program to model the transient heat transfer through LFC in the familiar environment of Microsoft Excel using VBA based on one-dimensional Finite Difference formulations. The modelling procedure has been systematically validated by comparisons with a number of analytical solutions and simulation results using ABAQUS/Standard. The next section will describe the basis of the modelling method which includes the development of one-dimensional Finite Difference formulation which can be used to solve transient heat conduction problems for porous material.

4.2.1 One-Dimensional Finite Difference Formulation

Assuming a homogenous and isotropic material, the general three-dimensional transient heat-conduction equation (based on Fourier's law of conduction) in Cartesian coordinates is (Holman, 2002):

$$\rho c \frac{\partial T}{\partial t} = \frac{\partial}{\partial x}\left(k \frac{\partial T}{\partial x}\right) + \frac{\partial}{\partial y}\left(k \frac{\partial T}{\partial y}\right) + \frac{\partial}{\partial z}\left(k \frac{\partial T}{\partial z}\right) \quad \ldots\ldots\ldots (4.1)$$

where

$T(x,y,z,t)$ is temperature (˚C);

$k(T)$ is temperature dependent thermal conductivity (W/mK);

ρ is material density (kg/m^3);

c is specific heat of material (J/kg°C);

t is time (sec);

x, y, z are Cartesian coordinates.

The right hand side of Equation 4.1 stand for the net heat conduction in a solid material, whereas the left hand side represents the accumulated internal energy.

If the thickness of the LFC panel is small in comparison to the other dimensions, the problem will reduce to a one dimensional heat transfer analysis, i.e. the heat flow is perpendicular to the face except near the edges. Hence, the governing Equation 4.1 with no heat generation reduces to:

$$\rho c \frac{\partial T(x,t)}{\partial t} = \frac{\partial}{\partial x}\left(k(T) \frac{\partial T(x,t)}{\partial x} \right) \quad \text{..... (4.2)}$$

where $0 \le x \le L$, for $t > 0$, L is the thickness of the panel

Assuming a homogeneous material and choosing the explicit method, the temperature of a volume cell (Figures 4.1 and 4.2) at a time step is computed directly based on the temperatures of the adjacent cells in the last time step which leads to a very straightforward scheme of computation (Wang HB, 1995):

(i) For a typical node m within the material (Figure 4.1):

$$T'_m = F_0 [\frac{2(k_{m-1,m} T_{m-1} + k_{m+1,m} T_{m+1})}{k_{m-1,m} + k_{m+1,m}} + T_m (\frac{1}{F_0} - 2)] \quad \text{....(4.3)}$$

where F_0 is defined as:

$$F_0 = \frac{(k_{m-1,m} + k_{m+1,m})\Delta t}{2\rho c(\Delta x)^2} \quad \text{………… ………….. (4.4)}$$

T'_m is the temperature of m in the subsequent time step and $k_{i,j}$ is the thermal conductivity at the average temperature of cells i and j:

$$k_{i,j} = k(\frac{T_i + T_j}{2}) \quad \text{……………………………….... (4.5)}$$

Numerical stability under the explicit scheme requires:

$$\Delta t \leq \frac{\rho c(\Delta x)^2}{(k_{m-1,m} + k_{m+1,m})} \quad \text{…………………………….. (4.6)}$$

(ii) For a boundary node, when subjected to convective and radiative boundary conditions (Figure 4.2):

$$T_1^{'} = 2F_0[T_2 + \frac{h\Delta x}{k_1}T_\infty + (\frac{1}{2F_0} - 1 - \frac{h\Delta x}{k_1})T_1) + \phi e\sigma[(T_\infty + 273)^4 - (T_1 + 273)^4]\frac{2\Delta t}{\rho c\Delta x} \text{ .(4.7)}$$

where F_0 is $F_0 = \frac{k_1 \Delta t}{\rho c(\Delta x)^2}$

$h(T)$ is convection heat transfer coefficient (W/m^{2}K);

T_∞ is the ambient temperature (°C);

ϕ is a geometric "view factor"

e is the effective emissivity

σ is Stefan-Boltzmann constant (5.67 x 10^{-8} W/m^2.K^4).

Numerical stability limits the time step to:

$$\Delta t \leq \frac{0.5\rho c(\Delta x)^2}{k_1}[1 + \frac{h\Delta x}{k_1} + \frac{\phi E\sigma\Delta x}{k_1} \cdot \frac{(T_1 + 273)^4}{T_1}]^{-1} \text{ … (4.8)}$$

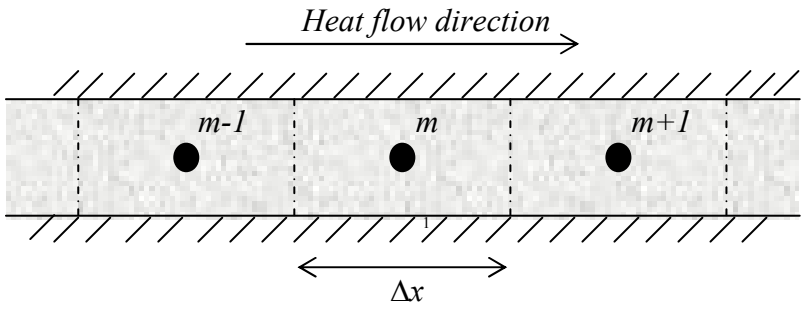

Figure 4.1 Finite Difference discretization for node *m* within the material

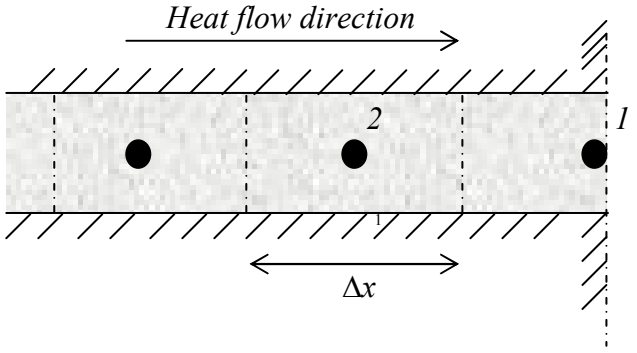

Figure 4.2 Finite Difference discretization for boundary node

4.2.2 Initial and Boundary Conditions

LFC panel is assumed to have a uniform initial temperature equal to the ambient temperature. On the unexposed boundary, the convective heat transfer coefficient (h) is assumed to be constant and the value is taken as 10 W/m^{2}K. The emissivity of the surface depends on the material. For concrete, the surface emissivity will be taken as 0.92 (Ozisik, 1985). The exposed boundary conditions are the recorded temperatures on the exposed surface of fire test specimens.

4.2.3 Validation of the heat conduction model

Sections 4.2.1 and 4.2.2 have comprehensively extracted the Finite Difference formulations to model the one-dimensional transient heat transfer through LFC and its initial and boundary conditions. It is important to verify the accuracy of this model through comparison with the available analytical and numerical solutions. To accomplish this validation, 3 different approaches have been taken as follows:

1. Verification of the conductive heat transfer simulation through a panel (referred to as case 1)
2. Verification of the convective heat transfer at boundaries of a panel (referred as to case 2)
3. Verification of the conductive heat transfer simulation with temperature-to dependent material properties (referred as case 3).

For case 1 and 2, analytical solutions are presented with constant material properties of LFC. Nevertheless no analytical solution is established when thermal properties of material change with temperature (case 3). Therefore, numerical simulation results using the generic commercial finite element package, ABAQUS, are employed to corroborate the Finite Difference formulations.

4.2.3.1 Conduction Heat Transfer with Constant Material Properties

Consider a one-dimensional heat transfer through LFC panel with thickness l and constant thermal conductivity k. The initial temperature of the panel is uniform and indicated by T_0 (Figure 4.3). If both surfaces of the LFC panel are suddenly changed to zero temperature (0°C), temperature development through the thickness of the panel at time t can be calculated as follow (Carslaw and Jaeger, 1959):

$$T = \frac{4T_0}{\pi} \sum_{n=0}^{\infty} \frac{1}{(2n+1)} e^{-\alpha(2n+1)^2 \pi^2 t / l^2} \sin\frac{(2n+1)\pi x}{l} \quad \ldots. (4.9)$$

where $\alpha = \frac{k}{\rho c}$, ρ is the density of the material and c is the specific heat.

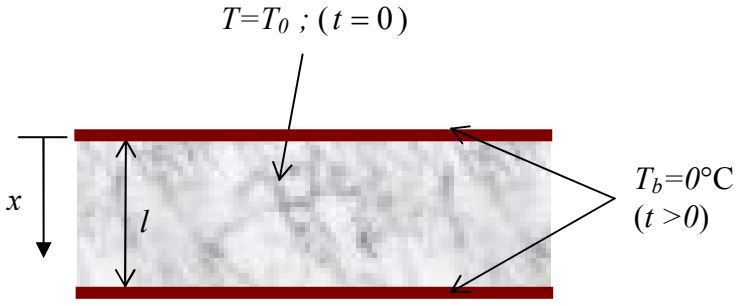

Figure 4.3 LFC panel with thickness *l*, both boundaries kept at zero temperature

Analysis has been carried out for an example of case 1 (Figure 4.3) with the material properties indicated in Table 4.1.

Table 4.1 Material properties of LFC to analyse example of case 1

LFC properties	Values
Density (ρ)	650 kg/m^3
Thickness of panel (l)	30 mm
Thermal conductivity (k)	0.206 W/mK
Specific heat (c)	1110 J/kg.°C
Initial temperature (T_0)	20°C

The temperature development of this example is achieved through both the analytical method (Equation 4.9) and the Finite Difference method. The results are compared in Figures 4.4 and 4.5. The thickness of the panel is divided into 6 elements and temperatures are calculated for the nodes indicating each element (5 internal nodes and 2 boundary nodes) and the time step of 5 seconds is used for this Finite Difference method. The infinite series in Equation 4.9 has been restricted to only 12 members for calculation purposes. It can be seen in Figures 4.4 and 4.5 that Finite Difference method can offer very accurate results for heat transfer analysis in solids with constant thermal properties regardless of its simple approach.

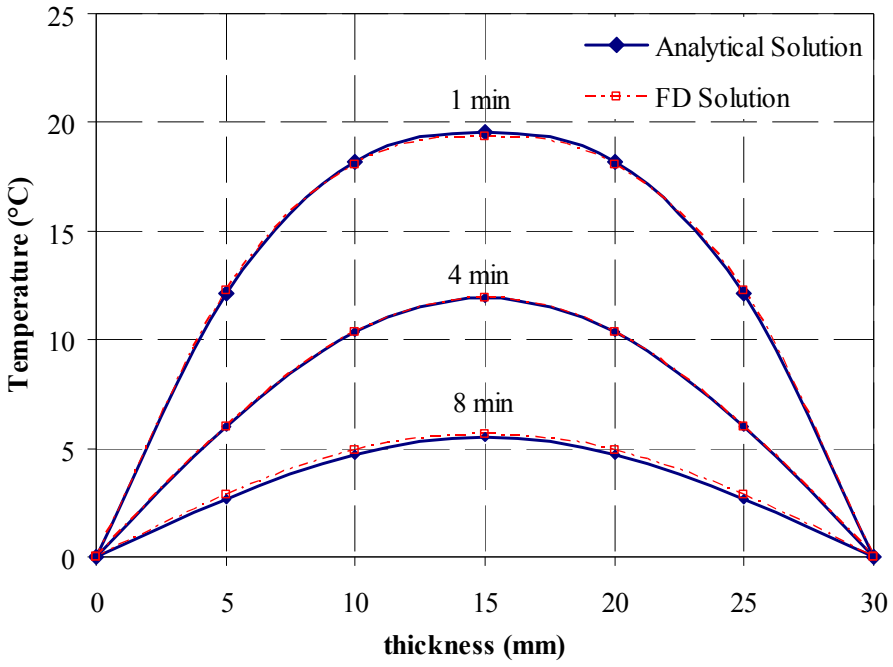

Figure 4.4 Temperature distribution across the thickness of a 30mm example panel attained by analytical method and Finite Difference method

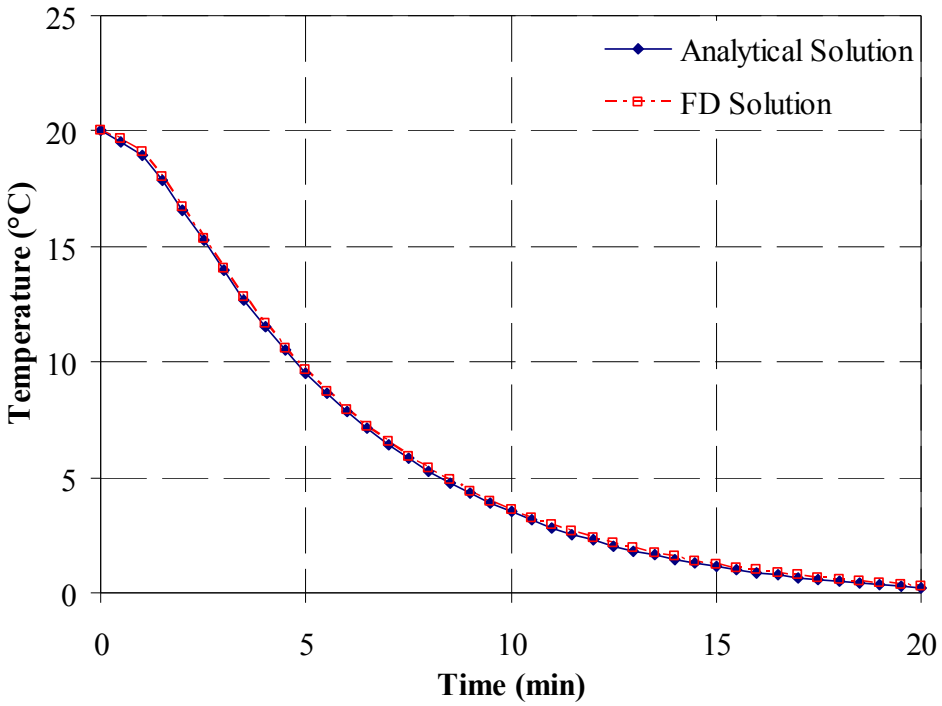

Figure 4.5 Temperature development at the midpoint of a 30mm example panel obtained by analytical method and Finite Difference method

4.2.3.2 Convection Heat Transfer with Constant Material Properties

Verification is also carried out for a problem where convective boundary conditions exist. Consider the one-dimensional heat transfer through a panel with thickness of *2L* and constant thermal conductivity of *k* shown in Figure 4.6. The initial temperature of the panel is T_0. The panel is suddenly taken to an ambient temperature of T_∞ and the convective heat transfer coefficient at the surfaces of the panel is *h*. If $\theta = T - T_\infty$, temperature development across the thickness of the panel at time *t* can be calculated using the following equation (Harmathy, 1988):

$$\frac{\theta}{\theta_0} = 2\sum_{n=1}^{\infty} \frac{\sin\lambda_n}{\lambda_n + (\sin\lambda_n)(\cos\lambda_n)} . \exp(-\lambda_n^2 \alpha t / L^2) . \cos(\lambda_n x / L) \quad \ldots . (4.10)$$

where $\alpha = \dfrac{k}{\rho c}$ and λ_n are roots of the equation: $\lambda_n \tan(\lambda_n) = \dfrac{hL}{k}$

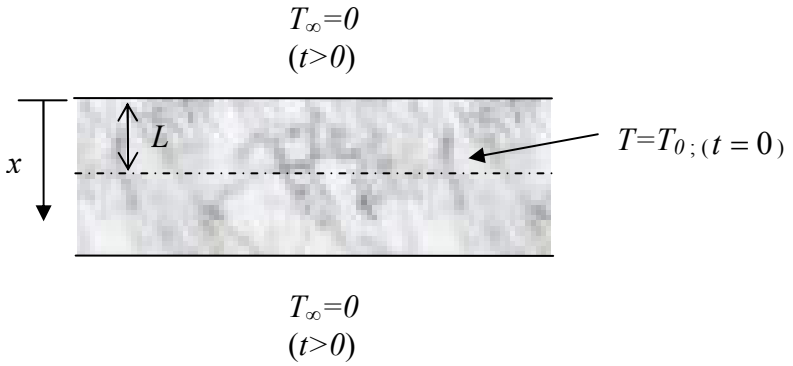

Figure 4.6. A panel with thickness *2L*, suddenly entered into an ambient zero temperature.

Analysis has been carried out for an example of case 2 (Figure 4.6) with the material properties indicated in Table 4.2.

Table 4.2 Material properties of LFC to analyse example of case 2

LFC properties	Values
Density (ρ)	650 kg/m^3
Thickness of panel (L)	15 mm
Thermal conductivity (k)	0.206 W/mK
Heat transfer coefficient (h)	10 W/m^{2}K
Specific heat (c)	1110 J/kg.°C
Initial temperature (T_0)	20°C
Ambient temperature (T_∞)	0°C

The first 20 roots of λ_n are used in Equation 4.10. The time step of 5 seconds is employed in the Finite Difference analysis and the thickness of the panel is divided by 7 nodes. The results are compared in Figures 4.7 and 4.8. Obviously results in Figures 4.7 and 4.8 showed that Finite Difference method is in good agreement with the analytical results.

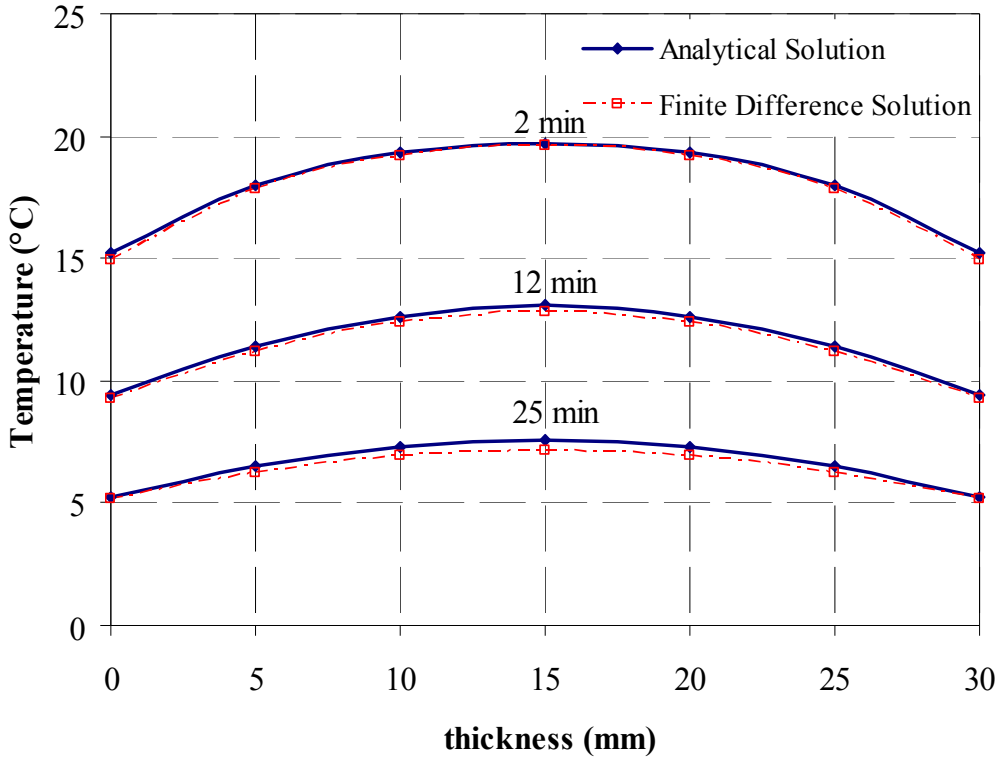

Figure 4.7 Temperature distributions across the thickness of a 30mm example panel with convective boundary condition attained by analytical method and Finite Difference method

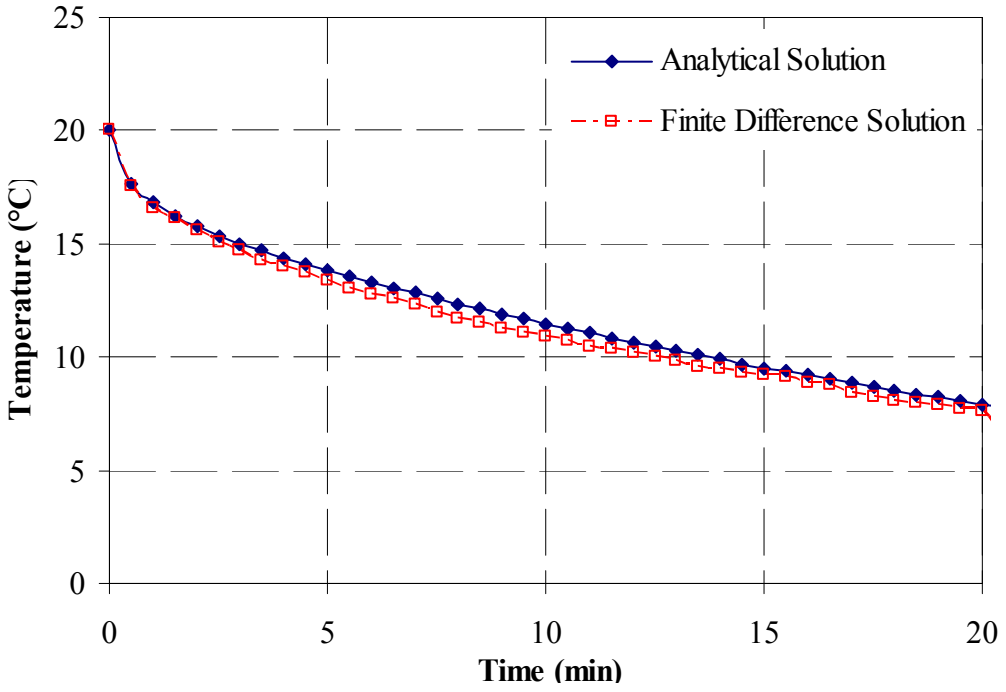

Figure 4.8 Temperature developments at the surface of a 30mm example panel with convective boundary condition attained by analytical method and Finite Difference method

4.2.3.3 Heat Transfer with Temperature-Dependent Thermal Properties

The thermal properties LFC are temperature-dependant. Since analytical solutions for heat transfer through this material is not available, another numerical method, Finite Element analysis, is employed for validation of Finite Difference analysis. For validation purpose, a 30mm LFC panel initially at 25°C is considered. The temperature-dependent thermal properties of the LFC panel are modelled as explained in Section 3.3.2 and Section 4.3, with density of 650 kg/m^3 at ambient temperature. One surface of the panel is exposed to high temperatures and the other side faces the ambient temperature of 25°C. Figure 4.9 illustrates the temperature curve obtained experimentally on the exposed surface of the panel and compares the temperature predictions of the unexposed side by the proposed Finite Difference analysis and by Finite Element analysis using the common software package, ABAQUS. The validity of Finite Difference formulations is confirmed yet again.

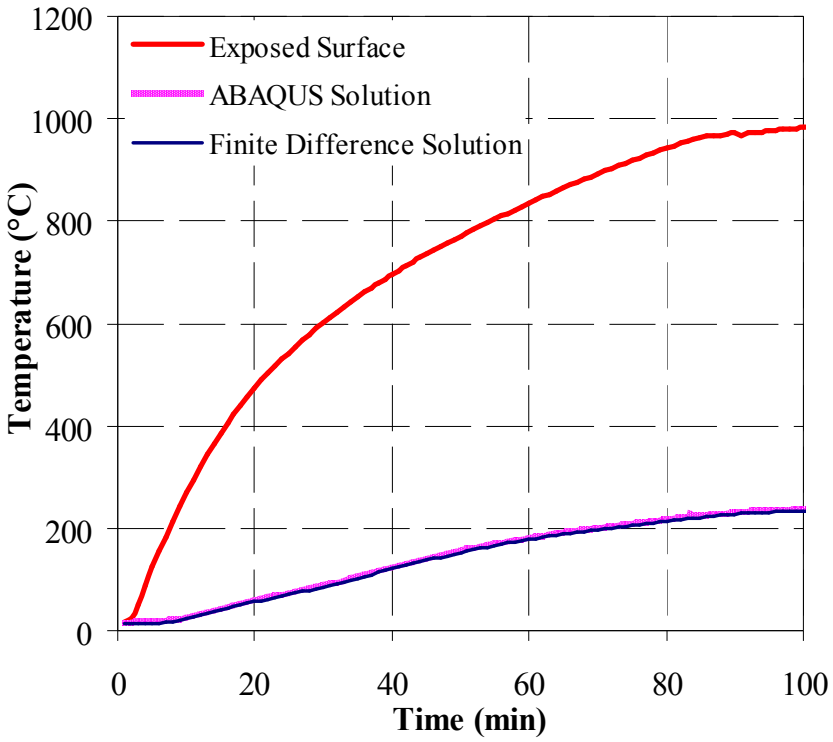

Figure 4.9 Temperature developments on the unexposed surface of a 30mm LFC panel attained by ABAQUS (Finite Element analysis) and Finite Difference method

The validation of Finite Difference formulations confirmed that even though explicit Finite Difference method is a fairly simple algorithm, it can still offer very precise results compared to analytical methods or other complicated numerical ones.

4.3 ANALYTICAL MODEL FOR THERMAL CONDUCTIVITY

4.3.1 Input data

LFC is a high porous material consisting of solid cement matrix and air pores introduced by the foam. The effective thermal conductivity of LFC may be calculated using the following equation (Yuan, 2009):

$$k^* = k_s \frac{k_g \varepsilon^{\frac{2}{3}} + (1-\varepsilon^{\frac{2}{3}})k_s}{k_g(\varepsilon^{\frac{2}{3}} - \varepsilon) + (1-\varepsilon^{\frac{2}{3}} + \varepsilon)k_s} \quad \ldots (4.11)$$

where k^* is the effective thermal conductivity of LFC, k_g is effective thermal conductivity of gas to account for heat transfer in the pores, k_s is the thermal conductivity of the solid and ε is the porosity of the material (the ratio of the volume of pore to the overall volume).

The porosity value of LFC was determined through the Vacuum Saturation Apparatus (Cabrera and Lynsdale, 1988) and the results are given in Table 3.5.

The pore size for the 650 kg/m^3 and 1000 kg/m^3 was determined to be 0.72mm and 0.55mm respectively as shown in Section 3.4.2.

4.3.2 Calculation procedure

From Equation 4.11, it is necessary to have the base value thermal conductivity k_s of the pure solid (cement paste) in order to obtain the effective thermal conductivity k^* of LFC. Because of the difficulty of making pure solid, the value of k_s is obtained through back calculation, using HGP test results of dried LFC. The HGP test results are given in Table 3.4. As explained previously, it is assumed that water evaporation occurs between 90-170^{o}C so the HGP results at 170^{o}C are considered acceptable for dried LFC. Using Equation 4.11 and given that the porosity values of LFC at 650 kg/m^3, 1000 kg/m^3 and 1850 kg/m^3 density are 75%, 50% and 12% respectively, the base value thermal conductivity of pure dried solid k_s may be calculated to be 0.52, 0.49 and 0.50 W/mK for the 650, 1000 and 1850 kg/m^3 density respectively. These values are sufficiently close to accept the accuracy of this procedure and an average value of 0.5 W/mK will be used as input data in later calculations. In the above calculations, the

effect of radiation within pores was not considered because of the relatively low temperature.

The thermal conductivity – temperature relationship of LFC may be divided into three segments: (1) an initially flat part with the thermal conductivity constant as that at ambient temperature, until water evaporation starts at the assumed temperature of 90^{o}C; (2) a linearly decreasing segment until all the water has evaporated and the LFC is dry, which is assumed at 170^{o}C; (3) increasing thermal conductivity with temperature due to radiation in the pores. The third segment is described using Equation 4.11.

For the LFC thermal conductivity at ambient temperature, the directly measured result may be used. However, this value can also be derived from the value of dried LFC, measured at 170°C. In this calculation, the LFC may be considered to be part dry LFC and part water and Equation 4.12, based on volume fraction, may be used to calculate the thermal conductivity of LFC at ambient temperature.

$$k_{amb} = V_w k_w + (1 - V_w) k_{dry} \quad \ldots (4.12)$$

where k_{amb} is the LFC thermal conductivity at ambient temperature; V_w is the volume percentage of water; k_w is the thermal conductivity of water (0.58 W/mK) and k_{dry} is the thermal conductivity of dry LFC (value in Table 3.4 for 170^{o}C).

For LFC density of 650 kg/m^3, k_{dry} = 0.131 W/mK (Table 3.4), V_w = 0.1677 (Table 3.2), giving k_{amb} = 0.206 W/mK. For LFC density of 1000 kg/m^3, k_{dry} = 0.235 W/mK (Table 3.4), V_w = 0.2618 (Table 3.3), giving k_{amb}=0.325 W/mK. These calculated ambient temperature thermal conductivity values are close to the HGP test values of 0.226 and 0.309 W/mK respectively.

Figure 4.10 shows the calculated effective thermal conductivity of LFC for the two densities considered in this study and compare these calculated values with those directly measured using the HGP method (Table 3.4 values). The agreement is excellent, but the analytical model is able to give the thermal conductivity – temperature relationships above 250°C.

To summarise, the following input data are required for determining thermal conductivity – temperature relationship of LFC:

Thermal conductivity of cement paste at ambient temperature (0.5 W/mK); Volume fracture of water at ambient temperature: V_w; Porosity; Pore size.

The calculation procedure is as follows:

1. Calculate thermal conductivity of dried LFC at ambient temperature: use Equation 4.11;

2. Followed by calculating thermal conductivity of LFC at ambient temperature: use Equation 4.12;

3. The thermal conductivity is taken as constant at the value calculated in step 2 from ambient temperature to 90°C;

4. The thermal conductivity reduces linearly from the value calculated in step 2 at 90°C to the value calculated in step 1 at 170°C;

5. Equation 4.11 is used for thermal conductivity at temperatures above 170°C.

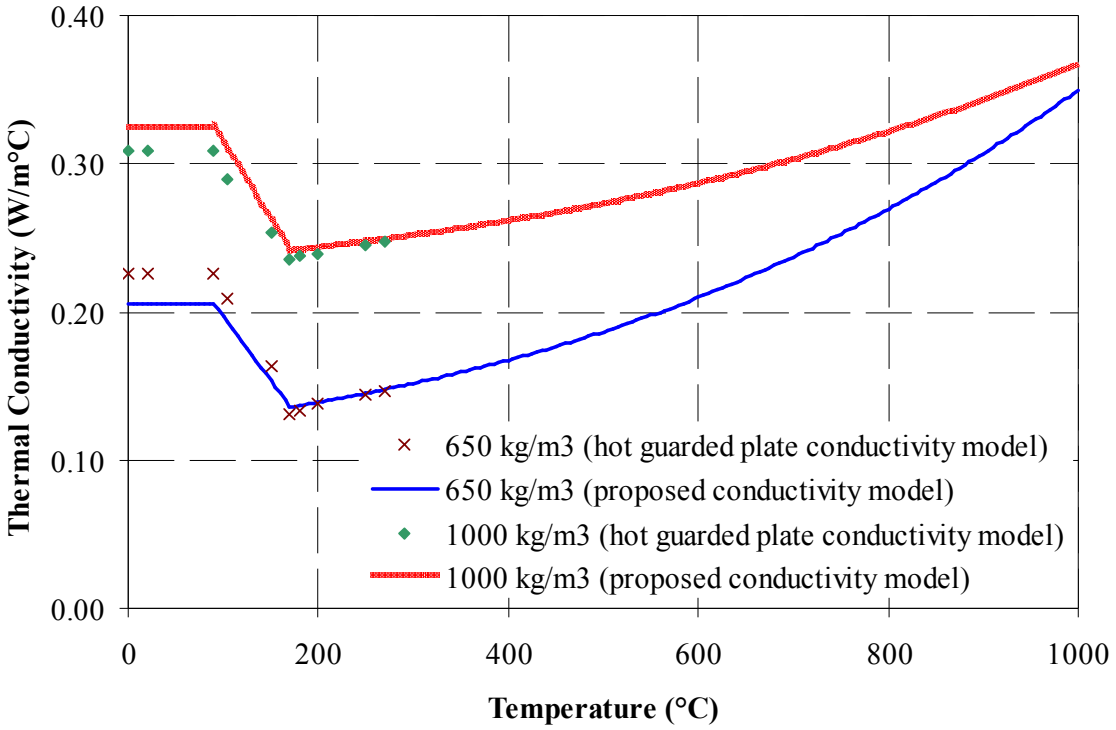

Figure 4.10 Effective thermal conductivity of LFC for 650 kg/m^3 and 1000 kg/m^3 densities

4.4 VALIDATION OF THERMAL PROPERTIES MODELS

In order to validate the proposed thermal property models for LFC presented in Chapter 3, thermal property values from these models were used as input material properties in the one-dimensional heat transfer program to predict temperature developments inside the LFC slab test samples described in Section 3.2.2 of this thesis. As mentioned in Section 3.2.6, it is acceptable to assume that heat transfer in the test samples is one-dimensional in the thickness direction of the LFC panel.

Measured experimental temperatures at all recording locations of the test specimens for both densities of LFC were compared with numerical analysis results, to provide comprehensive validation of the thermal property models proposed in Section 3.3 and 4.3. Thermal property values (theoretical thermal property model results) are considered and their prediction results compared.

As mentioned previously, the exposed surface temperatures are used as input data in the heat transfer analysis to eliminate uncertainty in the thermal boundary condition on the exposed side. Figures 4.11-4.14 compare the measured and numerical analysis results for the 650 kg/m^3 density specimens and Figures 4.15-4.18 are for the 1000 kg/m^3 density specimens.

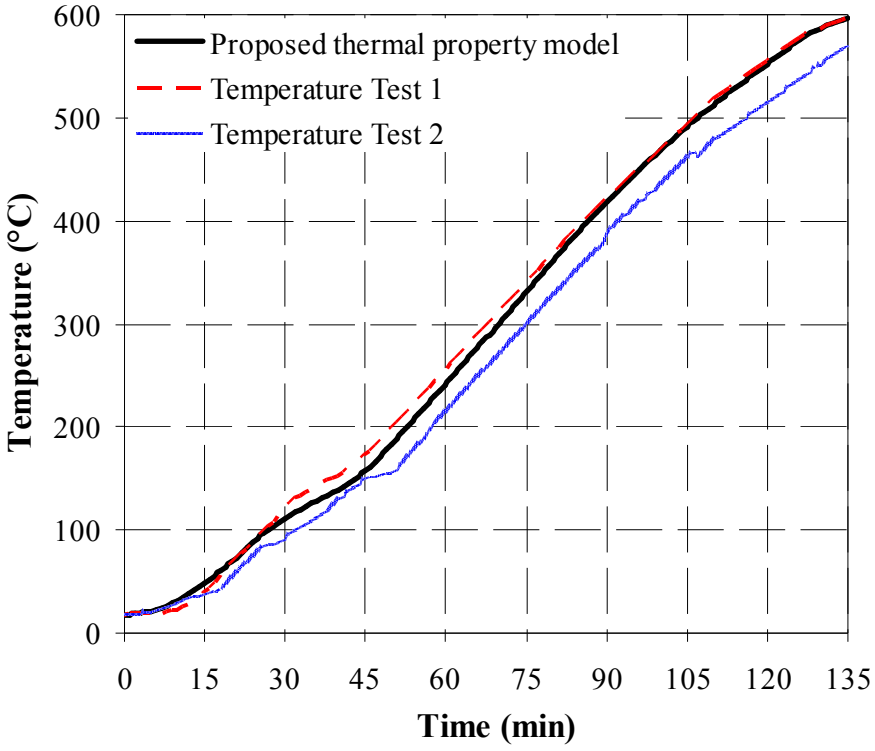

Figure 4.11 Comparison between test results and numerical analysis at 37.5mm from exposed surface for the 650 kg/m^3 density specimens

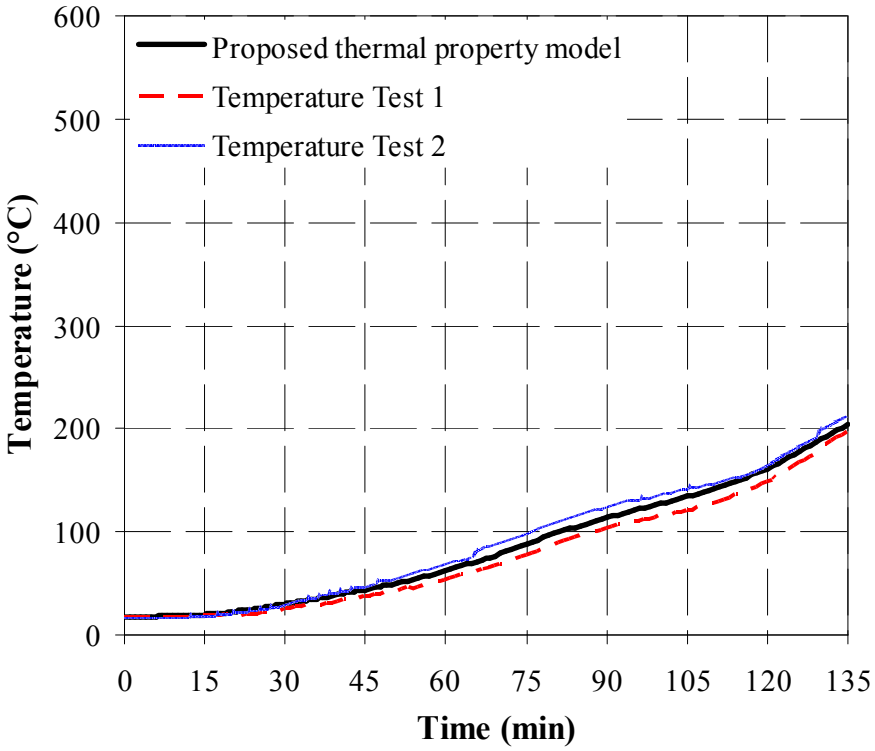

Figure 4.12 Comparison between test results and numerical analysis at 75.0mm from the exposed surface for the 650 kg/m^3 density specimens

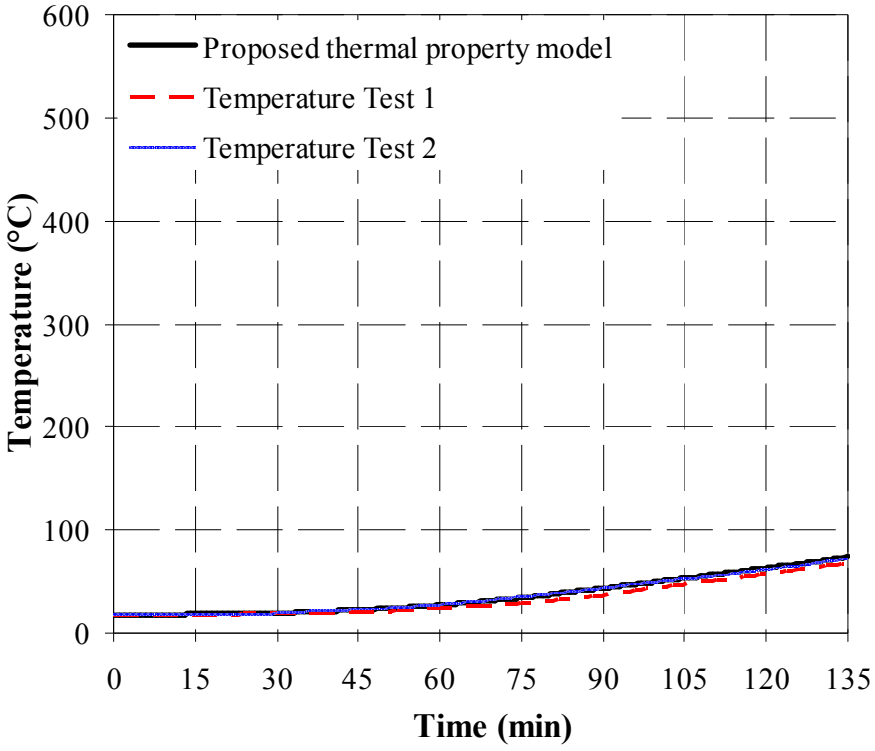

Figure 4.13 Comparison between test results and numerical analysis at 112.5mm from the exposed surface (mid-thickness) for the 650 kg/m^3 density specimens

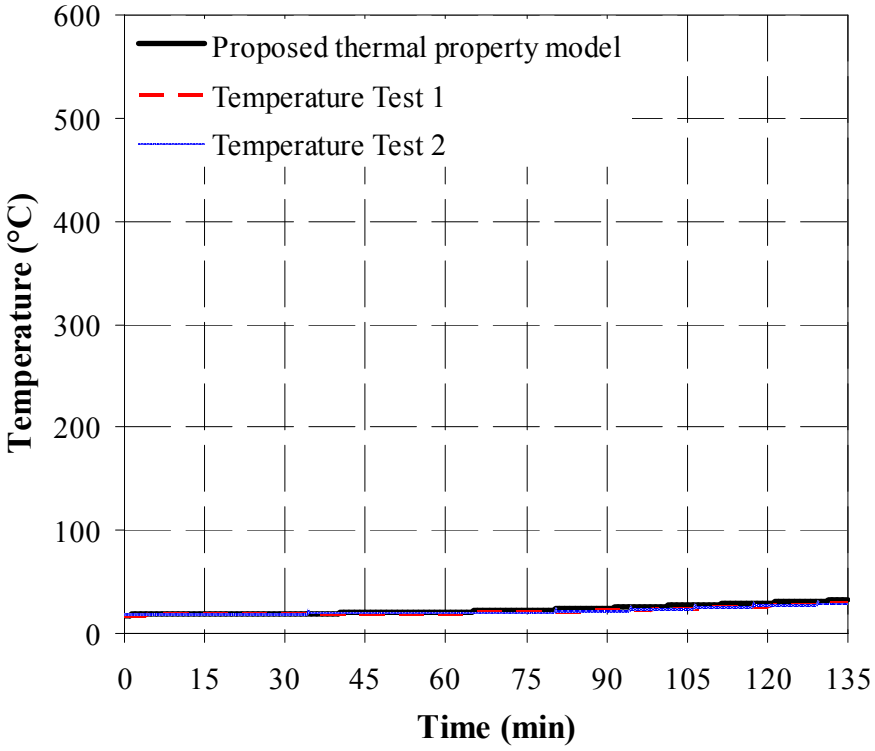

Figure 4.14 Comparison between test results and numerical analysis at the unexposed surface for the 650 kg/m^3 density specimens

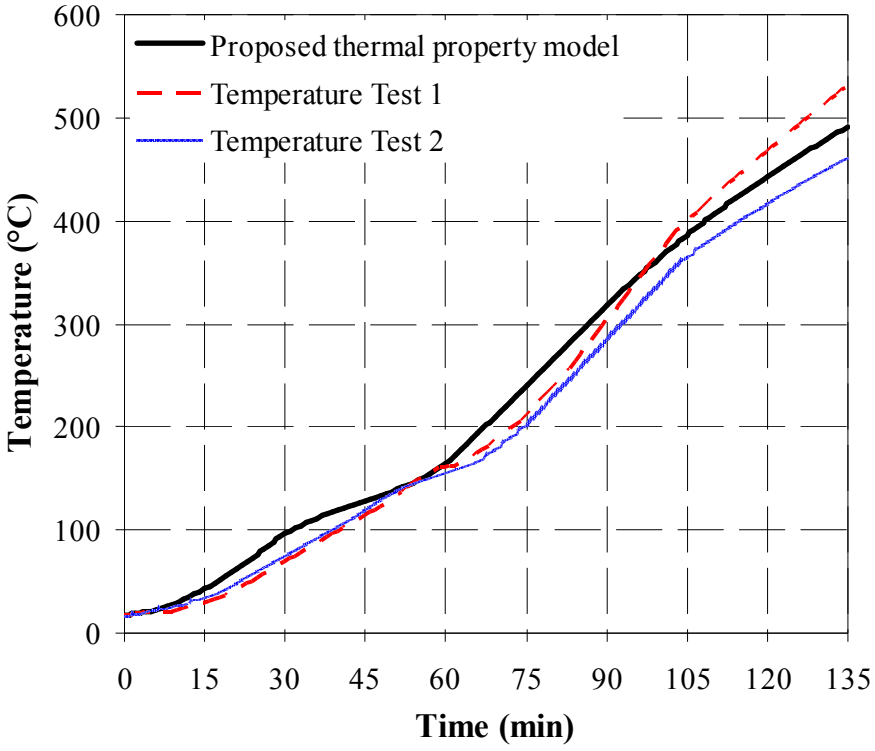

Figure 4.15 Comparison between test results and numerical analysis at 37.5mm from the exposed surface for the 1000 kg/m^3 density specimens

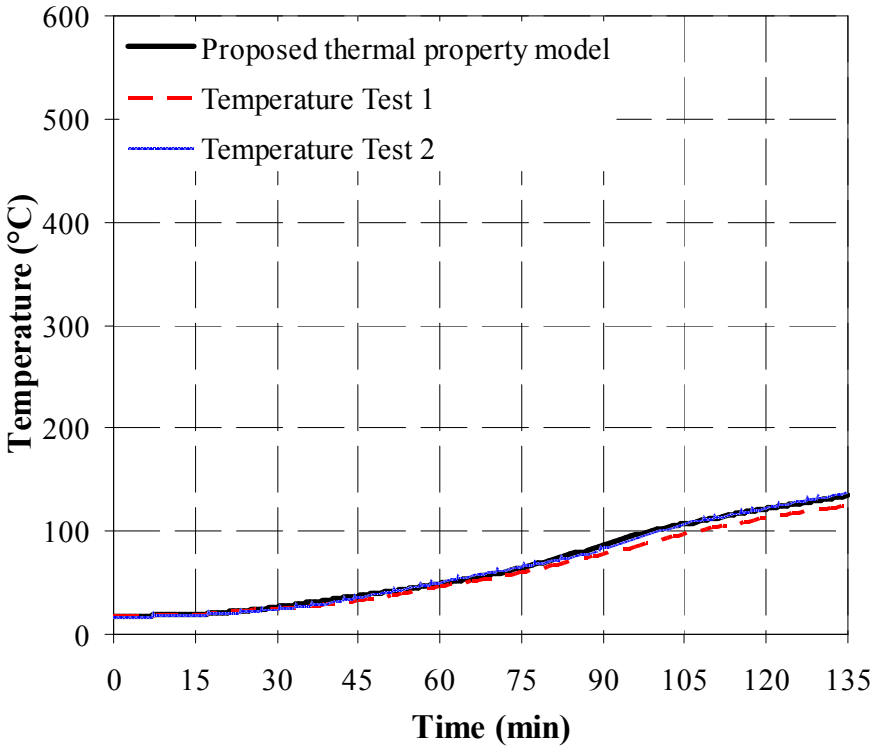

Figure 4.16 Comparison between test results and numerical analysis at 75.0mm from the exposed surface for the 1000 kg/m^3 density specimens

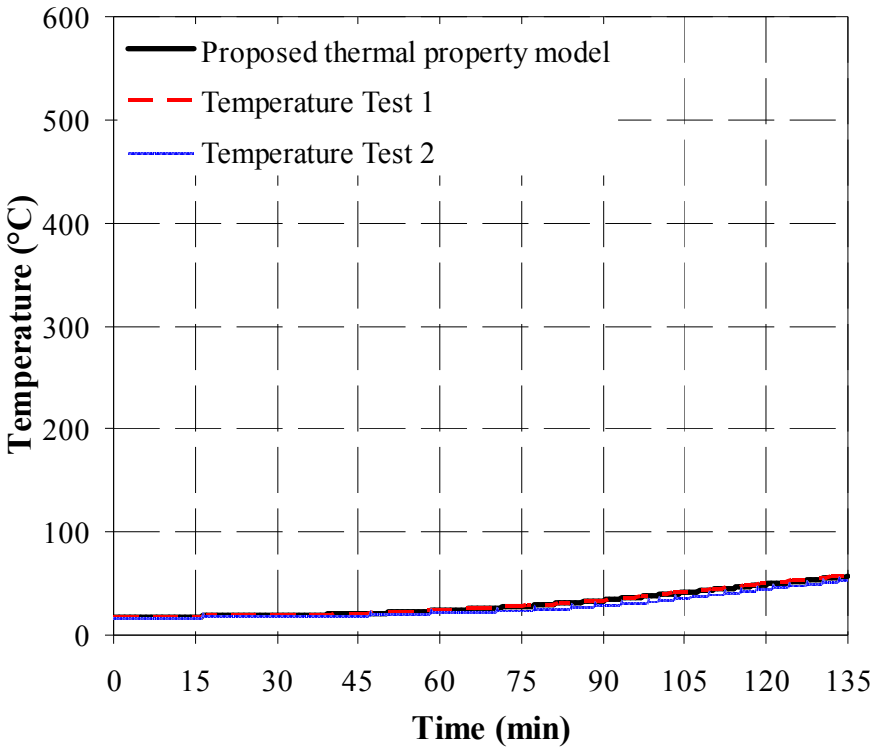

Figure 4.17 Comparison between test results and numerical analysis at 112.5mm from the exposed surface for the 1000 kg/m^3 density specimens

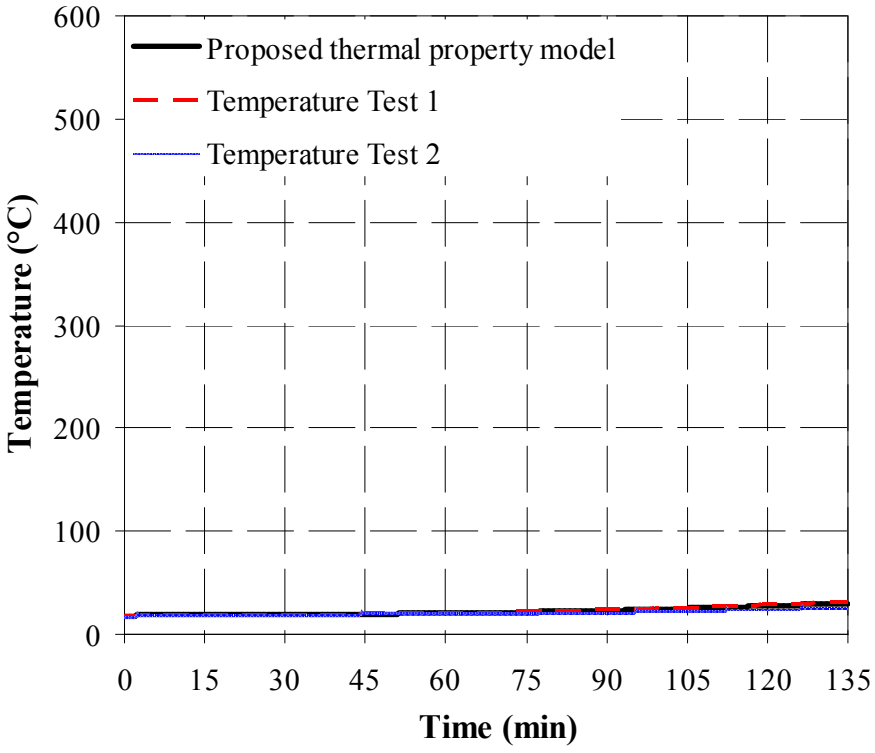

Figure 4.18 Comparison between test results and numerical analysis at the unexposed surface for the 1000 kg/m^3 density specimens

The results shown in Figures 4.11-4.18 clearly indicate close agreement between prediction and measured results of temperature throughout the thickness of the LFC samples. The comparison in Figure 4.10 is able to confirm accuracy of the proposed thermal conductivity model for temperatures not exceeding 250°C. Since temperatures from the LFC slab tests reached much beyond 250°C, these results confirm that the proposed thermal conductivity values at high temperatures are accurate.

4.5 SENSITIVITY STUDY

The previous section has shown that the proposed thermal property models for LFC are appropriate. Nevertheless, a number of assumptions have been introduced in the proposed models. It is important to examine the sensitivity of the temperature calculation results to these assumptions so that wherever necessary, critical factors in the proposed models are identified to enable accurate determination of their values. The results for both LFC densities are similar, so only the results for the 650 kg/m^3 density will be reported in this thesis.

In all simulations, the measured densities of LFC at high temperatures were used. This sensitivity study will concentrate on the specific heat-temperature model and the thermal conductivity-temperature model. The exposed boundary conditions are exposed surface temperature-time curves directly input from test measurements which are presented in the section following this sensitivity study. Parameters not mentioned in the discussion are kept equal to those given in previous sections.

4.5.1 Specific heat-temperature model

For the specific heat, the same thermal conductivity values from the proposed thermal conductivity model will be used and focus will be on the effects of moisture evaporation. Three cases will be considered: (1) Case 1: the proposed specific heat model with one additional specific heat for evaporation of the free water, (2) Case 2: constant specific heat without accounting for the effect of moisture evaporation, (3) Case 3: specific heat model including additional specific heats at three different temperature intervals to consider the three phases of water evaporation. Figure 4.19 compares specific heat for the three cases.

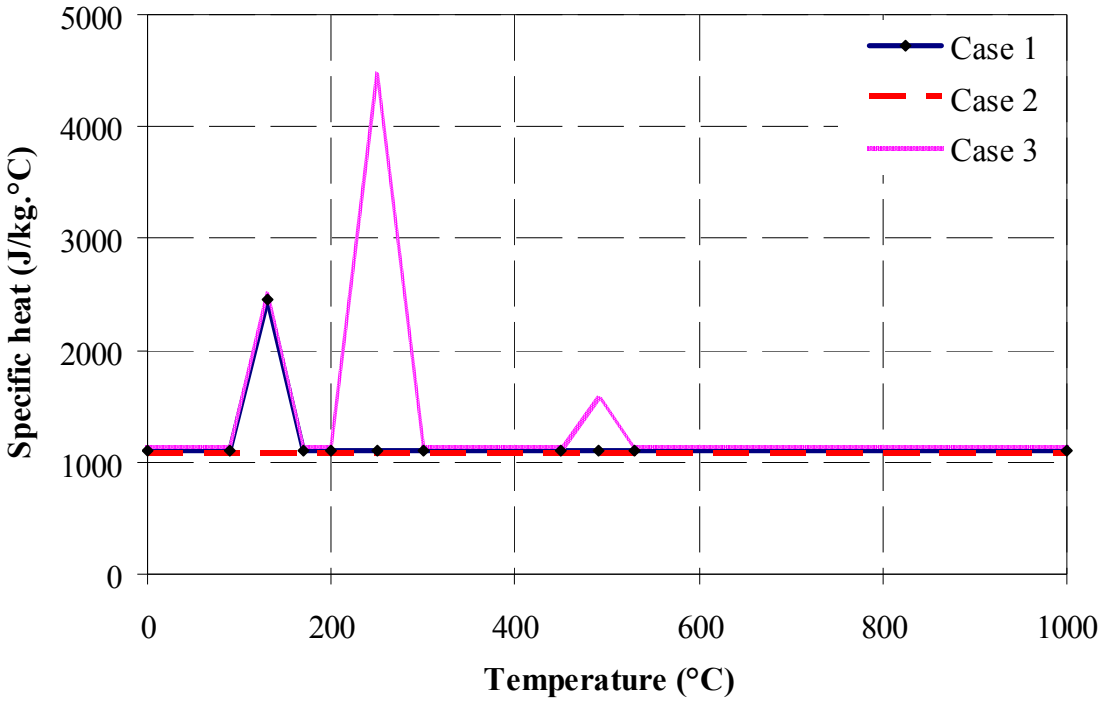

Figure 4.19 Specific heat models for all 3 cases considered for sensitivity study (LFC density of 650 kg/m^3)

Figures 4.20 to 4.23 show the results of comparison between predicted temperatures inside LFC by using different specific heat models. It is clear that using a constant specific heat model is not appropriate because this will miss the temperature plateau phase at around 90°C as seen in Figure 4.20. This difference in results is progressed further into the LFC specimen so Figure 4.21 shows quite large differences. In contrast, having too many spikes of additional specific heat to faithfully follow all the three phases of water evaporation does not appear to produce sensible results (refer Figures 4.22 and 4.23)

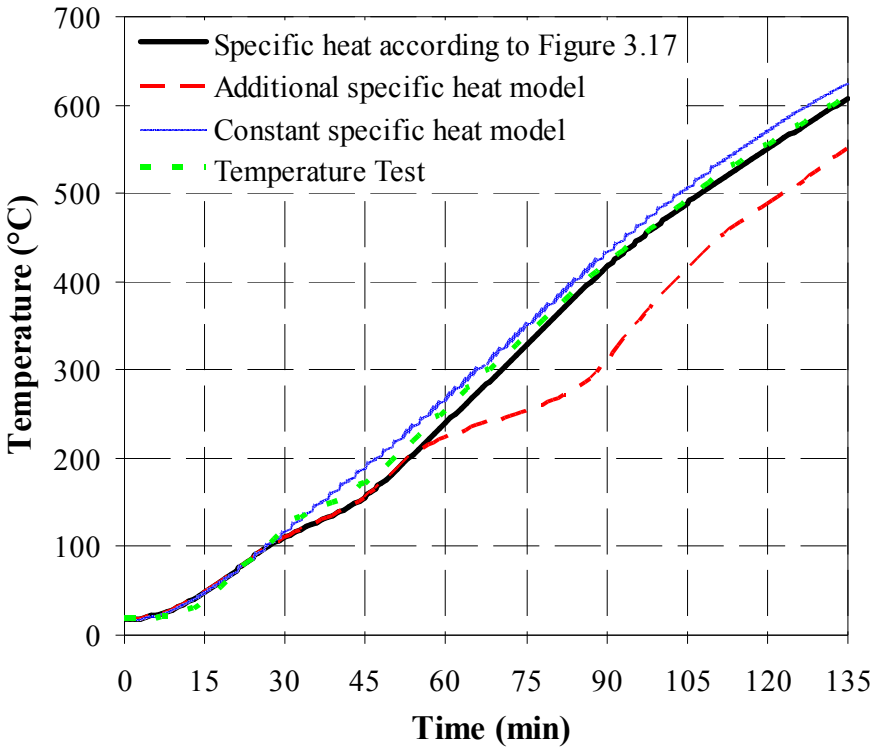

Figure 4.20 Sensitivity of LFC temperature to different specific heat models, 37.5mm from the exposed surface for the 650 kg/m^3 specimens

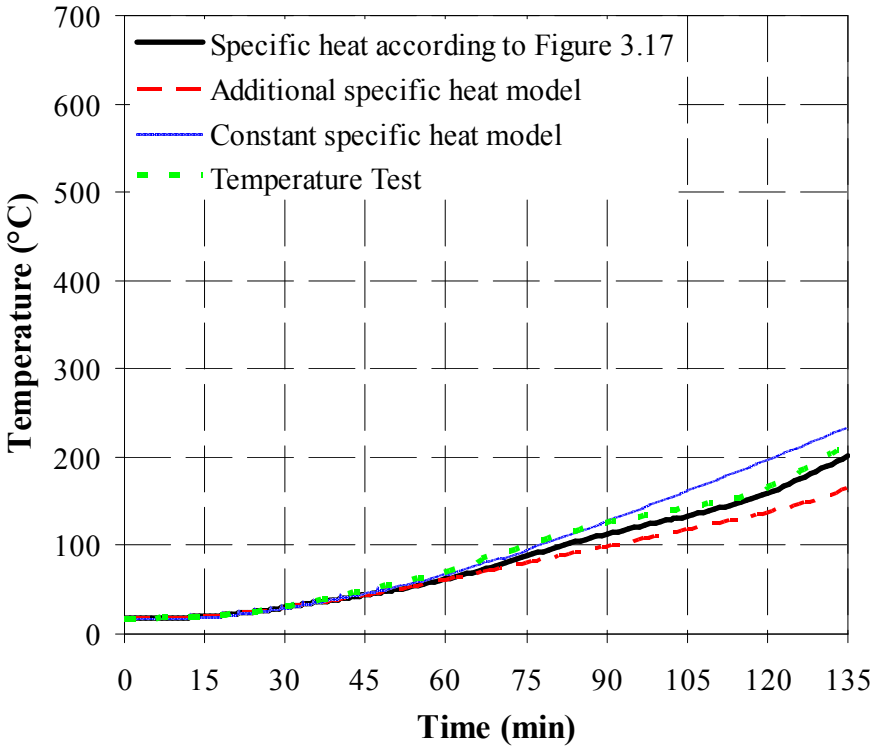

Figure 4.21 Sensitivity of LFC temperature to different specific heat models, 75.0mm from the exposed surface (mid-thickness) for the 650 kg/m^3 specimens

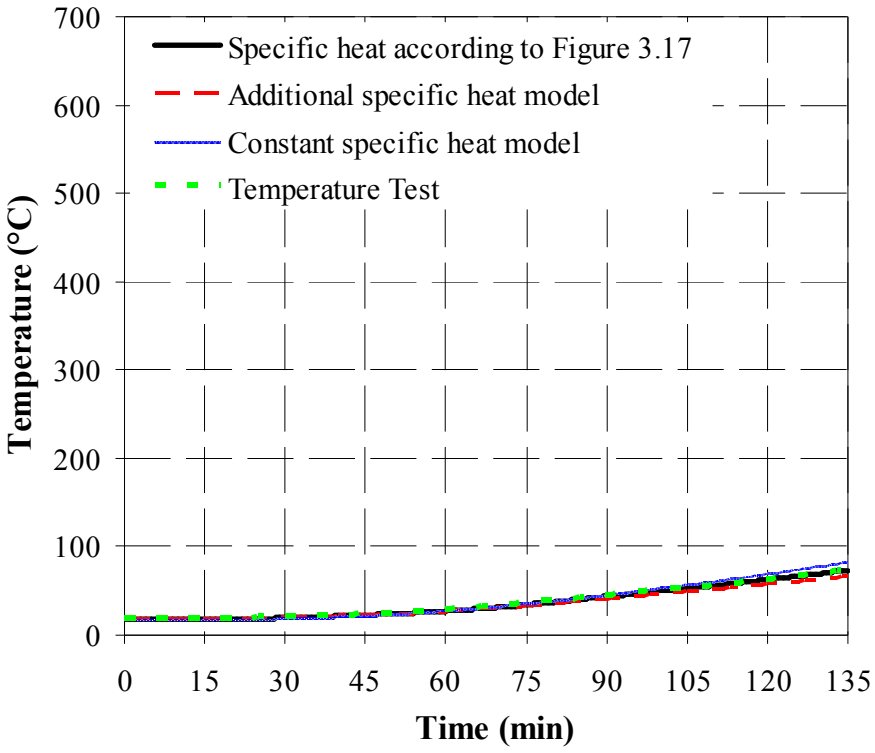

Figure 4.22 Sensitivity of LFC temperature to different specific heat models, 112.5mm from the exposed surface for the 650 kg/m^3 specimens

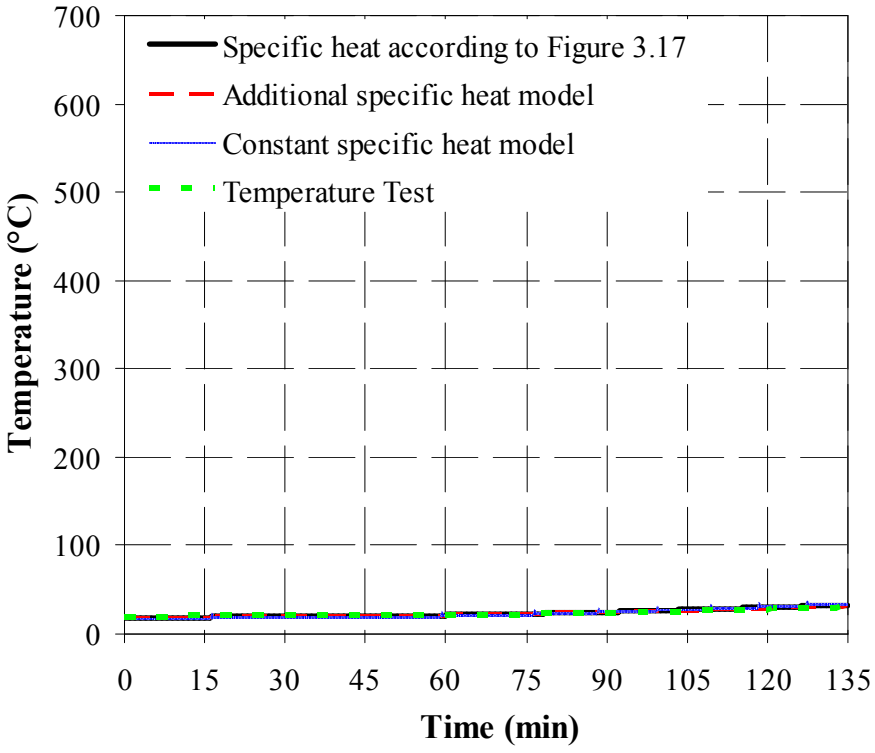

Figure 4.23 Sensitivity of LFC temperature to different specific heat models at the unexposed surface for the 650 kg/m^3 specimens

4.5.2 Thermal conductivity-temperature model

The proposed analytical thermal conductivity model will be used and the sensitivity study will focus on the pore size for the thermal conductivity model. For the 650 kg/m^3 density, an average pore size of 0.72 mm is found appropriate from an analysis of the internal structure of the sample shown in Figure 3.14 (Chapter 3). In the sensitivity study, the pore size was changed to 0.4 mm and 1.0 mm.

Figure 4.24 shows the LFC thermal conductivity-temperature relationships for different values of pore size. Figures 4.25-4.28 compare the predicted LFC temperatures at different distance from the exposed surface using these thermal conductivity curves and between the prediction results and the measured results. It is clear that the LFC temperatures are moderately sensitive to the pore size. However, because thermal conductivity deals with progressive heat transfer throughout the thickness, the difference in results becomes proportionally much greater at positions further away from the exposed surface. It is therefore important to obtain a sufficiently accurate value for the pore size. For LFC, as shown in Figure 3.14, although there are variations in the pore size for each density, these sizes may still considered to be relatively uniform so an average value of pore size may be used. The results of this study, by using the average pore size of 0.72mm, have been found to be acceptable.

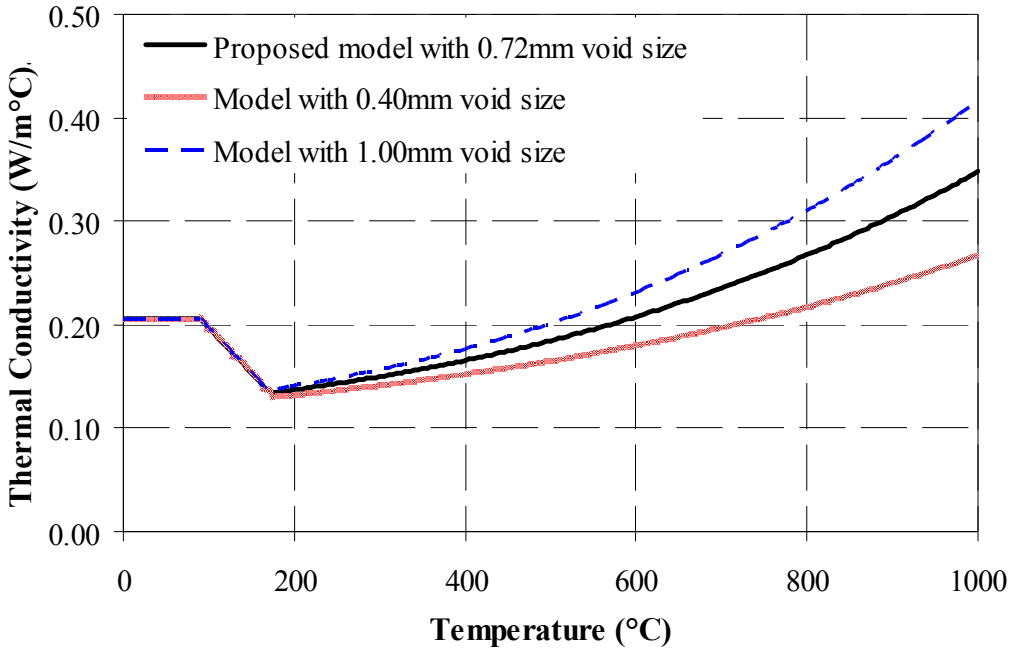

Figure 4.24 Comparison of LFC thermal conductivity using different pore sizes

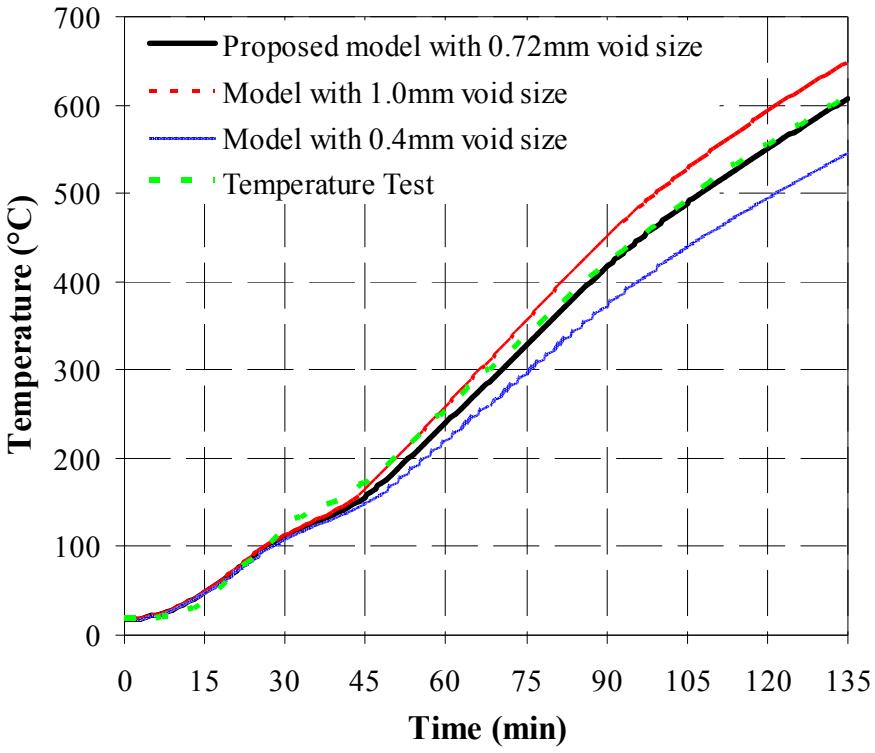

Figure 4.25 Sensitivity of LFC temperature to different pore sizes at 37.5mm from the exposed surface for the 650 kg/m^3 density specimen

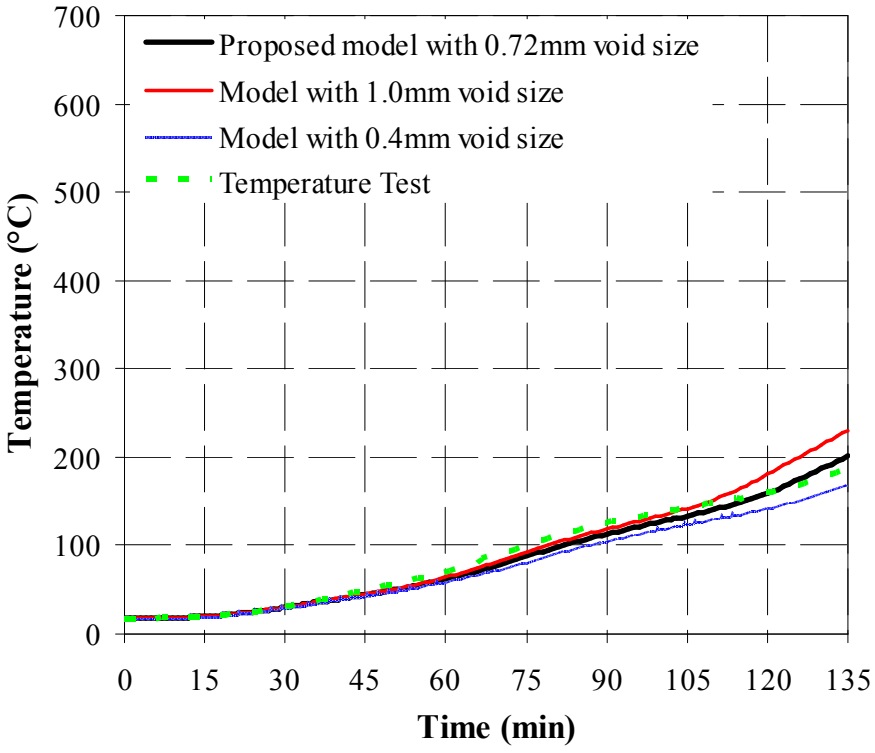

Figure 4.26 Sensitivity of LFC temperature to different pore sizes at 75.0mm from the exposed surface for the 650 kg/m^3 density specimen

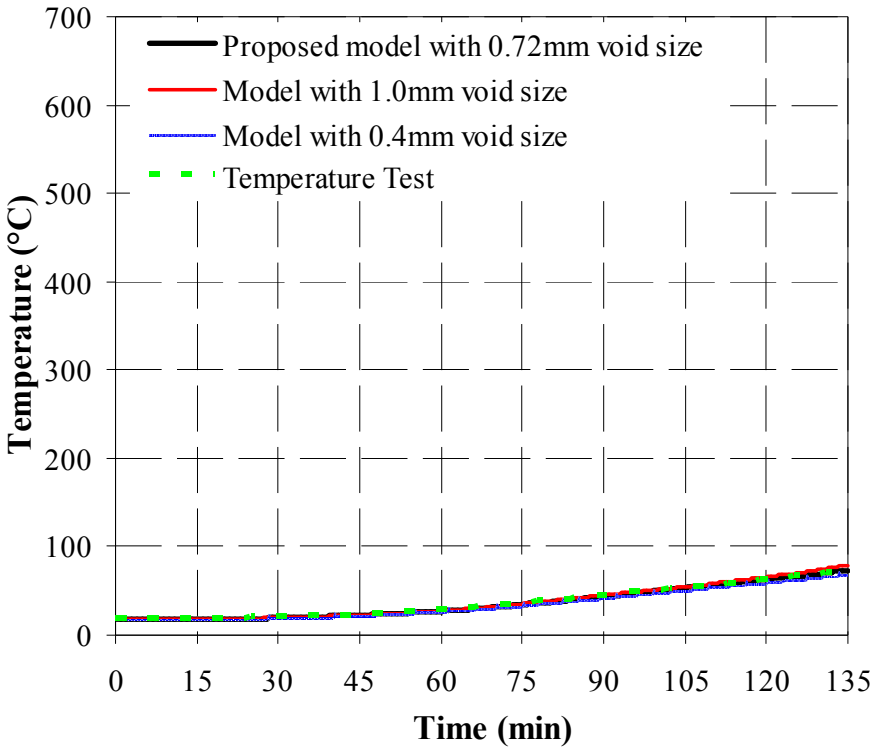

Figure 4.27 Sensitivity of LFC temperature to different pore sizes at 112.5mm from the exposed surface for the 650 kg/m^3 density specimen

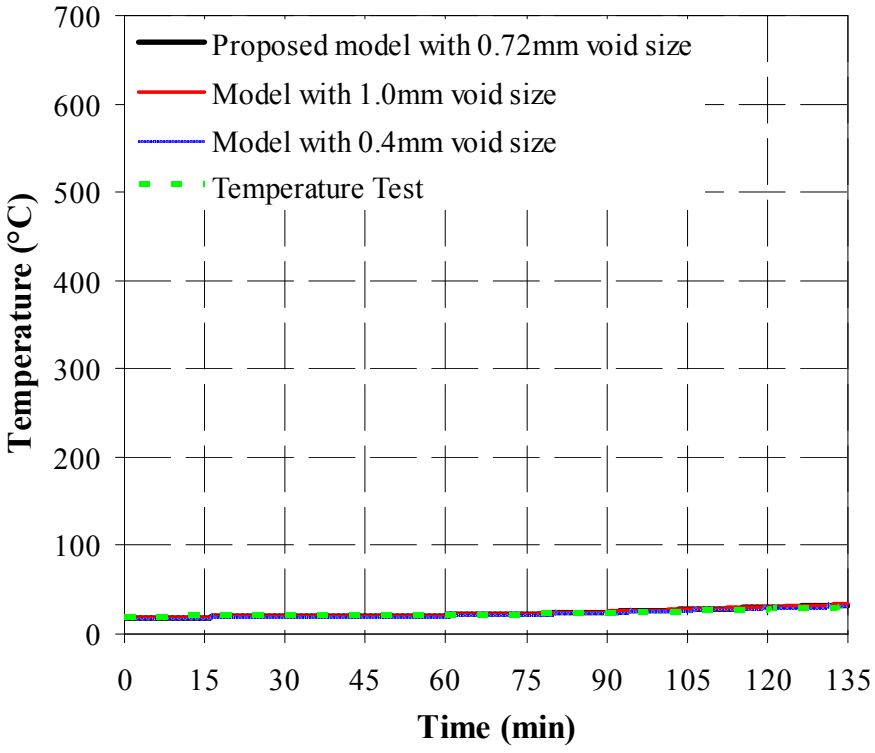

Figure 4.28 Sensitivity of LFC temperature to different pore sizes at the exposed surface for the 650 kg/m^3 density specimen

4.6 CONCLUSIONS

This chapter has presented the basis of the one-dimensional heat transfer modelling, the implementation of the method and the validation of thermal properties model of LFC panel. The comparison of test results with the numerical heat transfer analysis results using the proposed thermal property models is close, confirming the validity of the thermal conductivity models. Despite simplicity, the aforementioned analytical models for specific heat and thermal conductivity of LFC of different densities give accurate results. The superiority of the analytical model over the HGP test is that LFC of different densities may be now considered without relying on extensive tests. The prediction results are moderately affected by the air pore diameter. This suggests that the air pore size should be determined with accuracy, but the average pore diameter will be satisfactorily accurate. For LFC densities of 650 kg/m^3 and 1000 kg/m^3, the average pore diameter may be taken as 0.72mm and 0.55mm respectively. The proposed model is straightforward yet proficient and can be exploited to assist manufacturers to develop their products without having to carry out numerous large-scale fire tests in the future.

CHAPTER 5

EXPERIMENTAL STUDIES OF MECHANICAL PROPERTIES OF LFC EXPOSED TO ELEVATED TEMPERATURES

5.1 INTRODUCTION

Even though LFC has low mechanical properties compared to normal weight concrete (NSC), there is a potential of using this material as partition or load-bearing wall in low-rise residential construction. Before it can be considered for use as a load-bearing element in the building industry, it is necessary to acquire reliable information of its mechanical properties at ambient and elevated temperatures for quantification of its fire resistance performance. This chapter will present the results of experiments that have been carried out to examine and characterize the mechanical properties of LFC at elevated temperatures. Chapter 6 will present analytical models based on these experimental results.

A variety of test methods may be used to obtain different aspects of mechanical properties of materials at high temperatures, including the stressed test, the unstressed test, and the unstressed residual strength test (Phan and Carino, 2003). In this research, the unstressed test method was adopted for convenience. In the unstressed test, the sample was heated, without preload, at a steady rate to the predetermined temperature. While maintaining the target temperature, load was applied at a prescribed rate until sample failure. Because the temperature is unchanged, the test is also referred to as steady state test, as opposed to transient test in which the specimen temperature changes with time.

LFC with 650 kg/m^3 and 1000 kg/m^3 density were cast and tested. The details of the constituent material are shown in Table 2.6 (Chapter 2). The tests were carried out at

ambient temperature, 100, 200, 300, 400, 500, and 600°C. Compressive and three point bending tests were carried out.

5.2 POROSITY MEASUREMENTS AND PORE SIZE

The pore structure of cementitious material, determined by its porosity, is a very significant characteristic as it influences the properties of the material such as strength and durability. The porosity could therefore be a major factor influencing the material properties of LFC and an in-depth look into this aspect is essential to determine the relationships between porosity and material properties. Generally, the mechanical properties of LFC decrease with increasing porosity. The density of LFC may be diverse for the same water-cement ratio, through the integration of different amounts of foam, which may result in a different porosity and void sizes. For that reason, any change in the micro structure of LFC due to a variation in the void system may influence the mechanical properties considerably in relation to density.

Therefore, before the mechanical property tests were carried out, the porosity of LFC at elevated temperatures was measured according to the method described in Section 3.4.2. Table 5.1 indicates that replicate samples gave consistent results.

Table 5.1 Porosity of LFC obtained through Vacuum Saturation for mechanical properties test

Density (kg/m^3)	Sample	Porosity (%)			
		Ambient	200°C	400°C	600°C
650	1/1	74.8	74.9	75.9	76.3
	1/2	74.7	74.9	75.7	76.1
	1/3	74.8	75.0	76.1	76.5
1000	1/4	49.7	49.9	52.4	53.4
	1/5	50.0	50.4	52.5	53.7
	1/6	50.4	50.7	52.9	54.1

5.2.1 Effect of high temperature on porosity of LFC

Usually, the porosity of cement based material changes when the temperature increases. These changes in porosity can be characterized by considering phase changes in the concrete at different temperatures. Kalifa et al. (1998) in their research credited the increase in porosity with temperature to the release of chemically bound water and to the microcracking produced by expansion of the cement paste. Gallé and Sercombe (1999) attributed the growth of porosity to the formation of large capillary pores in the concrete which corresponds to the release of adsorbed water in capillary pores and release of chemically bound water in the hydrated cement paste. Gallé and Sercombe (1999) observed that macropores correlated to microcracks observed at the surface of specimens heated beyond 250°C. During the heating process, the authors observed from 300°C a number of cracks on the LFC specimens due to the heating, which could be concurrent with the growth of porosity and microstructural changes. Noumowé et al. (1996) confirmed by mercury intrusion porosimetry an increment in the pore sizes of concrete above temperature of 120 °C. Ye et al. (2007) attributed increase in porosity due to the decomposition of C–S–H and CH (main hydration products). These transformations formed additional void spaces in heated concrete.

Figure 5.1 presented the total porosity for each mix as a function of the temperature. LFC of both densities experienced a slight monotonous increase in porosity with temperature. The initial porosity for 650 and 1000 kg/m^3 density is 74.8% and 50.0% respectively. Between 200°C and 300°C, the porosity increased considerably for the higher density LFC while the increase was more moderate for the lower density LFC due to decomposition of the different amounts of calcium silicate hydrate gel and sulfoaluminate. At 300°C, the measured porosity for 650 kg/m^3 and 1000 kg/m^3 density is 75.5% and 51.9% correspondingly. For temperatures beyond 400°C, the measured porosity showed some increase corresponding to the decomposition of calcium hydroxide to form calcium oxide. At 600°C, the porosity is 76.3% and 53.7% for 650 and 1000 kg/m^3 respectively. Nevertheless, in general, due to the high porosity at ambient temperature, LFC may be considered to have almost constant porosity at different temperatures.

The pore size of LFC determined through image analysis tool presented in Section 3.4.3 of this thesis illustrate images of the internal structure of the 650 and 1000 kg/m^3 density LFC at ambient temperature which obviously demonstrates that the void sizes are not uniform and the average void size is primarily a function of the LFC density. The same analysis of the images was also done for both densities after being exposed to high temperatures and the results indicate that the void size did not change much from that at ambient temperature.

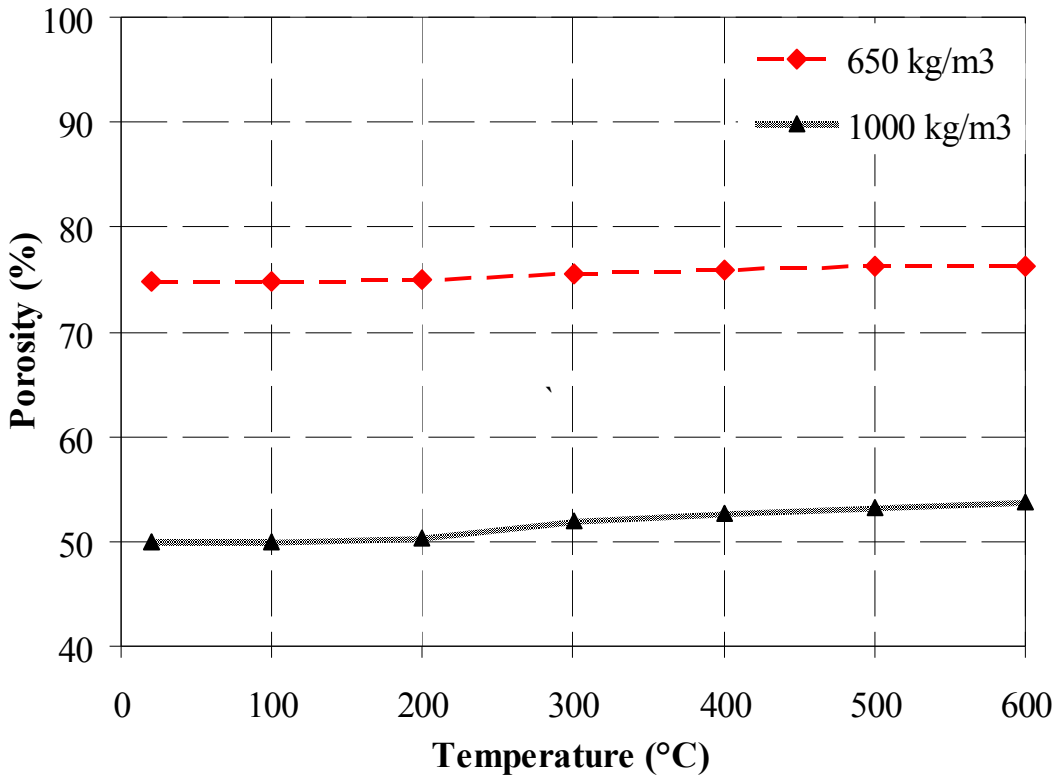

Figure 5.1 Porosity of LFC of two initial densities as a function of temperature

5.3 COMPRESSIVE TESTS

5.3.1 Heating of specimens

Two different electric furnaces were used for heating the LFC specimens to the various steady-state temperatures. One furnace had a maximum operating temperature of 450°C (low temperature furnace), and the second furnace had a maximum operating temperature of 1000°C (high temperature furnace). Each of the furnaces was capable of holding three specimens. The low temperature furnace had a temperature range of 50°C

to 450°C and was used for four of the reported thermal exposure conditions: 100°C, 200°C, 300°C and 400°C.

The furnace temperature exposure profiles were produced by a programmable microprocessor temperature controller attached to the furnace power supply and monitored by a Type K thermocouple located in the furnace chamber. The high temperature furnace (Figure 5.2) had a maximum operating temperature of 1000°C. This furnace was used for exposing concrete specimens to 500°C and 600°C. This furnace was also controlled by a programmable microprocessor temperature controller attached to the furnace power supply based on feed-back temperature reading from a Type K thermocouple located in the furnace chamber. Pre-testing checking of the furnaces showed that both furnace controllers and furnace power system could maintain furnace operating temperatures within ±1°C over the test range.

Figure 5.2 High temperature electric furnace with specimens

5.3.2 Test Set-up

The compressive tests were carried out on 100 x 200 mm cylinders. The specimens were removed from moulds after 24 hours of casting and then cured in a water tank at 20 ± 2°C for 28 days. Prior to testing, the specimens were removed from the curing

tank and put in the oven for 24 hours at 105°C. After 24 hours, all the specimens were removed from the oven and their ends were ground flat. To monitor the strain behaviour at ambient temperature during loading, two strain gauges was fitted on each sample for the ambient test only. These ambient temperature strain measurements were used to confirm that the strain calculated based on the displacement of the loading platen was of sufficient accuracy. Since it was difficult to measure strain at elevated temperatures, the displacement of the loading platen was used to calculate the strain for the elevated temperature tests. Four Type K thermocouples were installed in the central plane of each cylinder specimen to measure the specimen temperature, as shown in Figure 5.3.

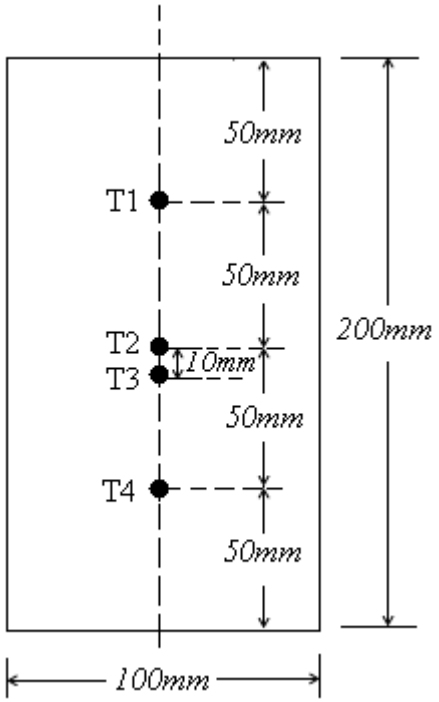

Figure 5.3 Typical 100 x 200 mm cylinder specimen with thermocouples arrangement

Loading was applied using an ambient temperature machine after removing the test samples from the furnace. Each specimen was wrapped with insulation sheets immediately after being removed from the electric furnace to minimise heat loss from the specimen to atmosphere. For each set, three replicate tests were carried out to check consistency of results. The target temperatures were 20°C (room temperature), 100, 200, 300, 400, 500, and 600°C.

During the loading process, the temperature of each sample (thermocouple T3) was measured and it was found that the temperature was stable throughout the testing period. Figures 5.4 shows typical temperature variations throughout the loading phase for specimens of 1000 kg/m^3 density. As can be seen, because the duration of loading was short (just over one minute), there was very little heat loss and the temperature change was less than 0.5^{o}C.

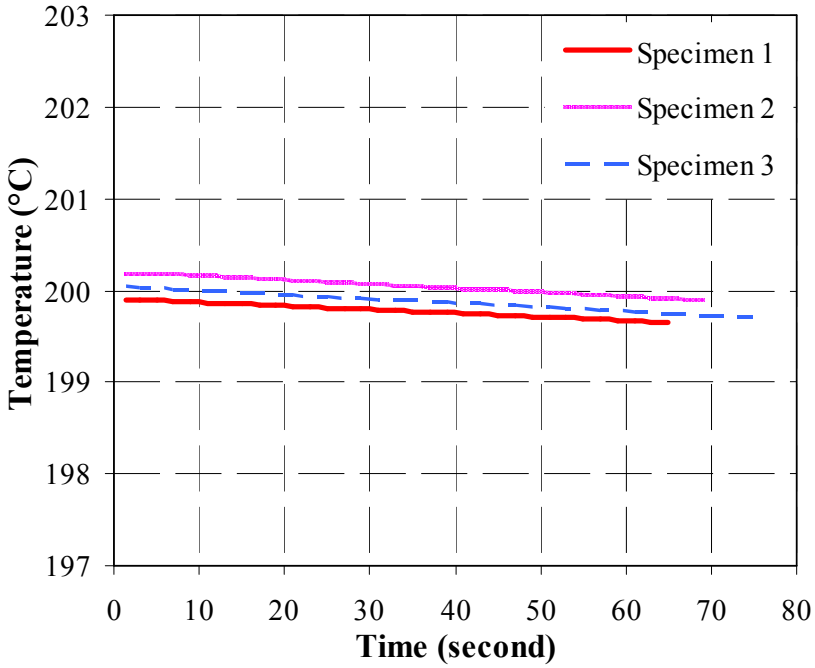

Figure 5.4 Temperature change during test of specimens of 1000 kg/m^3 density at target temperature of 200°C

5.3.3 Results and discussion

The compressive tests have yielded the following mechanical properties: compressive strength, compressive stress-strain relationship, modulus of elasticity in compression and failure mode in compression.

5.3.3.1 Effects of high temperature on compressive strength of LFC

As will be shown later in Section 5.3.3.2, the three duplicate tests of each series gave very consistent results so the average results may be used. As expected, for both densities, the LFC compressive strength decreased with temperature. Figures 5.5 and 5.6 present the compressive strength and normalized compressive strength of LFC at different temperatures. On initial heating, the LFC made with Portland cement CEM1

lost the absorbed, evaporable (or free) water and then the chemically bound water. The loss of water would induce micro cracking resulting in some reduction in strength. Between 90°C to 170°C, the compressive strength decreased slowly due to the release of free water and some of the chemically bound water. At this point, the reduction in concrete strength is not significant and the compressive strength of the LFC samples at 200°C still retained about 94% of the original unheated value. Between 200 °C and 400°C, decomposition of C-S-H gel and the sulfoaluminate phases caused cracks in the specimens (Taylor, 1992). These cracks had significant effects on the compressive strength of LFC (Ai et al., 2001). At 400 °C, the LFC strength retained only about 75% of its initial value for both densities. Further degradation and loss of strength continued to take place at high temperatures. At temperature of 600°C, the LFC retained only about 40% of the original strength for both densities. It should be pointed out that in this test, thermal shock should not be a problem. The specimens were heated slowly and no thermal crack was noticed before mechanical testing.

Since the compositions of both densities of LFC are identical, except for increased pores in the lower density LFC, it is not surprising that the normalised strength – temperature relationships of LFC of both densities are almost the same.

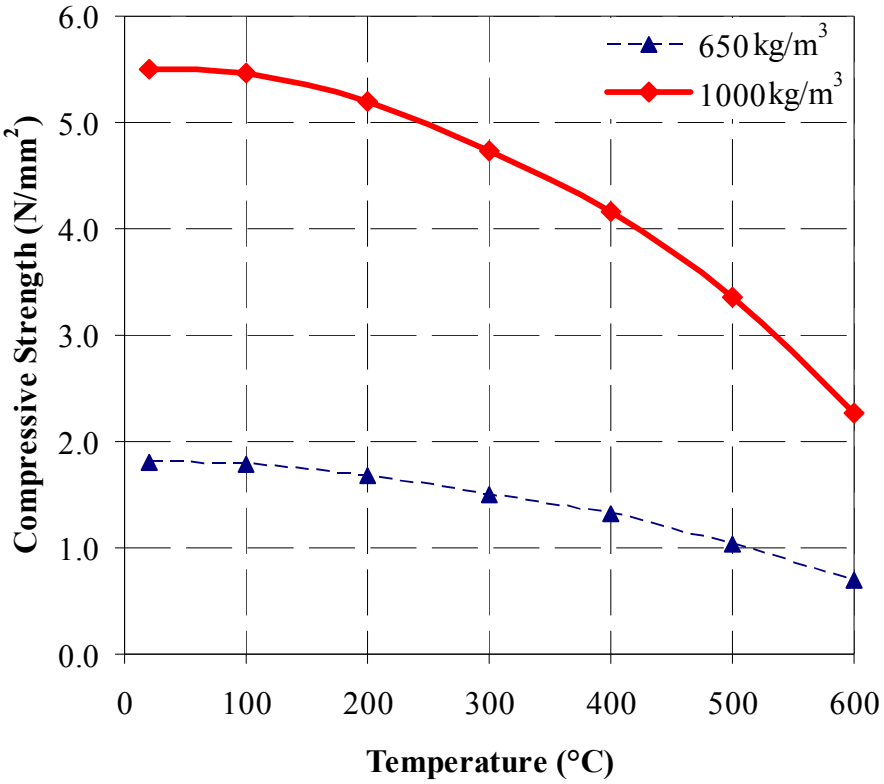

Figure 5.5 Compressive strength of LFC as a function of temperature

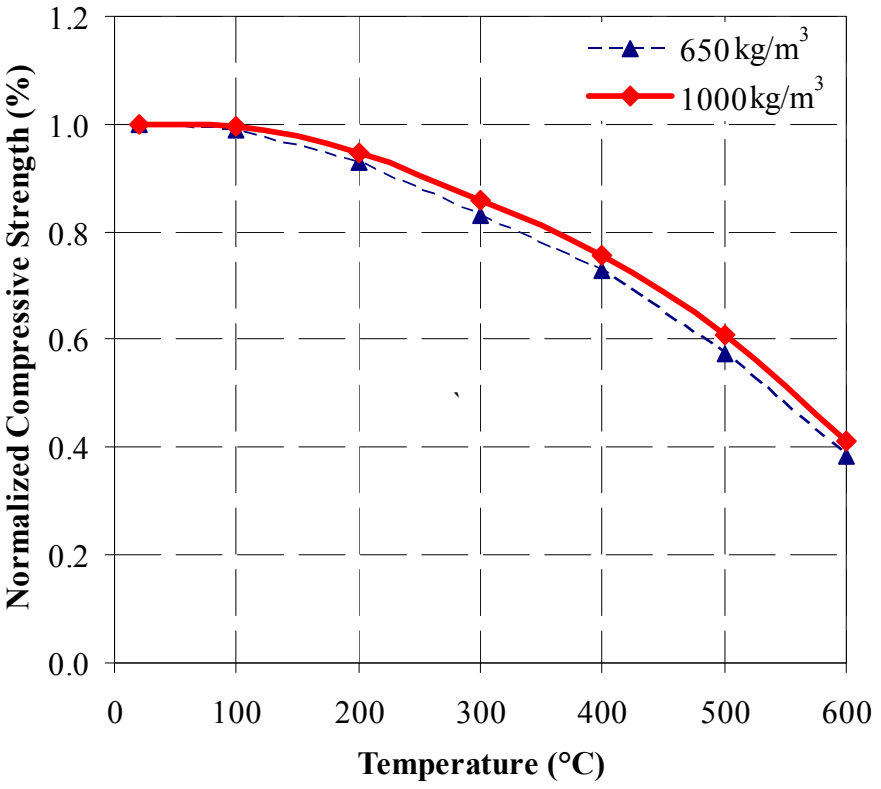

Figure 5.6 Normalized compressive strength of LFC as a function of temperature

5.3.3.2 Effects of high temperature on compressive stress-strain relationship of LFC

The engineering stress-strain relationships of LFC were determined from the measured load and deflection results using the original specimen cross-sectional area A_o and length L_o. Due to difficulty of using strain gauges at high temperatures, the deflection used to calculate the strain was that of the movement of the loading platen. Strains were measured at ambient temperature to confirm this method. Figure 5.7 compares the measured strain and that calculated using the displacement of the loading platen for the ambient temperature test. This comparison demonstrates that it is sufficiently accurate to use the loading platen displacement to calculate the axial strain of the test specimen.

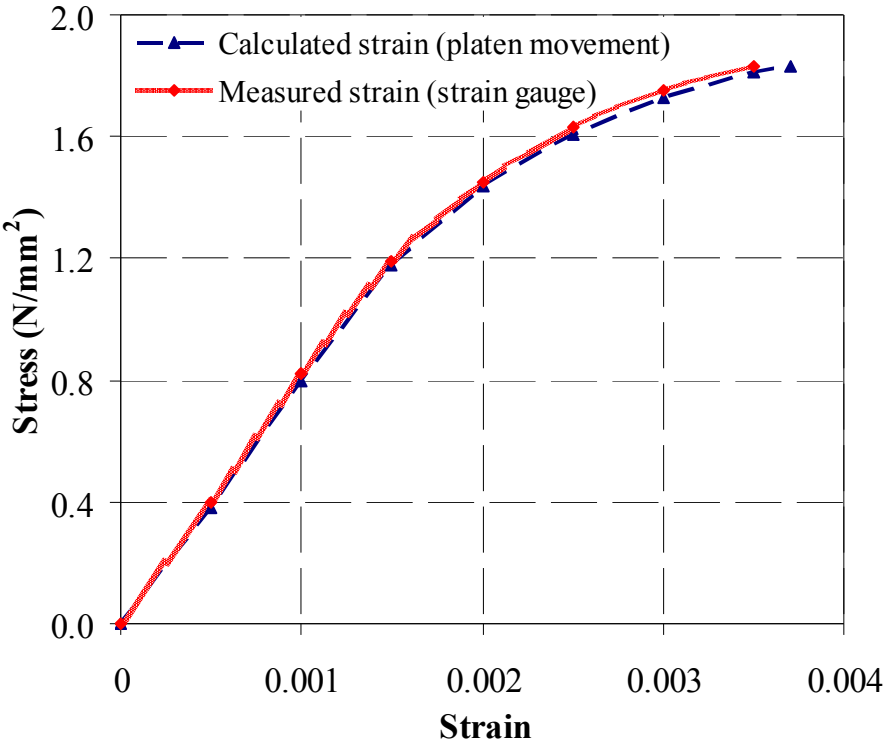

Figure 5.7 Comparison of measured strain and calculated strain (based on movement of the loading platen) for LFC of 650 kg/m^3 density at ambient temperature

The tests were displacement controlled where the crack continue to develop and grow after the peak load is reached. However, since the test specimens failed in a brittle manner after reaching the peak stress, it was not possible to obtain the descending branch of the stress-strain relationship. Figures 5.8-5.11 present typical stress-strain relationships for the three duplicate samples at different temperatures for the 650 kg/m^3

density specimens and Figures 5.12-5.15 are for the 1000 kg/m^3 density specimens. It was clear that all the three duplicate samples produced very consistent results. Figures 5.16 and 5.17 present the average stress-strain curves at all different testing temperatures for the two densities.

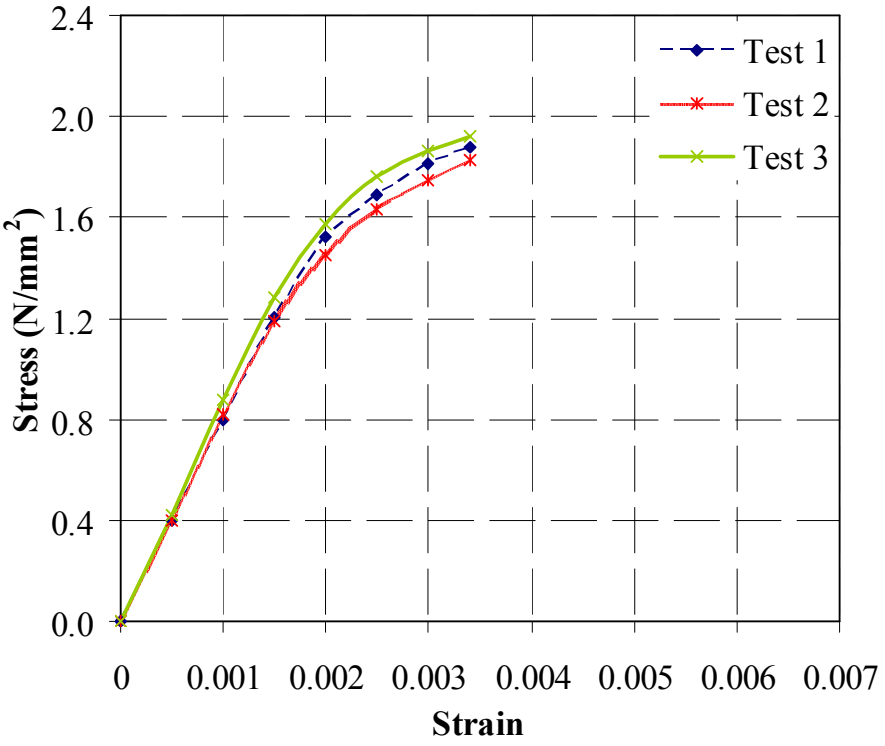

Figure 5.8 Stress-strain relationship for LFC of 650 kg/m^3 density at ambient temperature

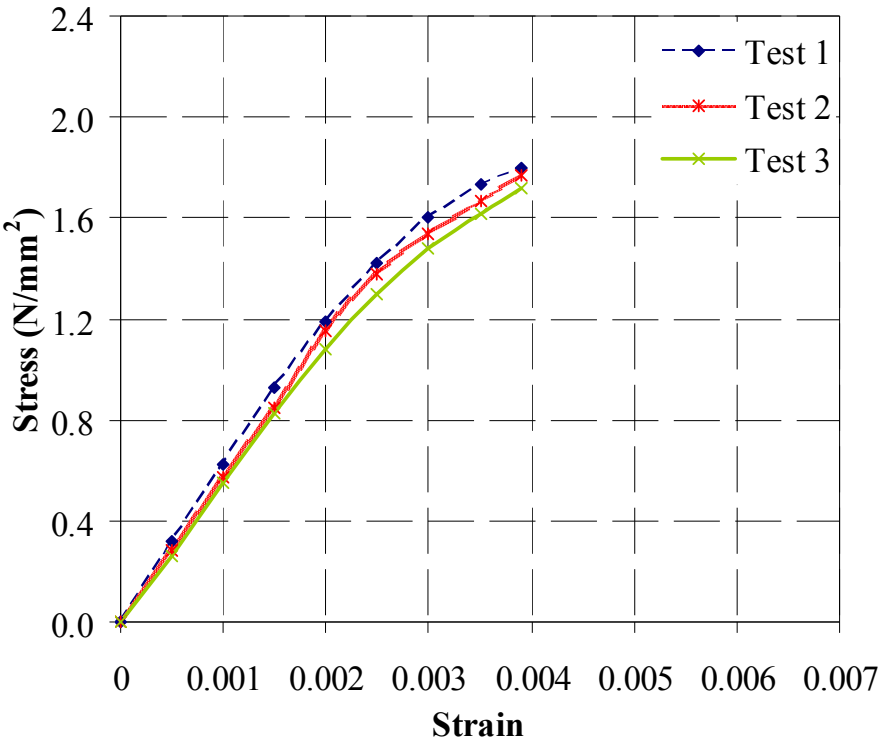

Figure 5.9 Stress-strain relationship for LFC of 650 kg/m^3 density at 200°C

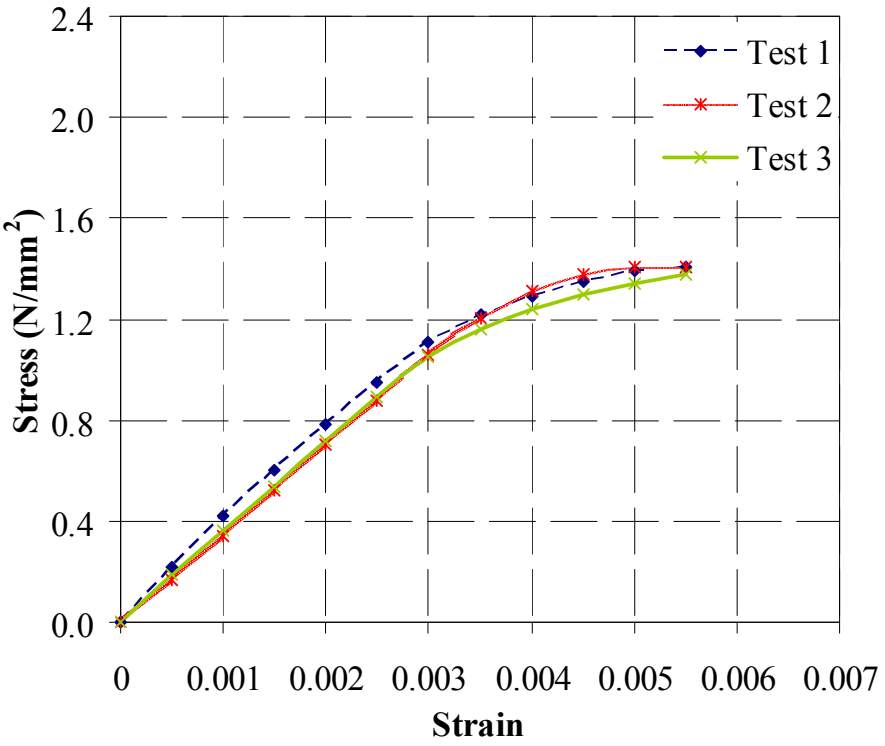

Figure 5.10 Stress-strain relationship for LFC of 650 kg/m^3 density at 400°C

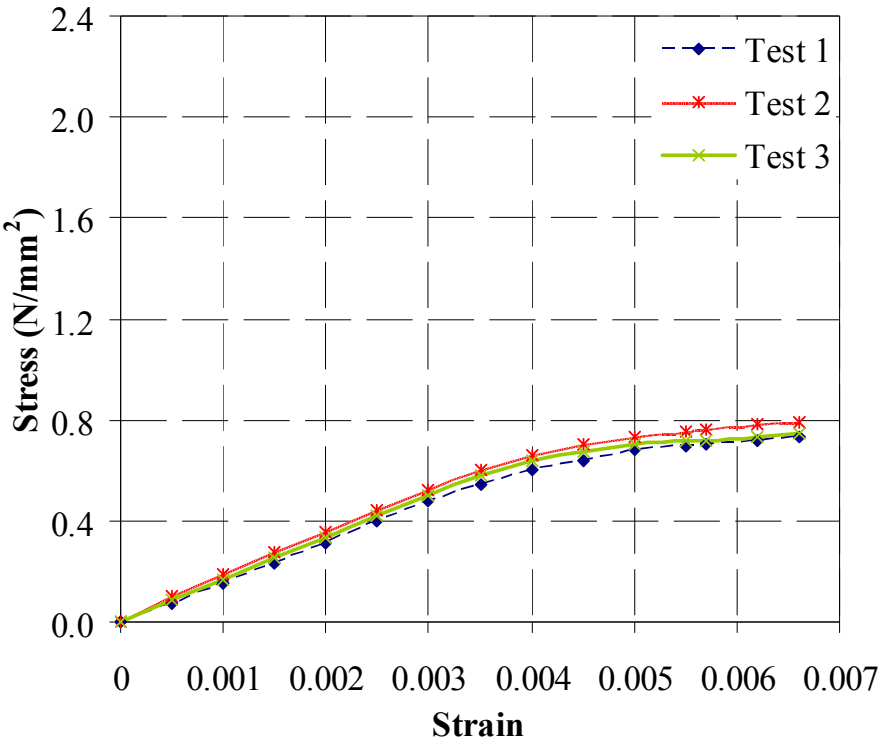

Figure 5.11 Stress-strain relationship for LFC of 650 kg/m^3 density at 600°C

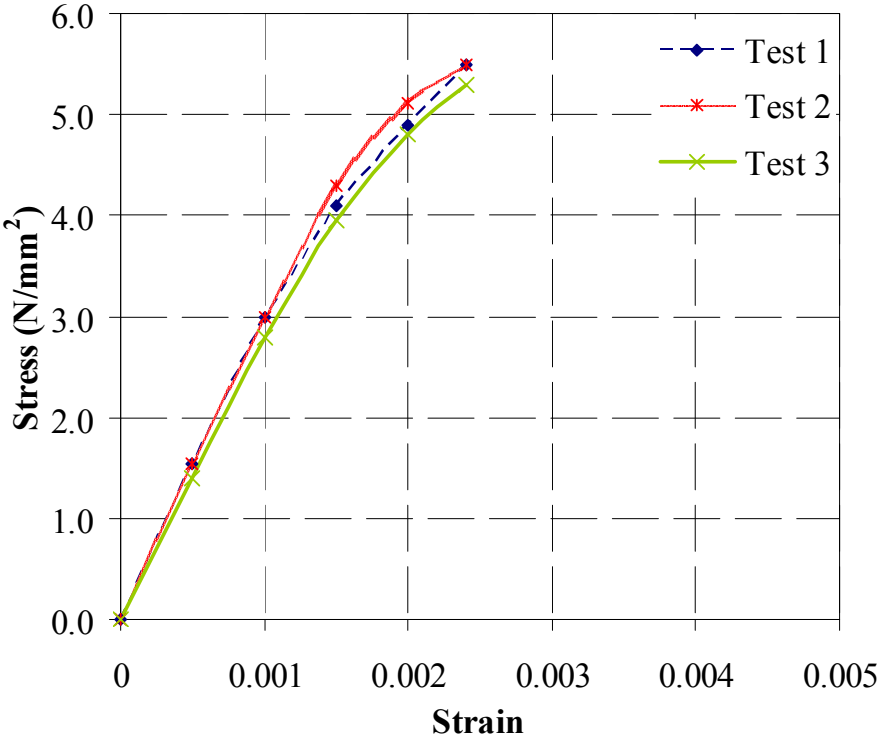

Figure 5.12 Stress-strain relationship for LFC of 1000 kg/m^3 density at ambient temperature

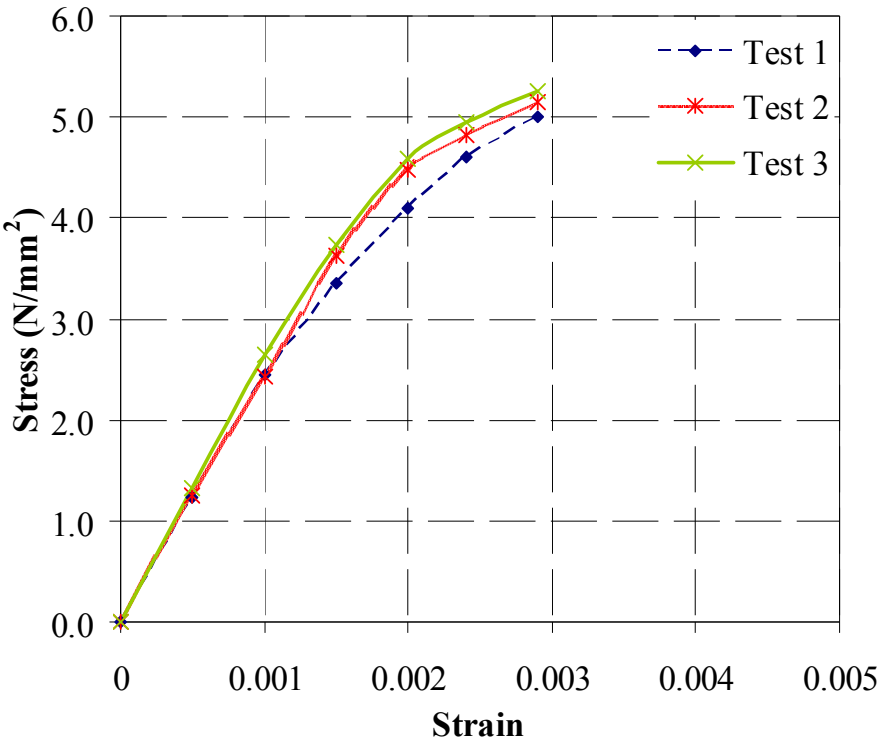

Figure 5.13 Stress-strain relationship for LFC of 1000 kg/m^3 density at 200°C

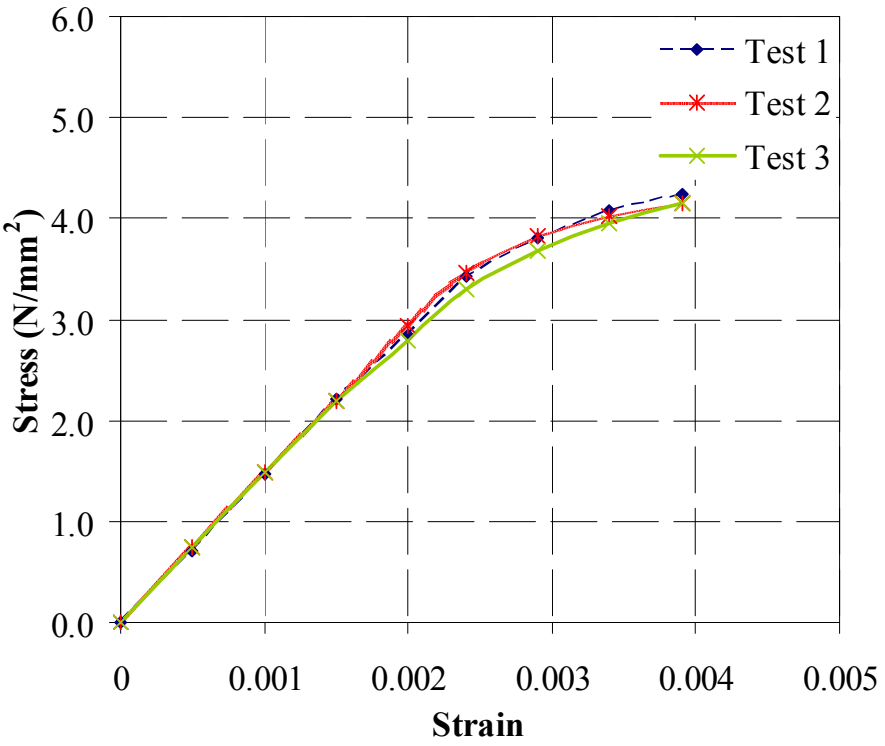

Figure 5.14 Stress-strain relationship for LFC of 1000 kg/m^3 density at 400°C

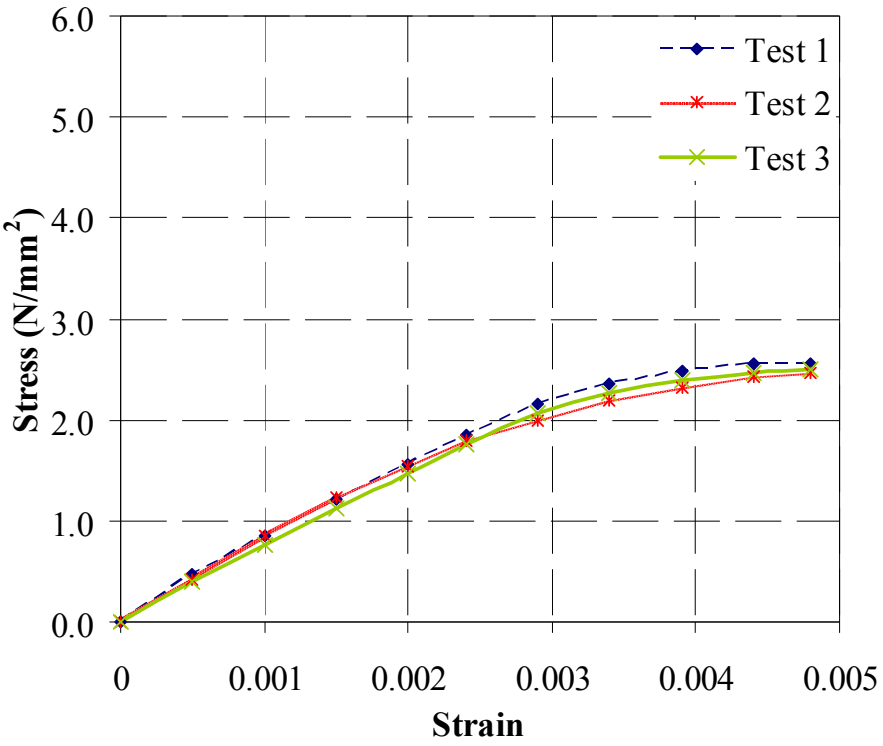

Figure 5.15 Stress-strain relationship for LFC of 1000 kg/m^3 density at 600°C

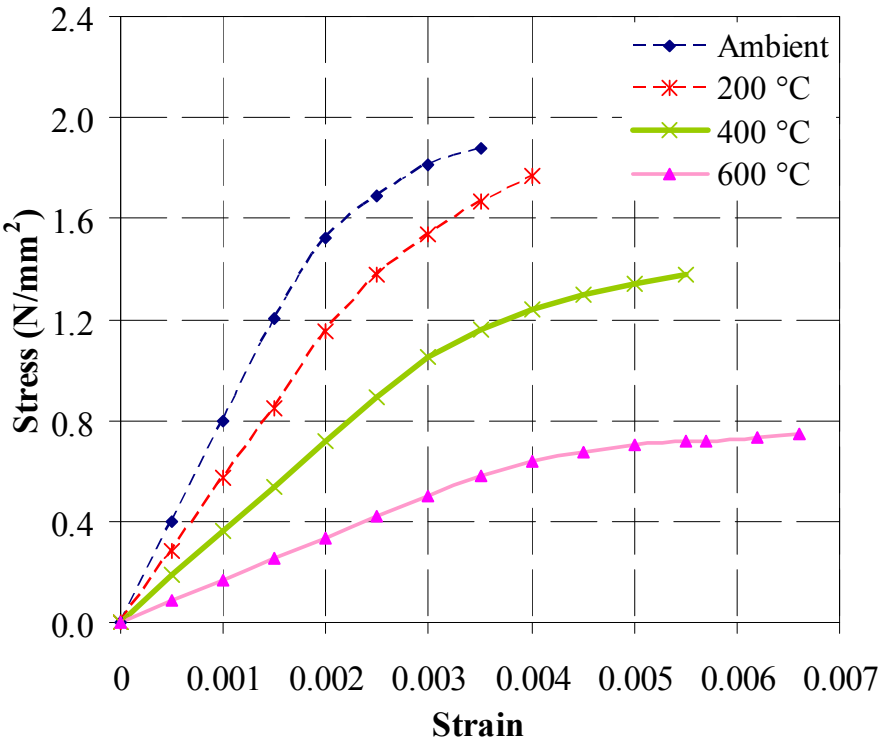

Figure 5.16 Average stress-strain relationships for LFC of 650 kg/m^3 density at different temperatures

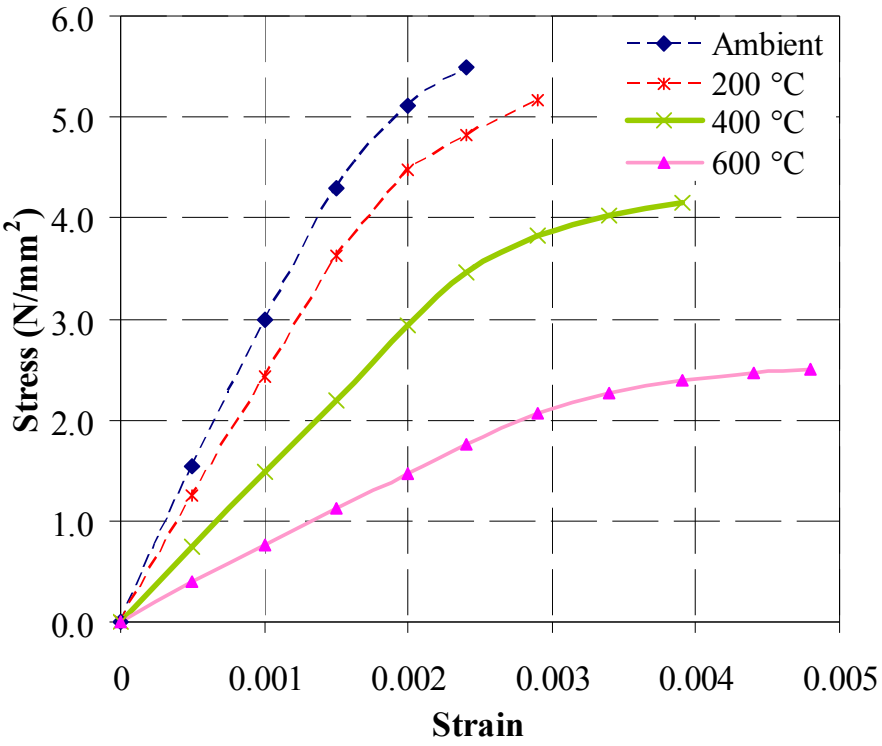

Figure 5.17 Average stress-strain relationships for LFC of 1000 kg/m^3 density at different temperatures

For both densities at all temperature levels, the ascending branch was linear for stress up to 75% of the peak strength. The strain corresponding to the peak strength increased at increasing temperatures. For LFC of 650 kg/m^3 density, the maximum strains were 0.0034, 0.0039, 0.0055 and 0.0066 at ambient temperature, 200°C, 400°C and 600°C respectively; for the 1000 kg/m^3 density, the corresponding values were 0.0024, 0.0029, 0.0039 and 0.0048 at ambient, 200°C, 400°C and 600°C respectively. The increase in strain results from opening of cracks initiated by the heating at higher temperatures.

Table 5.2 shows, for both densities and all temperatures, the elastic strain at the maximum stress, the maximum strain at the maximum stress and the ratio of these two strains. It appears that an average constant ratio of about 1.78 may be used for all cases.

Table 5.2 Elastic strain at the maximum stress, maximum strain at the maximum stress and the ratio of these two strains for both densities at different temperatures

Density (kg/m^3)	Temperature (°C)	Elastic strain at maximum stress	Maximum strain at maximum stress	Ratio of maximum strain at peak stress to elastic strain at peak stress
650	Ambient	0.0019	0.0034	1.79
	200	0.0022	0.0039	1.77
	400	0.0030	0.0055	1.83
	600	0.0037	0.0066	1.78
1000	Ambient	0.0013	0.0024	1.85
	200	0.0016	0.0029	1.81
	400	0.0023	0.0039	1.70
	600	0.0028	0.0048	1.71

5.3.3.3 Effect of high temperature on modulus of elasticity of LFC in compression

Figures 5.18 and 5.19 demonstrate the changes in modulus of elasticity of LFC in compression as a function of temperature. The modulus of elasticity was taken as the secant modulus at the point where the material changed from elastic to plastic behavior from the experimental compressive stress–strain curve. Compared to the reduction in LFC strength, the reduction in elastic modulus is greater. Both figures show that the loss in modulus of elasticity began immediately upon heating when the samples began to dry. The modulus of elasticity at 200°C, 400°C and 600°C was respectively about 75%, 40% and 25% of the original value for both densities.

As with changes in normalised strengths of LFC of both densities at elevated temperatures, the normalised modulus of elasticity of LFC of both densities at the same temperature was almost the same.

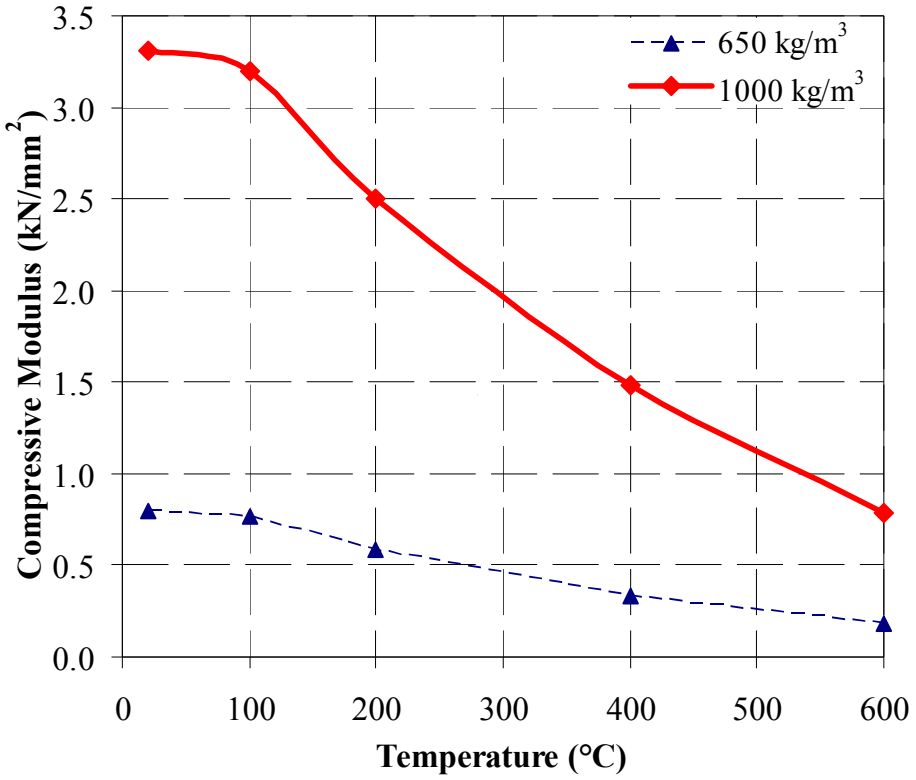

Figure 5.18 Compressive modulus of LFC as a function of temperature

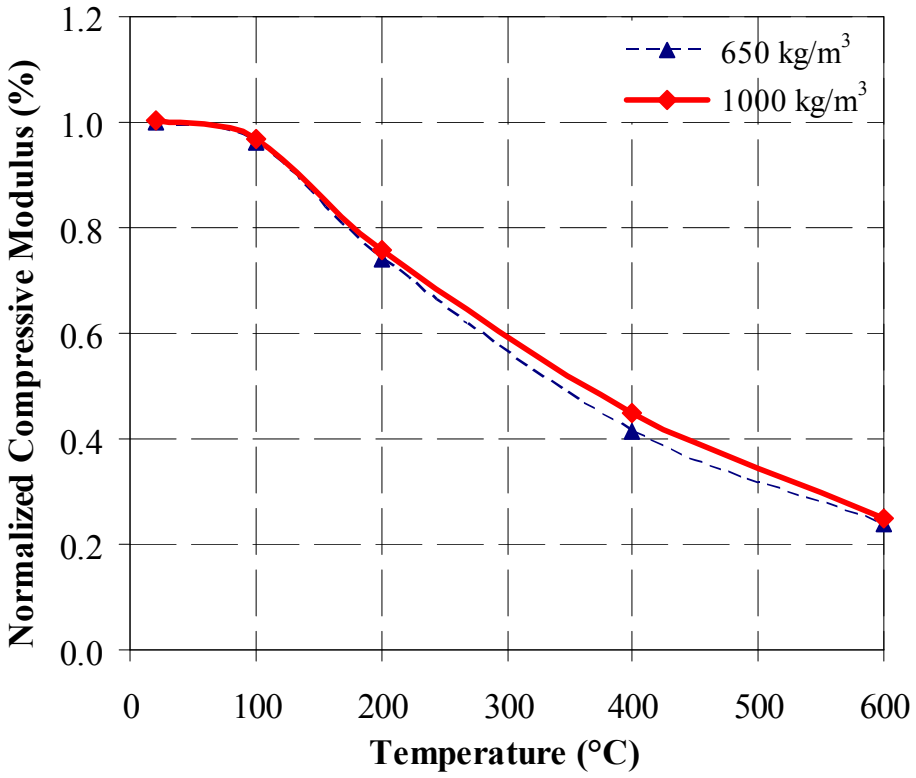

Figure 5.19 Normalized compressive modulus of LFC as a function of temperature

5.3.3.4 Effects of high temperature on LFC failure mode in compression

All the tested LFC specimens exhibited brittle failure at all temperatures levels, failing soon after reaching their peak strength. For the LFC of 650 kg/m^3 density, the end portion of the failed specimens resembled 'double cone pattern' (Figure 5.20b) at the top and bottom at 400°C. When exposed to temperature of 600 °C, the specimens crumbed and failed in an irregular pattern as shown in Figure 5.20(c). For LFC of 1000 kg/m^3 density, vertical cracks appeared in the broken specimens with double cone pattern at top and bottom at 400°C (Figure 5.21b); at 600 °C, it experienced the same mode of failure as the LFC of 650 kg/m^3 density (Figure 5.21c).

(a) at ambient *(b) at 400°C* *(c) at 600°C*

Figure 5.20 Failure modes of LFC of 650 kg/m^3 density at different temperatures

(a) at ambient *(b) at 400°C* *(c) at 600°C*

Figure 5.21 Failure modes of LFC of 1000 kg/m^3 density at different temperatures

5.4 THREE POINT BENDING TEST

5.4.1 Test set-up

Three methods may be used to obtain the tensile strength of concrete: direct tensile test, tensile splitting test or flexural (three point bending) test. For convenience in this study, the three point bending test was carried out. The preparation of samples followed a similar procedure as outlined above for the compression tests. The specimens were rectangular parallelepipeds of height *(h)* 25 mm, width *(w)* 125 mm and length L *(l)* 350 mm. As illustrated in Figures 5.22 and 5.23, the specimen was simply supported and was subjected to point load at the centre point. The length between the supports was L_s = 200 mm, giving a L_s/h aspect ratio of 8 and sufficient to ensure predominance of bending behaviour. The load-deflection was recorded for the evaluation of flexural tensile strength.

Figure 5.22 Three point bending test set up and specimen dimensions

Based on the sketch in Figure 5.23 and assuming linear elastic behaviour, the maximum flexural bending strength (f_{cr}) is at the centre (point *B*) which is defined as:

$$f_{cr} = \left(\frac{1}{4}PL\right) \Big/ \left(\frac{bd^2}{6}\right) = \frac{3PL}{2bd^2} \quad \ldots (5.1)$$

where $\frac{1}{4}PL$ is the bending moment at point *B* and $\frac{bd^2}{6}$ is the elastic modulus for rectangular cross-section. The flexural strength becomes tensile strength only if the material behaviour is linear until tensile failure.

The flexural modulus of elasticity may be calculated using the following equation:

$$E_{cr} = \frac{PL^3}{4bd^3 y} \quad \ldots (5.2)$$

where *y* is the maximum deformation at the centre of the beam.

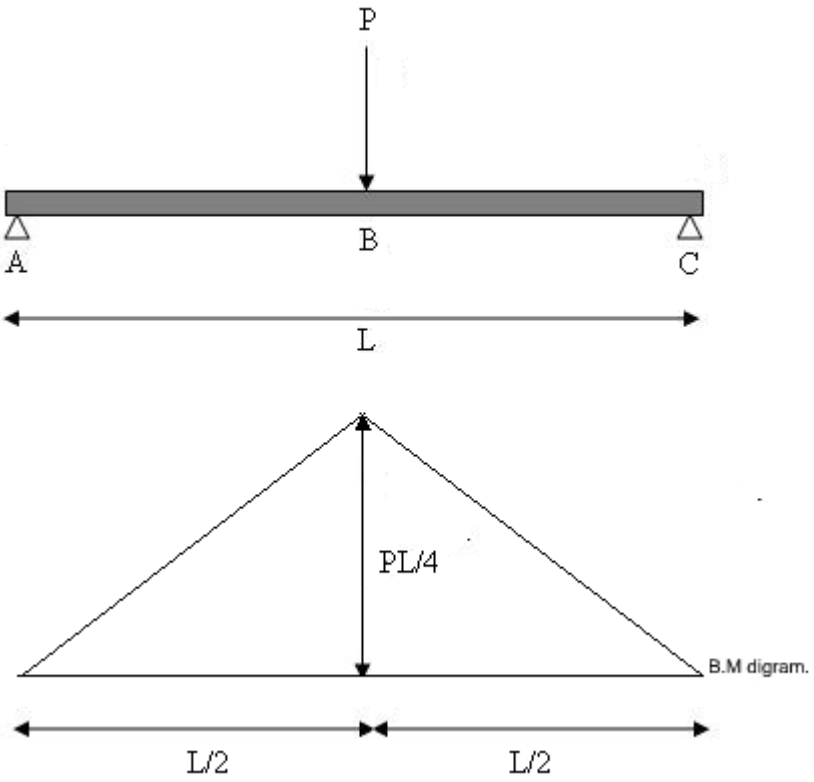

Figure 5.23 Simply supported specimen subjected to a concentrated load at mid span

5.4.2 Results and discussion

The bending tests have yielded the following mechanical properties: flexural tensile strength and flexural tensile modulus.

5.4.2.1 Effects of high temperature on flexural tensile strength of LFC

Since LFC is a brittle material, the bending test was intended to give a measure of the flexural tensile strength of the LFC. Figures 5.24 and 5.25 present the variation in flexural tensile strength of LFC as a function of temperature. The reduction in flexural tensile strength of LFC occurred predominantly after 90°C, regardless of the density of LFC. Consistent with changes in the aforementioned other mechanical properties of LFC, which indicates that the primary mechanism causing degradation is micro cracking, which occurs as the free water and chemically bound water evaporates from the porous body. When the chemical constitution of LFC started to break down between 200°C and 300°C due to decomposition of the C-S-H and sulfoaluminate phases ($3CaO.Al_2O_3.CaSO_4.12H_2O$ and $3CaO.Al_2O_3.3CaSO_4.31H$), cracks formed and there was a significant drop in tensile strength. At 400°C, the tensile strength was about 60% of the initial value for both densities. At 600°C, the flexural tensile strength achieved was only about 40% and 45% for 650 kg/m^3 and 1000 kg/m^3 densities respectively.

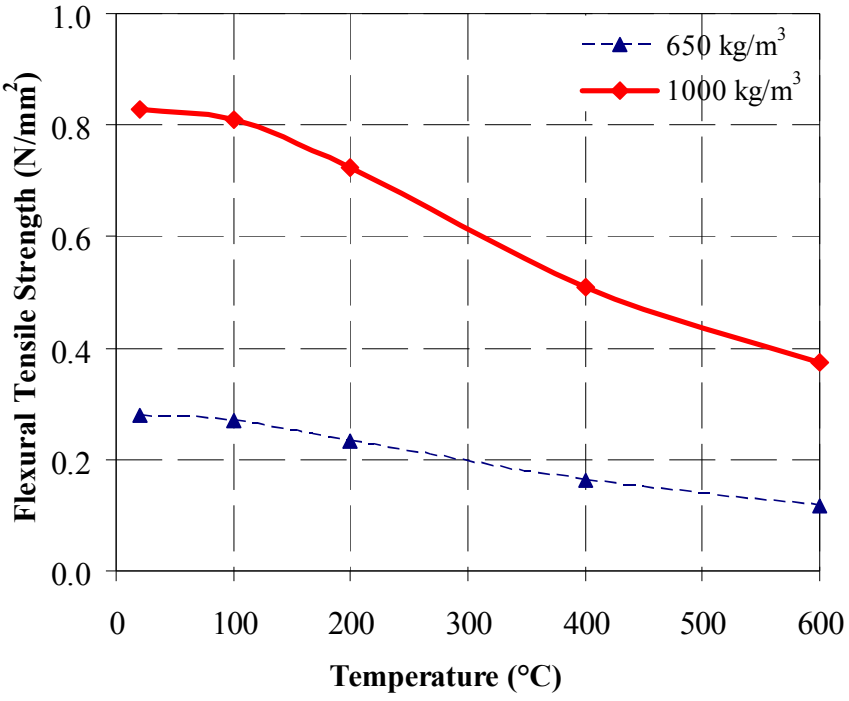

Figure 5.24 Flexural tensile strength of LFC as a function of temperature

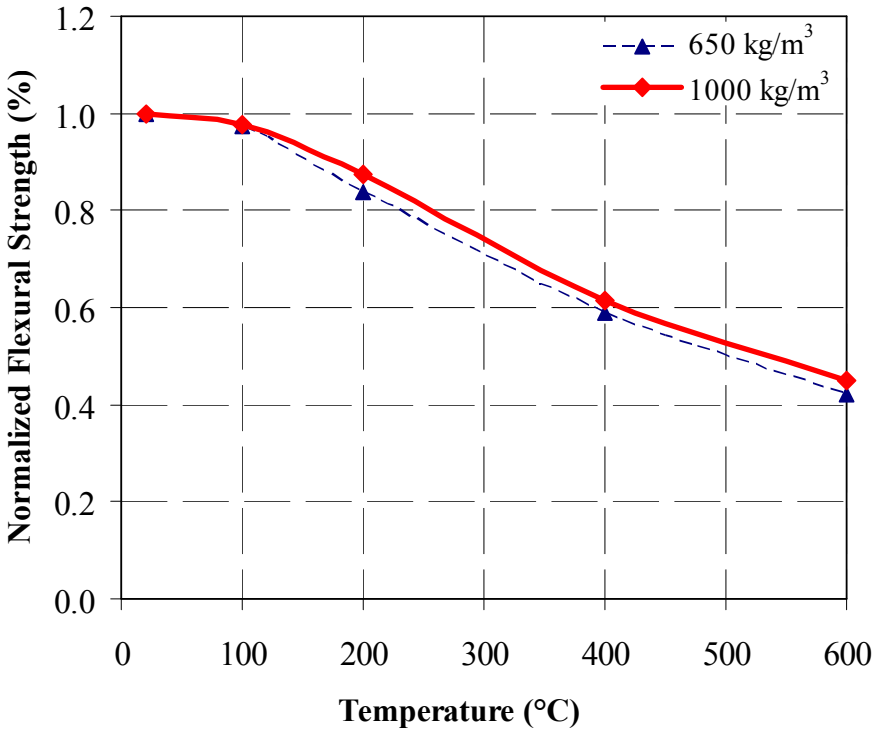

Figure 5.25 Normalized flexural tensile strength of LFC as a function of temperature

The normalized flexural tensile strength – temperature relationships for both densities are almost the same, which is consistent with other observed properties.

5.4.2.2 Effects of temperature on flexural tensile modulus of LFC

Figures 5.26 and 5.27 illustrate the changes in flexural modulus of LFC as a function of temperature and compare the flexural modulus with the compressive modulus obtained from the cylinder tests. Although there are some differences, the compressive modulus and flexural modulus values are very similar for both densities and at different temperatures.

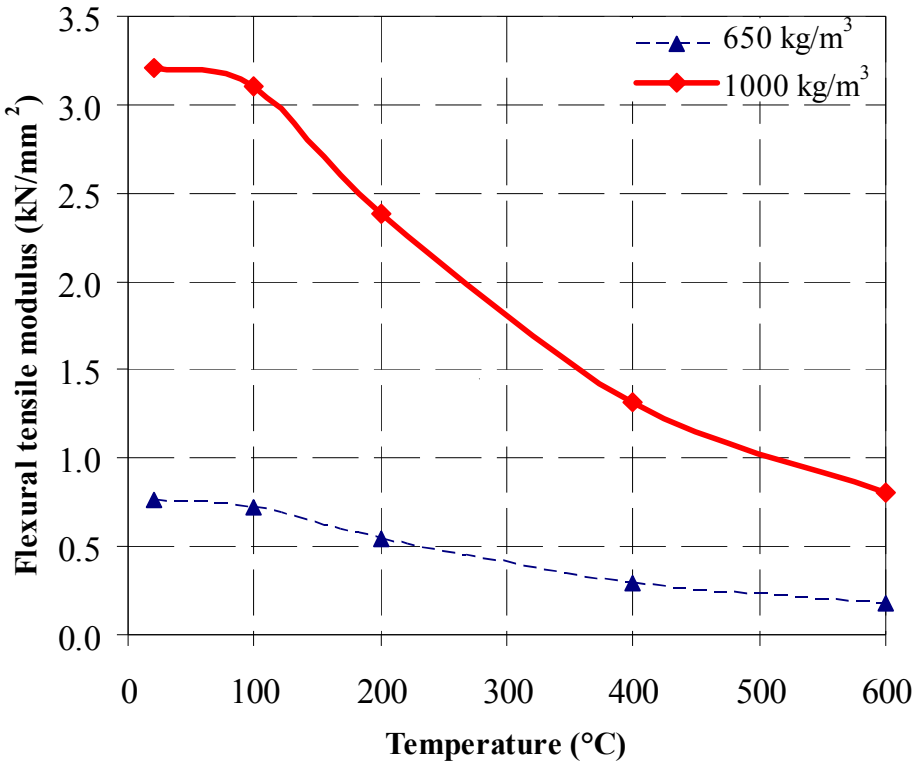

Figure 5.26 Flexural tensile modulus of LFC as a function of temperature

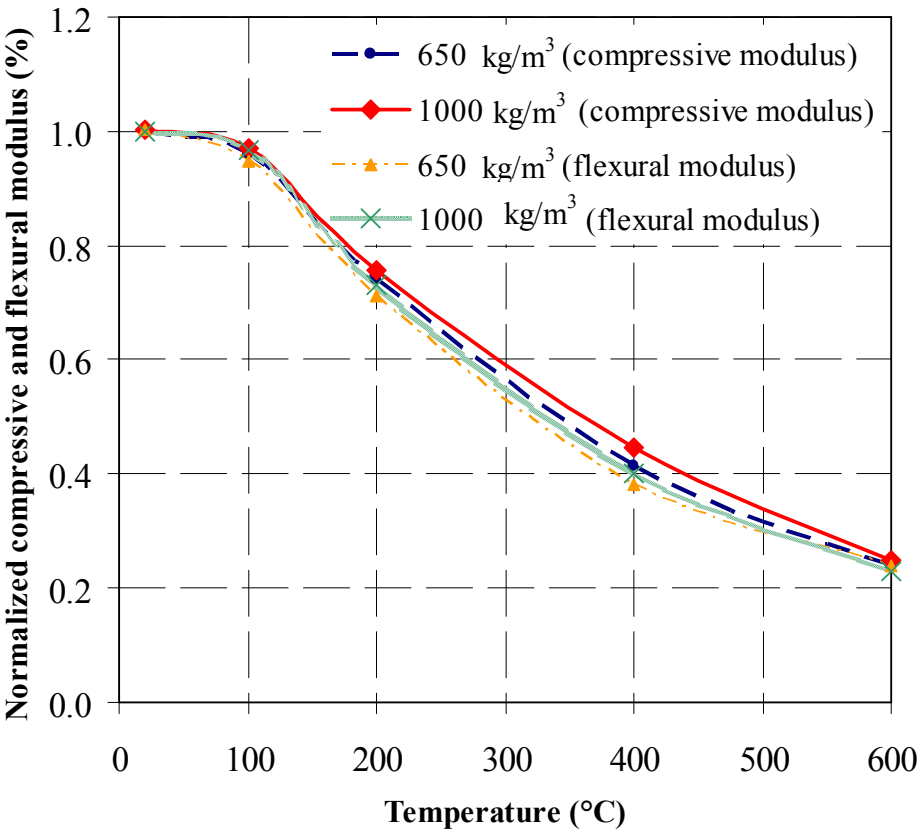

Figure 5.27 Comparison of normalized compressive modulus and flexural tensile modulus of LFC as a function of temperature

5.5 ADDITIONAL SPECIMENS FOR MECHANICAL PROPERTIES TEST

As outlined in Chapter 1, one of the objectives of this research was to assess and propose mechanical properties prediction equations of LFC based on comparison of the experimental results with existing models for normal weight concrete. Therefore, to get a good strength-porosity relationship and to observe the influence of voids on the mechanical properties of LFC of this study, additional compression tests were carried out on three additional LFC densities of 800, 1200 and 1400 kg/m^3. The average LFC compressive strength and porosity values were specified in Table 5.3 and Table 5.4 indicated the average modulus of elasticity in compression for all the three densities at different temperatures.

Table 5.3 Compressive strength and porosity of LFC for 800 kg/m^3, 1200 kg/m^3 and 1400 kg/m^3 density at different temperatures

Density (kg/m^3)	Average compressive strength (N/mm^2)				Average porosity (%)
	Ambient	200°C	400°C	600°C	
800	3.20	2.94	2.52	1.50	62
1200	11.61	10.40	8.21	4.82	44
1400	15.30	14.03	10.90	6.60	38

Table 5.4 Modulus of elasticity in compressive of LFC for 800 kg/m^3, 1200 kg/m^3 and 1400 kg/m^3 density at ambient temperature

Density (kg/m^3)	Average modulus of elasticity in compression (kN/mm^2)			
	Ambient	200°C	400°C	600°C
800	1.81	1.36	0.82	0.46
1200	7.69	5.78	3.47	1.93
1400	10.12	7.61	4.68	2.55

The results obtained will be further discussed in Section 6.2 and Section 6.3 of this thesis.

5.6 CONCLUSIONS

This chapter has presented the results of an extensive series of experimental studies to obtain compressive and tensile mechanical properties of LFC at elevated temperatures. Compressive cylinder tests and three point bending tests were carried out for a range of LFC densities at different temperatures from ambient up to 600^{o}C. The mechanical properties included compressive cylinder strength, compressive modulus of elasticity, compressive stress-strain relationship, strain at the maximum compressive stress, porosity, flexural bending strength and modulus of elasticity. The experimental results consistently demonstrated that the loss in stiffness for cement based material like LFC at elevated temperatures occurs predominantly after about 90°C, regardless of density. This indicates that the primary mechanism causing stiffness degradation is microcracking, which occurs as water expands and evaporates from the porous body. As expected, reducing the density of LFC reduces its strength and stiffness. However, for LFC of different densities, the normalised strength and stiffness (ratio of elevated temperature value to ambient temperature value) – temperature relationships are very similar. This chapter has principally focused on explanation of the experimental set-up and presenting the experimental results of the mechanical properties of LFC at elevated temperatures; Chapter 6 will present some quantitative information on the influence of voids on the mechanical properties of LFC and comparison between the experimental results and predictions of some existing predictive models based on normal weight concrete.

CHAPTER 6

MECHANICAL PROPERTY PREDICTIVE MODELS FOR LFC EXPOSED TO ELEVATED TEMPERATURES

6.1 MODELS FOR LFC MECHANICAL PROPERTIES

Since the LFC employed in this study used the same Portland Cement SEM1 as in normal weight concrete for which a number of mechanical property models have been developed, this chapter is intended to assess whether any of these models would be suitable for LFC. A two-stage comparison will be made: assessment of models at ambient temperature and assessment of models for elevated temperatures, based on ambient temperature results.

The aim of this investigation is to propose a procedure to predict the mechanical properties of LFC, based on existing mechanical property predictive models. This procedure is expected to assist manufacturers and future researchers to develop improved products with reduced cost of experimentation. Whilst full-scale tests to regulatory standards will still be necessary for final accreditation purpose, much of this may be avoided by developing a method to predict the mechanical properties of LFC at ambient and elevated temperatures during the development stage.

6.2 PREDICTION OF MECHANICAL PROPERTIES OF LFC AT AMBIENT TEMPERATURE

For LFC at ambient temperature, porosity represents the most important factor in affecting its strength. Hoff (1972) proposed a single strength-porosity model for cellular concrete with cement paste by combining the space taken by evaporable water and air-voids. Tam et al. (1987) reported a model for strength of LFC based on Feret's equations for a limited set of operating conditions. This equation was enhanced by

integrating the degree of hydration through Power's gel-space ratio concept. Balshin proposed an equation which provided a good fit to the plot of compressive strength against porosity for slate based autoclaved aerated concretes (Watson, 1980), at all ages of LFC made of cement paste containing high percentage of ash (Kearsley and Wainwright, 2002) and LFC containing high amount of fly ash as replacement to sand (Nambiar and Ramamurthy, 2008).

6.2.1 Strength-porosity relationship

Balshin (1949) strength-porosity relationship will be considered to assess the effects of porosity on compressive strength of LFC, which may be expressed using the following form:

$$f_c = f_{c,0}(1-\varepsilon)^n \quad \text{.....(6.1)}$$

where f_c is the compressive strength of LFC with porosity ε, $f_{c,0}$ is the compressive strength at zero porosity and n is a coefficient to be determined.

Figure 6.1 plots the recorded LFC compressive strength-porosity relationship for different LFC densities at ambient temperature (results of compressive strength presented in Table 5.3). Using Balshin's strength-porosity relationship, the best correlation is obtained with n=2.4, which was represented by the solid curve in Figure 6.1. A correlation coefficient of 0.914 indicates a good correlation between this model and the test results. Thus, the compressive strength of LFC at ambient temperature can be expressed as a power function of porosity as follow:

$$f_c = 39.2(1-\varepsilon)^{2.4} \text{.....(6.2)}$$

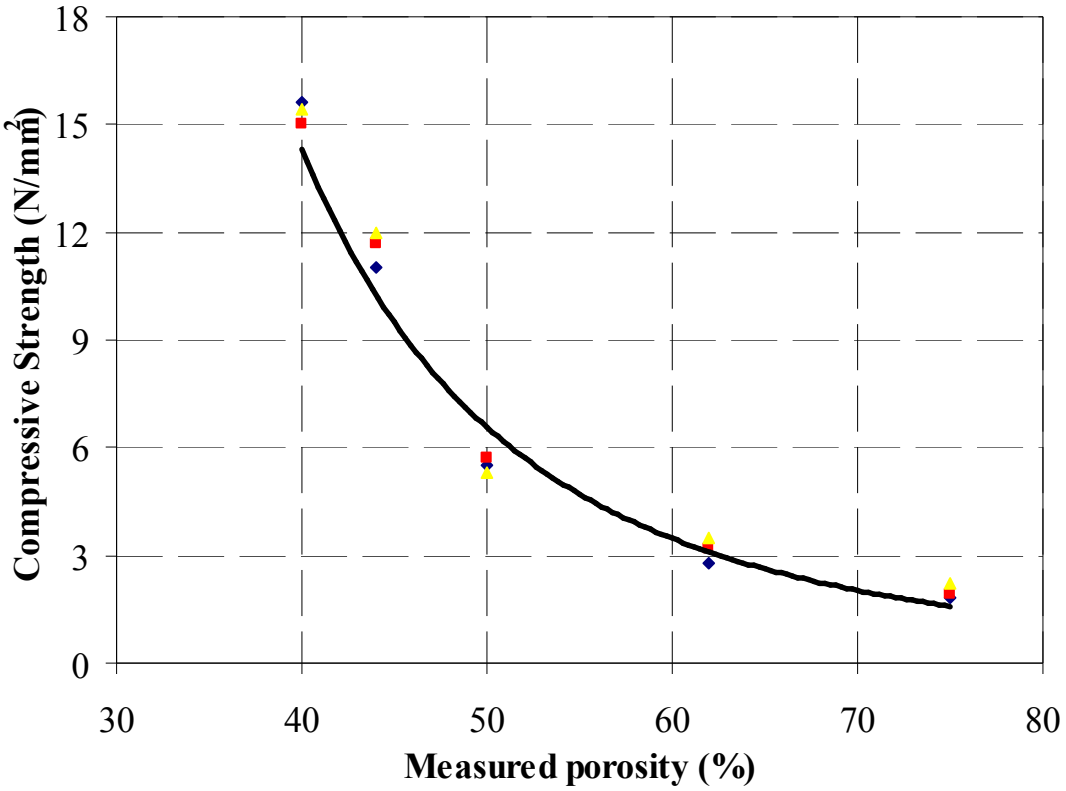

Figure 6.1 Compressive strength-porosity relation for LFC at ambient temperature

For interest, a similar study was carried out by others for LFC of different densities at ambient temperature. From the experimental results of this study for LFC at different temperatures, the same exercise was undertaken. The results are summarised in Table 6.1 and compared with results by others for other types of concrete. The *n* values of LFC obtained in this study show some consistency, but are different from other researchers. The *n* values of this study are much lower than from other studies, indicating that the LFC of this study suffered less void induced loss of strength.

Table 6.1 Comparison of *n*-values in strength-porosity model for different concretes

Researchers	Concrete type	Mix composition	Constants	
			$f_{c.0}$ (N/mm^2)	n
Hoff (1972)	LFC	Cement paste	115-290	2.7-3.0
Narayanan and Ramamurthy (2000)	Aerated concrete (non autoclaved)	Cement-sand	26.6	3.2
Kearsley and Wainwright (2002)	LFC	Cement with and without fly ash	188	3.1
Present work	LFC (ambient)	Cement-sand	39.2	2.4
	LFC (200°C)		38.5	2.4
	LFC (400°C)		28.1	2.4
	LFC (600°C)		19.5	2.6

6.2.2 Modulus of elasticity-porosity relationship

As acknowledged by the author, the strength-porosity relationship proposed by Balshin (Equation 6.1) has so far only been used to determine the compressive strength of porous material. This section will explore whether this equation (Equation 6.1) is also appropriate to establish the modulus of elasticity-porosity relationship for LFC. In order to do so, the experimental results of modulus of elasticity for all densities will be plotted as a function of porosity.

Figure 6.2 shows the recorded LFC modulus of elasticity-porosity relationship for different LFC densities at ambient temperature (results of modulus of elasticity in Table 5.4). Surprisingly, the same relationship can be used. The best correlation was found by using n=2.8, shown by the solid curve in Figure 6.2. A correlation coefficient of 0.936 indicates strong relationship between the model and the test results. Thus, the following modulus of elasticity-porosity relationship of LFC at ambient temperature is obtained:

$$E_c = 32.9(1-\varepsilon)^{2.8} \quad \text{.....(6.3)}$$

where E_c is the compressive modulus of LFC at ambient temperature and ε is porosity.

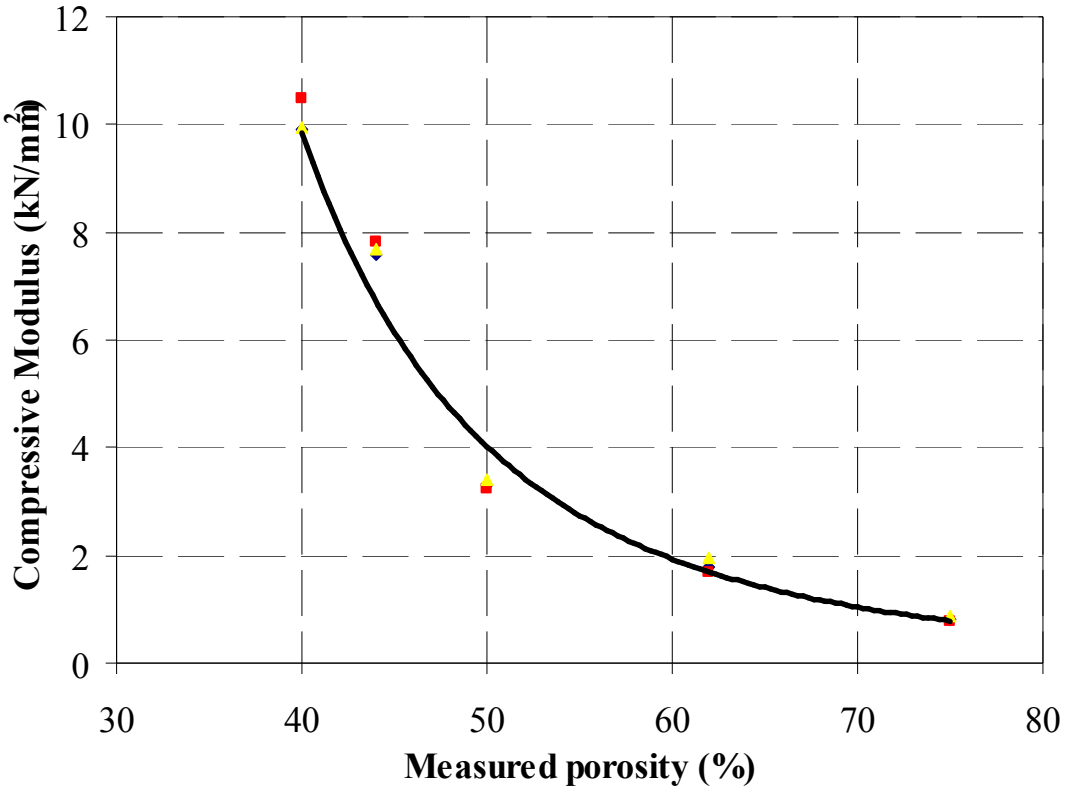

Figure 6.2 Modulus of elasticity-porosity relation for LFC at ambient temperature

From the experimental results of this study for LFC at different temperatures, the same exercise was undertaken to obtain the modulus of elasticity-porosity relationships. The results were summarised in Table 6.2 which shows a constant n value at different temperatures.

Table 6.2 Summary of $E_{c.0}$ and n values for modulus of elasticity-porosity relationship at different temperatures according to Balshin's model

Temperature (°C)	Constants	
	$E_{c.0}$ (kN/mm^2)	n
Ambient	32.9	2.8
200	24.7	2.8
400	15.0	2.8
600	8.2	2.8

6.2.3 Modulus of elasticity-compressive strength relationship

As presented in the literature review chapter (Section 2.2.5), Jones and McCarthy (2005) proposed a relationship linking the modulus of elasticity with the compressive strength of LFC (Equation 2.3) at ambient temperature. Although Equation 2.3 is considered applicable only for a minimum compressive strength of 5 N/mm^2, Figure 6.3 showed that the same modulus of elasticity-compressive strength relationship exists for LFC across the entire strength range.

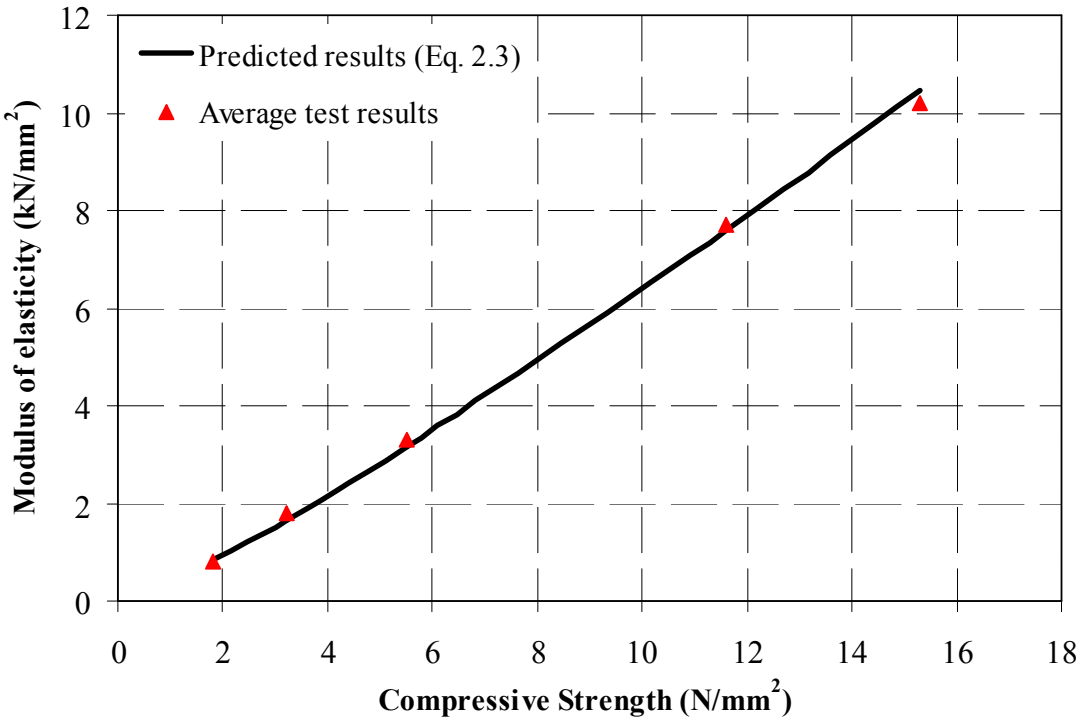

Figure 6.3 Modulus of elasticity-compressive strength relation for LFC at ambient temperature

6.2.4 Porosity-density relationship

Through using Equation 6.2 and Equation 6.3, it was possible to obtain an accurate assessment of the compressive strength and modulus of elasticity of LFC. Nevertheless, these models require input of the porosity value. Unfortunately, porosity was a property not frequently measured outside the laboratory, and therefore it is necessary to provide a model to obtain the porosity. The simplest method to calculate the porosity value was to relate it to LFC density. Since the pores inside LFC were created due to addition of

foams, by knowing the solid density of cement paste (without foam), one can easily predict the porosity of LFC of any other density using the following equation:

$$\varepsilon = \frac{\rho_{sc} - \rho_{dry}}{\rho_{sc}} \quad \ldots\ldots (6.4)$$

where ε is the porosity, ρ_{sc} is the solid density of cement paste (without foam) and ρ_{dry} is the dry density of LFC.

The accuracy of Equation 6.4 was checked by comparing the porosity values calculated using Equation 6.4 and the measured porosity values using the Vacuum Saturation Apparatus for different LFC densities, as shown in Figure 6.4. It should be noted that an average solid density of cement paste (ρ_{sc}) of 2100 kg/m^3 was established through the experiment. The agreement is excellent.

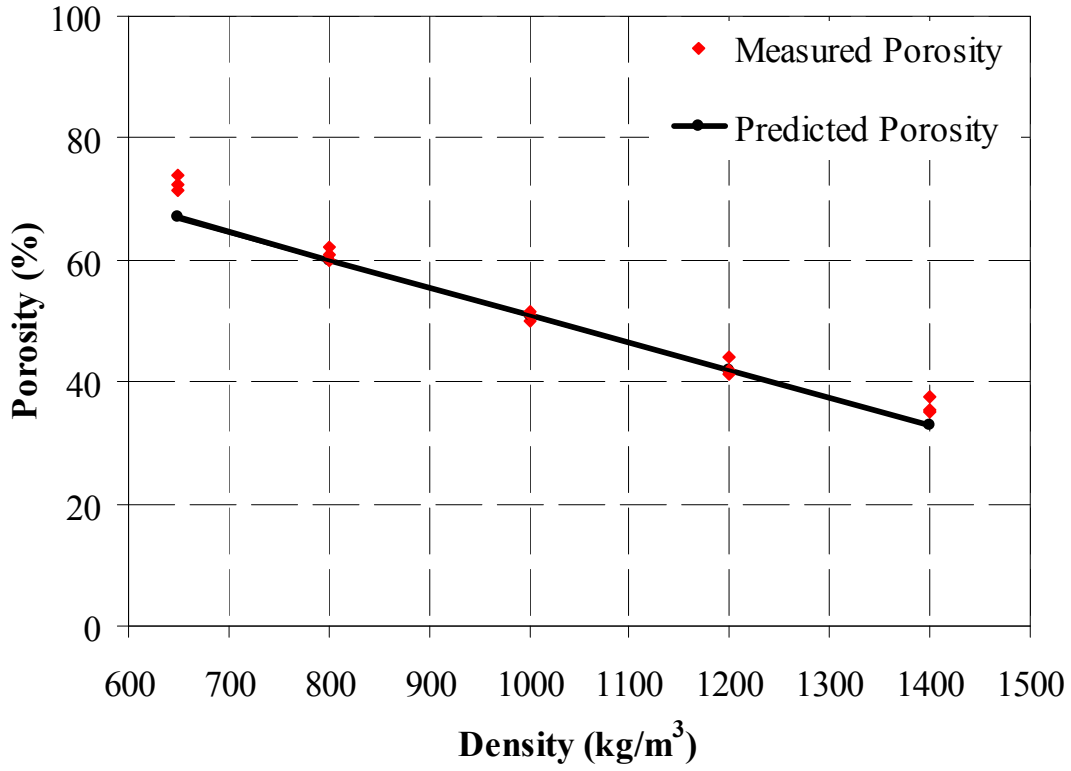

Figure 6.4 Comparison of predicted porosity with measured porosity as a function of density

6.3 PREDICTION OF MECHANICAL PROPERTIES OF LFC AT ELEVATED TEMPERATURES

As outlined in Section 2.4.2, a number of concrete mechanical property models have been proposed by others for normal weight concrete. This section was intended to assess the applicability of these models to LFC.

6.3.1 Compressive strength models for concrete at elevated temperatures

Several models have been proposed to estimate concrete compressive strength at high temperatures.

Li and Purkiss (2005) presented a review of the available models for the mechanical behaviour of concrete at elevated temperatures and provided comparisons between the existing models. Li and Purkiss (2005) suggested the following model to predict the compressive strength of concrete at elevated temperatures:

$$f_{cT} = f_c \cdot \left[0.00165 \cdot \left(\frac{T}{100} \right)^3 - 0.03 \cdot \left(\frac{T}{100} \right)^2 + 0.025 \cdot \left(\frac{T}{100} \right) + 1.002 \right] \quad \text{.....(6.5)}$$

where f_{cT} is the concrete compressive strength at elevated temperature, f_c is the concrete compressive strength at ambient temperature and T is temperature in ^{o}C.

The Eurocode 2 (2004) model is given below:

$$f_{cT} = f_c \qquad T \le 100°C \qquad \text{.....(6.6a)}$$

$$f_{cT} = f_c \cdot (1.067 - 0.00067 \cdot T) \qquad 100°C \le T \le 400°C \qquad \text{.....(6.6b)}$$

$$f_{cT} = f_c \cdot (1.44 - 0.0016 \cdot T) \qquad T \ge 400°C \qquad \text{.....(6.6c)}$$

Hertz (2005) in his study on concrete strength for fire safety design had derived an idealised data for the compressive strength of a number of concretes which included test series from more than 400 test comprising approximately 3000 specimens. The data covered a range of concretes with aggregates such as siliceous materials, limestone, granite, sea gravel, pumice, and expanded clay. He then proposed a model for

compressive strength of concrete at elevated temperatures that allowed for different types of aggregate to be differentiated as follows:

$$f_{cT} = f_c \cdot \left[\frac{1}{1 + \frac{T}{T_1} + \left(\frac{T}{T_2}\right)^2 + \left(\frac{T}{T_8}\right)^8 + \left(\frac{T}{T_{64}}\right)^{64}} \right] \text{.....(6.7)}$$

Assuming LFC as a type of lightweight aggregate concrete for application of Hertz's model, then T_1=100,000, T_2=1100, T_8=800 and T_{64}=940.

Figures 6.5 to 6.9 compare predictions of the above-mentioned models for all LFC densities at different temperatures against the experimental results from this study. As expected, the results showed that the Hertz (2005) model gave much higher results than the test results and was not appropriate for LFC. Both the Eurocode 2 (2004) and Li and Purkiss (2005) models seem to give good results and be suitable for LFC, with the Eurocode 2 predictions being slightly higher than the measured values.

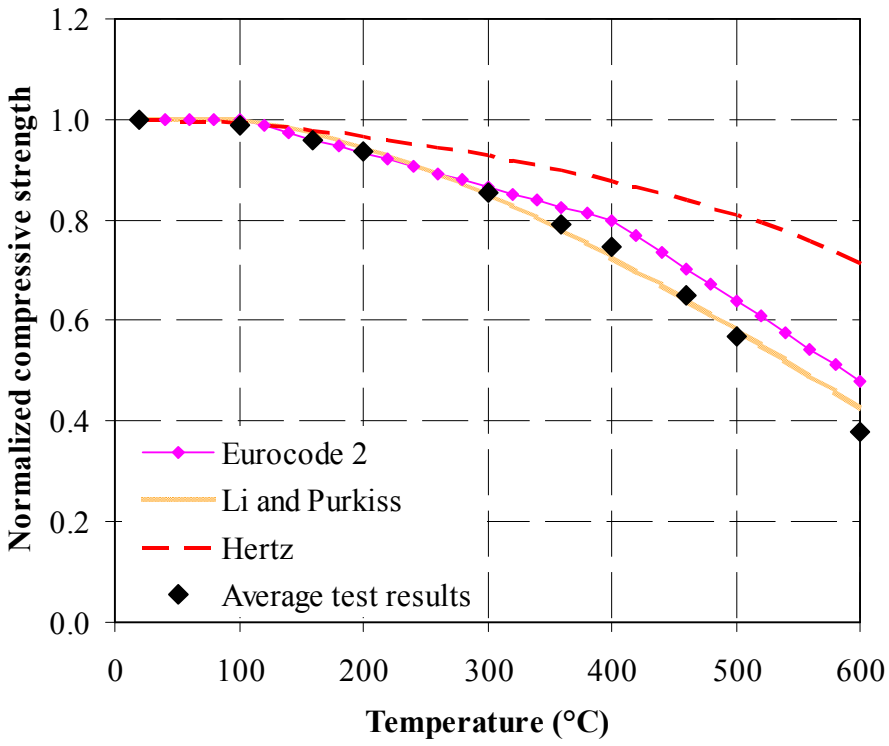

Figure 6.5 Comparison of normalized compressive strength-temperature relationships for 650 kg/m^3

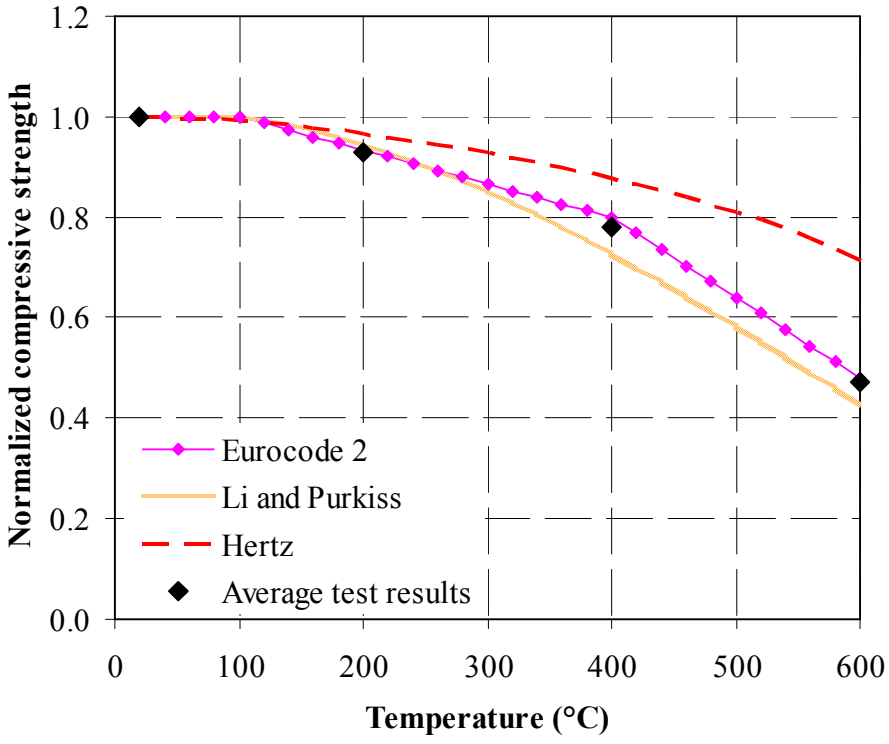

Figure 6.6 Comparison of normalized compressive strength-temperature relationships for 800 kg/m^3

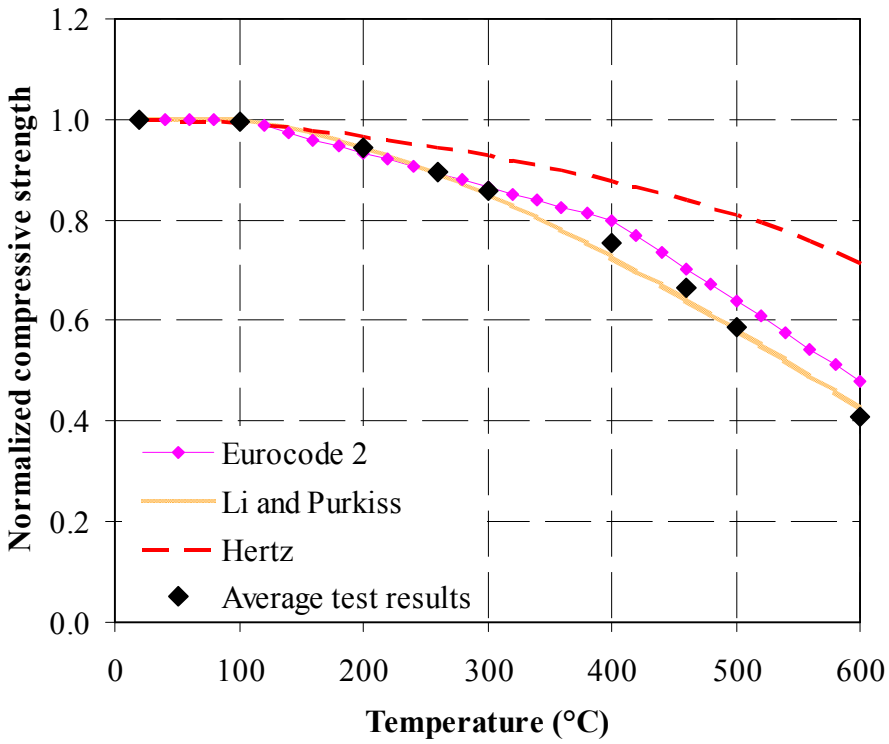

Figure 6.7 Comparison of normalized compressive strength-temperature relationships for 1000 kg/m^3

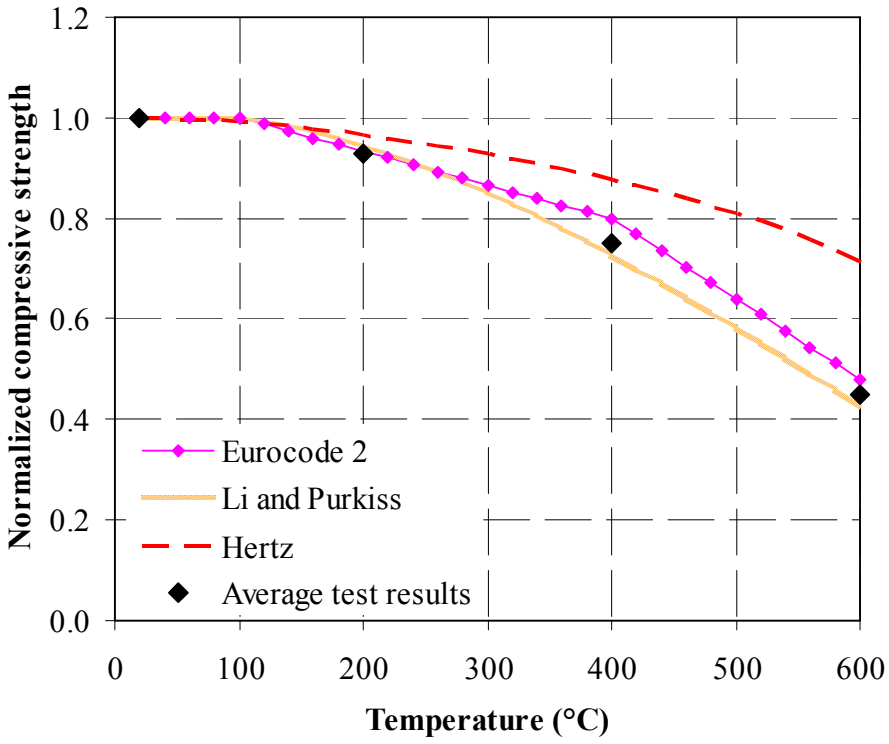

Figure 6.8 Comparison of normalized compressive strength-temperature relationships for 1200 kg/m^3

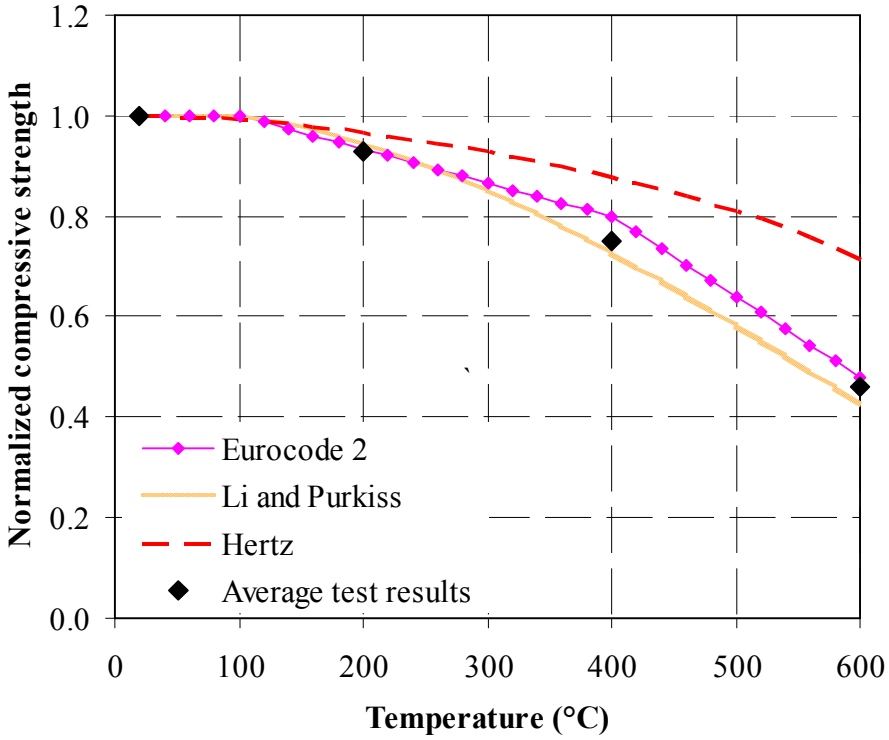

Figure 6.9 Comparison of normalized compressive strength-temperature relationships for 1400 kg/m^3

6.3.2 Models for modulus of elasticity of concrete at elevated temperatures

The elastic modulus of concrete would be affected primarily by the same factors influencing its compressive strength (Malhotra, 1982). Due to different definitions of modulus of elasticity and the difficulty of precisely calculating this value, it was not surprising that previous researchers have revealed great disparity in the experimental results. In this research, the modulus of elasticity was calculated as the secant modulus corresponding to 0.75 ultimate stress. The following models were considered.

Lu (1989), in his study on fire response of reinforced concrete beams, performed an unstressed test procedure to establish the modulus of elasticity of concrete when exposed to high temperatures. He proposed the following tri-linear expression between E_{cT} and T:

$$E_{cT} = (1 - 0.0015 \cdot T) \cdot E_c \qquad 20°C \le T \le 200°C \qquad \text{.....(6.8a)}$$

$$E_{cT} = (0.87 - 0.00084 \cdot T) \cdot E_c \qquad 200°C \le T \le 700°C \qquad \text{.....(6.8b)}$$

$$E_{cT} = 0.28 \cdot E_c \qquad T \ge 700°C \qquad \text{.....(6.8c)}$$

where E_{cT} and E_c are the modulus of elasticity of concrete at elevated and room temperature, respectively.

Li and Guo (1993) carried out an experimental investigation on strength and deformation of concrete under high temperature. They proposed a bi-linear model to predict the modulus of elasticity of concrete as given below:

$$E_{cT} = E_c \qquad 20°C \le T \le 60°C \qquad \text{.....(6.9a)}$$

$$E_{cT} = (0.83 - 0.0011 \cdot T) \cdot E_c \qquad 60°C \le T \le 700°C \qquad \text{.....(6.9b)}$$

The Eurocode 2 (2004) model did not explicitly give variation of modulus as a function of temperature. However, the compressive modulus may be calculated using the following equation:

$$E_{cT} = \frac{1.5 f_{cT}}{\varepsilon_{oT}} \qquad \text{.....(6.10)}$$

where f_{ct} is the peak stress and ε_{oT} is the strain at peak stress.

As will be shown later in Section 6.3.3, the strains at peak stress from Eurocode 2 (2004) did not agree with the measured values of this research. Therefore, the measured strains will be used in this assessment. This means that this exercise was not predictive, but merely to check whether Equation 6.10 is applicable.

Li and Purkiss (2005) developed a prediction model for modulus of elasticity of concrete based on published experimental data (Purkiss, 1996) and the data published

in Eurocode 2 (2004). They defined the elastic modulus as the initial tangent modulus and gave the following relationships:

$$E_{cT} = E_c \qquad T \le 60°C \qquad \text{.....(6.11a)}$$

$$E_{cT} = \frac{800 - T}{740} \cdot E_c \qquad 60°C \le T \le 800°C \qquad \text{.....(6.11b)}$$

Khennane and Baker (1993) in their research on concrete behavior under variable temperature and stress presented a plasticity model using a strain-rate formulation to depict the uniaxial response of concrete when subjected to combined thermal and mechanical actions and they proposed the following equation:

$$E_{cT} = (-0.001282 \cdot T + 1.025641) \cdot E_c \qquad 20°C \le T \le 800°C \qquad \text{.....(6.12)}$$

Figures 6.10 to 6.14 compare predictions of the various models with the test results for all densities at different temperatures. Except for the Lu (1989) and the Li and Guo (1993) models, all the other models give good predictions of the test results, particularly considering the relatively wide scatter of experimental results reported in literature. In conjunction with the conclusion drawn in the last section for compressive strength, both the Eurocode 2 (2004) and the Li and Purkiss (2005) models may be used. However, as previously mentioned, using the equation of Eurocode 2 (2004) was predicated on the assumption that an independent means of obtaining the strains at peak stresses can be established.

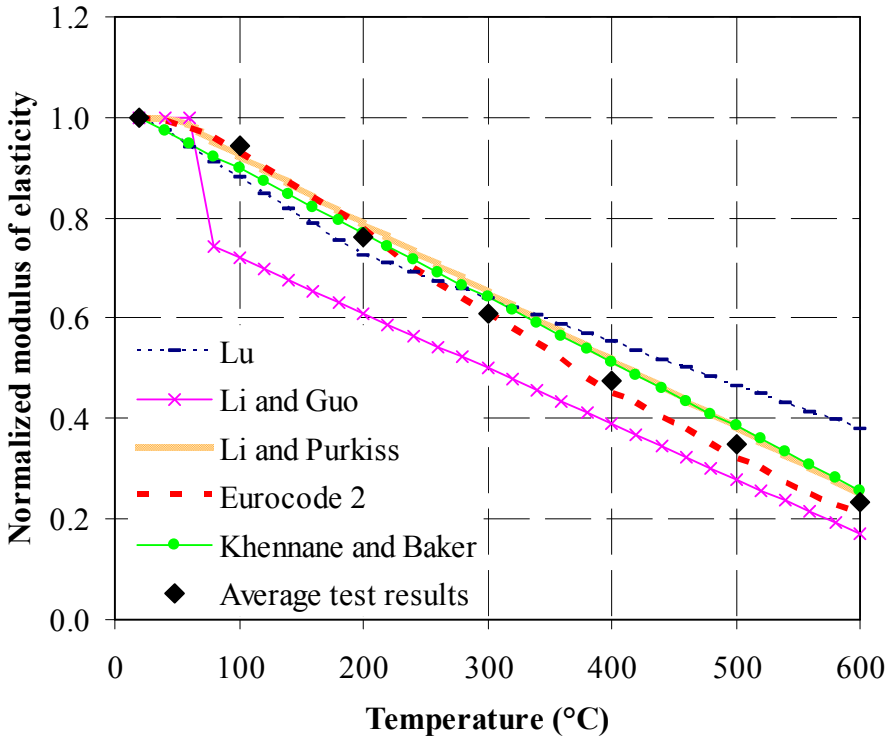

Figure 6.10 Comparison of normalized elastic modulus-temperature relationships for 650 kg/m^3

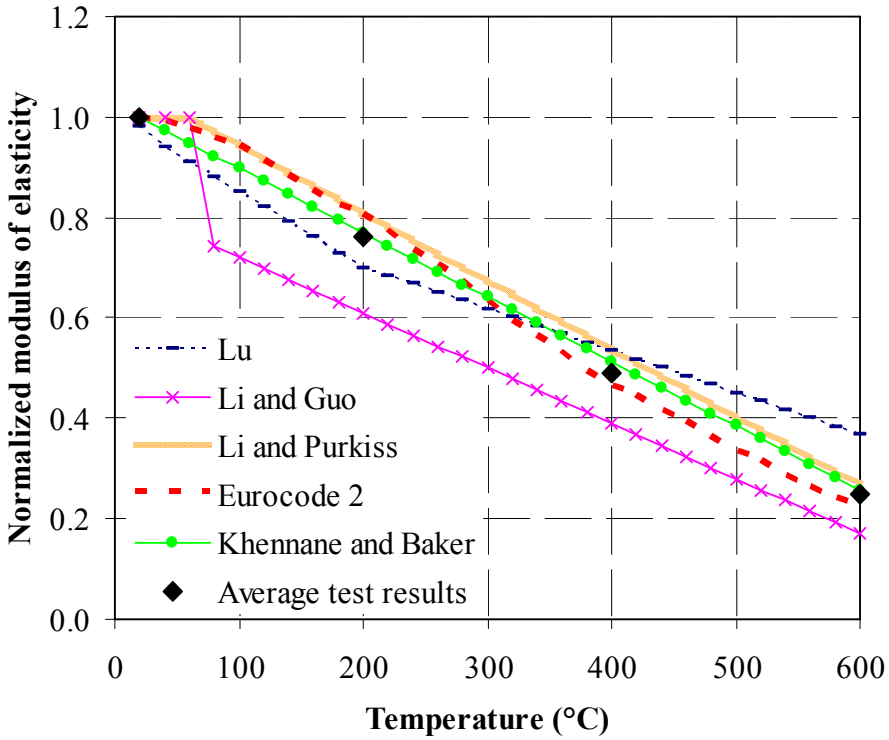

Figure 6.11 Comparison of normalized elastic modulus-temperature relationships for 800 kg/m^3

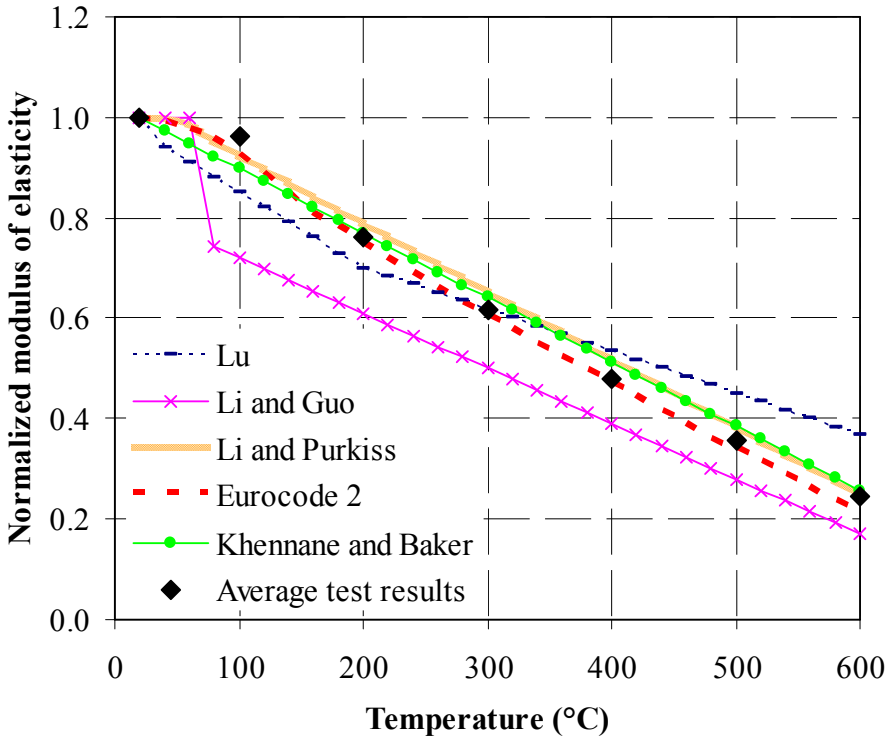

Figure 6.12 Comparison of normalized elastic modulus-temperature relationships for 1000 kg/m^3

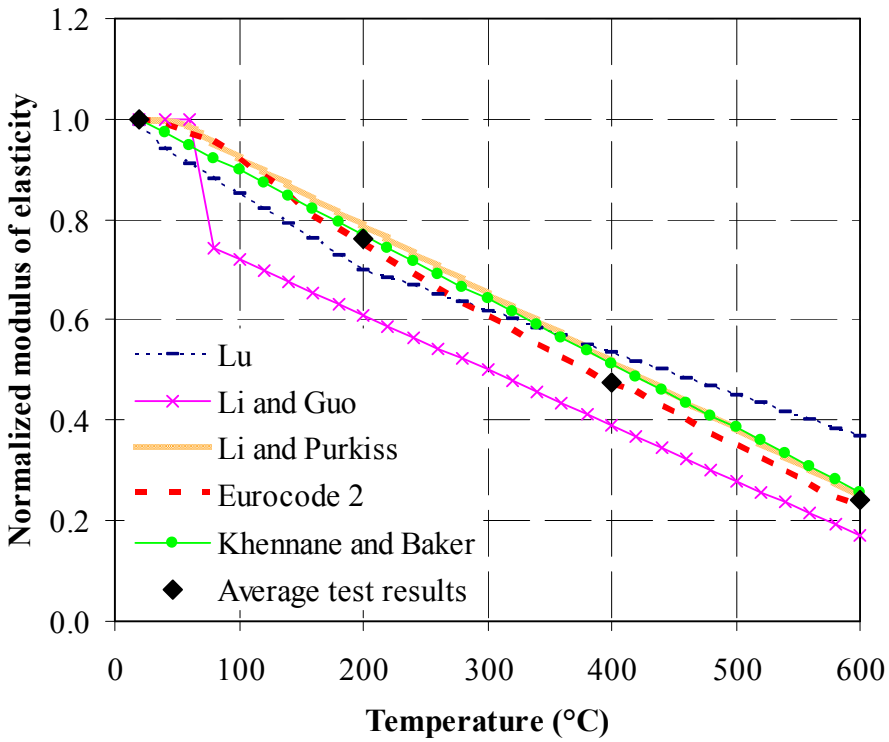

Figure 6.13 Comparison of normalized elastic modulus-temperature relationships for 1200 kg/m^3

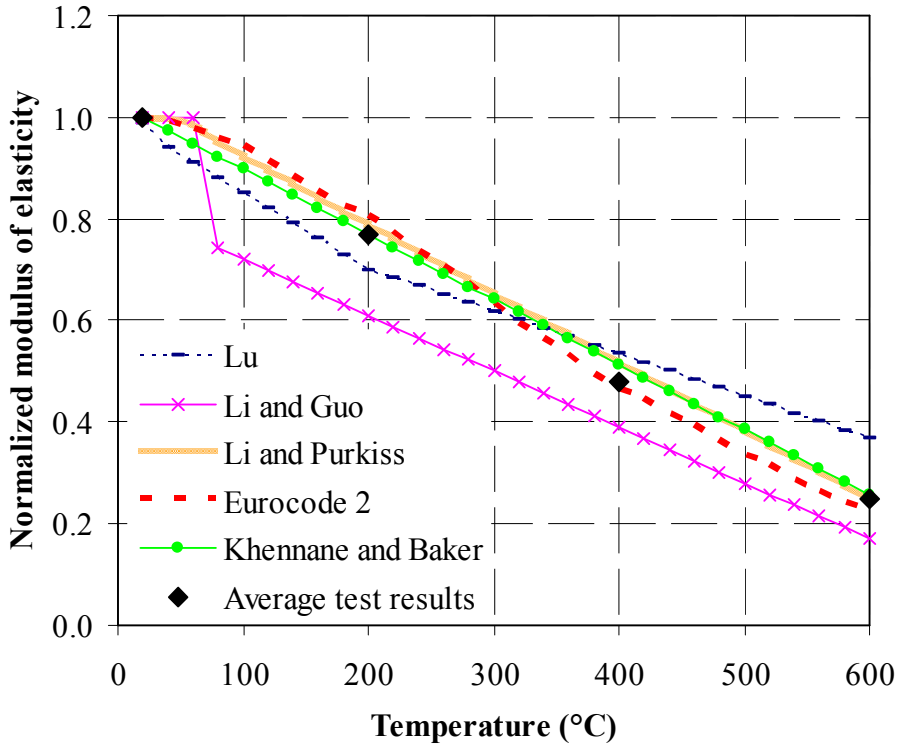

Figure 6.14 Comparison of normalized elastic modulus-temperature relationships for 1400 kg/m^3

6.3.3 Strain at peak compressive stress

For predicting LFC strain at the maximum compressive stress (ε_{oT}), the following models may be considered in regards to the models for cases where concrete specimens were not loaded during the heating process.

i.) ***Anderberg and Thelandersson*** **(1976)**

$$\varepsilon_{oT} = (0.00000167 \cdot T) + 0.002666 \qquad T \le 800°C \qquad \text{.....(6.13)}$$

ii.) ***Khennane and Baker*** **(1993)**

$$\varepsilon_{oT} = 0.003 \qquad 20°C \le T \le 200°C \qquad \text{.....(6.14a)}$$

$$\varepsilon_{oT} = (0.00001156 \cdot T) + 0.000686 \qquad T \ge 200°C \qquad \text{.....(6.14b)}$$

***iii.) Bazant and Chern* (1987)**

$$\varepsilon_{oT} = (0.0000064 \cdot T) - 0.00216 \qquad 20°C \le T \le 600°C \qquad \text{…..(6.15)}$$

***iv.) Li and Purkiss* (2005)**

$$\varepsilon_{oT} = \frac{2 \cdot f'_c}{E_c} + 0.21 \times 10^{-4} \cdot (T - 20) - 0.9 \times 10^{-8} \cdot (T - 20)^2 \qquad \text{…..(6.16)}$$

***v.) Eurocode 2* (2004)**

The Eurocode 2 relationship is reproduced in Table 6.3

Table 6.3 Temperature dependence of the strain at the peak stress point (Eurocode 2, 2004)

Temperature (°C)	Strain corresponding to peak stress
0	0.0025
100	0.0040
200	0.0055
300	0.0070
400	0.0100
500	0.0150
600	0.0250
700	0.0250
800	0.0250
900	0.0250
1000	0.0250

Figure 6.15 provides a comparison of the above-mentioned prediction models with the average test results for the two densities at different temperatures. It was clear from Figure 6.15 that the Eurocode 2 (2004) model appears to give the worst prediction. The model of Li and Purkiss (2005) provides the upper bound for ε_{oT} and the model of Anderberg and Thelandersson (1976) provided the lower bound. The results of the three

remaining models gave close agreement with the experimental results. Out of all the models, the Bazant and Chern (1987) prediction appeared to give the best agreement with these experimental results.

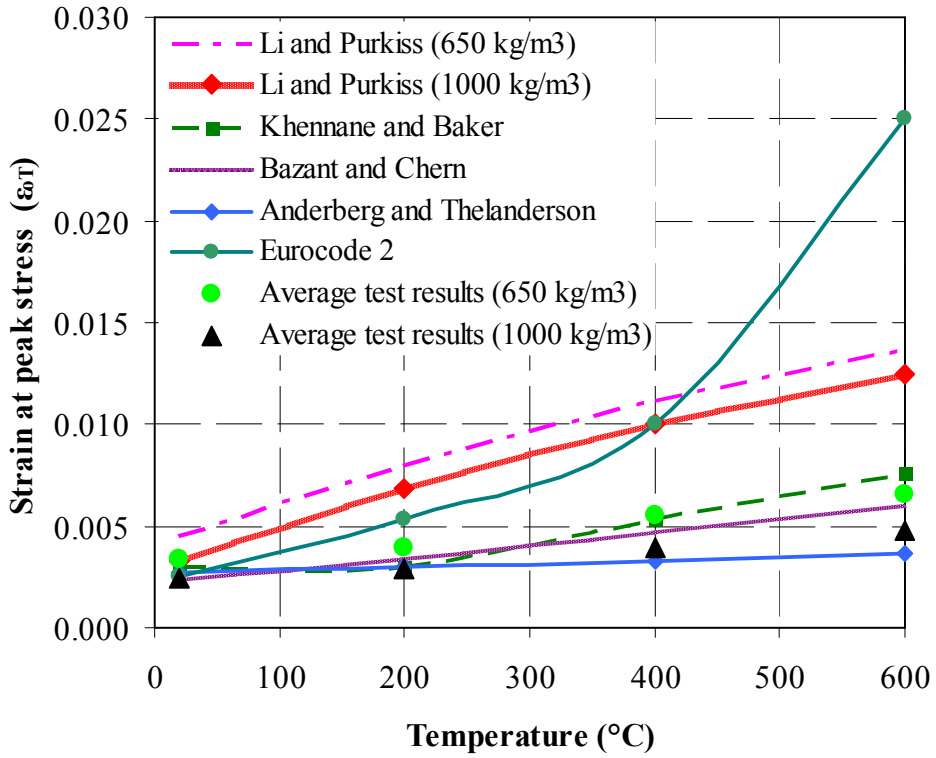

Figure 6.15 Comparison of strain at maximum stress-temperature relationships

Although the Eurocode 2 values of strain at peak stress cannot be used for LFC, the Eurocode 2 equation (Equation 6.10) does reveal that the strain at peak stress is simply 1.5 times the elastic strain at peak stress. In fact, based on the experimental results of this research, the strain at peak stress is about 1.78 times the elastic strain at peak stress.

For analysis of structural behaviour of LFC, it is more important to correctly predict the modulus of elasticity than the strain at peak stress. Therefore, this research recommends using the Li and Purkiss equation (Equation 6.11) to directly predict the modulus of elasticity change as a function of temperature. Using the Eurocode 2 model (Equation 6.6) for prediction of LFC strength at different temperatures and applying the constant ratio of 1.78 as obtained from this research, the variable LFC strain at peak stress for different densities can be obtained as a function of temperature.

Figure 6.16 compares the calculated strain at peak stress values with measured strain at peak stress values for both densities at different temperatures. The agreement is excellent.

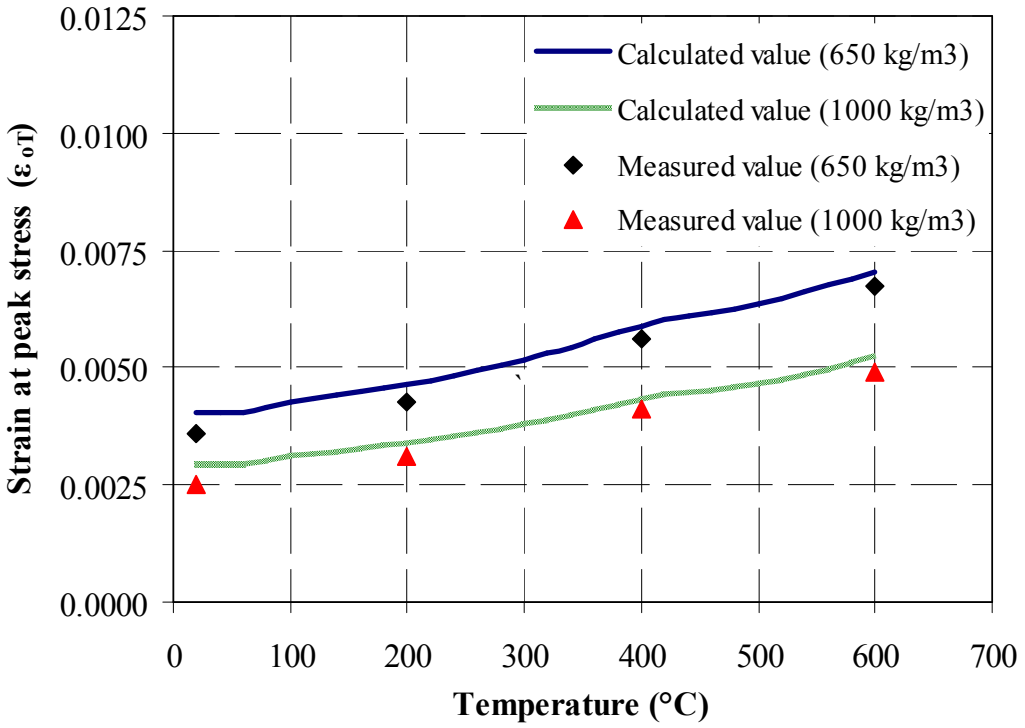

Figure 6.16 Comparison of calculated and measured strain at peak stress values for 650 and 1000 kg/m^3 densities at different temperatures

6.3.4 Stress-strain relationship of concrete exposed to elevated temperatures

The three models which will be considered for the stress-strain relationship of LFC were the Anderberg and Thelandersson (1976) model, Lie and Lin (1985) model and the Eurocode 2 (2004) model.

i.) Anderberg and Thelandersson model (1976)

This model was based on transient tests and the ascending compressive part of the relationship is:

$$f'_{cT} = E_{cT} \cdot \left[\varepsilon_{cT} - \frac{\varepsilon_{cT}^2}{2 \cdot \varepsilon_{oT}} \right] \text{.....(6.17)}$$

where E_{cT} is the modulus of elasticity of concrete at elevated temperature.

ii.) Lie and Lin model (1985)

This model includes an ascending and a descending branch. However, since only the ascending branch of LFC stress-strain relationship could be obtained, only the ascending branch equation will be given, which was as follows.

$$f'_{cT} = f_{cT} \cdot \left[1 - \left(\frac{\varepsilon_{oT} - \varepsilon_{cT}}{\varepsilon_{oT}} \right)^2 \right] \qquad \varepsilon_{cT} \le \varepsilon_{oT} \quad \text{.....(6.18)}$$

where f'_{cT} is the concrete compressive stress at elevated temperature, f_{cT} is the concrete compressive strength at elevated temperature, ε_{cT} is the concrete strain at elevated temperature and ε_{oT} is the strain at the maximum concrete stress.

iii.) Eurocode 2 model (2004)

The Eurocode 2 equation is:

$$f'_{cT} = \frac{3\varepsilon_{cT} f_{cT}}{\varepsilon_{oT}\left(2 + \left(\frac{\varepsilon_{cT}}{\varepsilon_{oT}} \right)^3 \right)} \quad \text{...(6.19)}$$

All three models require input of the LFC peak stress (f_{cT}) and strain at peak stress (ε_{cT}). For this exercise, the measured values were used so that this comparison does suffer from any inaccuracy in prediction of these input values.

Figures 6.17(a-d) and 6.18(a-d) compare predictions of the different models with the average test results for the two densities at different temperatures (ambient, 200°C, 400°C and 600°C). It should be pointed out that when using the Eurocode 2 model (Equation 6.19), the calculated strain at peak stress was used. Except for the Anderberg and Thelandersson (1976) model, Lie and Lin (1985) and Eurocode 2 (2004) model were almost identical and in good agreement with the experimental results for all densities at different temperatures.

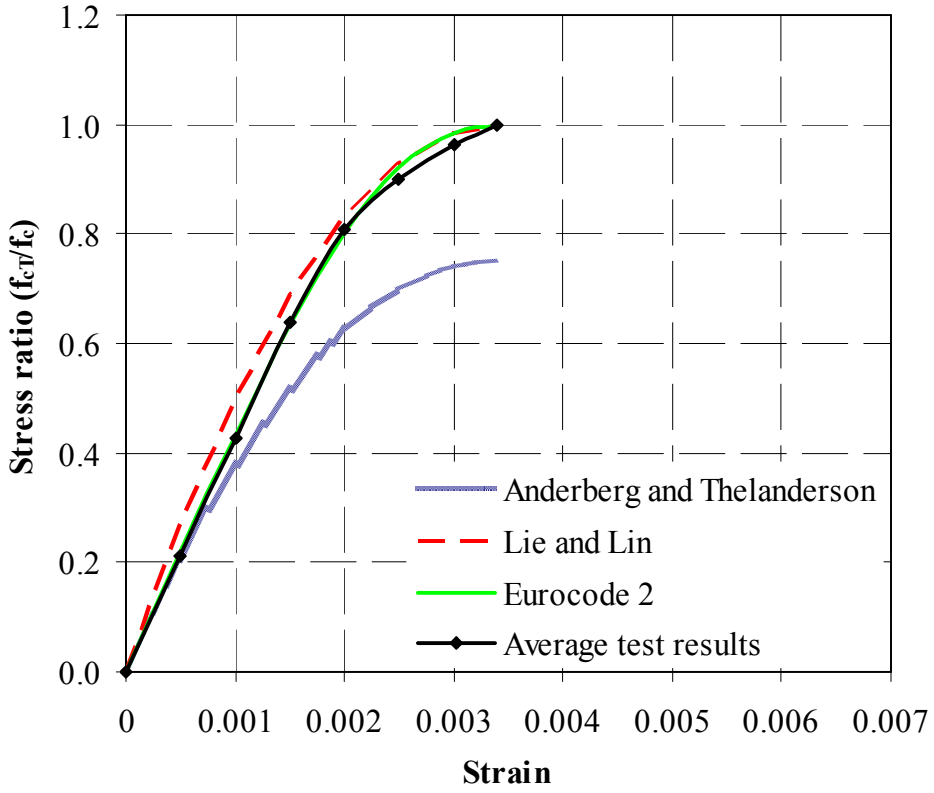

Figure 6.17(a) Stress-strain curves for 650 kg/m^3 density at ambient temperature

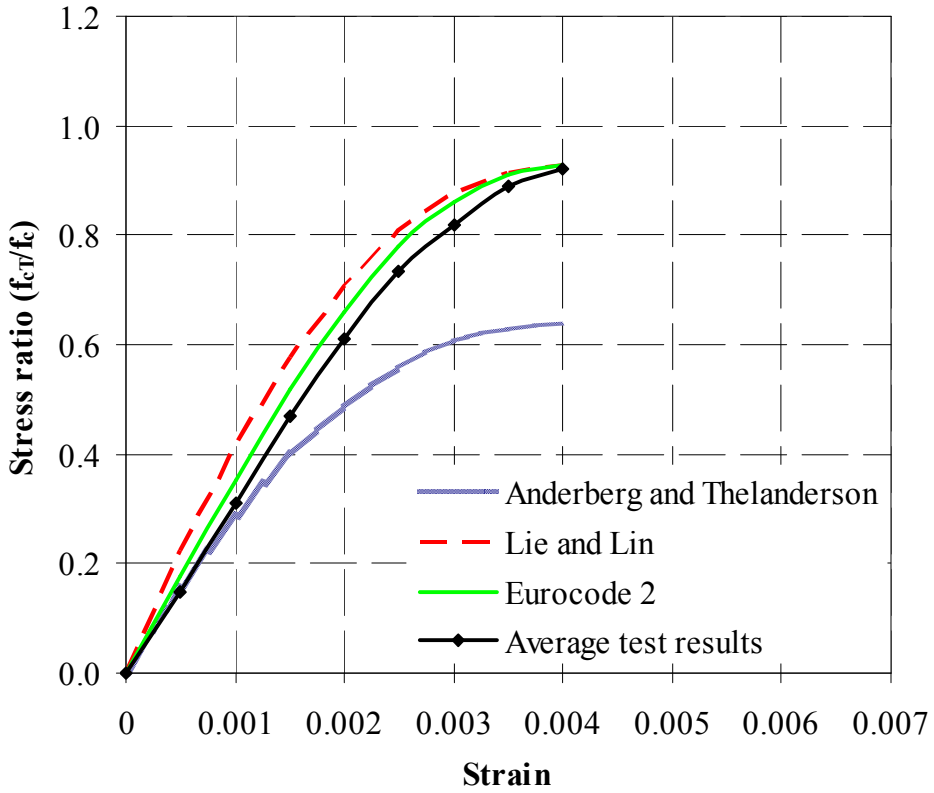

Figure 6.17(b) Stress-strain curves for 650 kg/m^3 density at 200°C

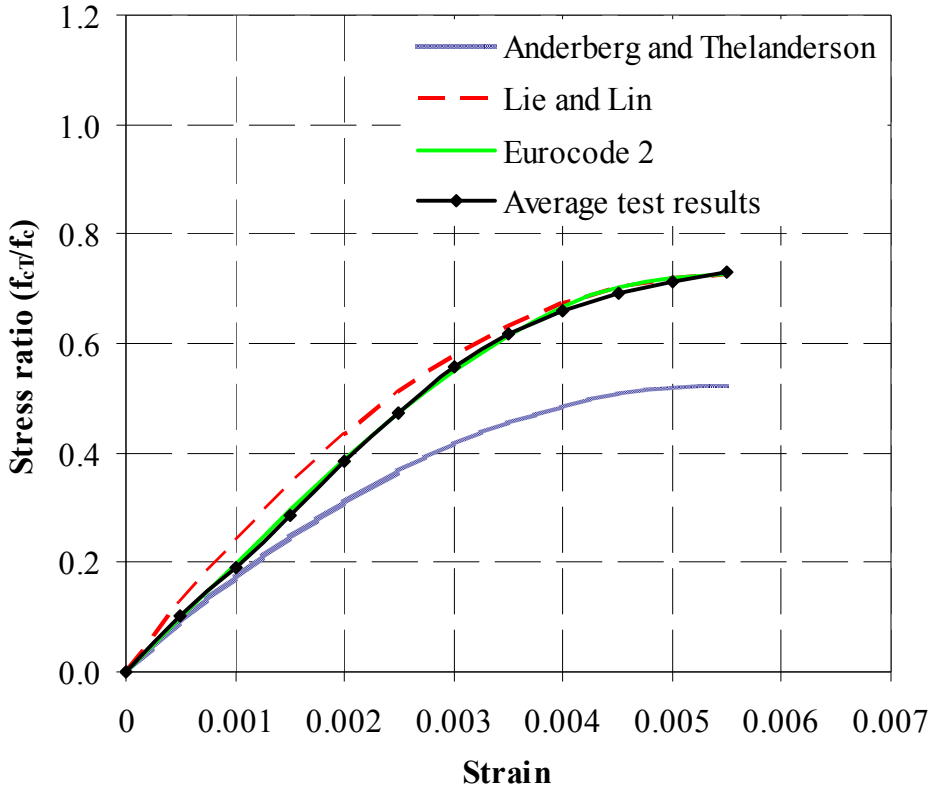

Figure 6.17(c) Stress-strain curves for 650 kg/m^3 density at 400°C

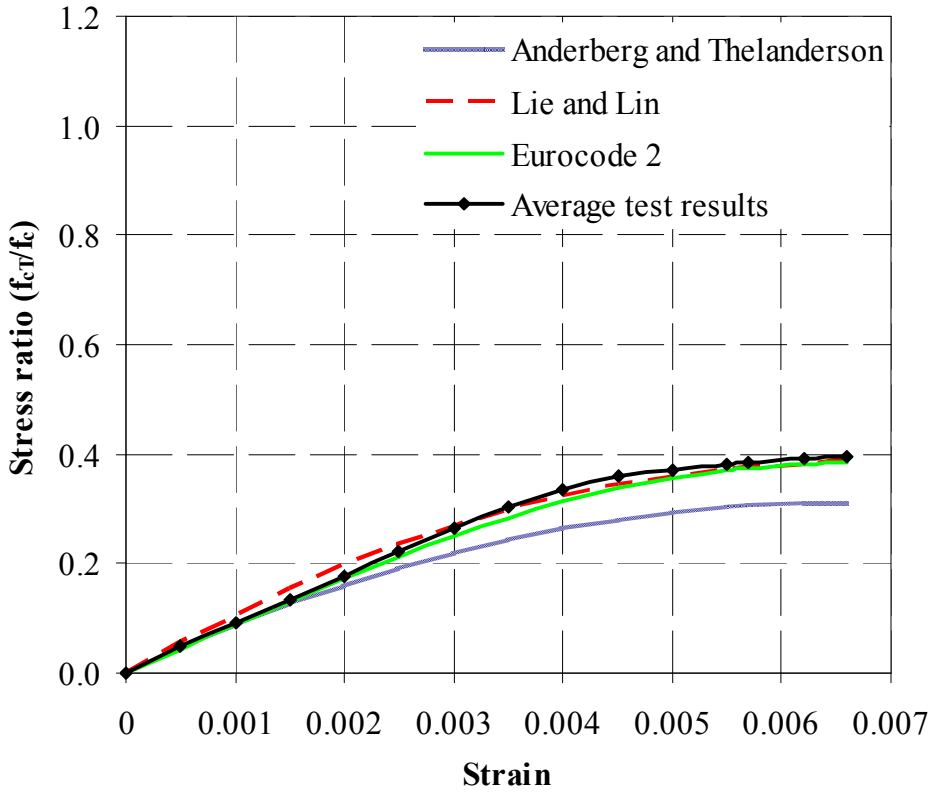

Figure 6.17(d) Stress-strain curves for 650 kg/m^3 density at 600°C

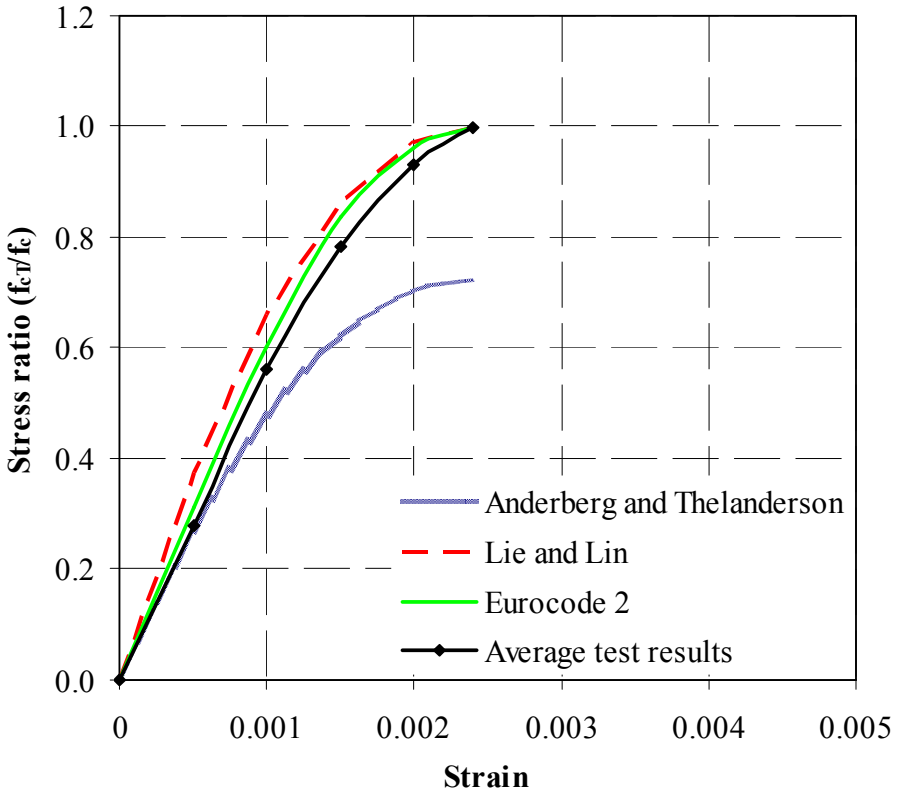

Figure 6.18(a) Stress-strain curves for 1000 kg/m^3 density at ambient temperature

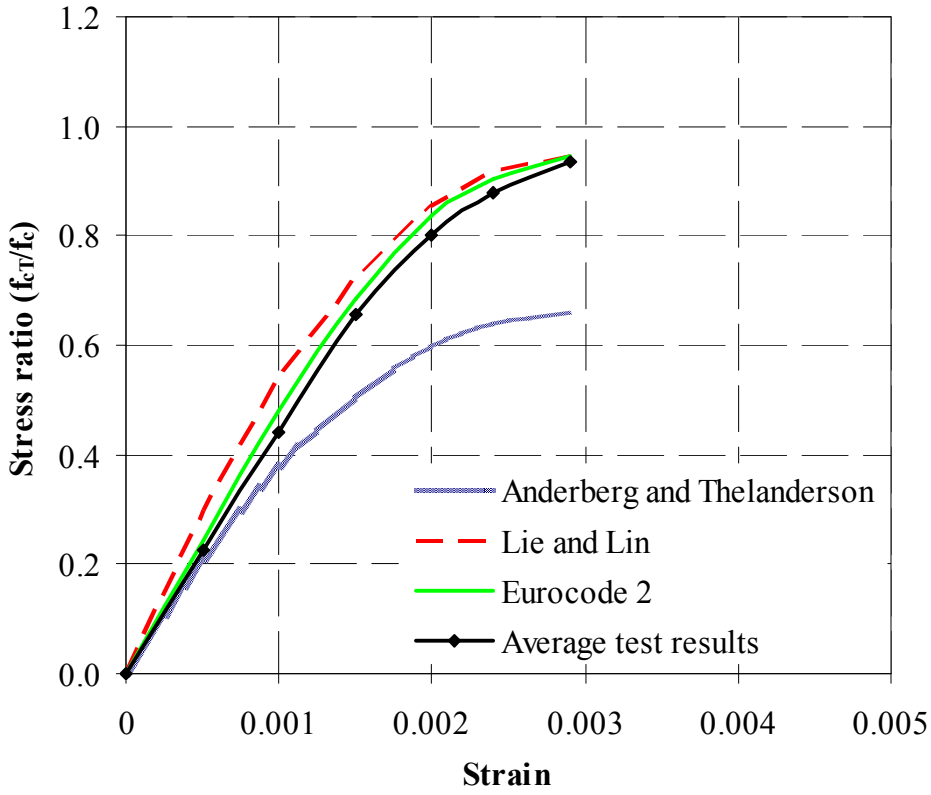

Figure 6.18(b) Stress-strain curves for 1000 kg/m^3 density at 200°C

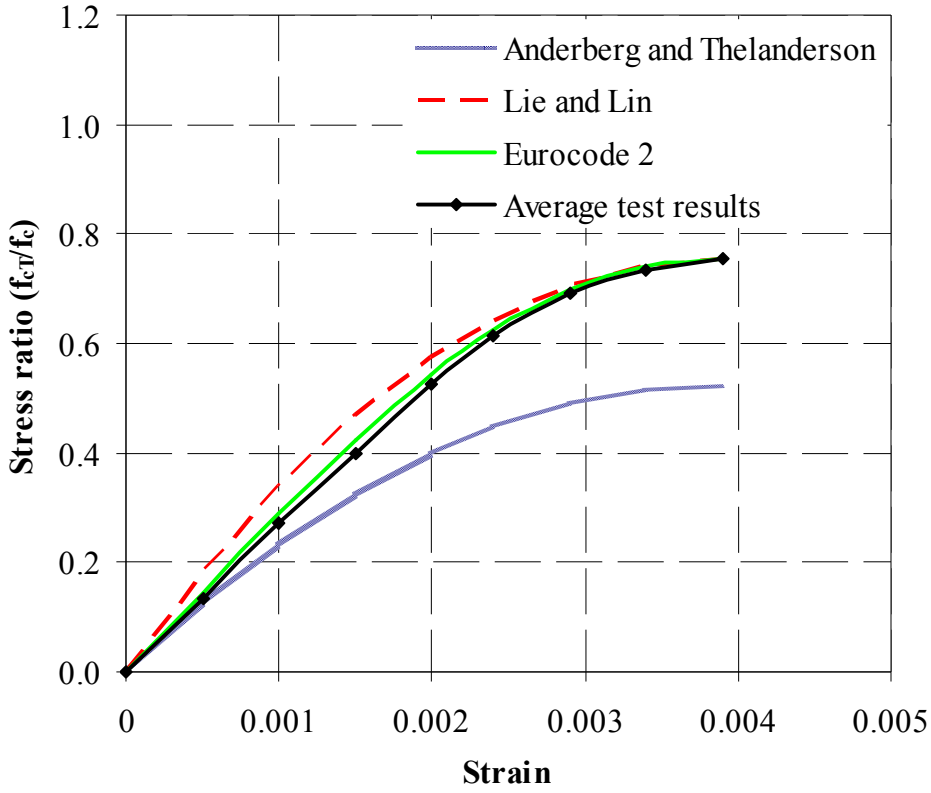

Figure 6.18(c) Stress-strain curves for 1000 kg/m^3 density at 400°C

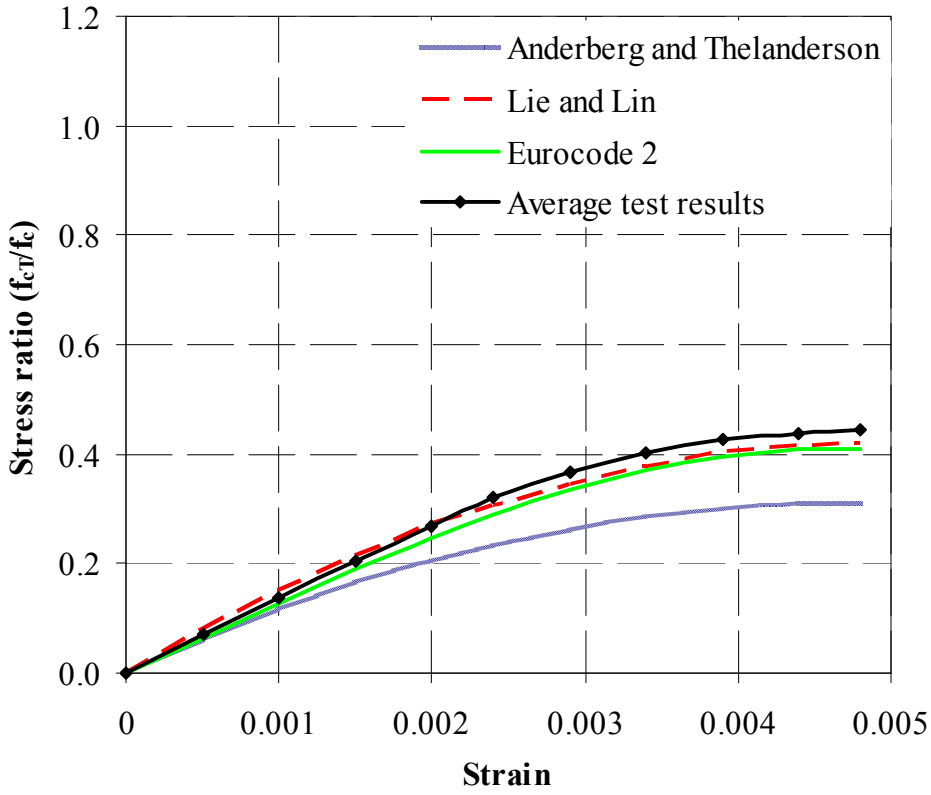

Figure 6.18(d) Stress-strain curves for 1000 kg/m^3 density at 600°C

Since the Eurocode 2 (2004) model is well established and accepted for use in fire engineering design of concrete structures, the author suggests adopting the Eurocode 2 (2004) model.

6.3.5 Flexural tensile strength of concrete exposed to elevated temperatures

There was very limited research related to tensile strength of concrete at elevated temperatures. Nevertheless, a few researchers such as Anderberg and Thelandersson (1976), Li and Guo (1993) and Terro (1998) have proposed prediction equations.

The Anderberg and Thelandersson (1976) model was:

$$f_{crT} = f_{cr} \cdot (-0.000526 \cdot T + 1.01052) \qquad 20°C \le T \le 400°C \quad \text{.....(6.20a)}$$

$$f_{crT} = f_{cr} \cdot (-0.0025 \cdot T + 1.8) \qquad 400°C \le T \le 600°C \quad \text{.....(6.20b)}$$

$$f_{crT} = f_{cr} \cdot (-0.0005 \cdot T + 06) \qquad 600°C \le T \le 1000°C \quad \text{.....(6.20c)}$$

where f_{crT} and f_{cr} are the tensile strength of concrete at elevated temperature and ambient temperature respectively and T is temperature in ^{o}C.

Li and Guo (1993) suggested the following equation based on the experimental results for tensile strength of concrete under high temperatures:

$$f_{crT} = f_{cr} \cdot (1 - 0.001 \cdot T) \qquad 20°C \le T \le 1000°C \quad \text{.....(6.21)}$$

Terro (1998) performed a numerical modeling of the behavior of concrete structures under fire condition and make recommendation as follows:

$$f_{crT} = f_{cr} \cdot \frac{f_{cT}}{f_c} \quad \text{.....(6.22)}$$

where f_{cT} is the concrete compressive strength at elevated temperature, f_c is the concrete compressive strength at ambient temperature.

Eurocode 2 (2004) gives:

$$f_{crT} = f_{cr} \qquad 20°C \le T \le 100°C \qquad \text{.....(6.23a)}$$

$$f_{crT} = f_{cr} \cdot (-0.002 \cdot T + 1.2) \qquad 100°C \le T \le 600°C \qquad \text{.....(6.23b)}$$

Figures 6.19 and 6.20 compare the predictions of the aforementioned models for LFC density of 650 kg/m^3 and 1000 kg/m^3 at different temperatures against the experimental results from this study. It is clear that the model of Anderberg and Thelandersson (1976) and Terro (1998) provide the upper bound for f_{ctT}, while the model of Li and Gao (1993) provides the lower bound for both densities. The Eurocode 2 (2004) model did not seem to fit well with the experimental results. Overall, the model proposed by Li and Gao (1993) seemed to provide the best agreement with the experimental results.

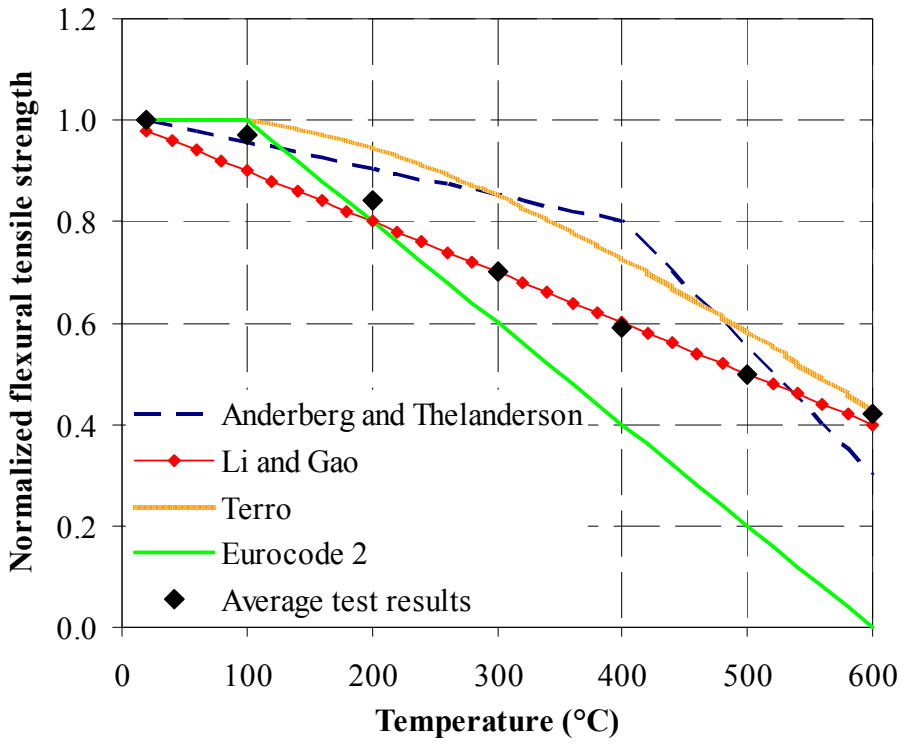

Figure 6.19 Comparison of flexural tensile strength-temperature relationships for 650 kg/m^3

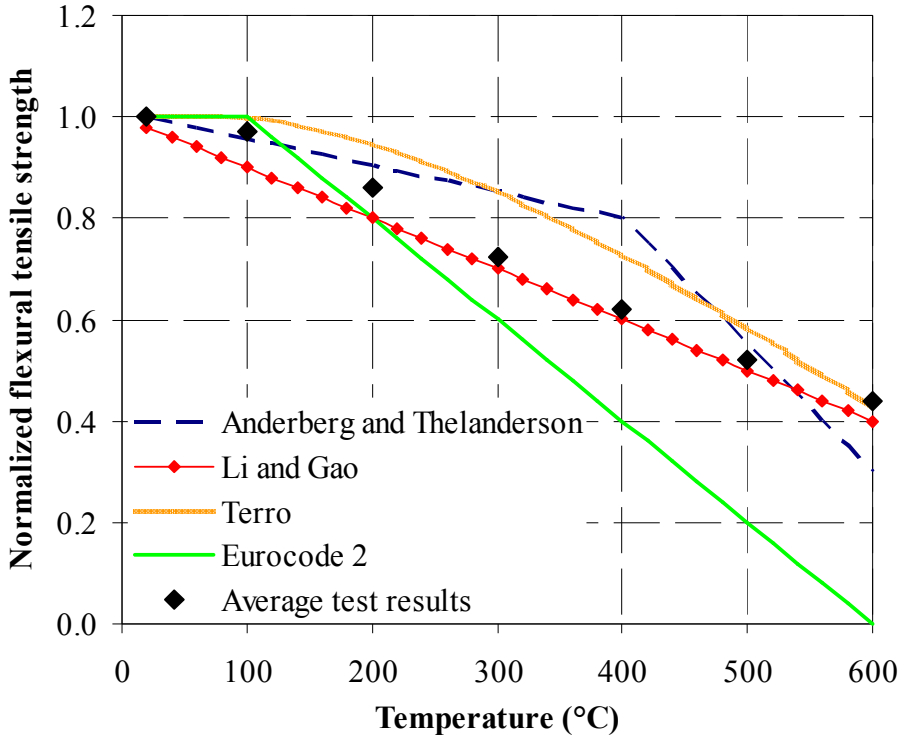

Figure 6.20 Comparison of flexural tensile strength-temperature relationships for 1000 kg/m^3

6.3.6 Procedure

The mechanical properties of LFC that influence the stress–strain relationship were the LFC strength, initial modulus of elasticity and strain at maximum stress. They experience significant changes at elevated temperatures. The LFC strength and initial modulus of elasticity decrease, while the absolute value of the strain at peak stress increases.

After a comprehensive assessment of all existing mechanical property predictive models, the following procedure may be used to predict the mechanical properties of LFC at high temperatures:

1. Obtaining dry density (ρ_{dry}) of LFC

2. Obtaining the solid density of cement paste (without foam) and then calculate the porosity (ε) of LFC using Equation 6.4.

3. Calculating the ambient temperature compressive strength (f_c) and modulus of elasticity (E_c) of LFC using Equation 6.2 and Equation 6.3 respectively. Values of 39.2 N/mm^2 and n=2.4 for the compressive strength and 32.9N/mm^2 and n=2.8 for the compressive modulus of elasticity should be used.

4. Eurocode 2 model (Equation 6.6) to calculate LFC compressive strength (f_{cT}) at high temperatures was used.

5. Calculating LFC modulus of elasticity (E_{cT}) at high temperatures using the Li and Purkiss model (Equation 6.11).

6. Multiplying the elastic strain at peak stress by 1.78 to give the strain at peak stress.

7. Using the Eurocode 2 equation (Equation 6.19) to calculate and plot the stress-strain relationship of LFC.

8. Calculating the tensile strength of LFC using the equation (Equation 6.21) of Li and Guo (1993).

6.4 PROPOSED PROCEDURE USING COMBINED MODEL

The above procedure has been implemented for all the tests carried out in this study. This section presents detailed comparison between the predicted stress-strain relationships using the above procedure and the experimental results. Figures 6.21(a-e) showed the comparison between the predicted stress-strain relationships using the proposed procedure and the average experimental results of different densities (650 kg/m^3 to 1400 kg/m^3) at different temperatures. Shown in these figures were also predicted stress-strain relationships if the measured ambient temperature strength and modulus of elasticity values were used instead of using the proposed strength-porosity (Equation 6.2) and modulus of elasticity-porosity (Equation 6.3) relationships. Overall the agreement was good, demonstrating the feasibility of using the proposed procedure to predict the mechanical properties of LFC of different densities at different temperatures by only knowing one single value of dry density (ρ_{dry}) of LFC. However, there was some inaccuracy in the stress-strain relationships using the proposed

procedure which was primarily a result of some inaccuracy in the proposed strength - porosity and modulus of elasticity – porosity relationships at ambient temperature. These figures showed that if the measured strength and modulus of elasticity were used, the predicted stress-strain relationships were in very close agreement with the test results. Therefore, it was recommended that ambient temperature mechanical tests should still be carried out to obtain the strength and modulus of elasticity values, rather than relying on the strength-porosity and modulus of elasticity-porosity models. The other high temperature mechanical property models (compressive strength ratio – temperature relationship, modulus of elasticity ratio – temperature relationship, strain at peak stress and stress-strain relationship) gave very accurate results.

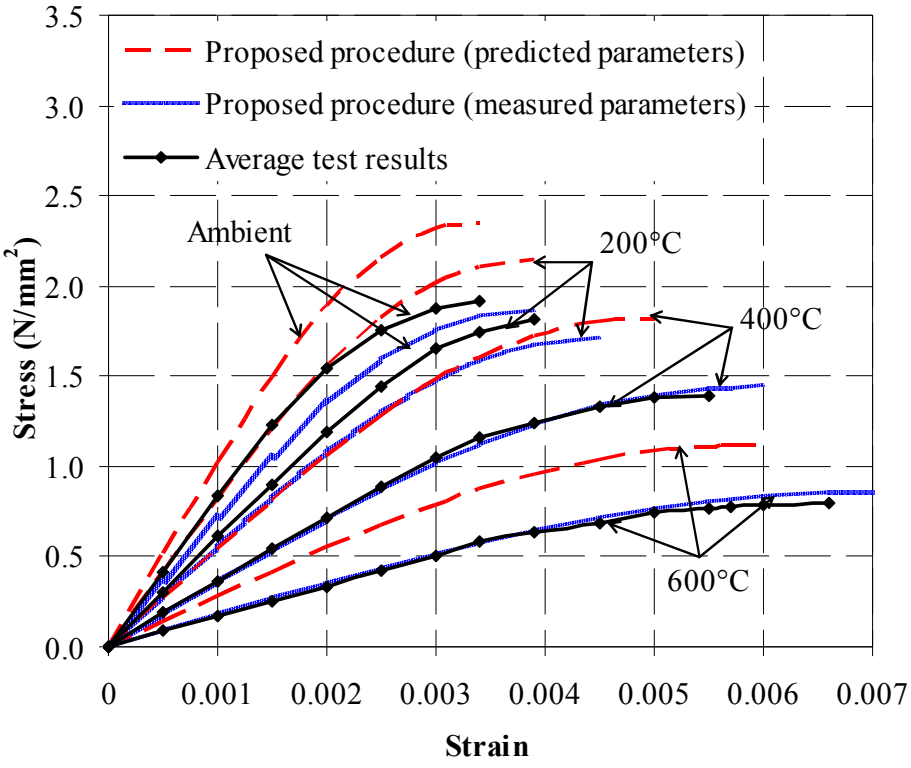

Figure 6.21(a) Comparison between the predicted stress-strain relationships using the proposed procedure and the average experimental results for 650 kg/m^3

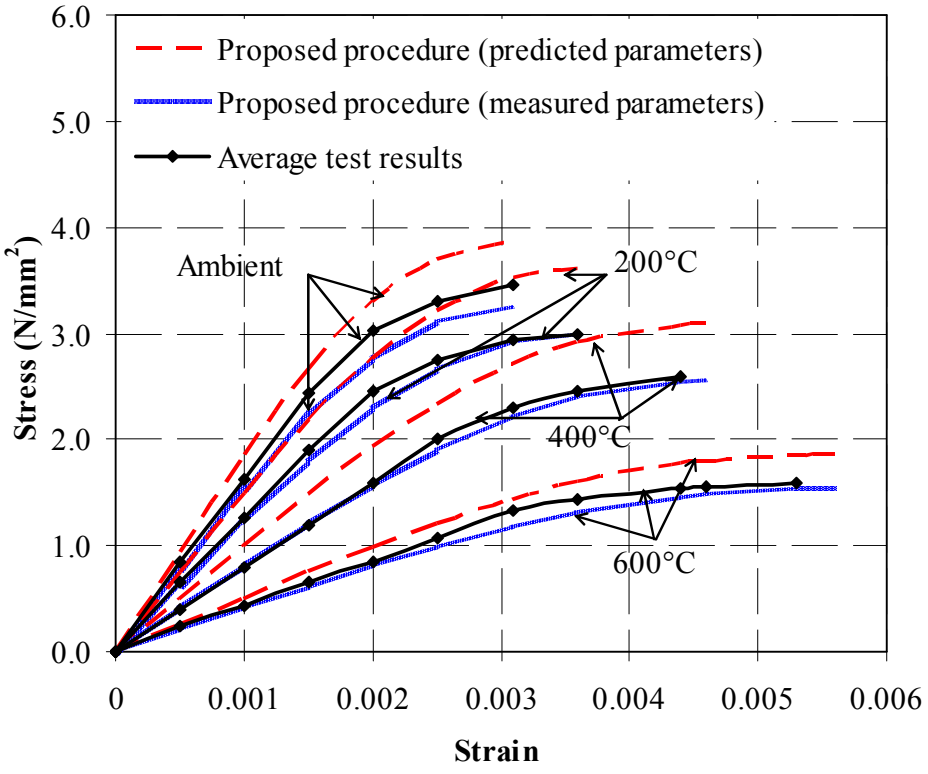

Figure 6.21(b) Comparison between the predicted stress-strain relationships using the proposed procedure and the average experimental results for 800 kg/m^3

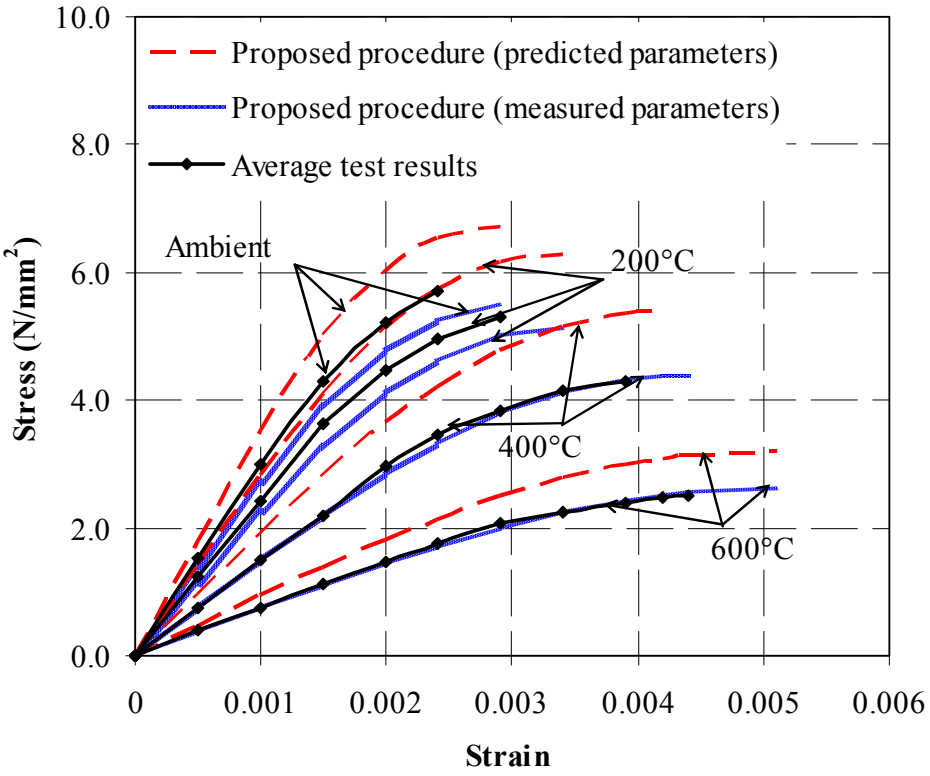

Figure 6.21(c) Comparison between the predicted stress-strain relationships using the proposed procedure and the average experimental results for 1000 kg/m^3

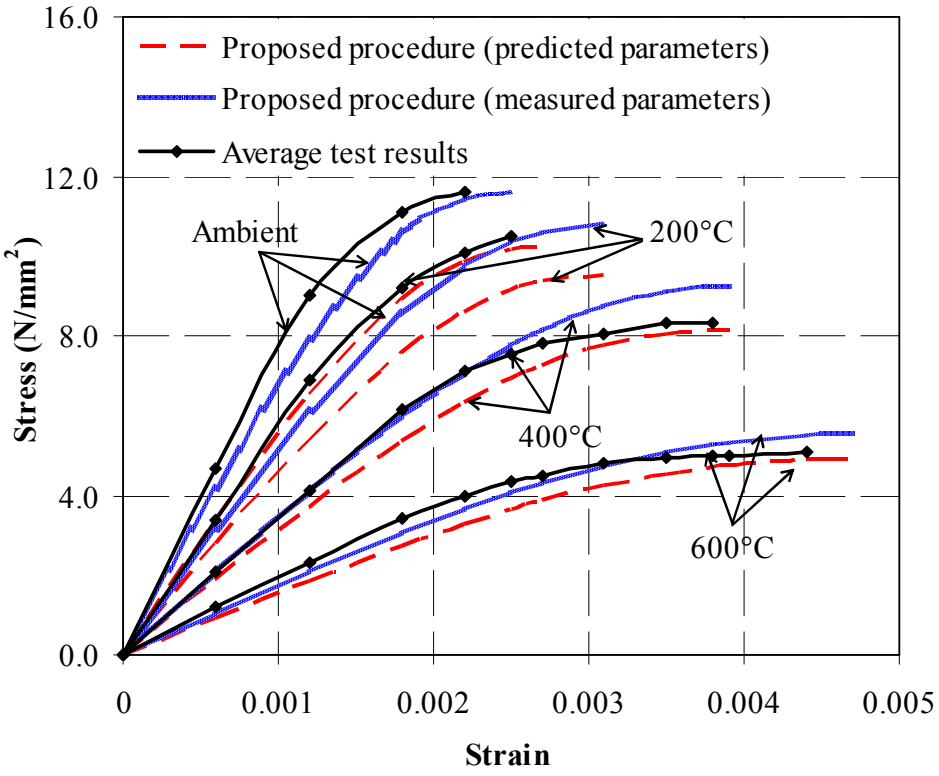

Figure 6.21(d) Comparison between the predicted stress-strain relationships using the proposed procedure and the average experimental results for 1200 kg/m^3

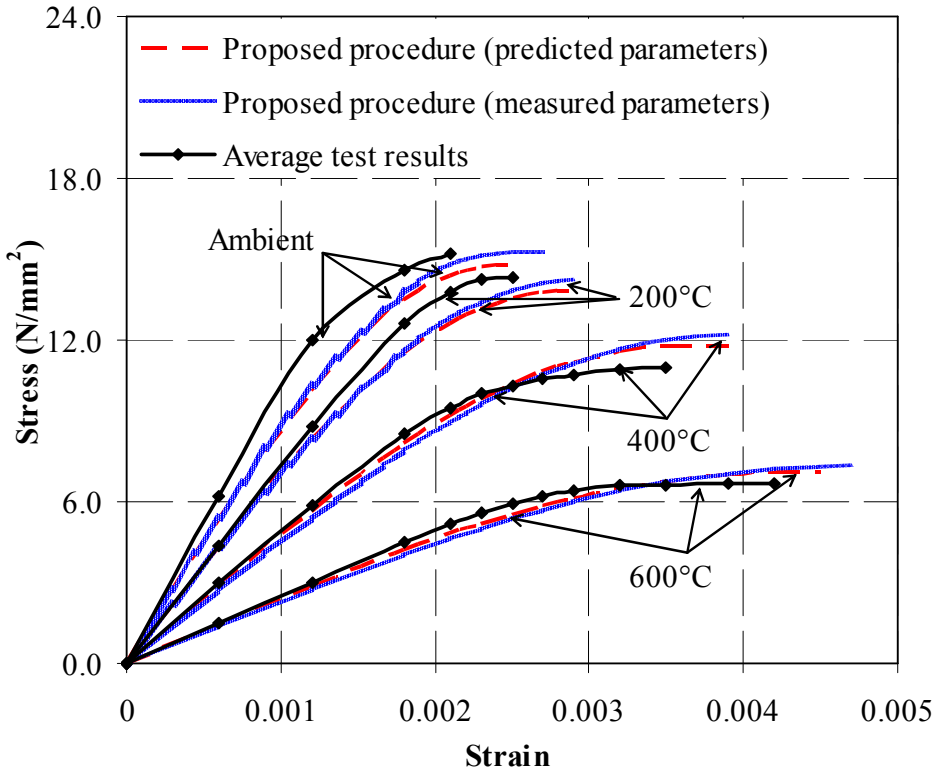

Figure 6.21(e) Comparison between the predicted stress-strain relationships using the proposed procedure and the average experimental results for 1400 kg/m^3

6.5 CONCLUSIONS

This chapter has presented a number of predictive models for mechanical properties of LFC exposed to elevated temperatures. The experimental results were compared with predictive models based on normal weight concrete. Since the mechanical properties of LFC come from Ordinary Portland Cement, thus the change in mechanical properties of LFC may be predicted using the mechanical property models for normal weight concrete. The following conclusions may be drawn:

(1) The Balshin equation (Equation 6.1) may be used to calculate both the ambient temperature compressive strength and compressive modulus of elasticity, as a function of porosity of LFC. Nevertheless, for improved accuracy, ambient temperature mechanical property tests were still recommended.

(2) For compressive strength at elevated temperatures, the well accepted Eurocode 2 (2004) model was applicable.

(3) For compressive modulus of elasticity at elevated temperatures, the Li and Purkiss (2005) model may be used.

(4) For LFC, the total strain at peak stress is approximately 1.78 times the elastic strain at peak stress.

(5) The Eurocode 2 (2004) equation may be used to obtain the compressive stress-strain relationship of LFC.

(6) The model of Li and Gao (1993) gave good prediction of the flexural tensile strength of LFC at elevated temperatures.

CHAPTER 7

STRUCTURAL PERFORMANCE OF ONE LFC BASED COMPOSITE WALLING SYSTEM

7.1 INTRODUCTION

LFC has very low thermal conductivity, making it a suitable material for building use as insulating or fire resisting material due to its porous internal structure. LFC can also be made to have a reliable amount of compressive resistance, making it possible to use LFC as load-bearing material. However, the experimental results on compressive properties of LFC presented in Chapter 5 indicated that LFC suffered from brittle failure. Therefore, a suitable method of using LFC in load-bearing construction would be to use it in composite action with steel, which has high ductility. This particular chapter explores the use of LFC in composite action with steel sheeting in lightweight composite walling construction. Should LFC be cast in-situ, the thin steel sheeting can be used as formwork during construction. Because of the low density of LFC, the pressure on the steel sheeting during construction would be much lower than using normal weight concrete, allowing thin steel sheeting to be used. Before such a system can be used in practice, it is necessary to carry out fundamental research to thoroughly investigate its behaviour.

This chapter presents the results of an experimental and analytical investigation into the structural behaviour of a composite panel system consisting of two outer skins of profiled thin-walled steel plates with lightweight foamed concrete (LFC) core under axial compression. A total of 12 tests were carried out, composed of two duplicates of 6 variants which were distinguished by two steel sheeting thicknesses (0.4mm and 0.8mm) and three edge conditions of the sheeting. The density of LFC core was 1000 kg/m^3. Experimental results include failure modes, maximum loads and load-vertical

strain responses. In analysis, full bond between the steel sheets and the concrete core was assumed and the LFC was considered effective in restraining inward buckling of the steel sheets. Using the effective width method for the steel sheets, the load carrying capacities of the test specimens were calculated and compared with the experimental results.

7.2 EXPERIMENTS

The experiments were designed to provide information on the load deformation response and failure modes of the specimens. The objective of the experiments was to enable development of a calculation method.

7.2.1 Geometrical descriptions of specimen

The dimensions of the test specimens were 400mm high by 400mm wide by 100mm thick. The short height of the specimens would mean that failure of the specimens would be governed by cross-sectional capacity. A total of 12 prototype specimens were tested under axial compression. These 12 specimens consisted of two duplicates of 6 types, being two steel thicknesses (0.4mm and 0.8mm) in combination with three edge conditions of the steel sheeting. Figure 7.1 showed details of the prototype specimen. The profiled steel sheeting was made in-house from plain sheeting of 0.4mm or 0.8mm thickness by fly press. The two profiled steel facings were connected using 6 x 10mm bolts and nuts.

Refer to Figure 7.2, the steel sheeting could have one of the three edge conditions: (a) the steel sheets do not cover the LFC panel thickness (referred to as no stopping edge), (b) the steel sheets cover the LFC panel thickness but were not joined (referred to as with stopping edges), (c) the steel sheets cover the LFC panel thickness and are joined by welding (referred to as welded stopping edge). These three steel sheeting edge conditions were investigated to assess the influence of the steel sheeting in restraining the LFC to improve its ductility.

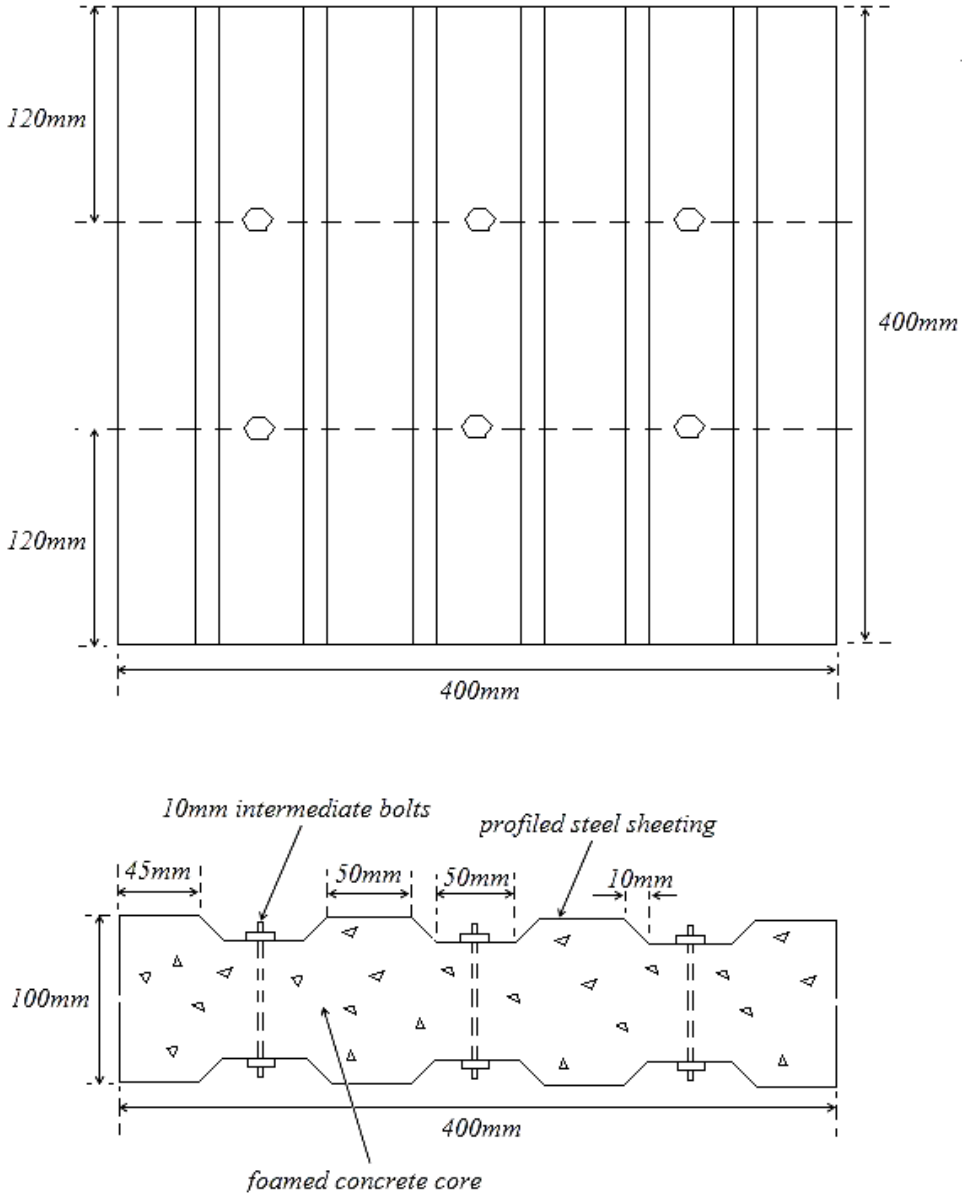

Figure 7.1 Details of prototype composite walling

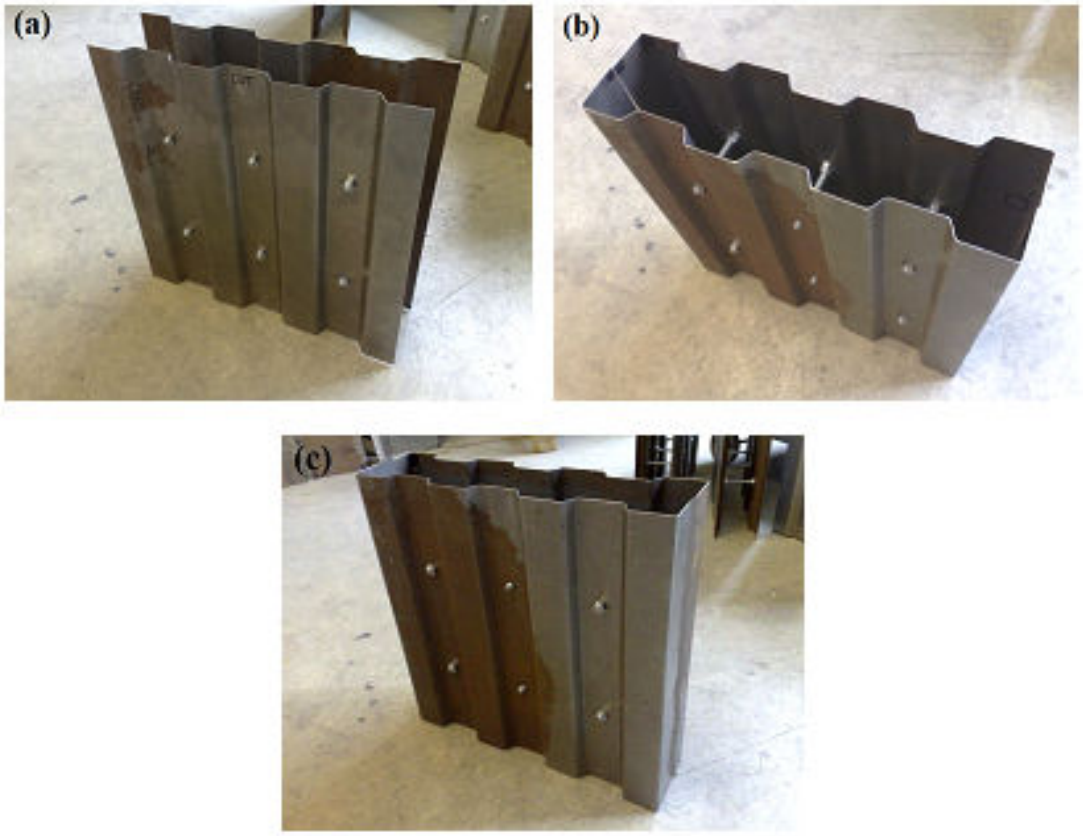

Figure 7.2 Steel sheeting edge conditions (a) no stopping edge (b) with stopping edge (c) with welded stopping edge

7.2.2 Casting, curing and instrumentation

All twelve specimens were cast in house on the same day so that the LFC core would have the same design strength. The LFC core used in this composite system was made from ordinary Portland cement, fine sand, water and stable foam with cement-sand ratio of 2:1 and the water-cement ratio of 0.5.

As mentioned in Section 2.6.1, LFC with density of 1000 kg/m^3 was chosen as it was found to have a useful amount of mechanical properties to construct a lightweight load-bearing walling system when in composite action with the profiled cold-formed thin-walled steel sheeting. Three LFC cubes and three cylinders were also cast on the day the composite panels were made. Additional two sets of three identical tests were also conducted to determine the strength of LFC core alone without any steel plate. Figure 7.3 shows the shapes of these two additional sets. These tests were carried out to establish the LFC core strength contribution factor when in composite action with the steel sheeting. These two shapes were used to determine the effects of profiling on

compressive strength of the core, as observed by Wright (1998). LFC was poured vertically similar to the direction of loading and the test samples were naturally cured in the indoor climate of the concrete lab. The composite panel was tested at 28 days after casting.

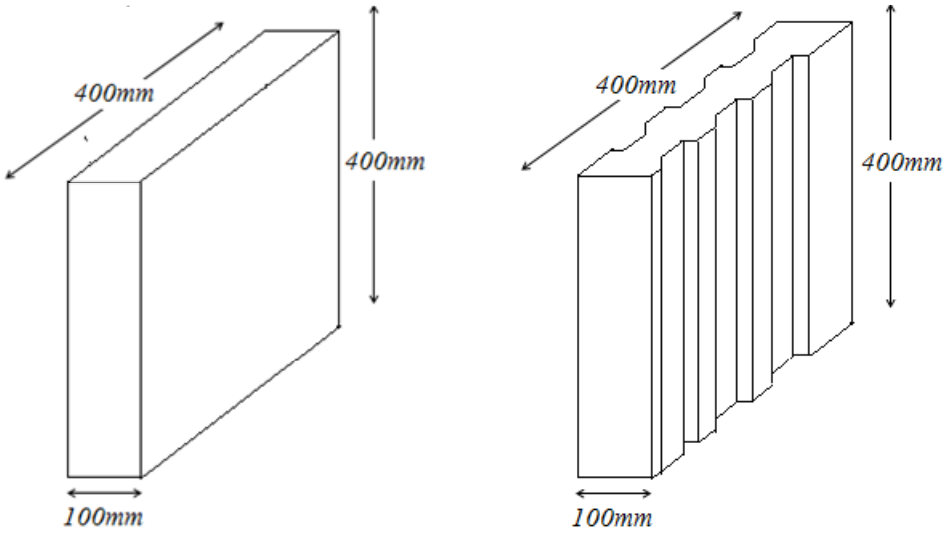

(a) rectangular LFC panel *(b) profiled LFC panel*

Figure 7.3 Dimensions of the two additional LFC core samples

A number of strain gauges were placed on the specimens and Figure 7.4 showed their locations on a sample. In all cases, the strain gauges were at mid-height (*h/2*) of the specimen.

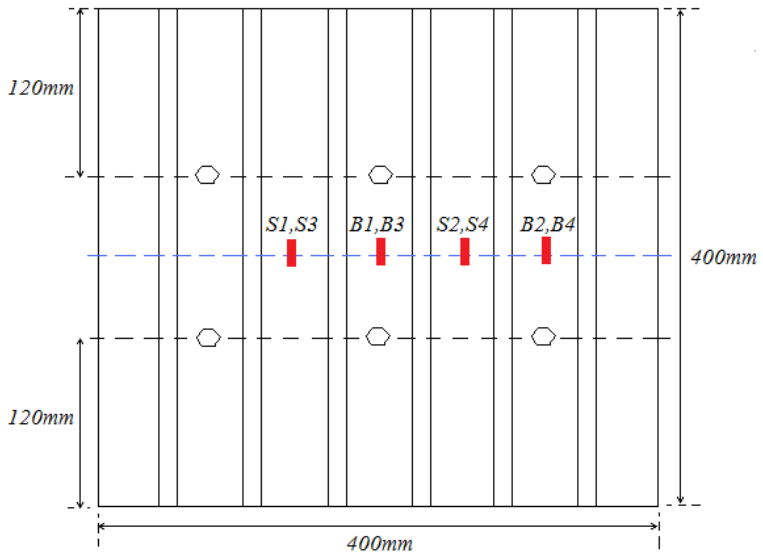

Figure 7.4 Strain gauge arrangements

7.2.3 Test set-up

The specimens were loaded in axial compression and the test was carried out in a universal compression testing machine with a maximum capacity of 2,500 kN after 28 days of casting (Figure7.5). The tests were displacement controlled. The top and bottom of the specimens were ground flat prior to testing so as to ensure equal load distribution. In addition to the strain gauges on the sample, the displacement of the loading platen was also recorded to measure axial deformation of the specimen. Observations were made on general behaviour including cracking of concrete, buckling of sheeting and failure mode.

Figure 7.5 Axial compression test set-up

7.2.4 Material properties

Three concrete cubes and 3 cylinders were cast and tested on the same days as the composite walling specimens. The cube tests after 28 days gave an average strength of 5.9 N/mm^2 and the cylinder tests provided an average strength of 5.1 N/mm^2. The test results were given in Table 7.1 and they were quite consistent. Table 7.1 also gave the results of the additional tests on the LFC panels. Data from the steel sheeting supplier gave yield strength of 280 N/mm^2 and a modulus of elasticity of 200,000 N/mm^2.

Table 7.1 Variation of compressive strength of LFC core for different shapes and dimension

Shapes	Dimension (mm)	Compressive strength (N/mm^2)			Average strength (N/mm^2)	Ratio of strength to cube strength
		Test 1	Test 2	Test 3		
Cube	100 x 100 x 100	5.7	6.2	5.9	5.9	1.00
Cylinder	100 ø x 200	4.9	5.1	5.3	5.1	0.86
Rectangular panel	400 x 400 x 100	4.1	4.0	4.3	4.1	0.69
Profiled panel	400 x 400 x 100	3.8	3.7	3.5	3.7	0.63

The strength ratio given in Table 7.1 indicated that the compressive strength of LFC was influenced by the shape and size of the specimens, which conforms to observed the behaviour of normal weight concrete. The average cylinder strength and rectangular panel strength were 15% and 30% lower than the cube strength respectively. The strength of the profiled panel was slightly smaller than the strength of the rectangular panel as found by Wright (1998).

7.3 TEST RESULTS AND OBSERVATIONS

Table 7.2 listed the ultimate strength (maximum load) of each specimen. Except for tests 9 and 10 which showed a difference of about 10%, other duplicate tests reached very similar ultimate strengths. Figures 7.6-7.11 present the load versus mid-height vertical strain relationships for the six types of specimens. The different strain gauges (S1-S4 and B1-B4) recorded very similar data so only data from one of each set (S1 on the steel surface without any mechanical connectors, B1 on the steel surface between the mechanical fasteners was taken into consideration.

Figures 7.6-7.11 indicated that in all cases, the strain gauge S1 recorded more elastic strains than B1, indicating participation of the mechanical fasteners. In all cases, the test sample was able to sustain the maximum applied load for a considerable axial deformation. The descending branch of all the load-strain curves was gradual, indicating good ductility of the test specimen.

Table 7.2 Summary of test results of composite walling under compression

Test no.	Reference *	Steel thickness (mm)	Ultimate strength (kN)
0	concrete alone	-	125
1	NSE1	0.4	161
2	NSE2		169
3	NSE3	0.8	240
4	NSE4		247
5	WSE1	0.4	175
6	WSE2		187
7	WSE3	0.8	263
8	WSE4		272
9	WE1	0.4	189
10	WE2		207
11	WE3	0.8	285
12	WE4		302

** NSE = no stopping edge; WSE = with stopping edge; WE = welded edge*

Table 7.2 showed that the ultimate strength of the specimens with stopping edge was about 10% higher than those without any stopping edge for both steel thicknesses. Panels with welded steel edges sustained on average 17% more load than those without stopping edge. In Section 7.4, it will be shown that these increases in strength can be attributed to the increase in effective width of the steel sheeting.

Figure 7.12 compares the load versus mid-height strain (point B1) relationships of the two steel sheeting thicknesses and three edge conditions. As expected, the ultimate load and axial stiffness of the composite panel increases with increasing steel thickness and improved edge condition.

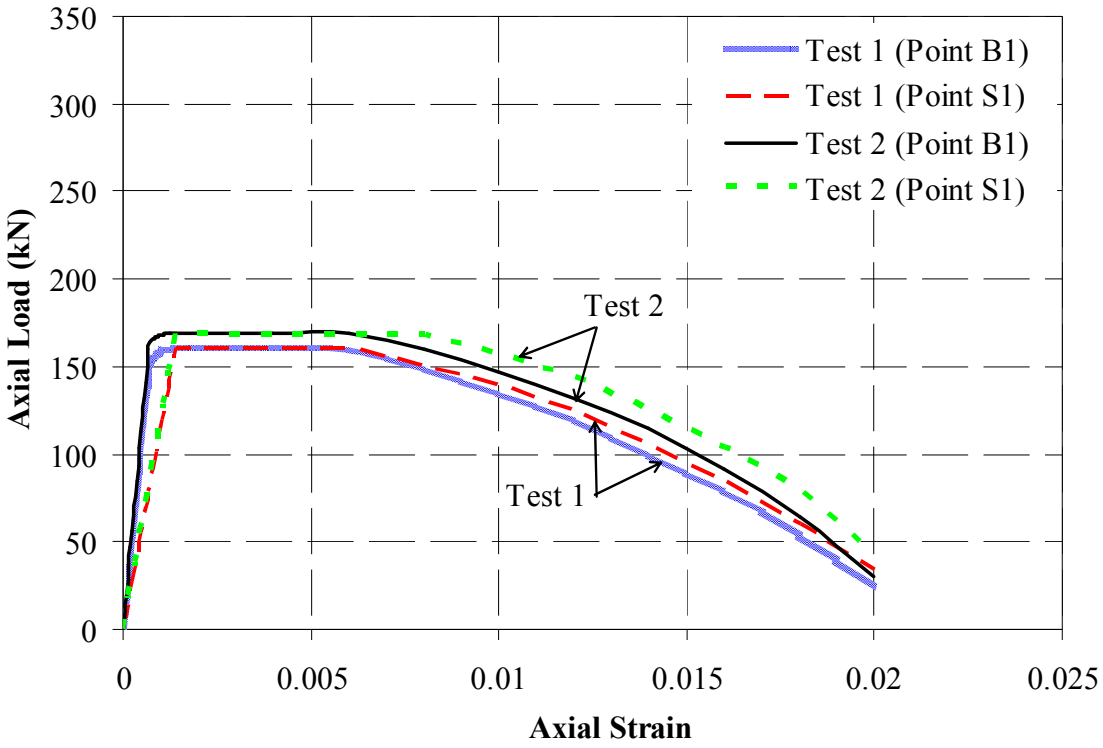

Figure 7.6 Load versus mid-height strain relationships for the panel with 0.4mm steel thickness and no stopping edge

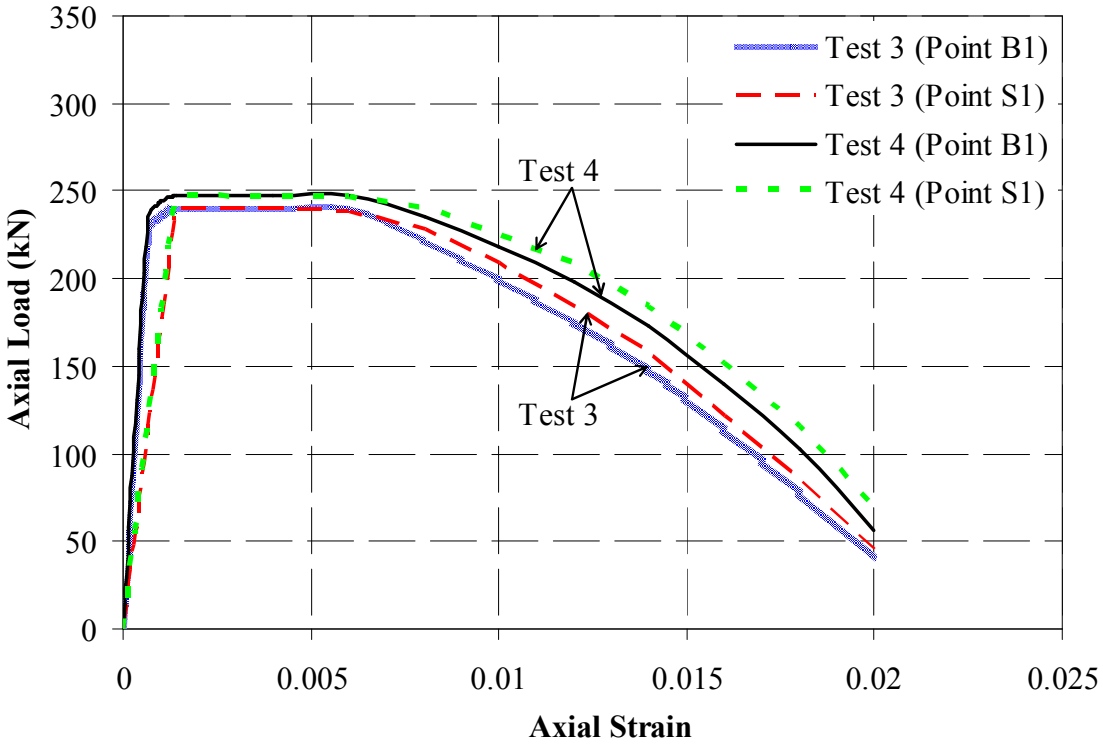

Figure 7.7 Load versus mid-height strain relationships for the panel with 0.8mm steel thickness and no stopping edge

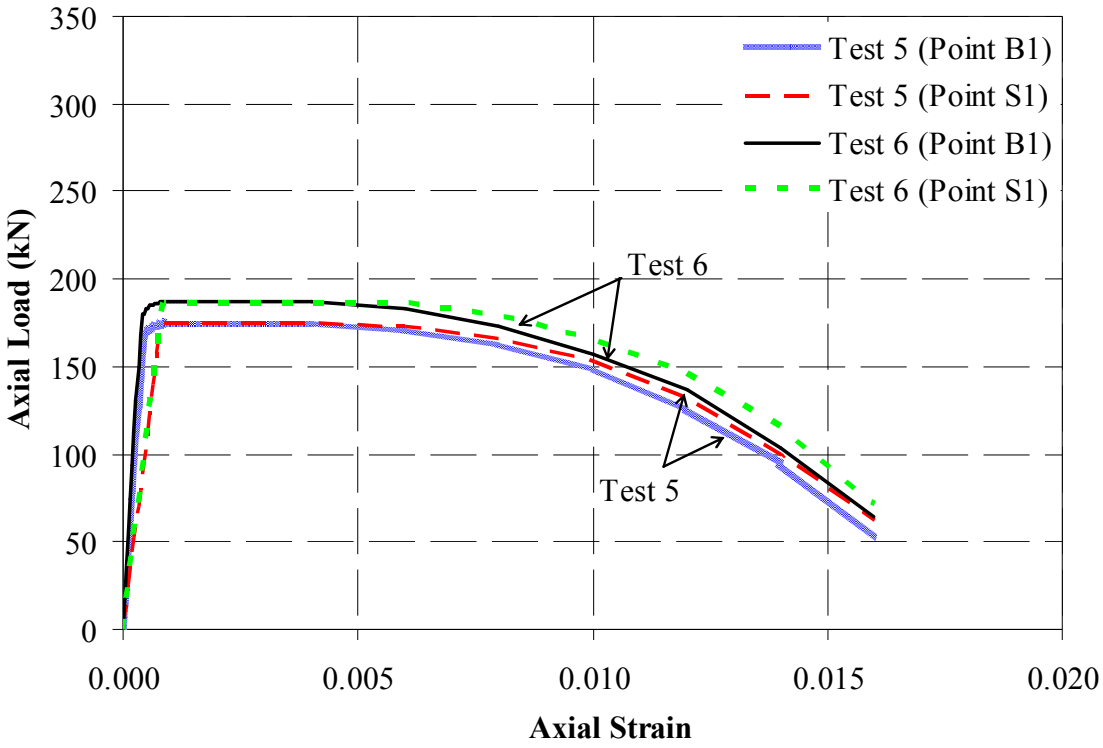

Figure 7.8 Load versus mid-height strain relationships for the panel with 0.4mm steel thickness and with stopping edge

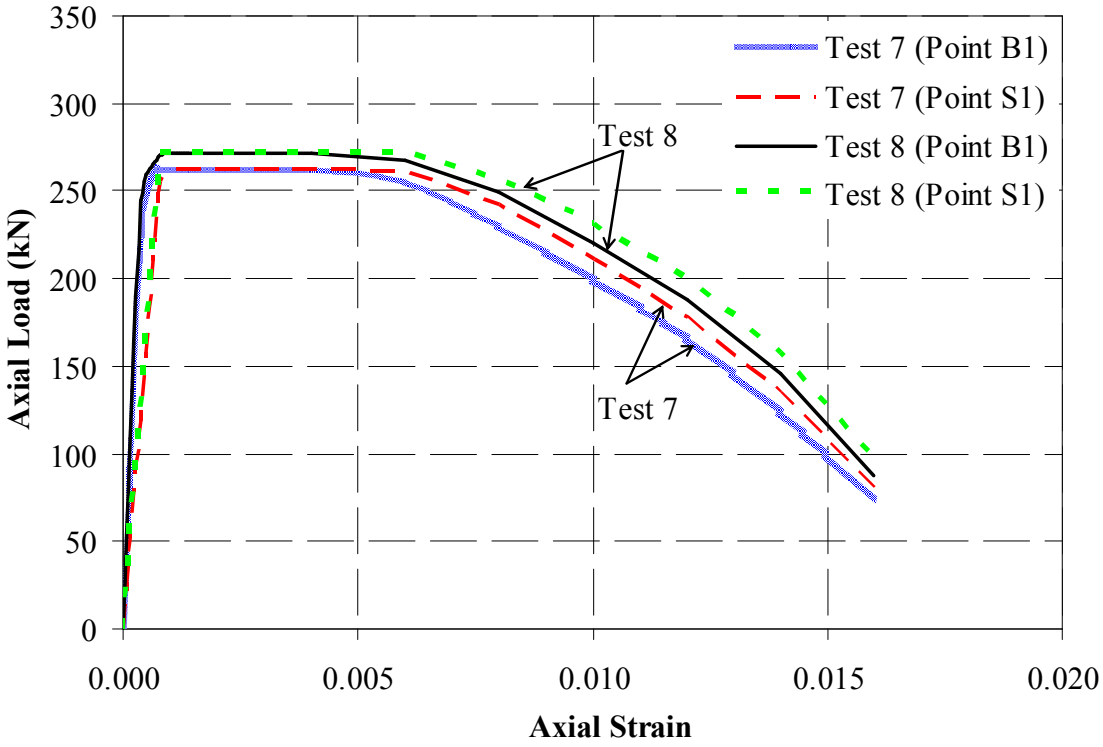

Figure 7.9 Load versus mid-height strain relationships for the panel with 0.8mm steel thickness and with stopping edge

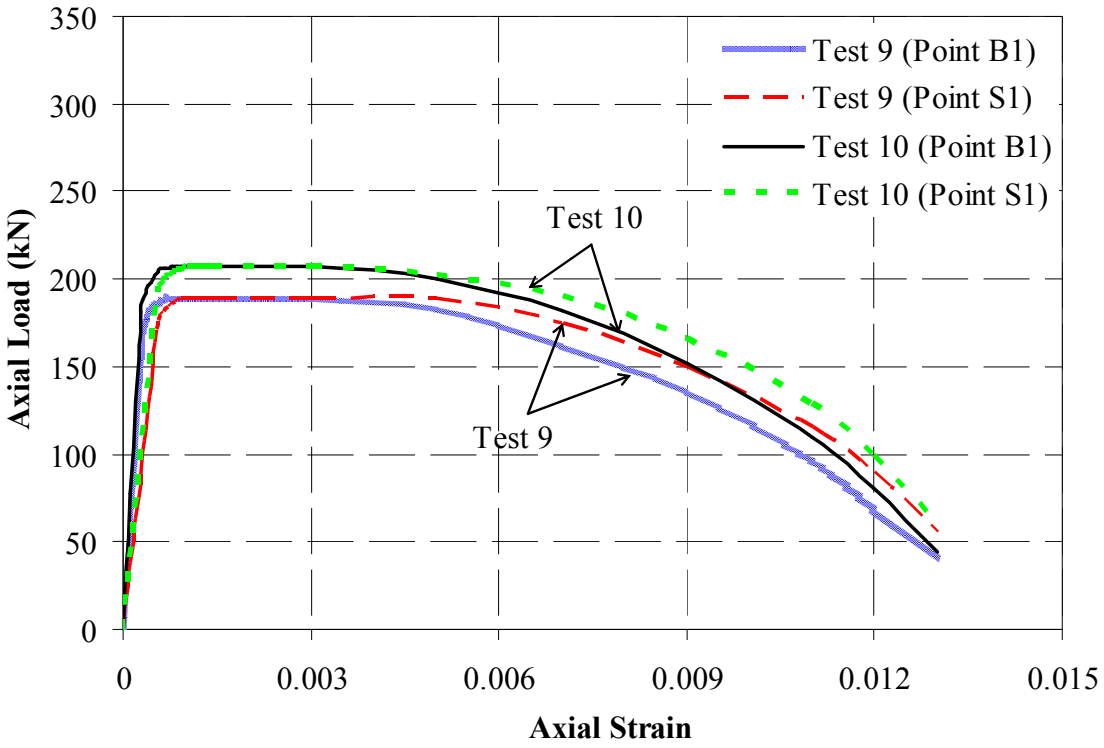

Figure 7.10 Load versus mid-height strain relationships for the panel with 0.4mm steel thickness and with welded edge

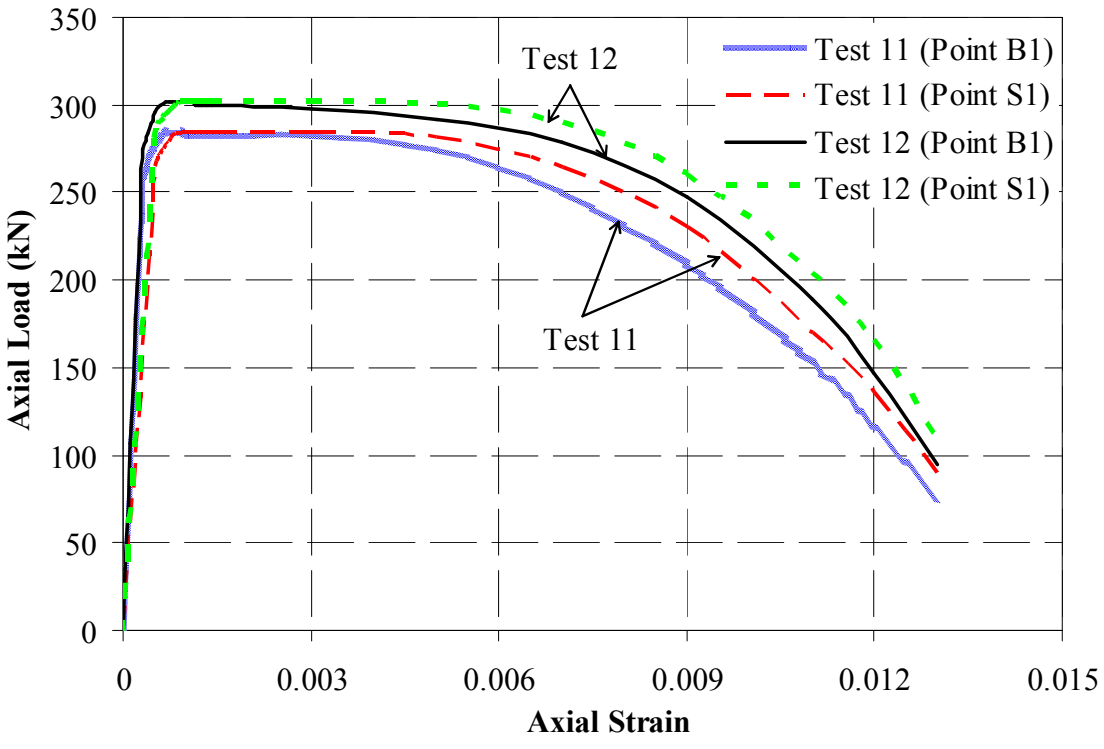

Figure 7.11 Load versus mid-height strain relationships for the panel with 0.8mm steel thickness and with welded edge

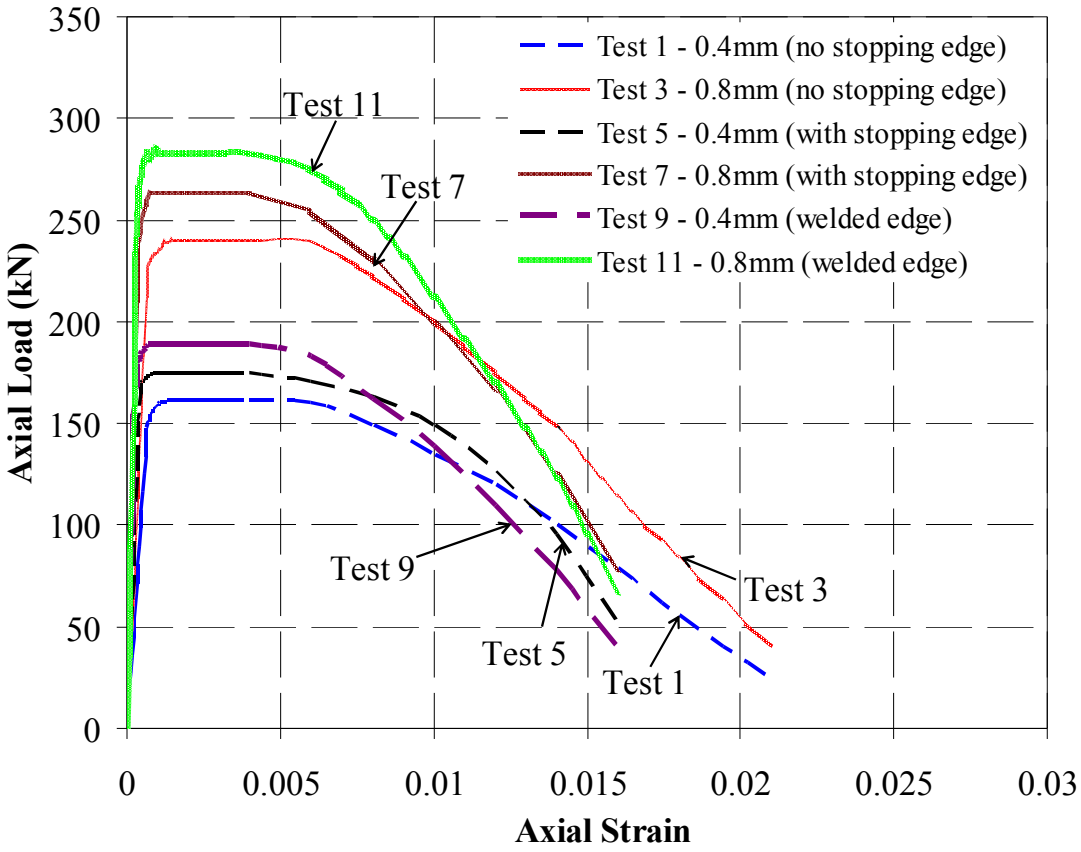

Figure 7.12 Comparison of load versus mid-height strain (point B1) relationships of the two steel sheeting thicknesses and three edge conditions and also with profiled panels without steel sheeting.

Figures 7.13 shows a failed sample for all three edge conditions; (a) without stopping edge, (b) with stopping edge and (c) with welded edge. The steel sheeting experienced local buckling before failure, but the LFC core of 1000 kg/m^3 density was capable of preventing the panel from inward buckling. In all cases, failure of the panel was initiated by local buckling of the steel sheeting, followed by crushing of the LFC core. Although the steel sheeting provided some ductility to the panel, the welded steel edges were not able to provide much confinement effect to the LFC panel. It should be pointed out that the line of bolts should not be a problem. The steel sheeting buckled and the bolts stopped that. There was no separation of the steel sheeting from the LFC core until near failure, indicating that the mechanical fasteners were able to hold the steel sheeting and the LFC core together to enable them to resist the applied load in composite action. Clearly, if composite walling system using LFC is to be used in real projects, bond between the profiled steel sheeting and the LFC infill should be

considered. However, it is expected that because LFC would be less demanding owing to its lower strength than normal weight concrete, the steel sheeting used in composite walling systems using normal weight concrete would still be suitable.

(a) failure mode of panel without stopping edge with outward buckling of steel

(b) failure mode of specimen with stopping edge

(c) failure mode of specimen with welded edge

Figure 7.13 Failure modes for composite panel without stopping edge

7.4 ANALYTICAL RESULTS

As previously described, the panels can be considered to be in composite action and the LFC core was able to prevent the steel sheeting from inward local buckling. Therefore, the test specimens will be analysed as a conventional composite walling system.

Since the test panels were short (height to thickness ratio=4), no global buckling was observed and the panel strength reached the cross-sectional resistance. Also experimental observation indicates that there was little evidence (e.g. bulging of the steel sheeting) of any confinement effect on the LFC core provided by the steel sheeting. Therefore the ultimate resistance of the panel, N_u may be calculated from:

$$N_u = N_s + N_c \quad \ldots.(7.1)$$

Where N_s is the resistance of the steel sheeting and N_c the resistance of the LFC core. The following sections will discuss how N_s and N_c may be obtained.

7.4.1 Steel sheeting resistance

7.4.1.1 Critical local buckling stress

The local buckling stress of the steel plate in concrete-filled steel section was influenced by the width to thickness ratio, boundary condition, initial geometric imperfection and residual stresses induced by welding or cold-formed process (Liang and Uy, 2000). For ideal steel plates, the critical elastic buckling stress can be determined by the following equation (Bulson, 1970):

$$\sigma_{cr} = \frac{k\pi^2 E_s}{12(1-v^2)(b/t_p)^2} \quad \ldots.(7.2)$$

where σ_{cr} is the local buckling stress, k is the elastic buckling coefficient, which accounts for the effect of the plate aspect ratio and boundary condition on the critical buckling stress, E_s is the modulus of elasticity of the steel, v is the Poisson's ratio, b is the width of the plate and t_p is the thickness of the plate.

7.4.1.2 Plate buckling coefficient

The plate buckling coefficient of the steel section depends on the boundary condition. Therefore, the buckling coefficient was a function of the boundary condition along the longitudinal edges and the type of loading. The *k* values for various common boundary conditions and loading cases are given by a few authors (Gerald and Becker, 1957), (Uy and Bradford, 1996). Gerard and Becker (1957) summarized the buckling coefficient, *k* as a function of plate boundary condition and aspect ratio (*a/b*). Gerard and Becker's results are based on steel plates in contact with rigid medium. Uy and Bradford (1996) recently proposed a slightly different set of plate buckling coefficients for steel plates in contact with elastic medium, which would be more suitable to the current problem. For the current research which had uniform distribution of compressive stress, the buckling coefficients were compared in Table 7.3.

Table 7.3 Buckling coefficient of steel plates under compression

Boundary condition	Buckling coefficient, *k*	
	Gerald and Becker (1957)	Uy and Bradford (1996)
S-F	0.425	0.8
S-S	4	5.6

** S-F – simply supported-free, S-S – simply supported-simply supported*

7.4.1.3 Effective width

For thin-walled structures, the current design method was to use an effective width to account for local buckling. According to Winter (1947), the effective width (b_{eff}) of a plate of width *b* can be calculated using the following equation:

$$\frac{b_{eff}}{b} = \sqrt{\left(\frac{\sigma_{cr}}{f_y}\right)}\left[1 - 0.22\sqrt{\left(\frac{\sigma_{cr}}{f_y}\right)}\right] \quad \ldots.(7.3)$$

Where b_{eff} is the effective width, *b* is the original width, σ_{cr} is the local buckling stress, and f_y is the yield stress. The yield stress f_y, multiplied by the effective width gives the ultimate strength of the plate approximately.

Liang and Uy (2000) conducted a theoretical study on the post-local buckling behaviour of steel plates in steel box columns filled with concrete, by using the finite element method. They found that the post-local buckling characteristics of steel plates in concrete filled thin-walled box columns have not been adequately studied theoretically and there is also lack of an efficient method for evaluating the initial local buckling loads of steel plates. They examined the effective width methods for the ultimate strength design of steel plates restrained by concrete and of short concrete-filled welded box columns in compression and proposed the following two effective width equations:

$$\frac{b_{eff}}{b} = 0.675\left(\frac{\sigma_{cr}}{f_y}\right)^{\frac{1}{3}} \qquad \text{for } \sigma_{cr} \le f_y \quad \ldots.(7.4)$$

$$\frac{b_{eff}}{b} = 0.915\left(\frac{\sigma_{cr}}{\sigma_{cr} + f_y}\right)^{\frac{1}{3}} \qquad \text{for } \sigma_{cr} > f_y \quad \ldots.(7.5)$$

The resistance of the steel sheeting can be calculated as:

$$N_s = b_{eff} \cdot t_p \cdot f_y \quad \ldots.(7.6)$$

7.4.2 Strength of LFC core

A study conducted by Wright (1998) established that there was a reduction in load carrying capacity in profiled concrete panel when compared to solid panel. He found that the extreme edges of the profiled panel did not present a solid mass of concrete and the extra bending stresses (due to any loading eccentricity or material non-uniformity) must be carried by only that concrete in the ribs of the profile. This reduces the load carrying capacity of the rib to resist the applied axial load.

Wright (1998) then derived an empirical correction to calculate the reduced concrete strength for uniform axial compression, where the reduction in concrete strength was assumed to be directly proportional to the extent of void created by profiling the compressed edge of the panel. A reduction factor, α, which was applied to the concrete strength was given as below:

$$\alpha = 1 - \frac{A_{vf}}{A_c} \quad \text{....(7.7)}$$

where A_{vf} is the area of the profile voids on one face and A_c is the area of concrete. For the tested samples, the calculated α value is 0.91.

The test results in Table 7.1 appeared to confirm the findings by Wright (1998) where the compressive strength of the profiled LFC panel was found to be lower than the concrete strength of the solid panel. Therefore, an experimental correction (α reduction factor in Equation 7.6) must be included when calculating the resistance of the LFC core in the composite walling system.

Based on this result, the resistance of the LFC core in the proposed composite walling system can be determined as follows:

$$N_c = 0.69 \cdot A_c \cdot f_{cu} \cdot \alpha \quad \text{....(7.8)}$$

The factor of 0.69 (see Table 7.1) takes into account the reduced strength of LFC in a panel construction compared to the cube strength of LFC, and it was determined by divided the average solid panel strength (4.1 N/mm^2) by the cube strength (5.9 N/mm^2). With the introduction of α calculated using Equation 7.7 (0.91), Equation 7.8 gives a final factor of 0.63 which was the same as the experimental result in Table 7.1, obtained by dividing the LFC strength in the profiled panel by the LFC cube strength.

7.4.3 Load carrying capacity of composite wall panels

Based on the discussion in the last section, the load carrying capacity (N_u) of the composite wall panel in axial compression, taking into consideration the effective width and concrete strength reduction factor for profiled shape, can be calculated by using the following equation:

$$N_u = 0.63 \cdot A_c \cdot f_{cu} + b_{eff} \cdot t_p \cdot f_y \quad \text{....(7.9)}$$

Table 7.4 presented the total effective width of steel sheeting for the two different thicknesses and the three different edge conditions, using the aforementioned two different methods of calculating the plate buckling coefficient and two methods of calculating the plate effective width. The total effective width coefficient was obtained

as the sum of effective widths of all the segments of the profiled steel sheeting divided by the total width of the steel sheeting.

Table 7.4 Effective width of steel plates in composite panel

Steel Thickness (mm)	Uy and Bradford *k* value		Gerard and Becker *k* value	
	Total effective width (b_e/b)			
	Winter (1947)	Liang and Uy (2000)	Winter (1947)	Liang and Uy (2000)
	(1)	(2)	(3)	(4)
	No stopping edges			
0.4	0.51	0.47	0.44	0.43
0.8	0.74	0.65	0.67	0.60
	With stopping edges			
0.4	0.49	0.46	0.43	0.41
0.8	0.74	0.66	0.67	0.59
	Welded edges			
0.4	0.54	0.49	0.47	0.45
0.8	0.82	0.71	0.74	0.66

It was interesting to notice that if the same plate buckling coefficient was used, the two different effective width methods (compare (1) with (2) or (3) with (4)) gave substantial differences in the total effective width of the steel sheeting, with the Liang and Uy (2000) method (Equations 7.4 and 7.5) of calculating the effective width giving results about 10% lower than the Winter (1947) method (Equation 7.3). Likewise, when the same effective width method was used, the two different methods of calculating the plate buckling coefficient (compare (1) with (3) or (2) with (4)) results in large differences in the total effective width of the steel sheeting, with the Uy and Bradford (1996) method giving values about 10% higher than the Gerard and Becker (1957) method. However, when the traditional Gerard and Becker (1957) plate buckling coefficient was combined with the traditional Winter effective width formula (column 3 in Table 7.4), the results were very similar to those obtained by combining the more recent plate buckling coefficient method of Uy and Bradford (1996) with the more recent effective method of Liang and Uy (2000) (column 2 in Table 7.4).

Table 7.5 compared the calculated and measured wall panel strengths for all the 12 tests using the different effective widths of Table 7.4. Due to the relatively low contribution by the steel sheeting to the strength of the panels, all four methods produced similar panel strengths. A statistical analysis was carried out to verify the homogeneity and the reliability of the predicted strength over experimental results obtained from the proposed equation (Equation 7.9). The mean x and standard deviation s, were calculated for each combination of design method as shown in Table 7.5. Overall, the ratio of predicted strength-experiment results using all the four methods indicated that the specimens were relatively homogeneous.

Among these four methods, both the effective widths (2) and (3) in Table 5 gave good estimation of panel strength. Among these two methods, the method (2) appeared to give slightly more accurate predictions. The results in Table 7.5 were also presented in Figures 7.14-7.16. It should be pointed out that the buckling coefficient for plates from Uy and Bradford (1996) and effective width formulation proposed by Liang and Uy (2000) respectively were derived for composite column design. From the results in Table 7.5, these models were also acceptable for design use for composite panel using LFC.

Table 7.5 Comparisons between predicted composite panel strengths and test results

Ref. No.	Predicted Strength (kN)				Ratio predicted/experiment			
	Gerard and Becker *k* value		Uy and Bradford *k* value		Gerard and Becker *k* value		Uy and Bradford *k* value	
	Liang and Uy	Winter	Liang and Uy	Winter	Liang and Uy	Winter	Liang and Uy	Winter
NSE1	169	171	174	177	1.05	1.06	1.08	1.10
NSE2					1.00	1.01	1.03	1.05
NSE3	245	259	256	273	1.02	1.08	1.07	1.14
NSE4					0.99	1.05	1.04	1.11
WSE1	177	179	182	187	1.01	1.02	1.04	1.07
WSE2					0.95	0.96	0.98	1.00
WSE3	270	288	286	306	1.03	1.09	1.09	1.16
WSE4					0.99	1.06	1.05	1.12
WE1	182	184	187	192	0.96	0.97	0.99	1.02
WE2					0.88	0.89	0.90	0.93
WE3	287	307	300	325	1.01	1.08	1.05	1.14
WE4					0.95	1.02	0.99	1.07
				Mean, x	0.9867	1.0242	1.0258	1.0758
				Standard deviation, s	0.0458	0.0596	0.0532	0.0674

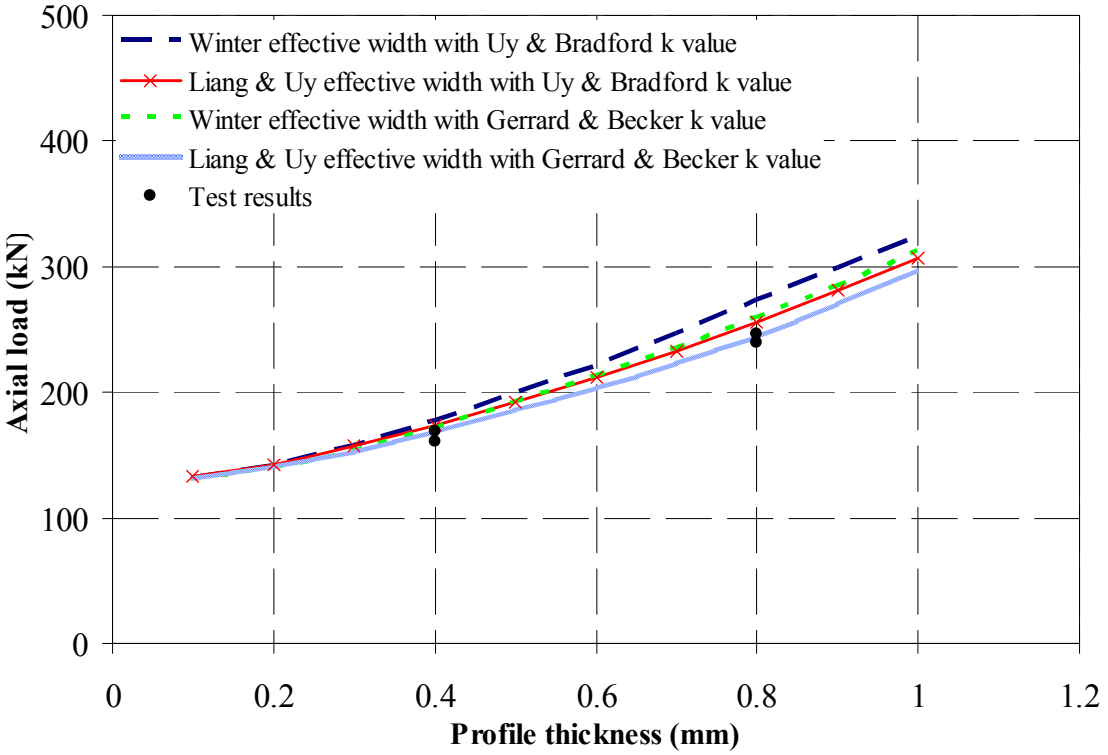

Figure 7.14 Comparisons between predicted strengths and test results for composite panel with no stopping edge

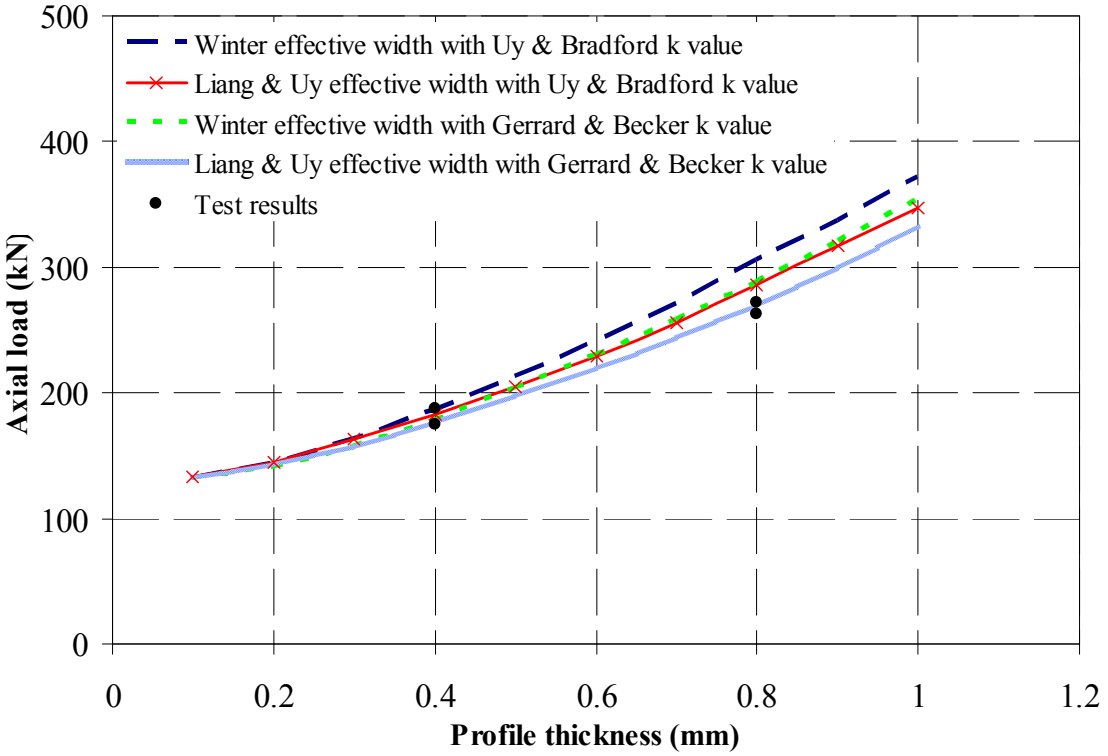

Figure 7.15 Comparisons between predicted strengths and test results for composite panel with stopping edge

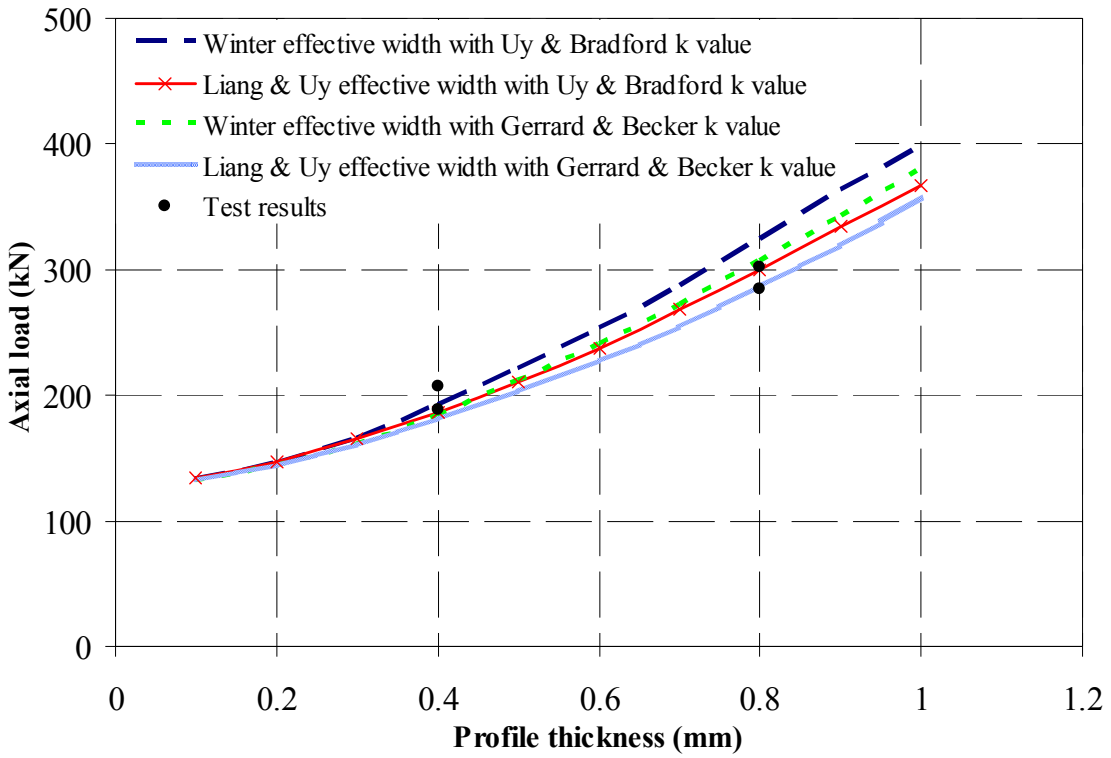

Figure 7.16 Comparisons between predicted strengths and test results for composite panel with welded edge

7.5 CONCLUSIONS

This chapter has described two series of tests on a new composite wall panel system consisting of two outer skins of profiled thin-walled steel sheeting with lightweight foamed concrete (LFC) core under axial compression, for steel sheeting thicknesses of 0.4mm and 0.8mm respectively. Each series of tests had three edge conditions for the sheeting. These tests provided information on the behaviour and failure mode of these panels. An analytical model has been developed to calculate the maximum load-bearing capacity of this type of wall system. It was found from the experimental investigation that the failure of the panel system was initiated by outward local buckling of the steel sheeting which was followed by concrete crushing of the LFC core and the LFC core of 1000 kg/m^3 density was sufficient to prevent the steel sheeting from inward buckling.

All the specimens showed good ductility, giving gradual reduction in load carrying capacity at increasing deformation. In contrast, without using steel sheeting, the core LFC panels experienced brittle failure after reaching the peak load. The increase in load carrying capacities of the panels with stopping edge and welded edge can be attributed

to the increased effective width of the steel sheeting. The load carrying capacities of panels with stopping edge and with welded edge were about 10% and 17% higher than those without any stopping edge for both steel sheeting thicknesses.

The proposed panel strength calculation model which takes into consideration the effect of profiling on concrete strength according to Wright was able to predict the axial capacity of the proposed panel very well. For calculating the steel sheeting effective width, the combination of Uy and Bradford plate local buckling coefficients with the Liang and Uy effective width formulation appeared to give the best agreement with the experimental results. Nevertheless, the traditional effective width method proposed by Winter in conjunction with the traditional plate local buckling coefficients of Gerard and Becker also gave close results compared to the experiments.

CHAPTER 8

INDICATIVE STUDY ON FIRE RESISTANCE AND STRUCTURAL PERFORMANCE OF LFC BASED SYSTEM

8.1 INTRODUCTION

This research so far has primarily concentrated on developing and validating thermal property models for LFC, characterizes its mechanical properties at high temperatures and concentrated on experimental and analytical studies of the structural behaviour and ultimate load carrying capacity of a composite walling system under axial compression. From the experimental verification, as expected the mechanical properties of LFC were reasonably low when compared to normal weight concrete. Nonetheless there was a potential of using LFC as fire resistant partition or as load-bearing walls in low-rise residential construction. In order to demonstrate the feasibility of this proposal, this chapter presents a preliminary feasibility study on its fire resistance and structural performance of LFC based system. The objectives of this feasibility study were:

- Investigating the fire resistance performance of LFC panels of different densities (650, 800, 1000, 1200 and 1400 kg/m^3) when exposed to fire on one side for different fire resistance ratings based on insulation requirement.

- Examining whether the composite walling system had sufficient load carrying capacity, based on compression resistance at ambient temperature.

8.2 ASSESSMENT OF FIRE RESISTANCE PERFORMANCE IN THE CONTEXT OF FIRE REQUIREMENTS STANDARD

When designing a building, a very significant consideration is how it will behave in fire and ensure the elements of structure will not collapse but remain standing or hold back the fire for a prescribed time. The building regulation stipulates the rules and the degree of fire resistance of the elements of structure. For example, BS 476 (1987) dictates the appropriate fire tests for these elements of structure and materials and grades the level of fire resistance.

The author planned to develop and utilize this LFC panel system in Malaysia therefore discussion in this section will include the fire requirements stipulated in the Malaysia standard as well. All building constructions in Malaysia have to abide by the fire requirements specified in Part VII of the UBBL (1997). These requirements include the restrictions on spread of flame and fire resistance of structural members. The Ninth Schedule of the UBBL gives the minimum requirements for fire resistance (in hours) for single-storey (Part II) and multi-storey (Part I) buildings of various types. It also gave the notional fire rating values of various common types of construction. Similar fire requirements standard can also be found in other building by-laws and codes. The minimum statutory fire rating requirements for elements of structure in Malaysia and England are summarised in Table 8.1, for brevity and easy comparison.

Table 8.1 Summary of minimum fire rating requirement in minutes for elements of structures in Malaysia and England (Hock and Giang, 1998)

Building category		Malaysia	England
Domestic	One storey	0	30
	2–3 Storey	30–60	30–60
Institutional	< 28 m	60–90	30–60–90
	> 28 m	90–120	120
Hotel	2 Storey	30–60	30
	3 Storey	60	60
	> 3 Storey	60–90–120	60–90–120
Office	< 7.5 m	0–30–60	30–60
	7.5–28 m	60–90	60–90
	> 28 m	60–90–120	120
Shop	< 7.5 m	0–30–60	60
	7.5–28 m	60–90	60–90
	> 28 m	60–120–240	120
Assembly	< 7.5 m	0–30–60	60
	7.5–28 m	60–90	60–90
	> 28 m	60–90–120	120
Storage	< 7.5 m	0–30–60	60–90
	7.5–15 m	30–60–120	90
	15–28 m	60–120–240	90–120
	> 28 m	240	120
Factory	< 7.5 m	0–30–60	60
	7.5–28 m	60–120–240	90–120
	> 28 m	120–240	120
Apartment	2–3 Storey	60	30
	> 3 Storey	60–90–120	60–90–120

8.3 FIRE RESISTANCE PERFORMANCE OF LFC PANELS

This section presented a limited amount of indicative study to investigate the fire resistance performance of LFC panels when exposed to fire on one side, based on thermal properties in Chapter 3 and Chapter 4.

For simplicity, the fire resistance requirement was based on thermal insulation, where the average temperature on the unexposed surface should not exceed 140^{o}C from ambient (BS476, 1987). For this predictive study, standard fire curve was used as input data and the thermal boundary condition (heat transfer coefficients) was according to EN 1991-1-2 (2004). The results were presented as the minimum thickness of the panel for the following different initial densities (kg/m^{3}) of LFC: 650, 800, 1000, 1200, 1400

and 1600. The heat transfer analysis was carried out for 30, 60, 90 and 1200 minutes of the standard fire exposure time.

Table 8.2 summarises the simulation results, presenting the minimum thickness of LFC required to achieve different fire resistance ratings for different densities. It was clear from Table 8.2 that as far as insulation performance was concerned, the lower the LFC density, the better. This was attributed to the lower thermal conductivity of lower LFC, as shown in Figure 4.10 (Chapter 4), repeated in Figure 8.1. Although Figure 8.1 indicated steeper upward trend in lower density LFC due to greater void size, less water inside lower density LFC would reduce the initial thermal conductivity considerably so that within the practical range of temperature, the thermal conductivity of lower density LFC was lower.

Table 8.2 Indicative LFC minimum thickness for different fire resistance ratings for fire exposure from one side

LFC Dry density (kg/m^3)	Minimum LFC thickness (mm) for fire resistance rating of			
	30 minutes	60 minutes	90 minutes	120 minutes
650	21.0	36.7	50.1	60.5
800	22.0	38.0	51.2	61.8
1000	23.1	39.1	52.3	63.2
1200	24.0	40.0	53.0	64.2
1400	26.9	43.5	55.9	67.4

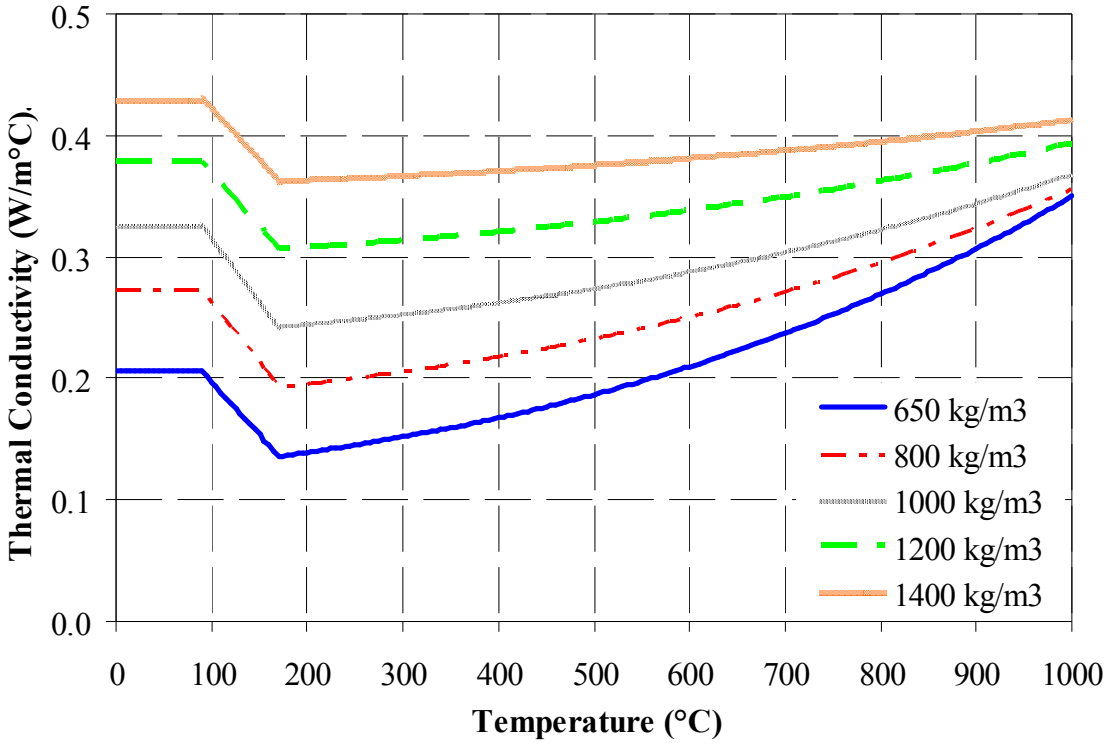

Figure 8.1 Thermal conductivity-temperature curves for all the densities used in this parametric study

The results in Table 8.2 indicated that although increasing LFC density would increase its specific heat, thus allowing more heat to be absorbed in LFC, as far as the unexposed surface temperature is concerned, which was used to assess insulation fire performance, thermal conductivity plays a more important role so that using higher density LFC had no advantage. The minimum thickness values in Table 8.2 were not particularly onerous. In fact, a single layer of 650 kg/m^3 density LFC of about 21 mm would achieve 30 minutes of standard fire resistance rating, more or less similar to gypsum plasterboard. This value is encouraging for application of LFC in building construction as fire resistant partitions.

From the indicative study results on LFC panels shown in Table 8.2, it can be concluded that if LFC panel of 100mm thickness of any density (650 to 1400 kg/m^3) was to be used in construction, it was able to meet the various fire rating requirements stipulated by the UBBL (1997) for thermal insulation. For domestic construction, a fire resistance rating of 30 minutes can be easily met by LFC panels.

8.4 FEASIBILITY OF USING LFC BASED COMPOSITE WALLING SYSTEM

The potential market for this composite walling system is low-rise residential construction. The practicability of this system was examined by analysing the investigation to verify whether the composite walling system has sufficient load carrying capacity**.** It was proposed to construct the interior load-bearing walls by using 100mm thick composite walls with 0.4mm steel sheeting, as tested in this research (presented in Chapter 7). Figure 8.2 showed the elevation section of a four-storey residential building and the floor span is 5m. Table 8.3 summarizes the applied loads on the interior walls (panels 1-4) supporting different floors.

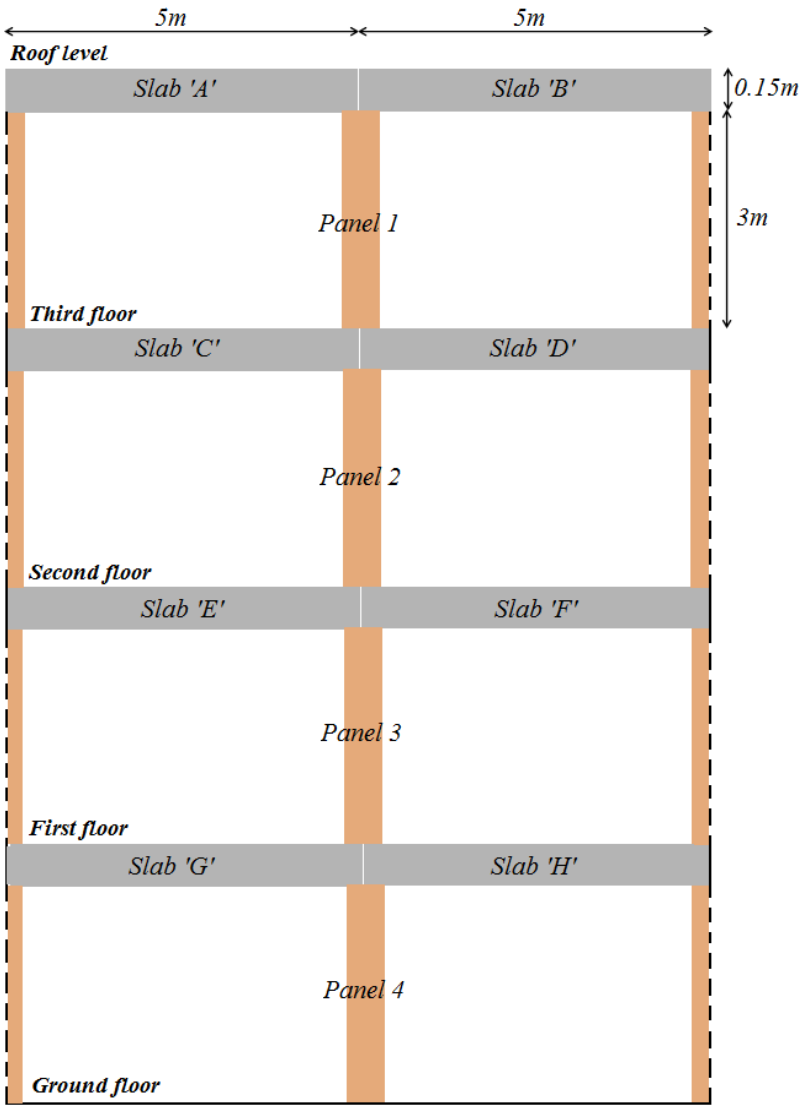

Figure 8.2 Arrangement of LFC composite wall panels for a four-storey residential building section.

Table 8.3 Design of prototype composite panel

Description	Unit	Value
Slab thickness	mm	150
Dead load (partitions and finishes)	kN/m^2	1.5
Imposed loads (floor)	kN/m^2	2.5
Self weight of slab (with normal weight concrete)	kN/m	=0.15*24*5=18.0
Partition and finishes	kN/m	=5*1.5=7.5
Characteristic dead load, G_k	kN/m	=18+7.5=25.5
Characteristic imposed load, Q_k	kN/m	=5*2.5=12.5
Design load, F	kN/m	=(1.4*25.5)+(1.6*12.5)=55.7
Self weight of the panel (100 mm thick wall of 1000 kg/m^3)	kN/m	3.2
Load carried by Panel 1	kN/m	55.7
Load carried by Panel 2	kN/m	114.6
Load carried by Panel 3	kN/m	173.5
Load carried by Panel 4	kN/m	232.4

Table 8.4 compared the applied loads (per 0.4m) on the different panels with the available panel strengths (per 0.4m) based on the experimental results in Table 7.2. It was expected that the 3m wall panel as proposed in Figure 8.2 will have a lower strength than the 400mm high test panels due to buckling. This will be further examined in Section 8.5, based on flexural buckling resistance. However, the results in Table 8.4 clearly indicated the 100mm thick panel with 0.4mm steel sheeting has sufficient cross-sectional resistance for four floors.

Table 8.4 Assessment of adequacy of 100mm thick wall with 0.4mm thick steel sheeting.

Description	Required load carrying capacity per 0.4m wide (kN)	Wall adequate based on average experimental results in Table 7.2 (Chapter 7)		
		no stopping edge (165kN)	with stopping edge (181kN)	with welded stopping edge (198kN)
Panel 1	= 0.4*55.7 = 23	√	√	√
Panel 2	= 0.4*114.6 = 46	√	√	√
Panel 3	= 0.4*173.5 = 70	√	√	√
Panel 4	= 0.4*232.4 = 93	√	√	√

8.5 EFFECT OF SLENDERNESS RATIO ON LOAD CARRYING CAPACITY OF COMPOSITE WALLING SYSTEM

It was expected that the strength of the proposed composite walling system will decrease increasing height due to buckling effect.

The flexural buckling resistance of panel under compression may be calculated using the well known Euler equation (Gere, 2004) given below:

$$P_{cr} = \frac{\pi^2 EI}{L_p^2} \quad \ldots\ldots(8.1)$$

where P_{cr} is the critical buckling load; EI ($=E_sI_s + E_cI_c$) is the flexural rigidity of the composite cross section with E_s and E_c being the Young's modulus of steel and LFC respectively and I_s and I_c being the second moment of area of the steel sheeting and LFC core respectively about the centre of the composite cross-section. E_s = 200,000 N/mm^2 and E_c = 3,300 N/mm^2. L_p is the length of composite panel.

Figure 8.3 clearly compared the buckling resistance of 400mm wide panels of two types of construction (with or without stopping edge) for panel heights ranging from 2m to 5m.

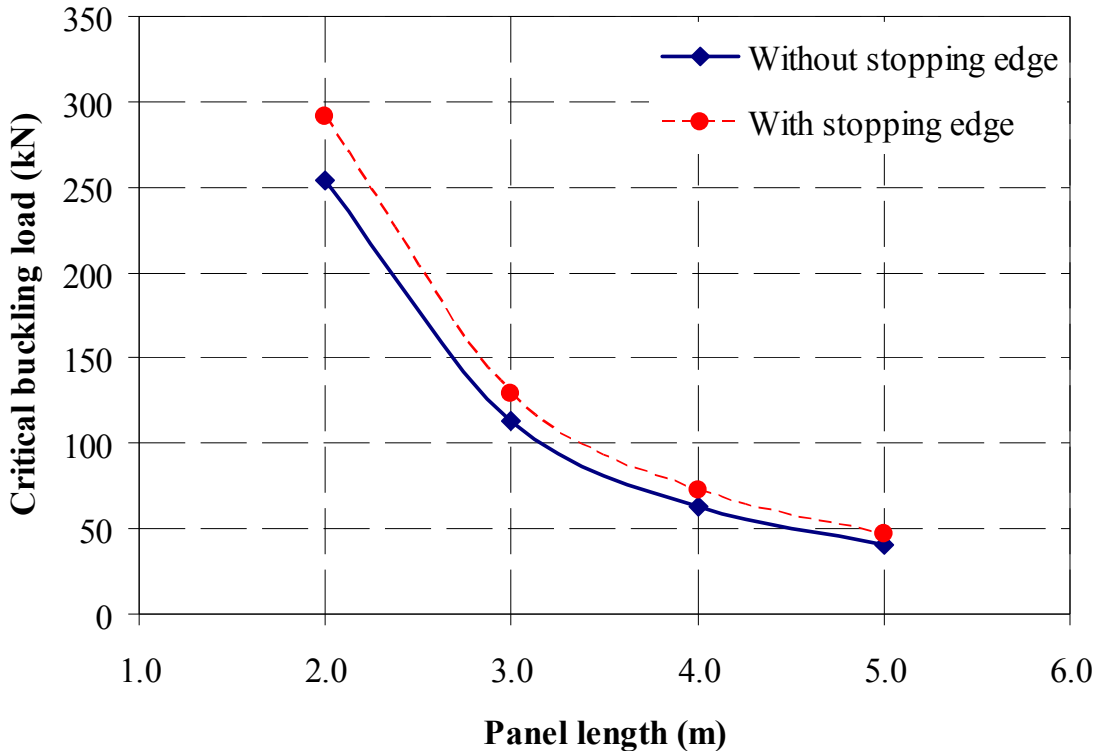

Figure 8.3 Relationship between critical load and panel height, panel width=400mm

Table 8.5 listed the applied loads (per 0.4m) for the different panels of the indicative building shown in Figure 8.1 with the calculated buckling strengths (per 0.4m) for different panel heights. The results showed that if the panel height does not exceed 3m, which would be sufficient to cover most cases of residential construction, the proposed panel system would have sufficient load carrying capacity. For heights of 4 and 5m, the proposed panel construction would not be sufficient for three storeys, but would be sufficient for one or two storey residential construction. For such heights, the panel thickness and steel sheeting thickness could be increased to increase the panel load carrying capacity. It should be pointed out that full composite action is not likely to take place between the steel sheeting and LFC core. Interaction between the steel sheeting and the LFC core was generated using mechanical bolts for the samples tested in this research. Nevertheless these mechanical fasteners that connected the two profiled steel facings with the concrete core were able to give some degree of composite action and preventing the steel from peeling off during loading. It is suggested that future work is necessary to develop a better bonding system for practical application. The main conclusion was that the LFC based composite walling system could be designed to resist the applied loads in low-rise residential construction.

Table 8.5 Assessment of adequacy of 100mm thick wall with 0.4mm thick steel sheeting for different panel lengths

Panel length (m)		2.0	3.0	4.0	5.0
Length-width ratio		5.0	7.5	10.0	12.5
Edge condition	Required load carrying capacity per 0.4m wide	Wall adequate based on critical buckling load calculation			
No stopping edge	Panel 1 (23kN)	√	√	√	√
	Panel 2 (46kN)	√	√	√	*x*
	Panel 3 (76kN)	√	√	*x*	*x*
	Panel 4 (93kN)	√	√	*x*	*x*
With stopping edge	Panel 1 (23kN)	√	√	√	√
	Panel 2 (46kN)	√	√	√	√
	Panel 3 (76kN)	√	√	*x*	*x*
	Panel 4 (93kN)	√	√	*x*	*x*
Welded edge	Panel 1 (23kN)	√	√	√	√
	Panel 2 (46kN)	√	√	√	√
	Panel 3 (76kN)	√	√	*x*	*x*
	Panel 4 (93kN)	√	√	*x*	*x*

8.6 SUMMARY

This short chapter has presented the results of a feasibility study to investigate the potential of using LFC in lightweight residential construction, considering the insulation performance for fire resistance and compressive resistance of LFC wall panels at ambient temperature.

From the fire resistance investigation, it had been concluded that the LFC based panel system exposed to the standard fire on one side can easily achieve the insulation performance requirement with a very small thickness, the minimum LFC panel thickness for the highest density (1400kg/m^3) being around 26.9mm, 43.5mm, 55.9mm and 67.4mm for 30, 60, 90 and 120 minutes of standard fire rating respectively. This performance was very similar to that provided by gypsum plasterboards. Because of the dominant role played by thermal conductivity, lighter LFC tends to perform better because of its low thermal conductivity.

From a comparison between squash resistance and Euler buckling load of LFC based composite walling systems against applied loads on a low-rise residential structure with typical floor loads and spans, it had been concluded that the LFC based walling system can be easily designed to achieve four storeys with typical floor heights between 2-5m.

Although there were a number of issues should still be investigated in detail in order to fine tune the design process, this study has confirmed the applicability of LFC based panel walling system to lightweight low-rise residential construction.

CHAPTER 9

CONCLUSIONS AND RECOMMENDATIONS FOR FUTURE WORK

This chapter presented a summary of the main conclusions of this study and gives some recommendations for future research on LFC.

9.1 SUMMARY AND CONCLUSIONS

Lightweight foamed concrete (LFC) was primarily used as a void filling and insulation material but it has a number of favourable characteristics such as light weight, good acoustic and insulation performance, ease in fabrication, environmentally sustainable, durable and cost effective. This had led LFC to be considered as a possible load-bearing material for building construction.

An extensive literature review in Chapter 2 had indicated that most of the researches have focused on LFC ambient temperature properties only and very little information was available on LFC thermal and mechanical properties at elevated temperatures. Also there were very few research studies to investigate structural performance and fire resistance of LFC based systems. Filling these major gaps in knowledge became the main objectives of this research. The following major tasks were undertaken to achieve the objectives of this research:

- Small-scale high temperature tests on LFC specimens (Chapter 3).
- Development of analytical models of thermal conductivity and specific heat of LFC (Chapter 3).
- Validation of thermal properties model and sensitivity study (Chapter 4).
- Mechanical properties tests of LFC at high temperatures (Chapter 5).

- Characterization of mechanical properties of LFC exposed to high temperatures (Chapter 5)

- Predictive equations for mechanical properties of LFC based on existing models for normal weight concrete (Chapter 6).

- Structural tests on prototype LFC based composite walling system consisting of two outer skins of profiled thin-walled steel sheeting with lightweight foamed concrete (LFC) core under axial compression (Chapter 7).

- Development of analytical model to calculate the maximum load-bearing capacity of this composite walling system (Chapter 7).

- Feasibility study on fire resistance and structural performance of LFC based system (Chapter 8).

From these research investigations, the following main conclusions may be drawn:

- For the purpose of establishing the thermal conductivity values of LFC at elevated temperatures, two methods may be considered: direct measurement using the hot guarded plate (HGP) test method and analytical method based on porous material. The analytical method has the advantage of providing fundamental understanding of the material and the thermal conductivity value can be determined with a minimum input of material property data at high temperatures. This contrasts with the HGP test method in which separate tests will be required for different temperatures. The superiority of the analytical model over the HGP test was that LFC of different densities may be now considered without relying on extensive tests.

- The development of the analytical method to determine the thermal conductivity of LFC at high temperatures was based on treating LFC as mix of dried LFC and water before completion of water evaporation and as mix of dried LFC and air voids afterwards. The thermal conductivity of dried LFC and average air void size should be determined in order to employ the analytical model. The void size may be acquired by taking a microscopic image of the LFC and the dried thermal conductivity value of LFC can be directly measured using the

HGP test or calculated if the LFC ambient temperature thermal conductivity was available. This chapter has presented detailed guidance on how to perform these calculations. A comparison between measured thermal conductivity results using the guarded hot plate test and the predicted thermal conductivity results using the theoretical model showed very good agreement.

- The specific heat of LFC can be approximated as the sum of a constant base value for the dried LFC and an additional value to allow for heat required to evaporate the free water.

- Given that the mechanical properties of LFC come from Ordinary Portland Cement, it has been confirmed that the reduction in mechanical properties of LFC can be predicted using the mechanical property models for normal weight concrete.

- From structural tests on LFC based composite walling system consisting of two outer skins of profiled thin-walled steel sheeting with LFC core under axial compression, for steel sheeting thicknesses of 0.4mm and 0.8mm respectively, it was found that all the specimens demonstrated good ductility, giving gradual reduction in load carrying capacity at increasing deformation. Failure of the composite walling was instigated by outward local buckling of the steel sheeting which was followed by concrete crushing of the LFC core. LFC was able to provide sufficient support to prevent the steel sheeting from inward buckling.

- Edge detailing of the LFC based composite walling system had some influence on the ultimate strength of the system. Covering the edges of the panels with steel sheeting improved the panel strength. Welding the steel sheeting at the edges (referred to as welded edge) to form a closed tubular construction gave higher load carrying capacity than without joining them (referred to as with stopping edges). Compared to LFC panels without the steel sheeting covering the edges, the load carrying capacities of panels with stopping edge and with welded edge were about 10% and 17% higher.

- The cross-sectional resistance of the LFC based composite walling system may be calculated by adding together the resistance of the steel sheeting and the

resistance of the profiled LFC core. For the LFC core, profiling results in a reduction of its strength due to unavoidable small eccentricity reducing the effectiveness of the LFC at the extremities of the core. The model proposed by Wright (1998), based on test results for normal weight concrete walling system, was found applicable to profiled LFC cores. In order to deal with local buckling of the steel sheeting, the combination of Uy and Bradford (1996) plate local buckling coefficients with the Liang and Uy (2000) effective width formulation to work out the steel sheeting effective width appears to provide the best agreement with the experimental results. Nevertheless, good agreements with test results were also established when using more traditional approach for the effective width method proposed by Winter (1947) in conjunction with the plate local buckling coefficients of Gerard and Becker (1957).

- The indicative study of fire resistance performance of LFC construction under standard fire exposure from one side has concluded that LFC has outstanding insulation performance for fire resistance and offers a practicable alternative to gypsum as the construction material for partition walls. For instant, a single layer of 650 kg/m^3 density LFC of about 21 mm would achieve 30 minutes of standard fire resistance rating, more or less similar to gypsum plasterboard.

- The results of a feasibility study on structural performance of composite panel system has confirmed it would be possible to design LFC based composite walling system to resist typical floor loads in low rise residential construction. For example, using 100mm LFC core and 0.4mm steel sheeting would give sufficient load carrying capacity for the construction of 4 storey buildings with 3m storey height.

9.2 RECOMMENDATION FOR FUTURE RESEARCH STUDIES

The author believes that this thesis represents the first comprehensive experimental and analytical study on thermal and mechanical properties of LFC at high temperatures and structural performance of composite walling system with LFC core. Inevitably, a number of assumptions have been made and some conclusions had been drawn based on limited available experimental data. While this study has filled some important gaps in knowledge related to LFC subject, it had also identified the need to execute more

comprehensive further research studies on LFC properties, structural behavior, fire resistance and other building construction requirements. In particular, this thesis recommends the following specific studies related to material specification, structural behaviour and fire resistance:

9.2.1 On material specification and properties

- The present study had concentrated on using a constant cement-sand ratio of 2:1 and water cement ratio of 0.5. Future work is necessary to look into different cement-sand ratios and water-cement ratios on thermal and mechanical properties of LFC at elevated temperatures.

- It was established from the literature review that utilization of fly ash as filler in LFC mix may contribute to better strength and thermal conductivity. Therefore it would be desirable for future studies to look into this effect.

- Similarly, it may be possible to improve the properties of LFC by using fibre, which may help reduce the size of the pores without increasing the LFC density.

- The present experimental and numerical studies on thermal and mechanical properties were limited to two LFC densities. Future studies should place greater emphasise on different densities as well.

- It would be ideal if the mechanical properties of LFC at elevated temperatures could be predicted numerically, taking into consideration the mechanical properties of the solid constituent and the effects of pores.

- The elevated temperature mechanical property tests presented in this study were under the steady state condition. Transient state tests, although being more difficult, may become necessary. Also, the tests in this study were conducted to obtain mechanical properties of unstressed samples at high temperatures. Other mechanical properties, including the effect of pre-stress, residual properties after cooling down, thermal strain at high temperatures, should also be investigated.

9.2.2 On structural behaviour

- This research had used one type of profiling. It would be interesting to conduct future studies to look into the effects of different steel profiling.

- The feasibility study in Chapter 8 used either the cross-sectional resistance of Euler buckling load as the upper limit. Future work is essential to establish empirical equations to consider their interactions.

- Interaction between the steel sheeting and the LFC core was generated using mechanical bolts for the samples tested in this research. For practical application, a better bonding system should be developed.

- The structural tests were conducted on individual samples. Connection between panels will have important influence on the entire panel behaviour. For practical construction, such detailing should be carefully investigated. It is recommended that full scale panel tests should be conducted.

- Bending and combined bending and axial compression behaviour should be investigated.

- More detailed numerical simulation methods should be developed for both local buckling effects and global structural behaviour.

9.2.3 On fire resistance

- This study had only carried out an indicative investigation of thermal insulation performance for fire resistance. Structural load-bearing capacity, one of the three requirements of fire resistance, should be investigated in the future. In particular, future investigation should include the effects of non-uniform temperature distribution in the LFC based system.

- This study had only focused on the structural behaviour of small scale composite panel system at ambient temperature. In order to demonstrate the structural performance of LFC based composite panel system in fire, future studies should concentrate on the effects of elevated temperatures on the strength of composite system.

- Fire integrity, related to preventing fire spread through gaps in construction, is one of the three requirements of fire resistance. Panel joining detailing will greatly affect fire integrity. Future research studies should be conducted to investigate this effect.

- Numerical methods should be developed to carry out combined heat transfer and structural behaviour analysis under fire condition.

- Performance based fire engineering, in which natural fire condition, as opposed to the standard fire condition, can be considered. Future research should extend the current studies to natural fire conditions.

- Methods of assessing and repairing fire damaged LFC construction should be developed.

REFERENCES

Ai, H., Young, J.F., and Scherer, G. W., "*Thermal expansion kinetics: Method to measure permeability of cementitious materials: II, application to hardened cement pastes*", J. Am. Ceram. Soc., 84, 385-391 (2001).

Aldridge, D., "*Introduction to foamed concrete: What, Why, and How?*", In: Dhir, R. K., Newlands, M. D., McCarthy, A., Editors; Use of foamed concrete in construction, London: Thomas Telford, 1-14 (2005).

Aldridge, D., and Ansell, T., "*Foamed concrete: production and equipment design, properties, applications and potential*", In: Proceedings of one day seminar on foamed concrete: Properties, applications and latest technological developments, Loughborough University (2001).

Anderberg, Y. and Thelandersson, S. "*Stress and deformation characteristics of concrete at high temperatures: Experimental investigation and material behavior model*", Bulletin 54, Sweden (Lund): Lund Institute of Technology (1976).

Ang, C. N., and Wang, Y. C., "*The effect of water movement on specific heat of gypsum plasterboard in heat transfer analysis under natural fire exposure*", J. Construct. Build. Mater., 18, 505-515 (2004).

ASTM C 177-97, "*Standard test method for steady-state heat flux measurements and thermal transmission properties by means of the guarded-hot-plate apparatus*", American Society for Testing and Materials (1997).

Balshin, M. Y., "*Dependence of mechanical properties of metal powders on porosity and limiting properties of metal–ceramic materials (in Russian)*", Dokl. Akad. Nauk. UzSSR, 67, 831-834 (1949).

Bazant, P., and Chern, J. C., "*Stress-induced thermal and shrinkage strains in concrete*", J. Eng. Mech., ASCE, 113, 1493–511 (1987).

Brady, K. C., Watts, G. R. A., and Jones, M. R., "*Specification for foamed concrete*", Prepared for Quality Services, Civil Engineering, Highways Agency (2001).

Brandt, A. M., "*Cement-Based Composites: Materials, mechanical properties and performance*", E & FN Spon, London, 117-118 (1995).

British Cement Association, "*Foamed concrete: Composition and properties*", Report Ref. 46.042, Slough: BCA (1994).

BS 476, "*Fire tests on building materials and structures, Part 20: Method for determination of the fire resistance of elements of construction*", General principles (1987).

BS EN 197-1, "*Cement: Composition, Specifications and conformity criteria for low heat common cements*", British Standards Institution, London (2000).

BS EN 12620, "*Aggregates for Concrete*", British Standards Institution, London (2002).

Bulson, P. S., "*The stability of flat plates*", Chatto and Windus, London (1970).

Burns, P. J., and Tien, C.L., "*Natural convection in porous media bounded by concentric spheres and horizontal cylinders",* Int. J. Heat Mass Transfer, 22, 929-939 (1979).

Cabrera, J. G., and Lynsdale, C. J., "*A new gas permeameter for measuring the permeability of mortar and concrete*", Mag. Concr. Res., 40, 177-182 (1988).

Carman, A. P., and Nelson, R. A., "*The thermal conductivity and diffusivity of concrete*", Bulletin No.122, University of Illinois Engineering Experiment Station, Urbana-Champaign (1921).

Carslaw, H.S. and Jaeger, J.C., "*Conduction of Heat in Solids*", 2nd ed., Oxford: Oxford University Press (1959).

CEN 1991-1-2, "*Eurocode 1, Actions on structures, Part 1.2: General actions - Actions on structures exposed to fire*", Brussels, European Committee for Standardisation (2002).

CEN 1992-1-2, "*Eurocode 2, Design of concrete structures, Part 1.2: General rules - Structural fire design*", Brussels, European Committee for Standardisation, Document (2004).

CEN 1994-1-2, "*Eurocode 4, Design of composite steel and concrete structures, Part 1.2: General rules - Structural fire design*", Brussels, European Committee for Standardisation (2005).

De Rose, L., and Morris, J., "*The influence of mix design on the properties of microcellular concrete*", In: Dhir, R. K., Handerson, N. A., Editors; Specialist techniques and materials for construction, Thomas Telford, London, 185-197 (1999).

Dransfield, J. M., "*Foamed concrete: Introduction to the product and its properties*", One day awareness seminar on 'Foamed concrete: properties, applications and potential' held at University of Dundee, Scotland, 1-11, 23rd March (2000).

Gallé, C. and Sercombe J., *"Permeability and pore structure evolution of silico-calcareous and hematite high-strength concretes submitted to high temperatures*", J. Mater. Struct., 34, 619-628 (2001).

Gerard, G., and Becker, M., "*Handbook of Structural Stability: Part I - Buckling of Flat Plates*", NACA TN 3781 (1957).

Gere, J. M., "*Mechanics of materials*", Belmont, US (2004).

Giannakou, A., and Jones, M. R., "*Potentials of foamed concrete to enhance the thermal performance of low rise dwellings*", In: Dhir, R. K., Hewelett, P. C., Csetenyi, L. J., Editors; Innovations and development in concrete materials and construction, Thomas Telford, United Kingdom, 533-544 (2002).

Hamidah, M. S,, Azmi, I., Ruslan, M. R. A., Kartini, K., and Fadhil, N. M., "*Optimisation of foamed concrete mix of different sand-cement ratio and curing conditions*", In: Dhir, R. K., Newlands, M. D., McCarthy, A., Editors; Use of foamed concrete in construction, Thomas, London, 37-44 (2005).

Harmathy, T.Z., "*The SFPE Handbook of Fire Protection Engineering*", Society of Fire Protection Engineers/National Fire Protection Association: Boston (1988).

Hertz, K. D., "*Concrete strength for fire safety design*", Mag. Concr. Res., 57, 445-453 (2005).

Hock, S. C., and Giang, T. H., "*Protection of steel structures - modern trend in fire safety engineering approach*", Malaysian Structural Steel Association Convention, Kuala Lumpur (1998).

Hoff, G. C., "*Porosity-strength considerations for cellular concrete*", J. Cement Concr. Res., 2, 91-100 (1972).

Holman, J. P., "*Heat Transfer*", Boston, London, McGraw-Hill, 9th ed. (2002).

Jones, M. R., "*Foamed concrete for structural use*", In: Proceedings of one day seminar on foamed concrete: properties, applications and latest technological developments, Loughborough University, 27-60 (2001).

Jones, M. R., and McCarthy, A., "*Preliminary views on the potential of foamed concrete as a structural material*", Mag. Concr. Res., 57, 21-31 (2005).

Jones, M. R., and McCarthy, A., "*Utilising unprocessed low-lime coal fly ash in foamed concrete*", Fuel, 84, 1398-1409 (2005).

Jones, M. R., and McCarthy, A., "*Behaviour and assessment of foamed concrete for construction applications*", In: Dhir, R. K., Newlands, M. D., McCarthy, A., Editors; Use of foamed concrete in construction, Thomas, London, 61-88 (2005).

Kalifa, P., and Tsimbrovska, M., "*Comportement des BHP à hautes températures - Etat de la question et résultats expérimentaux*", Cahier du CSTB, n°3078 (1998).

Kalliopi, K. A., "*Pore structure of cement-based materials: Testing, interpretation and requirements*", Taylor & Francis, 9-11 (2006).

Kearsley, E. P., "*The use of foamed concrete for affordable development in third world countries*", In: Dhir R. K., McCarthy M. J., editors, Appropriate concrete technology, E&FN Spon, London, 233-243 (1996).

Kearsley, E. P., and Mostert, H. F., "*Use of foam concrete in Southern Africa*", In: Proceedings from the ACI international conference on high performance concrete, SP 172-48, 919-934 (1997).

Kearsley, E. P., and Mostert, H. F., "*The use of foamed concrete in refractories*", In: Dhir, R. K., Newlands, M. D., McCarthy, A., Editors; Use of foamed concrete in construction, Thomas, London, 89-96 (2005).

Kearsley, E. P., and Mostert, H. F., "*Opportunities for expanding the use of foamed concrete in the construction industry* ", In: Dhir, R. K., Newlands, M. D., McCarthy, A., Editors; Use of foamed concrete in construction, Thomas, London, 143-154 (2005).

Kearsley, E. P., and Wainwright P. J., "*The effect of high fly ash content on the compressive strength of foamed concrete*", J. Cement Concr. Res., 31, 105-112 (2001).

Kearsley, E. P., and Wainwright P. J., "*Porosity and permeability of foamed concrete*", J. Cement Concr. Res., 31, 805-812 (2001).

Kearsley, E. P., and Wainwright P. J., "*The effect of porosity on the strength of foamed concrete*", J. Cement Concr. Res., 32, 233-239 (2002).

Kessler, H. G., "*Cellular lightweight concrete*", Concrete Engineering International, 56-60 (1998).

Khennane, A., and Baker G., "*Uniaxial model for concrete under variable temperature and stress*", J. Eng. Mech., ASCE, 119, 1507-1525 (1993).

Khoury, G. A., "*Compressive strength of concrete at high temperatures: A reassessment*", Mag. Concr. Res., 44, 291-309 (1992).

Khoury, G. A., Majorana, C. E., Pesavento, F., and Schrefler, B. A., "*Modelling of heated concrete*", Mag. Concr. Res., 54, 77–101 (2002)

Koudriashoff, I. T., "*Manufacture of reinforced foam concrete roof slabs*", J. American Concrete Institute, 21, 37-48 (1949).

Li, L., and Purkiss J. A., "*Stress–strain constitutive equations of concrete material at elevated temperatures*", J. Fire Safety, 40, 669-686 (2005).

Li, W., and Guo, Zh. H., "*Experimental investigation on strength and deformation of concrete under high temperature*" Chin. J. Build. Struct., 14, 8-16 (1993).

Liang, Q. Q., and Uy, B., "*Theoretical study on the post-local buckling of steel plates in concrete-filled box columns*" J. Comput. Struct., 75, 479-90 (2000).

Lie, T. T., and Lin, T. D., "*Fire performance of reinforced concrete columns*", In: ASTM STP 882, Fire Safety: Science and Engineering, 176-205 (1985).

Lin, W. M., Lina, T. D., and Powers-Couche, L. J., "*Microstructures of fire-damaged concrete*", J. American Concrete Institute Materials, 93, 199-205 (1996).

Lu, Zh. D., "*A Research on fire response of reinforced concrete beams*", PhD thesis, Tongji University (1989).

Malhotra, H.L., "*Design of Fire-Resisting Structures*", London, Surrey University Press (1982).

McGovern, G., "*Manufacture and supply of ready-mix foamed concrete*", One day awareness seminar on 'Foamed concrete: Properties, applications and potential' held at University of Dundee, 12-25 (2000).

Md Azree, O. M., "*Effect of using additives to the compressive strength of lightweight foamed concrete*", Master Dissertation, School of Housing, Building and Planning, University of Science Malaysia, Penang (2004).

MDC Legal Advisors, "*Uniform Building By-laws*", 8th ed., Malaysia, MDC Publishers Printers Sdn. Bhd. (1997).

Montgomery, R. "*Heat-resisting and refractory concretes*", Advanced Concrete Technology: Processes. Edited by Newman, J., and Choo, B. S., Elsevier Ltd, 4/1-4/13 (2003).

Nambiar, E. K. K., and Ramamurthy, K., "*Models relating mixture composition to the density and strength of foam concrete using response surface methodology*", J. Cement Concr. Compos., 28, 752-760 (2006).

Nambiar, E. K. K., and Ramamurthy, K., "*Influence of filler type on the properties of foam concrete*", J. Cement Concr. Res., 28, 475-80 (2006).

Nambiar, E. K. K., and Ramamurthy, K., "*Air-void characterization of foam concrete*", J. Cement Concr. Res., 37, 221-230 (2007).

Nambiar, E. K. K., and Ramamurthy, K., "*Models for strength prediction of foam concrete*", J. Mater. Struct., 41, 247-254 (2008).

Narayanan, N., and Ramamurthy, K., "*Prediction relations based on gel-pore parameters for the compressive strength of Aerated Concrete*", Concr. Sc. Eng., 1, 206-212 (2000).

Noumowe, A., "*Effet des hautes temperatures (20 °C– 600 °C) sur le beton*", Ph.D. thesis, Institute National des Sciences Appliquees (1995).

Ozisik, M. N., "*Heat Transfer: A Basic Approach*", New York, London, McGraw-Hill (1985).

Phan, L. T., and Carino N. J., "*Code provisions for high strength concrete strength temperature relationship at elevated temperatures*", J. Mater. Struct., 36, 91-98 (2003).

Purkiss, J. A., "*Fire safety engineering - design of structures*", Oxford: Butterworth Heinemann (1996).

Rahmanian, I., "*Fire resistance of gypsum board based systems*", First year Ph.D. progression report, School of Mechanical, Aerospace and Civil Engineering, University of Manchester (2008).

Ramamurthy, K., Nambiar, E. K. K., and Ranjani G. I. S., "*A classification of studies on properties of foam concrete*", J. Cement Concr. Compos., 31, 388-396 (2009).

Rostasy, F. S., Weiβ R., and Wiedemann G., "*Changes of pore structure of cement mortars due to temperature*", J. Cement Concr. Res., 10, 157-164 (1980).

Sach, J., and Seifert, H., "*Foamed concrete technology: possibilities for thermal insulation at high temperatures*", CFI Forum of Technology, DKG 76, No. 9, 23-30, (1999).

Schneider, U., and Herbst, H., "*Permeability and porosity of concrete at high temperature*", Technical report 403, Deutscher Ausschuss für Stahlbeton, Berlin, In German (1989).

Shanmugam, N. E., and Lakshmi, B., "*State of the art report on steel-concrete composite columns*" J. Constructional Steel Research, 57, 1041-1080 (2001).

Tam, C. T., Lim, T. Y., and Lee, S. L., "*Relationship between strength and volumetric composition of moist-cured cellular concrete*", Mag. Concr. Res., 39, 12-18 (1987).

Taylor, H. F. W., "*Cement Chemistry*", London: Academic Press (1992).

Terro, M. J., "*Numerical modeling of the behavior of concrete structures in fire*", J. American Concrete Institute Struct., 95,183-193 (1998).

Turner, M., "*Fast set foamed concrete for same day reinstatement of openings in highways*", In: Proceedings of one day seminar on foamed concrete: properties, applications and latest technological developments, Loughborough University, 12-18 July (2001).

Uy, B., and Bradford, M. A., "*Elastic local buckling of steel plates in composite steel-concrete members*", J. Eng. Struct., 18, 193-200 (1996).

Valore, R. C., "*Cellular concrete Part 1 Composition and methods of production*" J. American Concrete Institute, 50, 773-796 (1954).

Van Deijk, S., "*Foamed Concrete*", Concrete, 49-54, July/August (1991).

Van Deijk, S., "*Foamed Concrete*", A Dutch View, BRE, 2-8 (1992).

Visagie, M., and Kearsely E. P., "*Properties of foamed concrete as influenced by air-void parameters*", Concrete/Beton, 101, 8-14 (2002).

Wang, H. B., "*Heat Transfer Analysis of Components of Construction Exposed to Fire*", Department of Civil Engineering and Construction, University of Salford, Manchester (1995).

Watson, K. L., "*Autoclaved aerated concrete from slate waste Part 2: some property/porosity relationship*", Int. J. Lightweight Concr., 2, 121-123 (1980).

Weigler, H., and Karl, S., "*Structural lightweight aggregate concrete with reduced density - Lightweight aggregate foamed concrete*", Int. J. Lightweight Concr., 2, 101-104 (1980).

Winter, G., "*Strength of Thin Steel Compression Flanges*", Transactions, ASCE, 112, 527-554 (1947).

Wright, H. D., "*The axial load behaviour of composite walling*", J. Construct. Steel Research, 45, 353-375 (1998).

Wright, H. D., and Gallocher, S. C., "*The behaviour of composite walling under construction and service loading*", J. Construct. Steel Research, 35, 257-273 (1995).

Ye, G., Liu, X., De Schutter, G., Taerwe, L., and Vandevelde, P., "*Phase distribution and microstructural changes of SCC at elevated temperatures*", J. Cement Concr Res, 37, 978-987 (2007).

Yuan, J., "*Fire protection performance of intumescent coating under realistic fire conditions*", Ph.D. Thesis, School of Mechanical, Aerospace and Civil Engineering, University of Manchester (2009).

Appendix A: Publication 1

Construction and Building Materials xxx (2010) xxx–xxx

Contents lists available at ScienceDirect

Construction and Building Materials

journal homepage: www.elsevier.com/locate/conbuildmat

Elevated-temperature thermal properties of lightweight foamed concrete

Md Azree Othuman, Y.C. Wang *

School of Mechanical, Aerospace and Civil Engineering, University of Manchester, Manchester M60 1QD, UK

ARTICLE INFO

Article history:
Received 11 December 2009
Received in revised form 2 July 2010
Accepted 18 July 2010
Available online xxxx

Keywords:
Foamed concrete
Thermal conductivity
Thermal properties
Fire resistance
Porous material

ABSTRACT

This paper reports the results of an experimental and analytical study to quantify the thermal properties of lightweight foamed concrete (LFC) at high temperatures. The density of LFC ranges from 600 to 1800 kg/m^3. The primary objective of this study is to obtain the thermal conductivity of LFC at high temperatures so as to obtain material property data for prediction of fire resistance of LFC based systems. In the analytical approach, LFC is considered to be a two phase material with solid cement and air pores. Therefore, it is assumed that the thermal conductivity of LFC is a function of its porosity and pore size. The porosity of LFC can be easily obtained from the volume of foam inside the material. The effective pore size is based on the dominant internal pore size of the foamed concrete. The Hot Guarded Plate (HGP) test was carried out at different elevated temperatures for foamed concrete of different densities. The HGP test and analytical prediction results are in close agreement. To validate the thermal property results, transient heating tests were conducted in an electric kiln on LFC slabs and the recorded temperatures were compared with a validated one-dimensional heat transfer program in which the aforementioned thermal properties were treated as input data. Close agreement between the measured and predicted temperature results confirms the thermal property results.

1. Introduction

LFC is a material consisting of Portland cement paste or cement filler matrix (mortar) with a homogeneous pore structure created by introducing air in the form of small bubbles. It has a number of attractive characteristics such as good thermal and acoustic insulation, self flowing and being easy to fabricate. Its use so far has been mainly as a filler material in civil engineering works [1]. However, its good thermal and acoustic performance indicates its strong potential as a material in building construction. Although its mechanical properties are low compared to normal strength concrete, LFC may be used as partition or light load bearing walls in low-rise residential construction. The first stage to realize the potential of LFC in building construction is to obtain reliable thermal and mechanical properties of LFC at ambient and elevated temperatures. To date, although there have been many studies on thermal and mechanical properties of lightweight aggregate concrete at ambient and high temperatures, there is an almost complete lack of systematic research to investigate the thermal or mechanical properties of LFC at elevated temperatures. This paper reports the results of an experimental and numerical study to investigate and establish the thermal properties of LFC at high temperatures.

When LFC is exposed to high temperatures, the free water in the pores and some chemically bonded water in the hydrated cement paste are released, consuming a large amount of energy, just as what happens in normal weight concrete. A few authors have described, as follows, the reactions that occur in cement based material like LFC at high temperatures. Vaporization of the free water takes place at around 100 °C [2]. It is generally considered that the evaporable water is completely eliminated at 120 °C. Then between 180 and 300 °C, loss of the chemically bond water happens through decomposition of the C–S–H and carboaluminate hydrates [3]. The high temperatures in the range of 400–600 °C may then stimulate a series of reactions in the hardened LFC paste. These reactions originate with the complete desiccation of the pore system, followed by decomposition of the hydration products and the destruction of C–S–H gels [4]. The conversion of calcium hydroxide into lime and water vapour during heating may lead to serious damage due to lime expansion [5]. These changes will affect the thermal properties of LFC.

Since LFC is a porous material, its effective thermal conductivity will be affected by the air pores inside. Within each air pore, heat conduction will dominate at relatively low temperatures. At high temperatures, radiation will play a much more important role because the radiant heat transfer coefficient is related to temperature raised to power three. The effective thermal conductivity of LFC at elevated temperatures depends not only on the thermal conductivities of the cement and the air, but also radiation effect inside the air pores.

* Corresponding author. Tel.: +44 161 3068968.
E-mail address: yong.wang@manchester.ac.uk (Y.C. Wang).

0950-0618/$ - see front matter © 2010 Elsevier Ltd. All rights reserved.
doi:10.1016/j.conbuildmat.2010.07.016

Analytical models of thermal conductivity and specific heat of LFC will be proposed, based on the assumed internal structure (porous) and constituents (cement, water and air) of LFC. The density of LFC may be obtained by direct measurement. These thermal properties may then be used in heat transfer analysis to obtain thermal performance (temperature distributions) of LFC under different heating conditions. This research is mainly concerned with establishing thermal property models of LFC at high temperatures. To do so, the proposed thermal property models of LFC are used as input in a validated one-dimensional heat transfer analysis program [6]. A number of heating tests are also carried out on LFC specimens in which an LFC panel of 150 mm in thickness is subjected to heating from an electric kiln. The heating tests were carried out for LFC of densities of 650 kg/m^3 and 1000 kg/m^3. The numerical prediction results are then compared with the experimental results. Through correlation between the prediction and experimental results, the proposed thermal property models can be assessed. Although direct measurement of thermal conductivity of foamed concrete is possible, e.g. through the use of Hot Guarded Plate (HGP) test, the alternative analytical approach, to be proposed in this paper, has the advantage of being able to provide fundamental understanding of the parameters affecting thermal conductivity. This paper presents details of these studies.

2. Experimental set-up

Two sets of tests were carried out: the transient high temperature tests on LFC slabs in an electric kiln and the Hot Guarded Plate (HGP) test. The HGP tests were carried out to provide data to correlate with the analytical method for thermal conductivity and the electric kiln tests provided transient temperature information to validate the thermal property models.

For the electric kiln tests, LFC panels of two densities of 650 kg/m^3 and 1000 kg/m^3 were cast and tested. The 650 kg/m^3 density was selected so as to enable comparison of thermal performance between LFC and that of other building materials of similar density, such as gypsum board; the 1000 kg/m^3 density was considered because LFC of this density would have a useful amount of mechanical properties to make it viable as a light load bearing infill material, which may be combined with thin walled steel in lightweight composite panel construction.

All LFC panel specimens had dimensions of 430 mm × 415 mm in plan and 150 mm in thickness. Each specimen was placed horizontally on top of an electric kiln as the source of heat, so that one side of the panel was subjected to kiln temperature and the other side faced up to the room temperature, as shown in Fig. 1. The heating chamber has an internal diameter of 64.8 mm and 53.4 cm height. A cross section through the electric kiln and the test specimen is shown in Fig. 2. There was a 280 mm × 265 mm opening on the top lid of the kiln, which allowed exposure of the lower side of the panel to elevated temperatures. A 30 mm thick layer of glass wool with the same opening size was laid under the specimen to insulate the contact surface of the top lid. The kiln temperature was increased to about 1200 °C.

2.1. Thermocouple arrangement

Heat transfer through each test LFC panel is assumed to be one dimensional. Therefore, to investigate temperature developments through each LFC panel, Type K thermocouples were placed throughout the thickness of the LFC specimen at the centre of the panel. Five thermocouples (T1–T5) were installed: on the exposed side, on the unexposed side and at quarter, half and three-quarter thickness, as shown in Fig. 3, being 37.5 mm, 75 mm and 112.5 mm from the heated surface. To check the assumption of one-dimensional heat flow inside the LFC panel, four additional thermocouples (T6–T9) were positioned at two corners of a 150 × 150 mm square in the centre region of the specimen, as shown in Fig. 3. One thermocouple was place inside the kiln, at an approximate distance of 50 mm from the exposed surface of the panel, to record the kiln temperature.

2.2. Specimen preparation

All LFC samples were made in house. The stable foam was produced using foam generator Portafoam TM2 System (Fig. 4), purchased from the Malaysian manufacturer (www.portafoam.com). This system runs from an air compressor and consists of a main generating unit, a foaming unit, and a lance unit. The foaming agent used was Noraite PA-1 (protein based) which is suitable for LFC densities ranging from 600 kg/m^3 to 1600 kg/m^3. Noraite PA-1 comes from natural sources and has a weight of around 80 g/l and expands about 12.5 times when used with the Portafoam foam generator. The aforementioned thermocouples were positioned during casting the LFC specimens. These thermocouples were found to be in the correct positions once the samples dried. Three identical specimens were prepared for each density and were tested at 14 days after mixing.

Fig. 1. A typical set-up for the small-scale fire test.

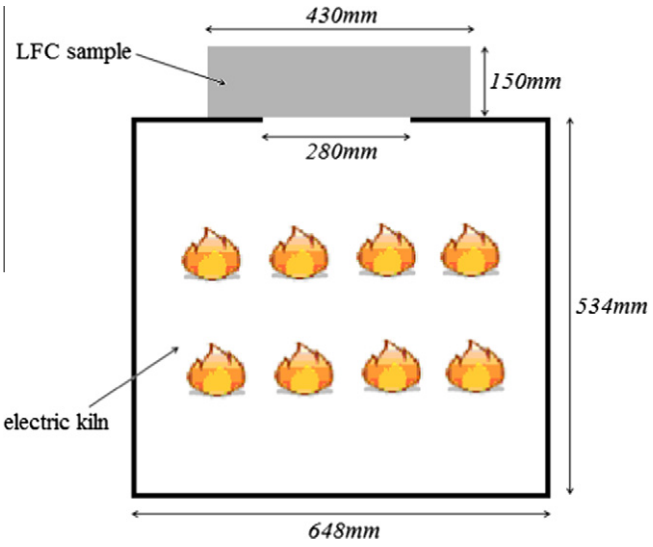

Fig. 2. Cross section through the electric kiln and test specimen in elevation.

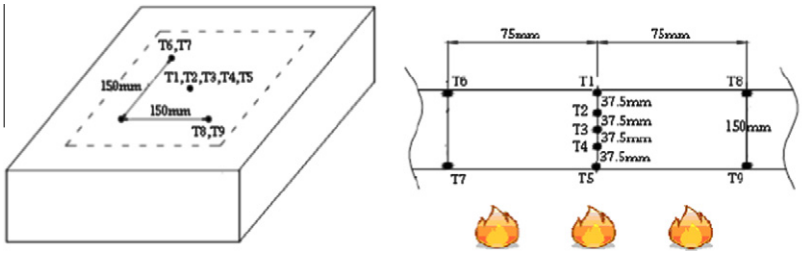

Fig. 3. Thermocouple layout on LFC specimens on plan and throughout thickness.

2.3. Kiln specifications and temperature

LFC is considered to be non-reactive so its thermal properties are temperature dependent only. Therefore, at this stage of the study an electric kiln was deemed satisfactory as the source of heat and a Harrier Top Loading Electric Kiln was used for the experiments. The kiln temperature was controlled in such a way that its temperature–time relationship resembled that of the standard fire curve according to the British Standard for fire resistance testing BS476 [7]. However, since this study relates the thermal properties of LFC to its temperature, rather than that of the air, and the recorded LFC slab surface temperatures were used as input data, the kiln simply acted as a heating source. It was not important that its heating curve did not follow that of the standard fire curve exactly. Fig. 5 shows the heating curve achieved in the kiln, which is compared to a standard cellulosic fire curve (BS476).

2.4. Hot guarded plate (HGP) test

The HGP test followed the ASTM procedure in Ref. [8]. The basic HGP method consists principally of a hot plate and a cold plate. In a HGP test, the test specimen is placed on a flat plate heater assembly consisting of an electrically heated inner plate (main heater) surrounded by a guard heater. The guard heater is carefully controlled to maintain the same temperature on both sides of the gap separating the main and the guard heaters. This prevents lateral heat flow from the main heater and ensures that heat from the electric heater flows in the direction of the specimen. On the opposite side of the specimen are additional flat plate heaters (cold plate) that are controlled at a fixed temperature selected by the operator. For a given heat input to the main heater, the hot plate assembly rises in temperature until the system reaches equilibrium.

The final hot plate temperature depends on the electrical power input, the thermal resistance of the specimen, and the temperature of the cold plate. The average thermal conductivity, k, of the specimen is determined from the Fourier heat flow equation:

$$k = \frac{W}{A}\left[1 \times \frac{d}{\Delta T}\right] \quad (1)$$

where W is the electrical power input to the main heater, A is the main heater surface area, ΔT is the temperature difference across the specimen, and d is the specimen thickness.

Based on the assumption that LFC is a homogeneous porous material, an analytical approach for its thermal conductivity will be provided. The analytical approach has the advantage of providing fundamental understanding of the material and the thermal conductivity value can be determined with a minimum input of material data at high temperatures. This contrasts with the HGP test in which separate tests will be necessary for different temperatures. Nevertheless, the HGP test can be used to provide the base value of thermal conductivity of solid cement and also an independent set of thermal conductivity values to validate the analytical approach.

Table 1 presents the HGP test results.

3. Thermal-physical properties of LFC

LFC can be considered as a non-reactive material and therefore its thermal properties can be considered to be temperature dependent only. Given that there is mass transfer involving water movement, precise treatment of thermal performance of LFC in fire should include combined heat and mass transfer. However, mass transfer can be rather complex to deal with and many of the mass transfer related material properties are different to obtain. An alternative treatment is to carry out heat transfer analysis only, but taking into consideration the effects of mass transfer in heat transfer properties. The validity of such a treatment has been demonstrated by Ang and Wang [9] on gypsum plaster, which has similar mass and heat transfer phenomena. The main effect of mass transfer, caused by moisture movement, is included in heat transfer analysis by modifying the specific heat of LFC. This will be explained in detail in Section 3.2.

Apart from specific heat, the other two properties that will be required as input data in heat transfer analysis is density and thermal conductivity of LFC. Sections 3.1 and 3.3 will explain how their values will be obtained in this study.

In fire resistance design, the fire temperature is treated as input information. To calculate temperatures in the construction element exposed to the given fire environment, it is necessary to determine the thermal boundary condition between the fire and

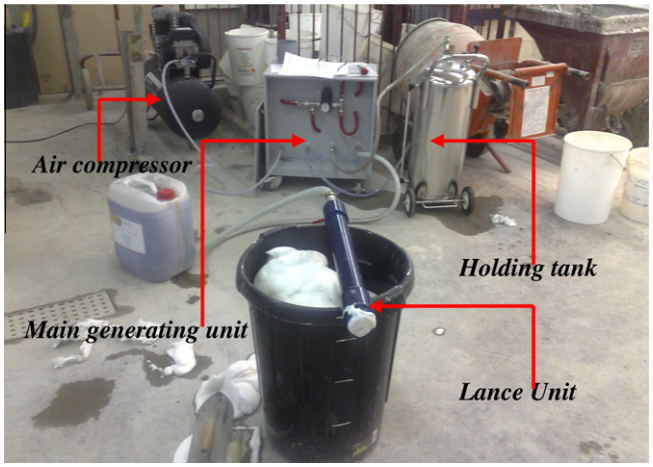

Fig. 4. Portafoam TM2 foam generator system.

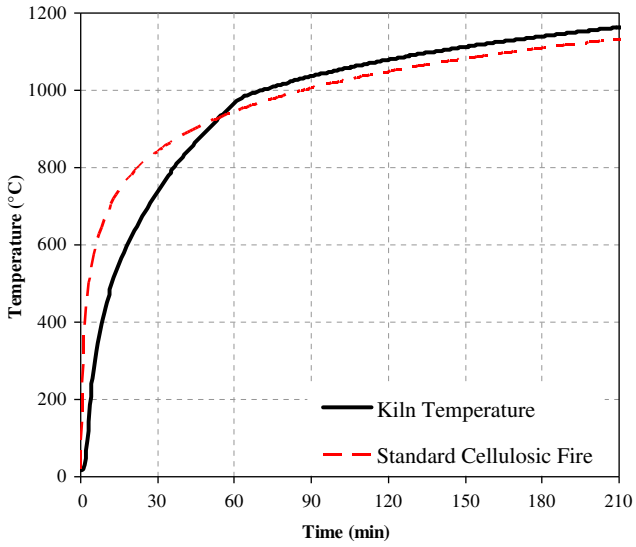

Fig. 5. Time–temperature curve for the kiln against standard cellulosic fire curve.

Table 1
Thermal conductivity of LFC at different temperatures obtained through Hot Guarded Plate tests.

Density (kg/m^3)	Thermal conductivity at different temperatures (W/m °C)							
	20 °C	90 °C	105 °C	150 °C	170 °C	180 °C	200 °C	250 °C
650	0.226	0.226	0.209	0.163	0.131	0.133	0.138	0.144
1000	0.309	0.309	0.289	0.253	0.235	0.238	0.239	0.245
1850	0.484	0.484	0.472	0.449	0.433	0.433	0.433	0.434

the surface of the construction element, including convective and radiant heat transfer. However, since the purpose of this study is to obtain thermal properties of LFC, the measured exposed surface temperature will be taken as input data so as to eliminate the uncertainty caused by the unknown thermal boundary condition.

3.1. Effects of moisture content and dehydration reactions on LFC density

LFC contains free water and chemically bond water. The free water content in LFC depends on the density (i.e., the free water content for the 650 kg/m^3 density is 1.7% by weight and that for the 1000 kg/m^3 density is 3.2% by weight based on experiment data). Evaporation of the free and of some of the chemically bond water will cause dehydration in LFC, which will affect all the aforementioned three items of thermal properties of LFC.

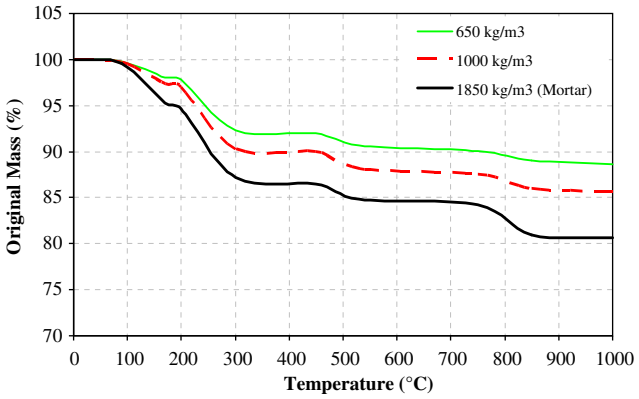

Fig. 6. Percentage of original density at different temperatures.

The dehydration process starts as early as 90 °C. In the range of 90–170 °C, the evaporable free water and part of the chemically bond water escapes. The evaporable free water may be considered to have been completely eliminated by 170 °C. Some chemically bond water is also lost through decomposition of the Calcium Silicate Hydrates (C–S–H) gel that takes place between 120 °C and 140 °C and decomposition of ettringite around 120 °C [10]. In the temperature range between 200 °C and 300 °C, some of the chemically bond water is released from further decomposition of the C–S–H gel and the sulfoaluminate phases ($3CaO{\cdot}Al_2O_3{\cdot}CaSO_4{\cdot}12H_2O$ and $3CaO{\cdot}Al_2O_3{\cdot}3CaSO_4{\cdot}31H$) of the cement paste [10]. Further dehydration occurs at around 450 °C, which corresponds to decomposition of $Ca(OH)_2 \rightarrow CaO + H_2O$ and it's completed at 530 °C [10]. At the second dehydration reaction, 75% of the chemically combined water is vaporised and the remaining 25% is then evaporated at the third dehydration reaction.

The previously described three stages of dehydration are accompanied by water loss or reduction in density of LFC. Fig. 6 shows recorded densities of LFC at different temperatures, as ratio of the original density for two different initial density values, 650 kg/m^3 and 1000 kg/m^3. These values are also compared to the density change of mortar (density 1850 kg/m^3).

Table 2
Density change values due to the dehydration process.

Actual density (kg/m^3)	Remain density after first dehydration (kg/m^3)	Remain density after second dehydration (kg/m^3)	Remain density after third dehydration (kg/m^3)	Remain density after final dehydration (kg/m^3)
650	637	603	590	579
1000	973	903	881	860
1850	1763	1613	1569	1500

Table 3
Base value of specific heat for 650 kg/m^3 density.

Material	Weight per 100 l of LFC (kg)	Fractional weight (%)	Specific heat of component (J/kg °C)	Contribution to specific heat of LFC (J/kg °C)
Cement	36.77	62.01	920	571
Sand	18.38	31.01	800	248
Water (with foam)	4.14	6.98	4180	292
Total	57.97	100.00	–	1110

Table 4
Base value of specific heat for 1000 kg/m^3 density.

Material	Weight per 100 l of LFC (kg)	Fractional weight (%)	Specific heat of component (J/kg °C)	Contribution to specific heat of LFC (J/kg °C)
Cement	53.96	58.89	920	542
Sand	26.98	29.44	800	236
Water (with foam)	10.69	11.67	4180	488
Total	94.32	100.00	–	1265

The results presented in Fig. 6 were obtained by directly weighing samples after heating them to different temperatures. Usually thermo gravimetric analysis (TGA) may be performed to determine changes in weight at increasing temperatures. However, due to limitation in experimental facility, this study used manual recording according to the following procedure: three 100 × 100 mm × 100 mm LFC cubes of each density (650, 1000 and 1850 kg/m^3) were heated to different temperatures and then kept at the desired temperature for 24 h. Their weight was recorded afterwards to obtain weight loss. The procedure was continued until a maximum temperature of 1000 °C.

The three curves are similar and the three dehydration phases can be clearly seen in Fig. 6. This figure also shows a further weight loss phase, occurring between 750 °C and 850 °C, which can be assigned to the release of carbon dioxide (CO_2) from calcium carbonate ($CaCO_3$) [10]:

$$CaCO_3 \rightarrow CaO + CO_2$$

Table 2 summarises the density change values for the four phases (three phases of dehydration and final phase of CO_2 release) of weight loss.

3.2. Specific heat for heat transfer analysis only

The specific heat of LFC may be divided into two parts: the base value corresponding to a mixture of the dry components and the effect of water evaporation. The base value of the dry components may be calculated using the mixture law as follows [11]:

$$C_p = \sum_{i-1}^{n} F_i C_{pi} \quad (2)$$

where C_p is the overall specific heat capacity, C_{pi} is component specific heat, F_i is the weight fraction of each component and $\sum F_i = 1$.

According to the mixture law and bearing in mind the three phase of dehydration, the base value of specific heat of LFC should consist of four segments: from ambient temperature to the start of the first phase, from the end of the first phase to the standard of the second phase, from the end of the second phase to the start of the third phase, and after the end of the third phase. However, existing literature, including fire resistant design codes for concrete structures such as EN 1992-1-2 [12] and EN 1994-1-2 [13], suggest that the base value may be taken as a constant value as that at ambient temperature. Since LFC differs from normal concrete only in terms of density, the base value of LFC is also considered constant over the entire temperature range. Tables 3 and 4 give the weights of different components of the two densities of LFC (650 kg/m^3 and 1000 kg/m^3) and the base value of specific heat at ambient temperature.

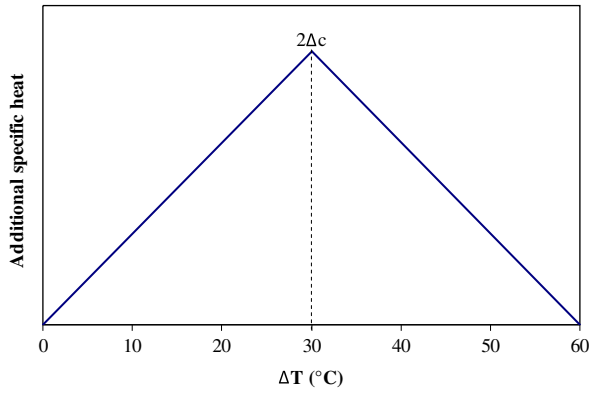

Fig. 7. Additional specific heat for evaporation of free water [8].

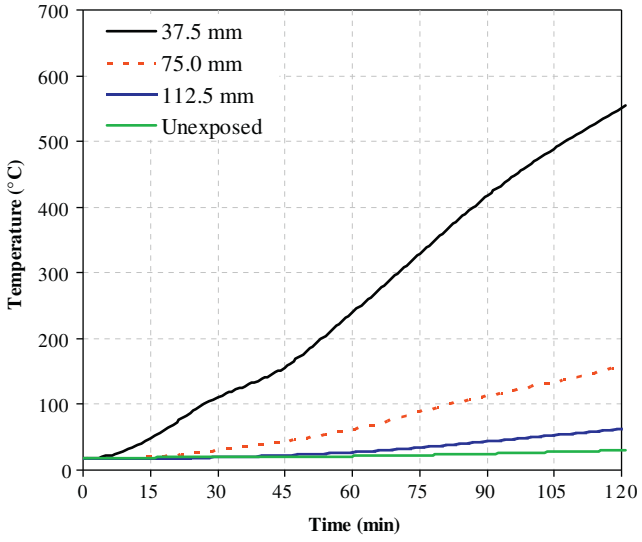

Fig. 8. Temperature distributions in 650 kg/m^3 density specimen.

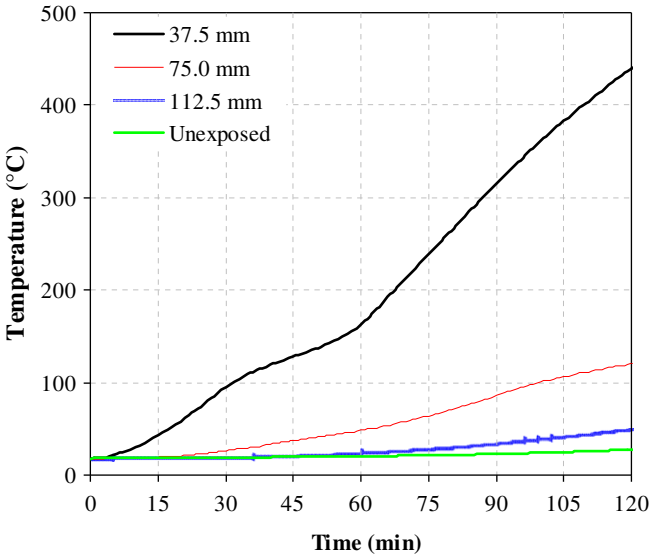

Fig. 9. Temperature distributions in1000 kg/m^3 density specimen.

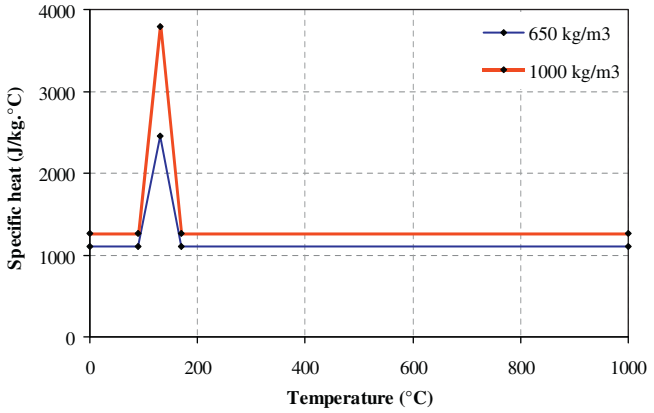

Fig. 10. Specific heat of LFC (650 kg/m^3 and 1000 kg/m^3 density) versus temperature.

In addition to the base value of specific heat, heat is also required to evaporate water from LFC. Therefore, the specific heat of LFC should be obtained from [9]:

$$C_p = C_{p,dry} + C_{add} \quad (3)$$

where $C_{p,dry}$ is 1110 J/kg °C for LFC of 650 kg/m^3 and 1265 J/kg °C for LFC of 1000 kg/m^3 as calculated previously (Tables 3 and 4) and C_{add} is the additional heat required to drive off water. C_{add} should be variable during the water evaporation temperature range to reflect that start and completion of water evaporation are gradual processes. A triangular distribution of specific heat over the water evaporation temperature range is typically assumed as shown in Fig. 7. In this figure, Δc is the average additional specific heat.

Many previous studies [2,10] have assumed that water is simply evaporated at the evaporation temperature range. Consequently, the area within the triangle in Fig. 7 is the latent heat of evaporation of water. However, Wang [11] suggested that due to water movement, this was not sufficient and a higher value of specific heat should be applied. This has been confirmed by Ang and Wang [9] who carried out a combined heat and mass analysis. In this study, the average additional specific heat for LFC was calculated as follows:

$$\Delta c = \frac{2.26 \times 10^6}{\Delta T} \times e \times f \ (\mathrm{J/kg\,^\circ C}) \quad (4)$$

In which the value of 2.26×10^6 J/kg is the latent heat of evaporation of water, Δc is the average additional specific heat, e is dehydration water content (percentage by total weight), ΔT is the magnitude of the temperature interval during which water is evaporated and f is a modification factor accounting for water movement. A value of $f = 1.4$ was used. This value was established by Ang and Wang [9] for gypsum. Ang and Wang who also found that this value to be relatively insensitive to different values of permeability provided the permeability is high. It was considered that both LFC and gypsum plaster are highly permeable materials so they should have a similar value of f. Since temperature rise in LFC is much more sensitive to changes in thermal conductivity than in specific heat, it was decided not worthwhile to refine the value of f. According to this procedure, the peak values of additional specific heat for LFC of 650 kg/m^3 and 1000 kg/m^3 densities are 2455 J/kg °C and 3796 J/kg °C respectively.

Since there are three phases of dehydration as explained previously, the above additional specific heat should be applied during each dehydration phase. Again, as like in calculating the base value of specific heat, existing literature, including fire resistance design codes for concrete, only considers the first phase of dehydration

Table 5
Porosity of LFC obtained through Vacuum Saturation Apparatus.

Sample	Dry density (kg/m^3) W_{dry}	Air saturated density (kg/m^3) W_{sat}	Water saturated density (kg/m^3) W_{wat}	Porosity (%)
650/1	650	899	565	74.6
650/2	649	912	562	75.1
650/3	653	908	571	75.7
1000/1	1004	1294	719	50.4
1000/2	1007	1287	737	50.9
1000/3	1002	1278	725	49.9

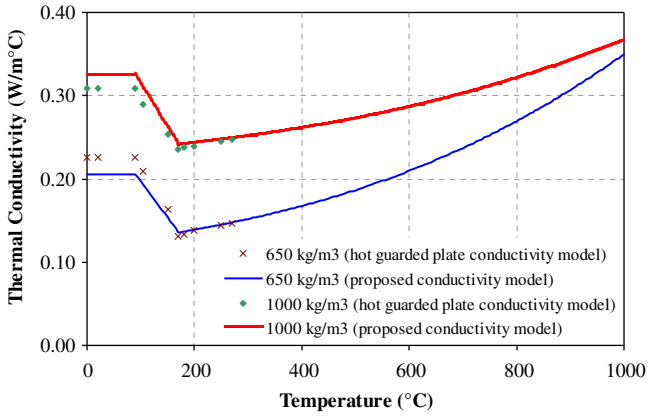

Fig. 12. Effective thermal conductivity of LFC for 650 kg/m^3 and 1000 kg/m^3 densities.

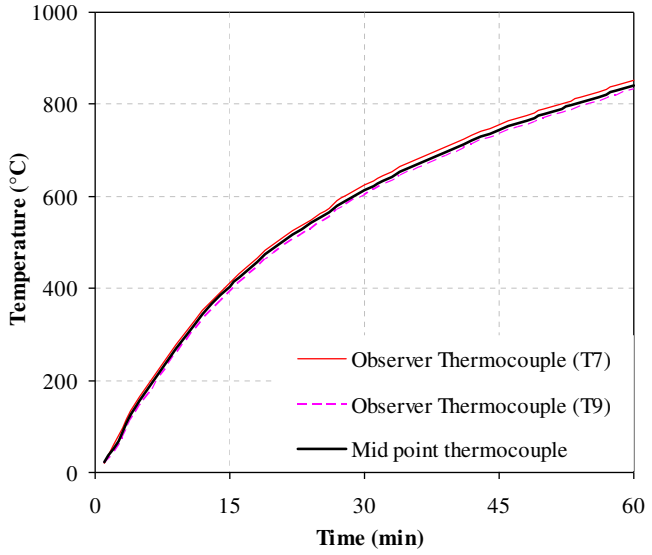

Fig. 13. Temperature readings on top surface (exposed side) of one 650 kg/m^3 density test observer thermocouples in (Test 2).

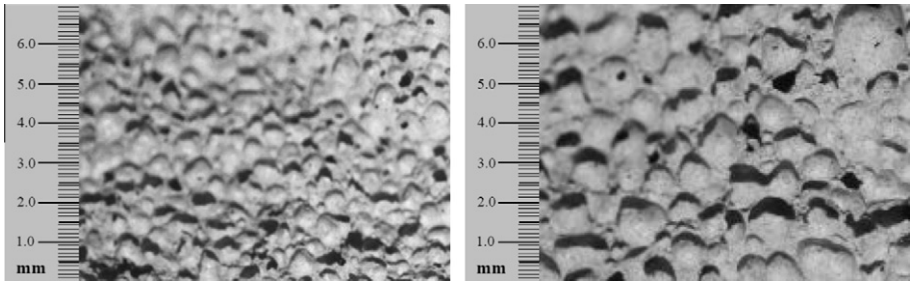

Fig. 11. Pore sizes for 1000 kg/m^3 (left) and 650 kg/m^3 (right) densities.

due to evaporation of the free water. Therefore, the specific heat-temperature relationship of concrete has only one peak, corresponding to the first phase. This appears to have been confirmed from the experimental results of this research. Figs. 8 and 9 show typical recorded temperatures inside LFC. The temperature plateau between 90 and 170 °C is clearly noticeable, reflecting the first phase of dehydration. Afterwards, the temperature development is smooth and continuous without any plateau at the other two dehydration phases. Therefore, in this paper, the additional specific heat will only be applied to the first phase of dehydration.

It can be seen from Figs. 8 to 9 that it takes longer time for LFC specimen of 1000 kg/m^3 density to reach 200 °C compared to LFC specimen of 650 kg/m^3 density. This is attributed to higher thermal capacitance value (density times specific heat) for LFC specimen of 1000 kg/m^3 density, which allow more heat to be absorbed thus slowing down the rate of heating.

As a summary, Fig. 10 shows the temperature-dependent specific heat of LFC for both densities of 650 kg/m^3 and 1000 kg/m^3.

3.3. Thermal conductivity

LFC is a high porous material consisting of solid cement matrix and air pores introduced by the foam. The effective thermal conductivity of LFC may be calculated using the following equation [14]:

$$k^* = k_s \frac{k_g \varepsilon^{\frac{2}{3}} + (1-\varepsilon^{\frac{2}{3}})k_s}{k_g(\varepsilon^{\frac{2}{3}}-\varepsilon) + (1-\varepsilon^{\frac{2}{3}}+\varepsilon)k_s} \quad (5)$$

where k^* is the effective thermal conductivity of LFC, k_g is effective thermal conductivity of gas to account for heat transfer in the pores, k_s is the thermal conductivity of the solid and ε is the porosity of the

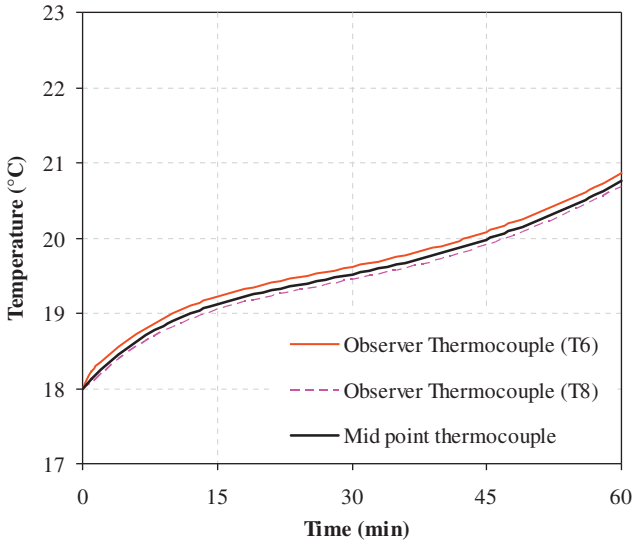

Fig. 14. Temperature readings on bottom surface (unexposed side) of one 650 kg/m^3 density test observer thermocouples in (Test 2).

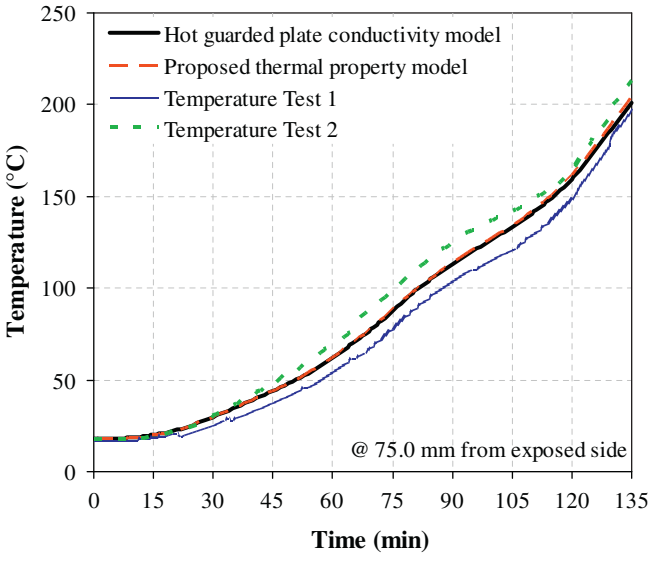

Fig. 16. Comparison between test results and numerical analysis at 75.0 mm from the exposed surface for the 650 kg/m^3 density specimens.

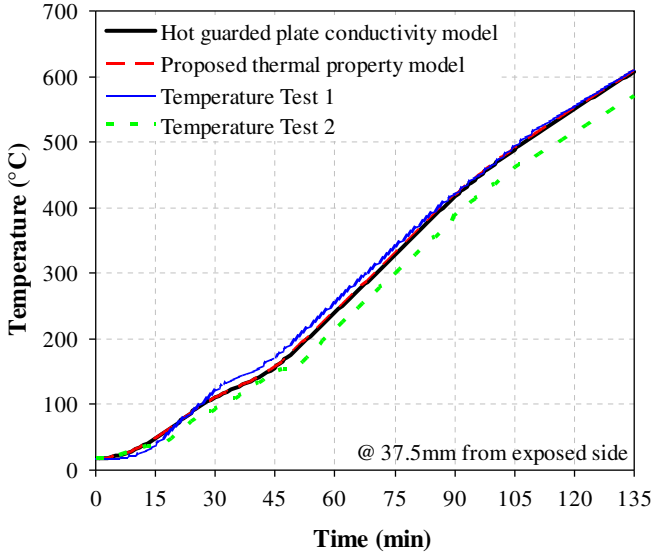

Fig. 15. Comparison between test results and numerical analysis at 37.5 mm from exposed surface for the 650 kg/m^3 density specimens.

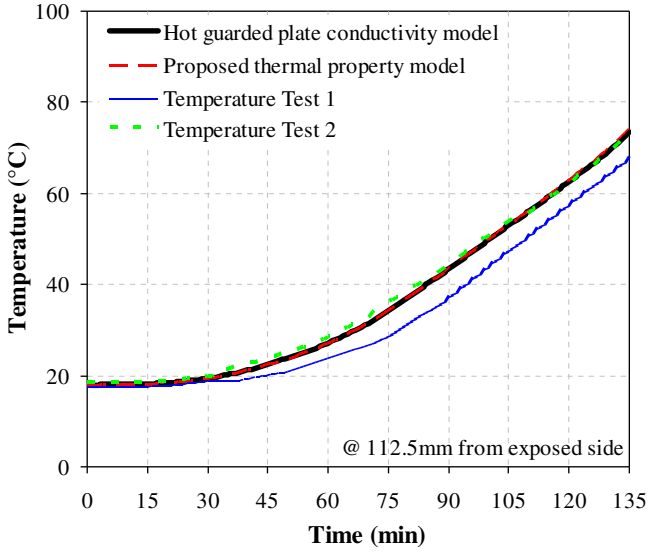

Fig. 17. Comparison between test results and numerical analysis at 112.5 mm from the exposed surface (mid-thickness) for the 650 kg/m^3 density specimens.

material (the ratio of the volume of void pore to the overall volume).

The porosity value of the LFC was determined through the Vacuum Saturation Apparatus [15]. The measurements of LFC porosity were conducted on slices of 68 mm diameter cores cut out from the centre of 100 mm cubes. The specimens were dried at 105 °C until constant weight had been attained and were then placed in a desiccator under vacuum for at least 3 h, after which the desiccator was filled with de-aired, distilled water. The porosity was calculated using the following equation:

$$P = \frac{(W_{sat} - W_{dry})}{(W_{sat} - W_{wat})} \times 100 \quad (6)$$

where P = porosity (%); W_{sat} = weight in air of saturated sample; W_{wat} = weight in water of saturated sample and W_{dry} = weight of oven-dried sample. The measured results are given in Table 5.

For analysis purpose, the porosity values are taken as 75% and 50% for LFC of densities of 650 kg/m^3 and 1000 kg/m^3 respectively.

From Eq. (5), it is necessary to have the base value thermal conductivity k_s of the pure solid in order to obtain the effective thermal conductivity k^* of LFC. Because of the difficulty of making pure solid, the value of k_s is obtained through back calculation, using HGP test results of dried LFC. The HGP test results are given in Table 1. As explained previously, it is assumed that water evaporation occurs between 90 and 170 °C so the HGP results at 170 °C are considered acceptable for dried LFC. Using Eq. (5) and given that the porosity values of LFC at 650 kg/m^3, 1000 kg/m^3 and 1850 kg/m^3 density are 75%, 50% and 12% respectively, the base value thermal conductivity of pure solid k_s may be calculated to be 0.52, 0.49 and 0.50 W/m °C for the 650, 1000 and 1850 kg/m^3 density respectively. These values are sufficiently close to accept the accuracy of this procedure and an average value of 0.5 W/m °C will be used as input data in later calculations. In the above calcula-

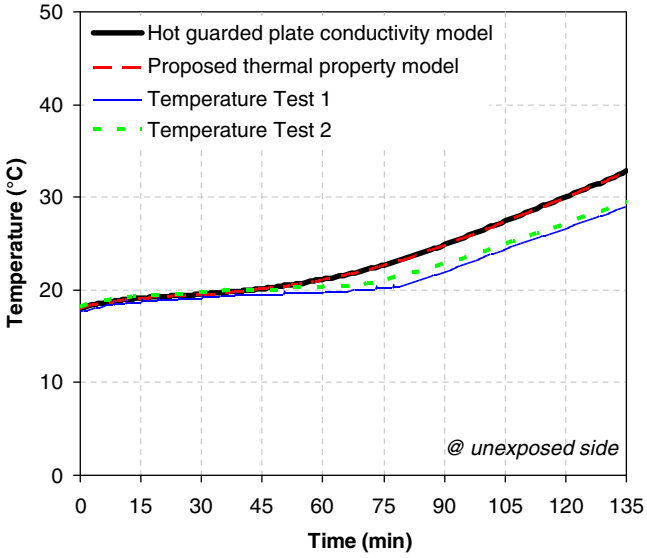

Fig. 18. Comparison between test results and numerical analysis at the unexposed surface for the 650 kg/m^3 density specimens.

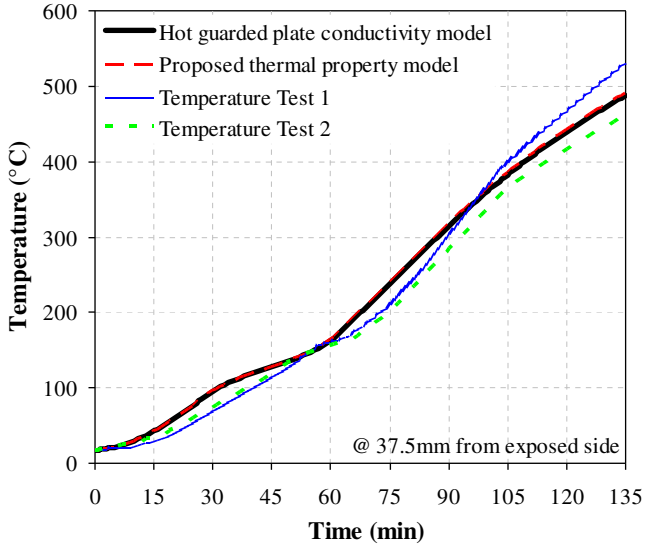

Fig. 19. Comparison between test results and numerical analysis at 37.5 mm from the exposed surface for the 1000 kg/m^3 density specimens.

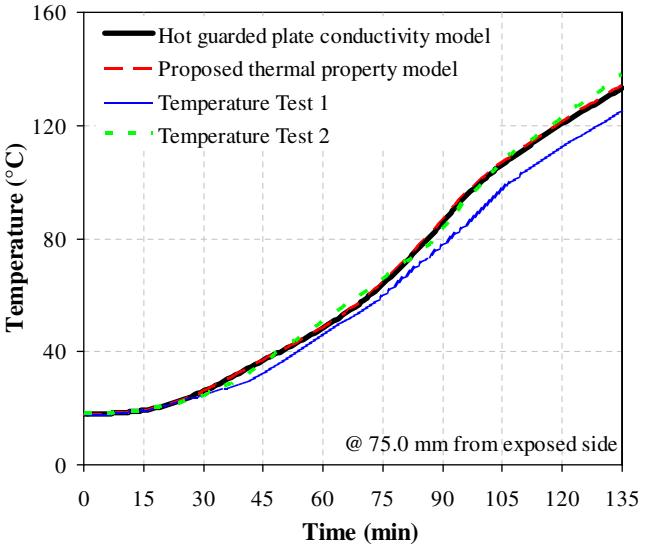

Fig. 20. Comparison between test results and numerical analysis at 75.0 mm from the exposed surface for the 1000 kg/m^3 density specimens.

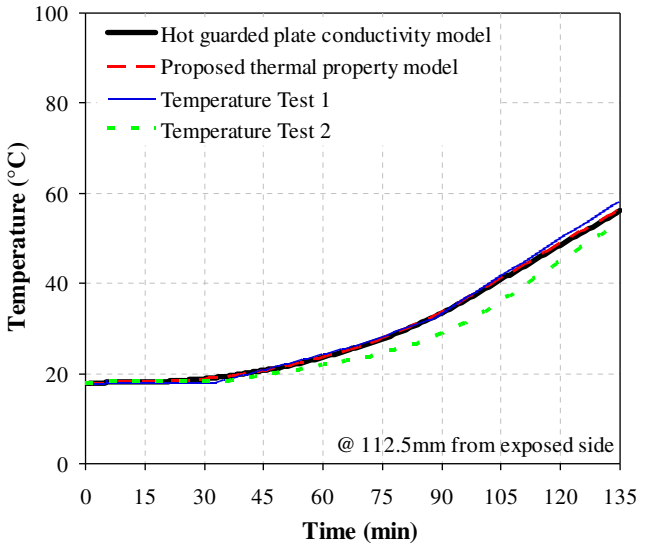

Fig. 21. Comparison between test results and numerical analysis at 112.5 mm from the exposed surface for the 1000 kg/m^3 density specimens.

tions, the effect of radiation within pores was not considered because of the relatively low temperature.

Although the HGP tests give directly the thermal conductivity values of LFC at different temperatures, these values can be calculated now that the base thermal conductivity value of the pure solid has been obtained. The thermal conductivity – temperature relationship of LFC may be divided into three segments: (1) an initially flat part with the thermal conductivity constant as that at ambient temperature, until water evaporation starts at the assumed temperature of 90 °C; (2) a linearly decreasing segment until all the water has evaporated and the LFC is dry, which is assumed at 170 °C; (3) increasing thermal conductivity with temperature due to radiation in the pores. The third segment is described using Eq. (5).

For the LFC thermal conductivity at ambient temperature, the LFC may be considered to be part dry LFC and part water and Eq. (7), based on volume fraction, may be used to calculate the thermal conductivity of LFC at ambient temperature.

$$k_{amb} = V_w k_w + (1 - V_w) k_{dry} \tag{7}$$

where k_{amb} is the LFC thermal conductivity at ambient temperature; V_w is the volume percentage of water; k_w is the thermal conductivity of water (0.58 W/m °C) and k_{dry} is the thermal conductivity of dry LFC (value in Table 1 for 170 °C).

For LFC density of 650 kg/m^3, k_{dry} = 0.131 W/m °C (Table 1), V_w = 0.1677, giving k_{amb} = 0.206 W/m.°C. For LFC density of 1000 kg/m^3, k_{dry} = 0.235 W/m °C (Table 1), V_w = 0.2618, giving k_{amb} = 0.325 W/m °C. These calculated ambient temperature thermal conductivity values are close to the HGP test values of 0.226 and 0.309 W/m °C respectively.

To obtain the thermal conductivity of gas in the air pores, it is necessary to include the effects of radiation within the pores at high temperatures. Assuming the air pores may be represented by uniform distribution of spherical pores of diameter d_e, the effective thermal conductivity of the gas at elevated temperatures may be analytically derived to give the following equation [14]:

$$\lambda_g = 4.815 \times 10^{-4} T^{0.717} + \frac{2}{3} \times 4 d_e \sigma T^3 \tag{8}$$

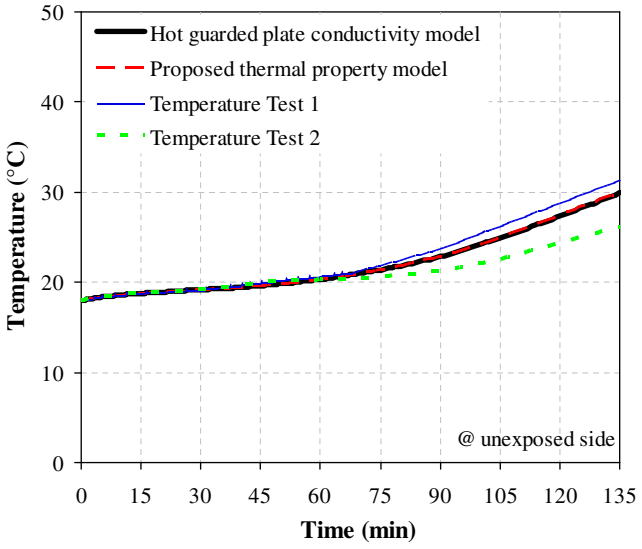

Fig. 22. Comparison between test results and numerical analysis at the unexposed surface for the 1000 kg/m^3 density specimens.

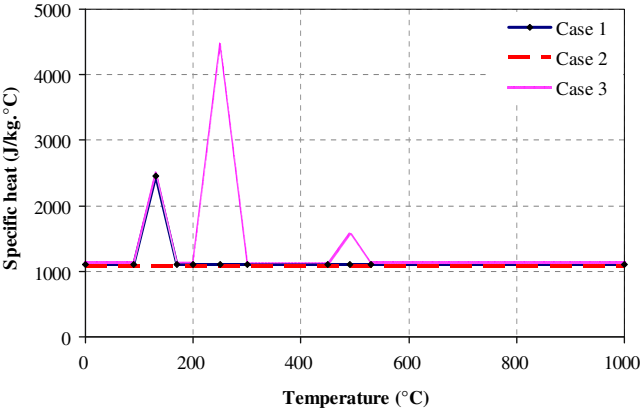

Fig. 23. Specific heat models for all three cases considered for sensitivity study (LFC density of 650 kg/m^3).

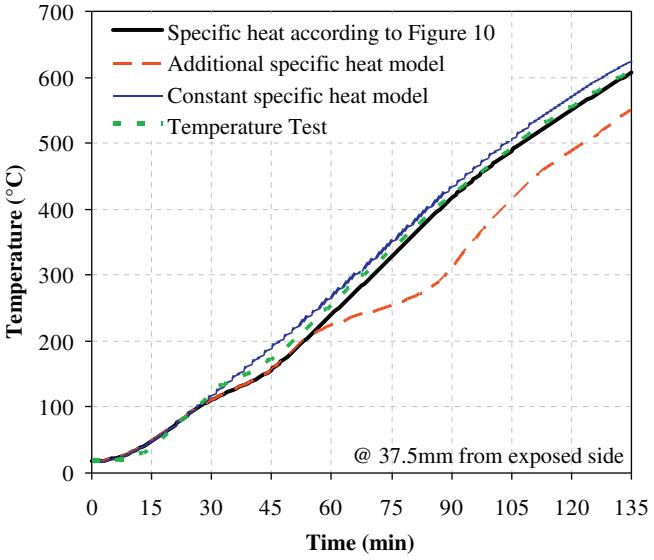

Fig. 24. Sensitivity of LFC temperature to different specific heat models, 37.5 mm from the exposed surface for the 650 kg/m^3 specimens.

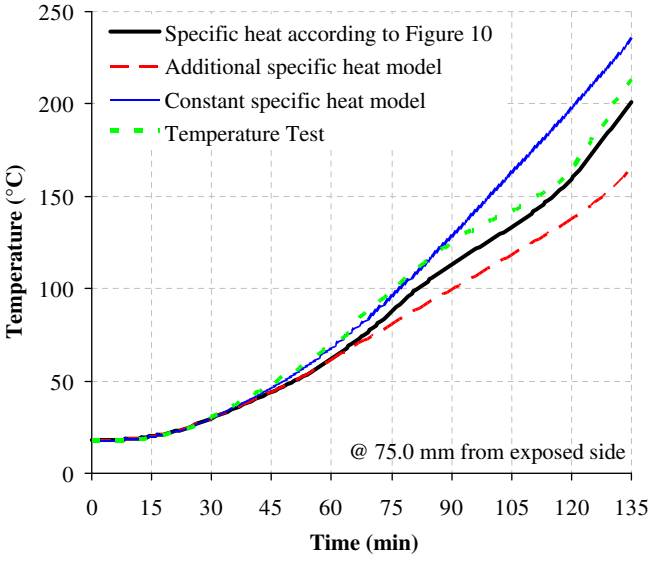

Fig. 25. Sensitivity of LFC temperature to different specific heat models, 75.0 mm from the exposed surface (mid-thickness) for the 650 kg/m^3 specimens.

where the first term is the gas thermal conductivity without the effect of thermal radiation and the second term represents the effect of radiation within the air pores.

Although there is also convection with the air pores, due to the small size of the pores (never larger than 5 mm), natural convection in the pores can be neglected.

In order to calculate the effective thermal conductivity of gas inside the air pores, it is necessary to establish the pore size. Fig. 11 shows images of the internal structure of the 1000 kg/m^3 and 650 kg/m^3 density LFC. Clearly the pore sizes are not uniform. However, these two figures do clearly indicate that there is a dominant pore size and that the dominant pore size is primarily a function of the LFC density. The dominant pore size tends to increase as the LFC density reduces due to the higher quantity of foam used. From an analysis of the internal images of the two densities of LFC, the dominant pore size of the 650 kg/m^3 and 1000 kg/m^3 density LFC has been determined as 0.72 mm and 0.55 mm respectively. Detailed investigation of the effects of pore size and distribution indicates that provided the total porosity is the same and there is a dominant pore size, the thermal conductivity of porous material may be calculated using the dominant pore size.

To summarise, Fig. 12 shows the calculated effective thermal conductivity of LFC for the two densities studied in this paper and compare these calculated values with those directly measured using the HGP method (Table 1 values).

4. Validation of thermal properties models

To validate the above proposed thermal property models for LFC, these thermal property values from these models were used as input data in a one-dimensional heat transfer program to predict temperature developments inside the LFC test samples described in Section 2 of this paper. Details of theoretical background and validations of the one-dimensional finite difference heat transfer have been presented elsewhere by Rahmanian [6]. As mentioned in Section 2.1, it is assumed that heat transfer in the test samples is one-dimensional in the thickness direction of the panel. To confirm this, thermocouples were installed on the exposed and unexposed surfaces of the sample in the middle and near the four corners. Figs. 13 and 14 compare these observa-

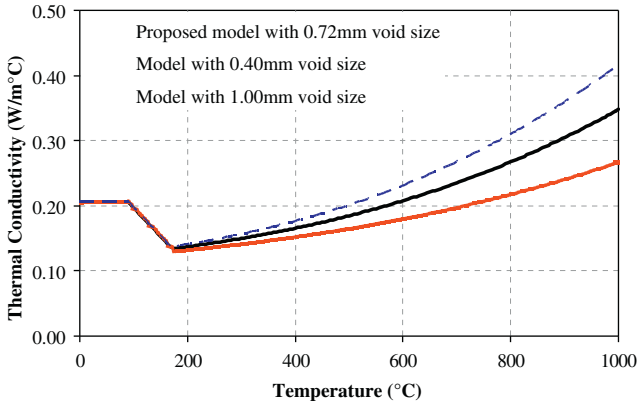

Fig. 26. Comparison of LFC thermal conductivity using different pore sizes.

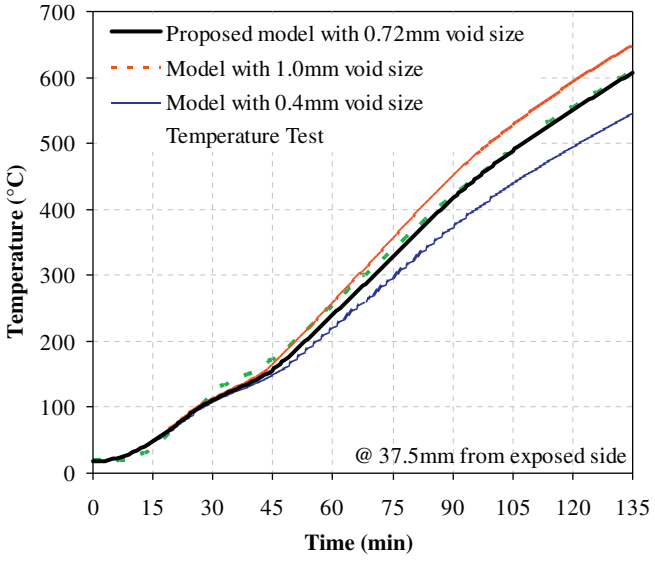

Fig. 27. Sensitivity of LFC temperature to different pore sizes at 37.5 mm from the exposed surface for the 650 kg/m^3 density specimen.

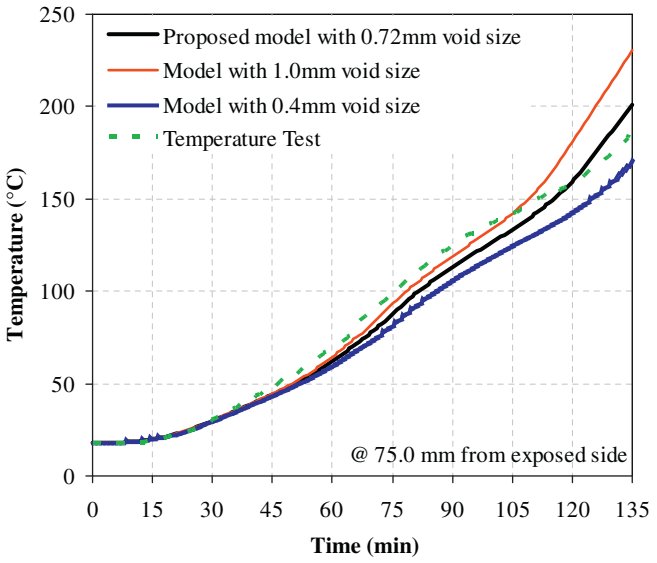

Fig. 28. Sensitivity of LFC temperature to different pore sizes at 75.0 mm from the exposed surface for the 650 kg/m^3 density specimen.

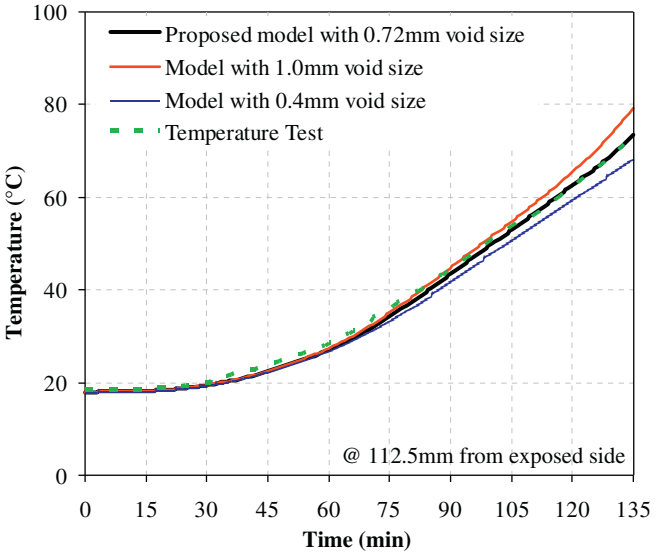

Fig. 29. Sensitivity of LFC temperature to different pore sizes at 112.5 mm from the exposed surface for the 650 kg/m^3 density specimen.

tions. The five thermocouples on each surface of the sample recorded very similar temperatures, thus confirming the one-dimensional heat transfer assumption.

To provide comprehensive validation of the thermal property models proposed in Section 3.3 the measured experimental temperatures at all recording locations of the test specimens for both densities of LFC were compared with numerical analysis results using the one-dimensional heat transfer program developed by Rahmanian [6] and the two sets of thermal property values (hot guarded plate conductivity model and the theoretical thermal property model results) as input data. As mentioned previously, the exposed surface temperatures were used as input data in the heat transfer analysis to eliminate uncertainty in the thermal boundary condition on the exposed side. Figs. 15–18 compare the measured and numerical analysis results for the 650 kg/m^3 density specimens and Figs. 19–22 are for the 1000 kg/m^3 density specimens.

From the results shown in Figs. 15–22, the following observations may be made:

(1) The two replicate tests of each LFC specimen gave close results throughout the long durations (over two hours) of all the tests, confirming the consistency of the LFC mix and the heating test procedure.
(2) The predicted temperatures, using as input data the directly measured thermal conductivity values from the HGP tests and the proposed specific heat model, are very close to the measured temperatures, confirming the validity of the specific heat model.
(3) Close agreement between prediction results of temperature throughout the thickness of the LFC samples, using the HGP test results and the proposed analytical model for thermal conductivity, confirms that the proposed analytical model for thermal conductivity is appropriate.

4.1. Sensitivity study

The previous section has shown that the proposed thermal property models for LFC is appropriate. Nevertheless, a number of assumptions have been introduced in the proposed models. It is important to examine the sensitivity of the temperature calculation results to these assumptions so that wherever necessary, critical factors in the proposed models are identified to enable accurate determination of their values. The results for both LFC densities are similar, so only the results for the 650 kg/m^3 density will be reported in this paper.

In all simulations, the measured densities of LFC at high temperatures were used. This sensitivity study will concentrate on the specific heat model and the thermal conductivity model. For the specific heat, the same thermal conductivity values from the HGP tests will be used and focus will be on the effects of moisture evaporation. Three cases will be considered: (1) the proposed specific heat model with one additional specific heat for evaporation of the free water, (2) constant specific heat without accounting for the effect of moisture evaporation, (3) specific heat model including additional specific heats at three different temperature intervals to consider the three phases of water evaporation. Fig. 23 compares specific heat for the three cases.

For the thermal conductivity model, the proposed analytical thermal conductivity model will be used and the sensitivity study will focus on the pore size. For the 650 kg/m^3 density, an average pore size of 0.72 mm was found appropriate from an analysis of the internal structure of the sample shown in Fig. 11. In the sensitivity study, the pore size was changed to 0.4 mm and 1.0 mm.

Figs. 24 and 25 show representative results of comparison between predicted temperatures inside LFC by using different specific heat models. It is clear that using a constant specific heat model is not appropriate because this will miss the temperature plateau phase at around 90 °C as seen in Fig. 24. This difference in results is progressed further into the LFC specimen so Fig. 25 shows quite large differences. In contrast, having too many spikes of additional specific heat to faithfully follow all the three phases of water evaporation does not appear to produce sensible results.

Fig. 26 shows the LFC thermal conductivity–temperature relationships for different values of pore size. Figs. 27–30 compares the predicted LFC temperatures at different distance from the exposed surface using these thermal conductivity curves and between the prediction results and the measured results. It is clear that the LFC temperatures are moderately sensitive to the pore size. Because thermal conductivity deals with progressive heat transfer throughout the thickness, the difference in results becomes proportionally much greater at positions further away from the exposed surface. It is therefore important to obtain a sufficiently accurate value for the pore size. For LFC, as shown in Fig. 11, although there are variations in the pore size for each density, these sizes may still considered to be relatively uniform so an average value of pore size may be used. The results of this study, by using the average pore size of 0.72 mm, have been found to be acceptable.

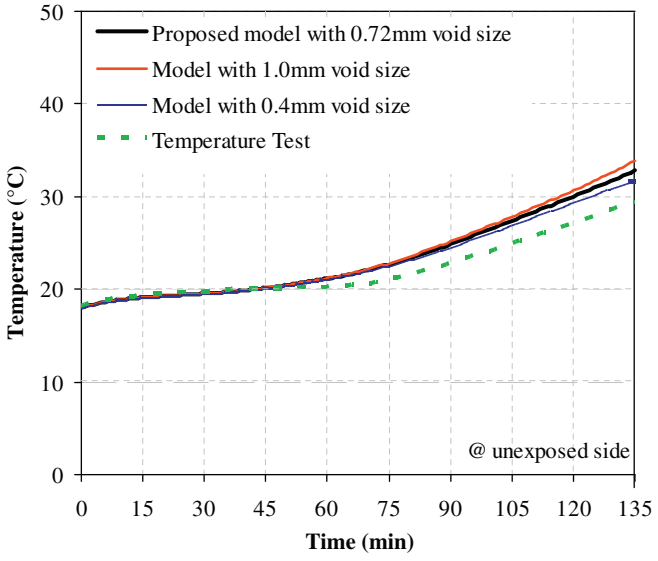

Fig. 30. Sensitivity of LFC temperature to different pore sizes at the exposed surface for the 650 kg/m^3 density specimen.

4.2. Fire resistance

This paper has mainly concentrated on developing and validating thermal property models for LFC, including density, specific heat and thermal conductivity. Even though the mechanical prop-

Table 6
Indicative LFC minimum thickness for different fire resistance ratings for fire exposure from one side.

LFC density (kg/m^3)	Minimum LFC thickness (mm) for fire resistance rating of			
	30 min	60 min	90 min	120 min
650	21.0	36.7	50.1	60.5
1000	23.1	39.1	52.3	63.2

erties of LFC are expected to be low in comparison with normal strength concrete, there is a potential of using LFC as fire resistant partition or as load bearing walls in low-rise residential construction. Therefore, this section presents a limited amount of indicative study to investigate the fire resistance performance of LFC panels exposed to fire on one side.

Table 6 presents the minimum LFC thickness necessary to achieve different standard fire resistance ratings. For simplicity, the fire resistance requirement is based on thermal insulation, i.e. the average temperature on the unexposed surface should not exceed 140 °C from ambient [7]. For this predictive study, the thermal boundary condition (heat transfer coefficients) was according to EN 1991-1-2 [16].

The results in Table 6 indicates that although increasing LFC density would increase its specific heat, thus allowing more heat to be absorbed in LFC, as far as the unexposed surface temperature is concerned which is used to assess insulation fire performance thermal conductivity plays a more important role so that using higher density LFC has no advantage.

The minimum thickness values in Table 6 are not particularly onerous. In fact, a single layer of 650 kg/m^3 density LFC of about 21 mm would achieve 30 min of standard fire resistance rating, more or less similar to gypsum plasterboard. This is encouraging for application of LFC in building construction as fire resistant partitions.

5. Conclusions

This paper has presented two methods to determine thermal conductivity values of lightweight foamed concrete (LFC) at elevated temperature: direct measurement using the hot guarded plate (HGP) test method and analytical solution. The analytical method is based on treating LFC as mix of dried LFC and water before completion of water evaporation at 170 °C and mix of dried LFC and air pores afterwards. To use the analytical model, the thermal conductivity of dried LFC and average air pore size should be obtained. The dried LFC thermal conductivity value may be directly measured using the HGP test or calculated if the LFC ambient temperature thermal conductivity is available. The average pore diameter may be obtained by taking a microscopic image of the LFC. A specific heat model has also been proposed in this paper, in which the specific heat of LFC is made of a constant base value and an additional value between 90 and 170 °C to account for water evaporation. From the results of comparison between elevated temperature tests on LFC panels and numerical heat transfer analysis using the different thermal property models, the following conclusions may be drawn:

(1) Despite simplicity, the aforementioned analytical models for specific heat and thermal conductivity of LFC of different densities give accurate results. The superiority of the analytical model over the HGP test is that LFC of different densities may be now considered without relying on extensive tests.
(2) The prediction results are moderately affected by the air pore diameter. This suggests that the air pore size should be determined with good accuracy, but the average pore diameter will be sufficiently accurate. For LFC densities of 650 kg/m^3 and 1000 kg/m^3, the average pore diameter may be taken as 0.72 mm and 0.55 mm respectively.
(3) An indicative study of fire resistance of LFC construction with standard fire exposure from one side has concluded that LFC offers a feasible alternative to gypsum as the construction material for partition walls.

References

[1] Hamidah MS, Azmi I, Ruslan MRA, Kartini K, Fadhil NM. Optimisation of foamed concrete mix of different sand–cement ratio and curing conditions. In: Dhir RK, Newlands MD, McCarthy A, editors. Use of foamed concrete in construction. London: Thomas; 2005.
[2] Noumowe A. Effet des hautes temperatures (20 °C–600 °C) sur le beton. PhD thesis, Institute National des Sciences Appliquees; 1995.
[3] Khoury GA. Compressive strength of concrete at high temperatures: a reassessment. Mag Concr Res 1992;44(161):291–309.
[4] Rostasy FS, Weiβ R, Wiedemann G. Changes of pore structure of cement mortars due to temperature. Cem Concr Res 1980;10(2):157–64.
[5] Lin WM, Lin TD, Powers LJ. Microstructures of fire-damaged concrete. ACI Mater J 1996;93(3):199–205.
[6] Rahmanian I. Fire resistance of gypsum board based systems. First year. PhD progression report, School of Mechanical, Aerospace and Civil Engineering, University of Manchester; 2008.
[7] BS476. Fire tests on building materials and structures. Part 20: method for determination of the fire resistance of elements of construction (general principles); 1987.
[8] ASTM. Standard test method for steady-state heat flux measurements and thermal transmission properties by means of the guarded-hot-plate apparatus, ASTM C 177-97. American Society for Testing and Materials; 1997.
[9] Ang CN, Wang YC. The effect of water movement on specific heat of gypsum plasterboard in heat transfer analysis under natural fire exposure. Constr Build Mater 2004;18(7):505–15.
[10] Taylor HFW. Cement chemistry. London: Academic Press; 1992.
[11] Wang HB. Heat transfer analysis of components of construction exposed to fire. PhD thesis, Department of Civil Engineering and Construction, University of Salford, Manchester; 1995.
[12] CEN. Eurocode 2. Design of concrete structures. Part 1.2: general rules – structural fire design. DD EN 1992-1-2; 2004.
[13] CEN. Eurocode 4. Design of composite steel and concrete structures. Part 1.2: general rules – structural fire design. DD ENV 1994-1-2; 2005.
[14] Yuan J. Fire protection performance of intumescent coating under realistic fire conditions. PhD thesis, School of Mechanical, Aerospace and Civil Engineering, University of Manchester; 2009.
[15] Cabrera JG, Lynsdale CJ. A new gas permeameter for measuring the permeability of mortar and concrete. Mag Concr Res 1988;40(144):177–82.
[16] BS EN. Eurocode 1. Actions on structures. Part 1.2: general actions – actions on structures exposed to fire. EN 1991-1-2; 2002.

Appendix B: Publication 2

CONCRETE RESEARCH LETTERS

www.crl.issres.net

Vol. 1 (1) – August 2010

An Experimental Investigation of Mechanical Properties of Lightweight Foamed Concrete Subjected to Elevated Temperatures up to 600°C

Md Azree Othuman Mydin[C], Y. C Wang

School of Mechanical, Aerospace and Civil Engineering, University of Manchester, Manchester M60 1QD, UNITED KINGDOM

Received: 05/08/2010 – Revised 28/09/2010 – Accepted 29/09/2010

Abstract

Although Lightweight Foamed Concrete (LFC) has low mechanical properties compared to normal weight concrete, there is a possibility of using this material as partition or load-bearing wall in low-rise residential construction. Before it can be considered for use as a load-bearing element in the building industry, it is essential to obtain reliable information of its mechanical properties at ambient and elevated temperatures for quantification of its fire resistance performance. This paper will reports the results of experimental works that have been performed to examine and characterize the mechanical properties of LFC subjected to elevated temperatures. LFC with 650 and 1000 kg/m^3 density were cast and tested under compression and three point bending. The tests were carried out at ambient temperature, 100, 200, 300, 400, 500, and 600°C. The experimental results of this study consistently demonstrated that the loss in stiffness for cement based material like LFC at elevated temperatures occurs predominantly after about 90°C, regardless of density. This indicates that the primary mechanism causing stiffness degradation is microcracking, which occurs as water expands and evaporates from the porous body. As expected, reducing the density of LFC reduces its strength and stiffness. However, for LFC of different densities, the normalised strength and stiffness (ratio of elevated temperature value to ambient temperature value) – temperature relationships are very similar.

Keywords: Lightweight foamed concrete; Lightweight concrete; Concrete material properties; Elevated temperatures; High temperatures, Lightweight material.

1. Introduction

LFC is defined as a cementitious material having a minimum of 20 per cent by volume of mechanically entrained foam in the mortar slurry [1] in which air-pores are entrapped in the matrix by means of a suitable foaming agent. The air-pores are initiated by agitating air with a foaming agent diluted with water; the foam then carefully mixes together with the cement slurry to form LFC. Integrating the air-pores into the base matrix gives a low self-weight, high workability, excellent insulating values, but lower strength in contrast to normal strength concrete. LFC can be fabricated anywhere in any shape or building unit size. Over the past 20 years, LFC has primarily been used around the world for bulk filling, trench reinstatements, backfill to retaining walls and bridge abutments, insulation to foundations and roof tiles, sound insulation, stabilising soils

(especially in the construction of embankment slopes), grouting for tunnel works, sandwich fill for precast units and pipeline infill. However, in the last few years, there is developing interest in using LFC as a lightweight non-structural and semi-structural material in buildings to take advantage its lightweight and good insulation properties [2].

It should be pointed out that most of the investigations on LFC so far have focused on its ambient temperature properties only [3-8]. Among these, the majority are about mechanical properties of LFC [3,6,7] with only a very few on its thermal properties [4]. Quantitative information on fire resistance performance is extremely sparse. Nevertheless these available investigations do give some useful data of LFC mechanical properties at ambient temperature which can be used as the basis of further research.

For cement-based material like LFC, the degradation mechanisms upon exposure to high temperatures comprise of mechanical damage as well as chemical degradation; where each mechanism is dominant within a specific temperature range. Lin et al. [9] conducted studies to examine the microstructure of concrete exposed to elevated temperatures in both actual fire and laboratory conditions with the assistance of Scanning-Electron-Microscopy (SEM) and stereo microscopy. They established that the absorption of moisture from the surrounding medium provides a mechanism for the rehydration of calcium oxide and un-hydrated cement grains that refilled the void spaces. They observed long irregular fibers of calcium silicate hydrate (C-S-H) gel merged with ettringite (hexacalcium aluminate trisulfate hydrate) and calcium hydroxide (C-H) crystals formed as a result of rehydration.

In a study carried out by Schneider and Herbst [10], chemical reactions and the behaviors of calcium hydroxide, calcium carbonate, calcium silicate hydrate, non-evaporable water and micropores under various temperatures was examined. They found that the major increase of concrete permeability and porosity at high temperature was primarily produced by arising micro cracks and by changes of material inner structure, as well as by crack opening due to high gas pressure values. As a result, the permeability of concrete depends not only on temperature levels, moisture content and gas pressure but also upon the degree of cracks development.

As a two phase material with solid cement and air voids, the degradation mechanisms of LFC are principally caused by deprivation of the cement paste. Even though both mechanical and chemical degradation result in degradation of mechanical properties, the mechanisms take place at considerably different temperature ranges. The dehydration process in the cement paste becomes significant at temperatures above about 110 °C [11] and diminishes the calcium silicate hydrate (C-S-H) links which provide the primary load-bearing formation in the hydrated cement. Furthermore, due to low permeability of the cement paste, internal water pressure is built up during dehydration of the hydrated C-S-H, which increases internal stresses and induce micro cracks in the material from about 300°C, resulting in decreased strength and stiffness of the material [12]. At higher temperatures around 450°C, calcium hydroxide ($Ca(OH)_2$), which is one of the most vital compounds in cement paste, dissociates, resulting in the shrinkage of LFC [13]. If the hot LFC is exposed to water, as in fire fighting, CaO in LFC turns into $Ca(OH)_2$ to cause cracking and destruction of LFC. It is still extremely difficult to accurately predict these mechanisms and experimental investigation remains essential.

Therefore, the aim of this study is to experimentally examine and characterize the mechanical properties of LFC at elevated temperatures. Tests were carried out at different temperatures up to 600°C. Extensive compressive and bending strength tests will be performed for LFC of densities of 650 kg/m^3 and 1000 kg/m^3.

2. Significance of research

LFC is a relatively new construction material compared to normal strength concrete. The major factor limiting the use of LFC in applications is insufficient knowledge of the material performance at elevated temperatures. In building application, load carrying capacity and fire resistance are the

most important safety requirements. In order to comprehend and eventually predict the performance of LFC based systems, the material properties at ambient temperature and elevated temperatures must be known at first stage. To be able to predict the fire resistance of a building structure, the temperatures in the structure must be determined. For quantification of structural performance, knowledge of the mechanical properties, at elevated temperatures of the material is essential. LFC mechanical properties will be established, including compressive strength, compressive modulus, strain at maximum compressive strength, compressive stress-strain relationship, failure modes, flexural tensile strength and flexural tensile modulus.

3. Mix design and material constituents of LFC

The LFC used in this study was made from ordinary Portland cement, fine sand, water and stable foam. Table 1 lists the details of the constituent materials. The main objectives of this research are to determine the mechanical properties of LFC at high temperatures. Therefore only a constant cement-sand ratio of 2:1 and water-cement ratio of 0.5 were used for all batches of LFC samples made for this research. A high cement-sand ratio (2:1) was chosen to achieve better compressive strength and water-cement ratio of 0.5 was found acceptable to achieve adequate workability [14]

LFC samples of two densities of 650 and 1000 kg/m^3 were cast and tested for mechanical properties test. The 650 kg/m^3 density was selected so as to enable comparison of mechanical performance between LFC and that of other building materials of similar density, such as gypsum board; the 1000 kg/m^3 density was used because LFC of this density would have a useful amount of mechanical properties to make it viable as a light load bearing infill material, which may be combined with thin-walled steel in lightweight composite panel construction.

Table 1 Constituent materials used to produce LFC

Constituents	Type
Cement	Ordinary Portland cement [15]
Sand	Fine sand with additional sieving to eradicate particles greater than 2.36 mm, to improve the LFC flow characteristics and stability [16]
Stable foam	Noraite PA-1 (protein-based) surfactant with unit weight of around 70 to 80 gram/litre produced from Portafoam TM2 System. The surfactant solution consists of one part of surfactant to 33 parts of water.

All LFC samples for mechanical properties test were made in house. The stable foam was produced using foam generator Portafoam TM2 System (Figure 1), acquired from the Malaysian manufacturer (www.portafoam.com). This system runs from an air compressor and consists of a main generating unit, a foaming unit, and a lance unit. The protein based foaming agent used was Noraite PA-1 which is suitable for LFC densities ranging from 600 kg/m^3 to 1600 kg/m^3. Three identical specimens were prepared for each density and were tested at 28 days after mixing.

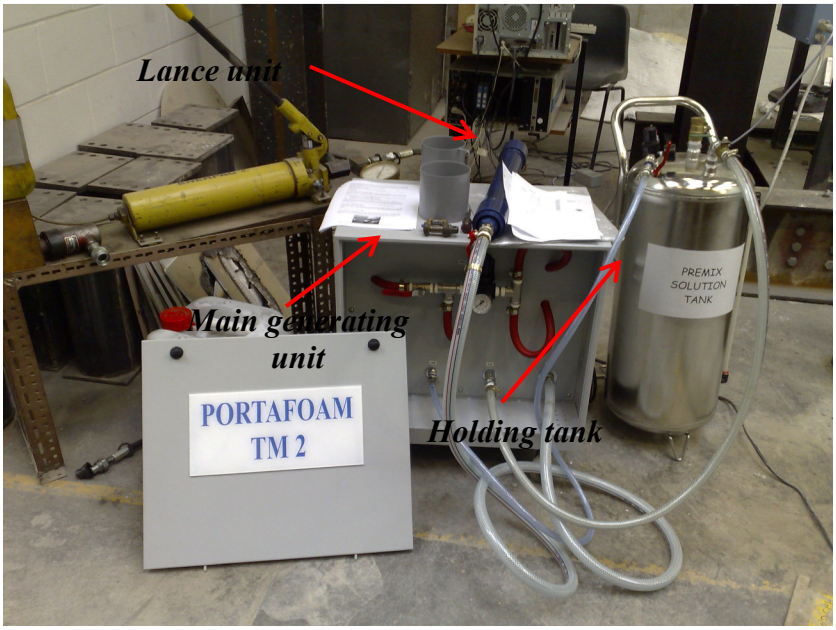

Figure 1. Portafoam TM2 foam generator system.

4. Test methods

A variety of test methods may be used to obtain different aspects of mechanical properties of materials at high temperatures, including the stressed test, the unstressed test, and the unstressed residual strength test [17]. In this research, the unstressed test method was adopted for convenience. In the unstressed test, the sample is heated, without preload, at a steady rate to the predetermined temperature. While maintaining the target temperature, load is applied at a prescribed rate until sample failure. Because the temperature is unchanged, the test is also referred to as steady state test, as opposed to transient test in which the specimen temperature changes with time.

4.1 Heating of specimens

Electric furnace was used for heating the LFC specimens to the various steady-state temperatures (100°C, 200°C, 300°C, 400°C, 500°C and 600°C). The furnace temperature exposure profiles were produced by a programmable microprocessor temperature controller attached to the furnace power supply and monitored by a Type K thermocouple located in the furnace chamber. Pre-testing checking of the furnaces showed that the furnace controller and furnace power system could maintain furnace operating temperatures within ±1°C over the test range.

4.2 Compression Test

The compressive strength tests were carried out on 100 x 200 mm cylinders. To monitor the strain behaviour at ambient temperature during loading, two strain gauges were fitted on each sample for the ambient test only. Since no strain measurement was made at elevated temperatures, the ambient temperature strain measurements were used to confirm that the strain calculated based on the displacement of the loading platen was of sufficient accuracy. Four Type K thermocouples were installed in the central plane of each cylinder specimen. Loading was applied using an ambient temperature compression machine (Figure 2) after removing the test samples from the furnace (Figure 3). To minimise heat loss from the specimen to atmosphere, each specimen was wrapped with insulation sheets immediately after being removed from the electric furnace. For each set of test, three replicate tests were carried out to check consistency of the results.

Figure 2. Compression test using ambient temperature machine

Figure 3. High temperature electric furnace with specimens

4.3 Three point bending test

For convenience in this study, the three point bending test was carried out. The preparation of samples followed a similar procedure as delineated above for the compression tests. The specimens were rectangular parallelepipeds of height *(h)* 25 mm, width *(w)* 125 mm and length *(l)* 350 mm. As shown in Figure 4, the LFC specimen was simply supported and was subjected to point load at the centre point. The length between the supports was L_s = 200 mm, giving a L_s/h aspect ratio of 8 and sufficient to ensure predominance of bending behaviour. The load-deflection was recorded for the evaluation of flexural tensile strength.

Figure 4. Three point bending test set up and specimen dimensions

4.4 Porosity measurements

The porosity of LFC was determined by using the Vacuum Saturation Apparatus [18]. The porosity was calculated using the following equation:

$$\varepsilon = \frac{(W_{sat} - W_{dry})}{(W_{sat} - W_{wat})} \times 100 \quad .....(1)$$

where ε is the porosity (%), W_{sat} is the weight in air of saturated sample, W_{wat} is the weight in water of saturated sample and W_{dry} is the weight of oven-dried sample.

5. Results and discussion

5.1 Porosity of LFC

Usually, the porosity of cement based material changes when the temperature increases. These changes in porosity can be characterized by considering phase changes in the concrete at different temperatures. Figure 5 presents the total porosity for each mix as a function of the temperature. LFC of both densities experienced a slight monotonous increase in porosity with temperature. The initial porosity for 650 and 1000 kg/m^3 density was 74.8% and 50.0% respectively. Between 200°C and 300°C, the porosity increased considerably for the higher density LFC while the increase was more moderate for the lower density LFC due to decomposition of the different amounts of calcium silicate hydrate gel and sulfoaluminate. At 300°C, the measured porosity for 650 and 1000 kg/m^3 density was 75.5% and 51.9% correspondingly. For temperatures beyond 400°C, the measured porosity showed some increase corresponding to the decomposition of calcium hydroxide to form calcium oxide. At 600°C, the porosity was 76.3% and 53.7% for 650 and 1000 kg/m^3 respectively. Nevertheless, in general, due to the high porosity at ambient temperature, LFC may be considered to have constant porosity at various elevated temperatures.

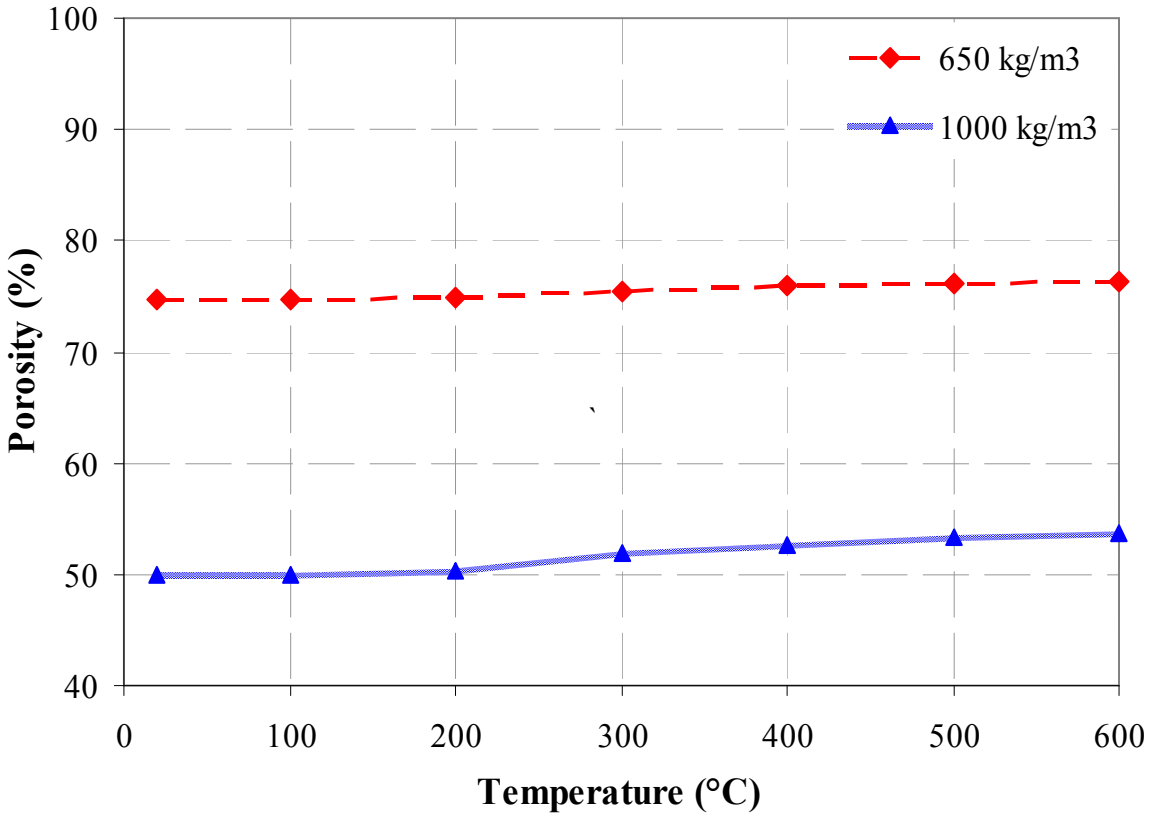

Figure 5. Porosity of LFC as a function of temperature

Figures 6 show the pore size of LFC determined through image analysis tool which illustrate images of the internal structure of the 1000 kg/m^3 and 650 kg/m^3 density LFC at ambient temperature. From Figures 6, it can be seen that the void sizes are not uniform and the average void size is primarily a function of the LFC density. The same analysis of the images was also done for both densities after being exposed to high temperatures and the results indicate that the void size did not change much from that at ambient temperature.

(a) 650 kg/m^3 density

(b) 1000 kg/m^3 density

Figure 6. Pore sizes of LFC

5.2 Compressive strength of LFC

Figure 7 and Figure 8 illustrate the compressive strength and normalized compressive strength of LFC as a function of temperature. It can be seen from Figures 7 and 8 that, for both densities, the LFC compressive strength decreased with temperature. On initial heating, the LFC made with Ordinary Portland Cement lost the absorbed, evaporable (free) water and then the chemically bound water. The loss of water would induce micro cracking resulting in some reduction in compressive strength. The compressive strength decreased slowly between 90°C to 170°C which due to the release of free water and some of the chemically bound water. The decrease in compressive strength between 20°C and 150°C corresponds to a reduction of the cohesion of the Van der Waal forces between the calcium silicate hydrate layers [18]. This decreases the surface energy of calcium silicate hydrate and leads to the formation of silanol groups (Si–OH: OH–Si) that presents weaker bonding strength. However, because this change only affects the concrete superficially, the reduction in concrete strength is not significant and the compressive strength of the LFC samples at 200°C still retained about 94% of the original unheated value. Between 200 °C and 400°C, decomposition of C-S-H gel and the sulfoaluminate phases caused cracks in the specimens [13]. These cracks had significant effects on the compressive strength of LFC [20]. At 400 °C, the LFC strength retained only about 75% of its initial value for both densities. Further degradation and loss of strength continued to take place at high temperatures. At temperature of 600°C, the LFC retained only about 40% of the original strength for both densities. Since the compositions of both densities

of LFC are identical, except for increased pores in the lower density LFC, it is not surprising that the normalised strength – temperature relationships of LFC of both densities are almost the same.

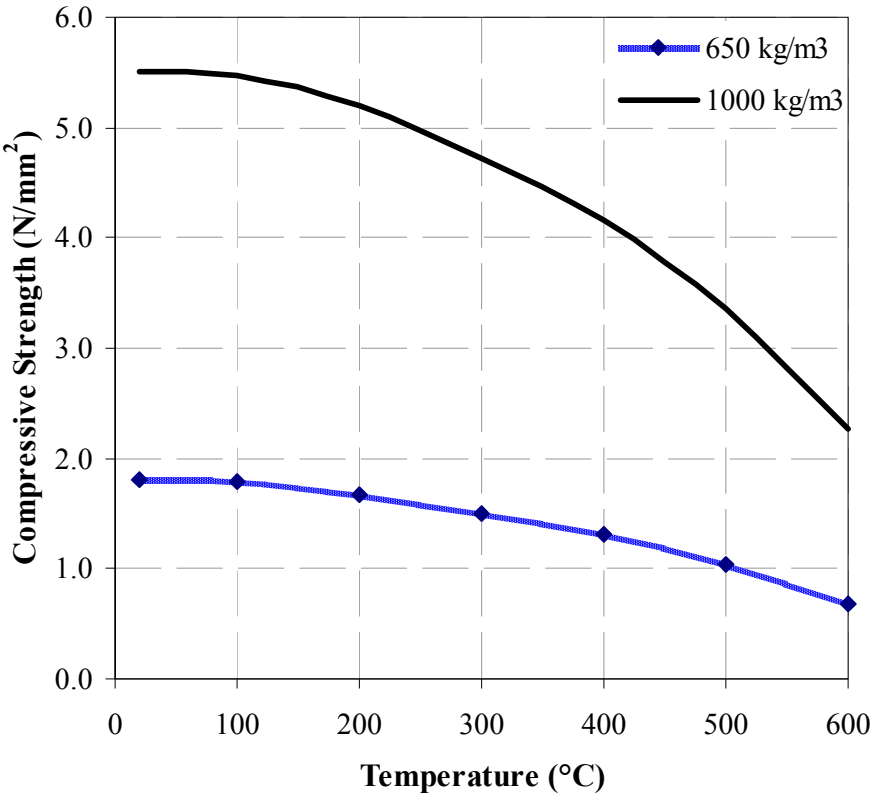

Figure 7. Compressive strength of LFC as a function of temperature

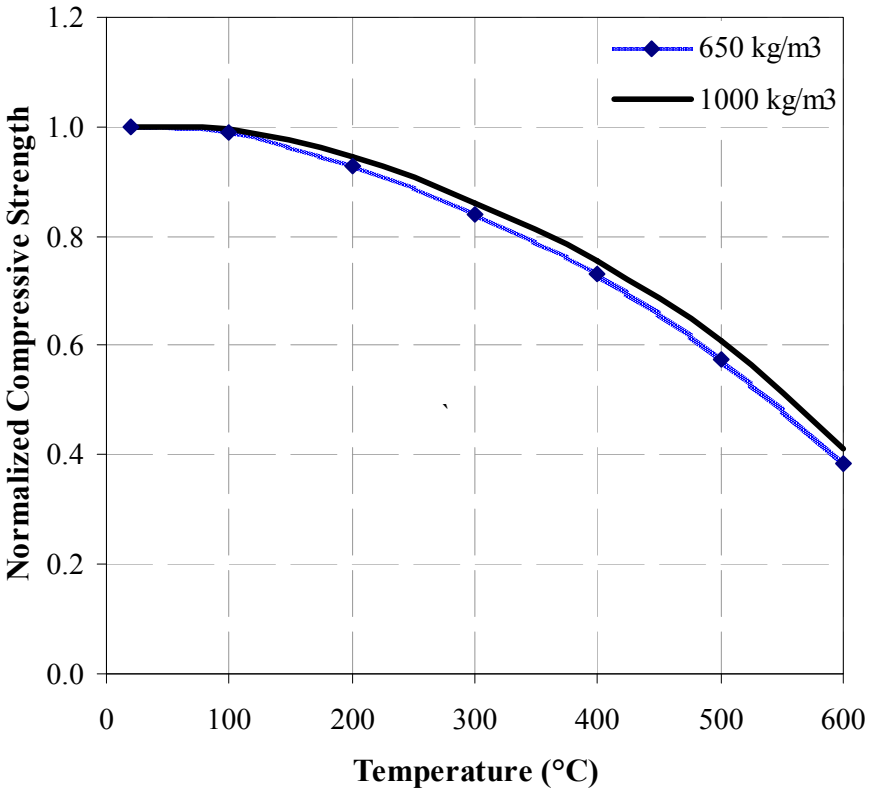

Figure 8. Normalized compressive strength of LFC as a function of temperature

5.3 Compressive stress-strain relationship of LFC

The tests were displacement controlled where the crack continued to develop and grew after the peak load was reached. However, since the test specimens failed in a brittle manner after reaching the peak stress, it was not possible to obtain the descending branch of the stress-strain relationship. Figures 9 and 10 present the average stress-strain curves at all different testing temperatures for the two densities.

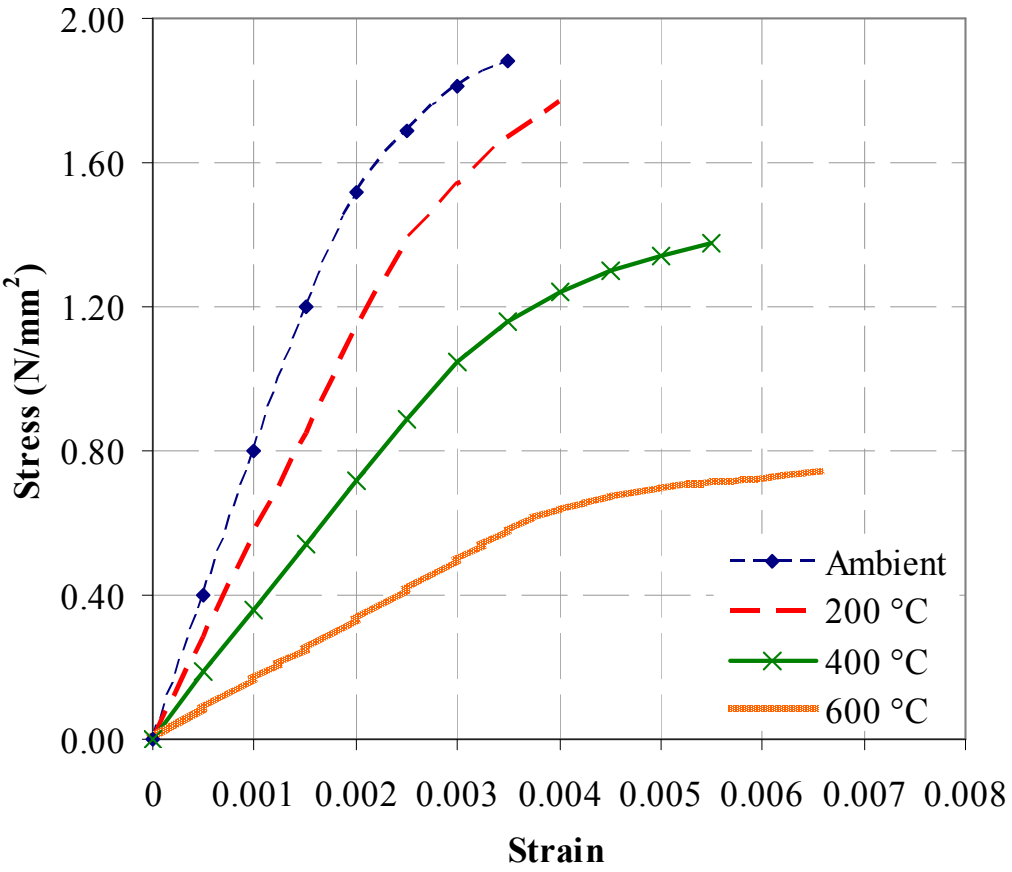

Figure 9. Average LFC stress-strain relationships for 650 kg/m^3 density at different temperatures

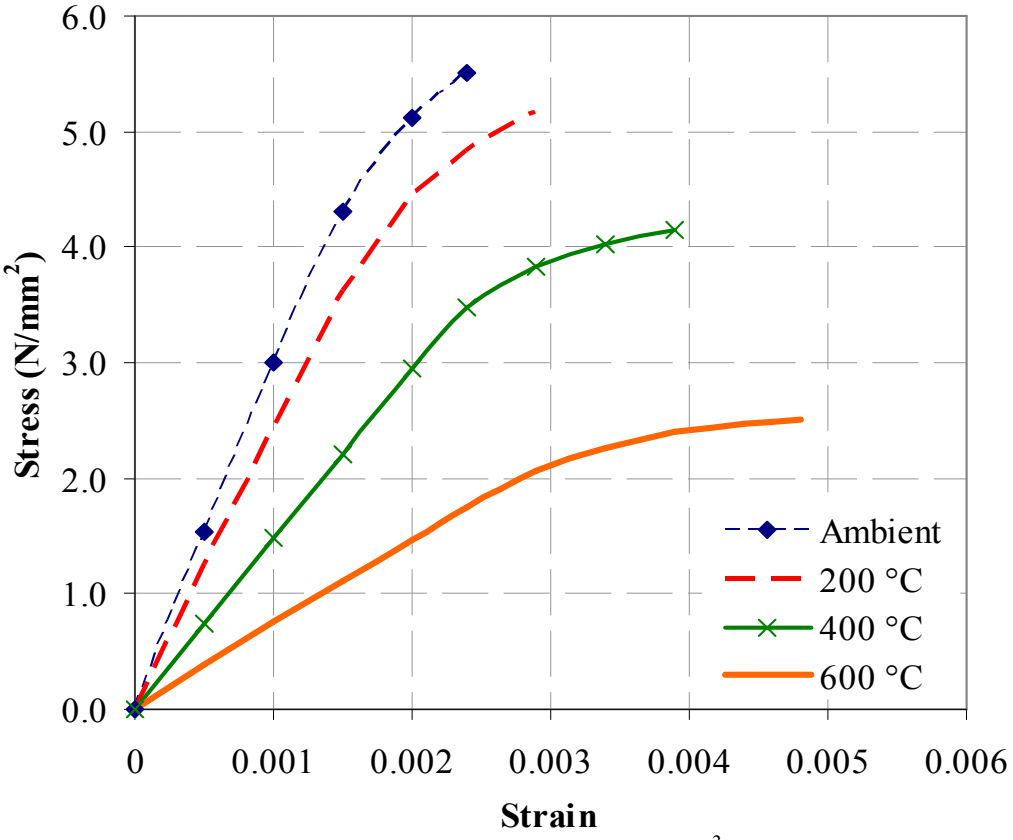

Figure 10. Average LFC stress-strain relationships for 1000 kg/m^3 density at different temperatures

It can be seen from Figures 9 and 10 that for both densities at all temperature levels, the ascending branch was linear for stress up to 75% of the peak strength. The strain corresponding to the peak strength increased at increasing temperatures. For LFC of 650 kg/m^3 density, the maximum strains were 0.0034, 0.0039, 0.0055 and 0.0066 at ambient temperature, 200°C, 400°C and 600°C respectively; for the 1000 kg/m^3 density, the corresponding values were 0.0024, 0.0029, 0.0039 and 0.0048 at ambient, 200°C, 400°C and 600°C respectively. The increase in strain results from opening of cracks initiated by the heating at higher temperatures.

5.4 Modulus of elasticity of LFC in compression

Figures 11 and 12 demonstrate the changes in modulus of elasticity of LFC in compression as a function of temperature. The modulus of elasticity was taken as the secant modulus at the point where the material changed from elastic to plastic behavior from the experimental compressive stress–strain curve. Compared to the reduction in LFC strength, the reduction in elastic modulus is greater. Both figures show that the loss in modulus of elasticity began immediately upon heating when the samples began to dry. The modulus of elasticity at 200°C, 400°C and 600°C was respectively about 75%, 40% and 25% of the original value for both densities. As with changes in normalised strengths of LFC of both densities at elevated temperatures, the normalised modulus of elasticity of LFC of both densities at the same temperature are almost the same.

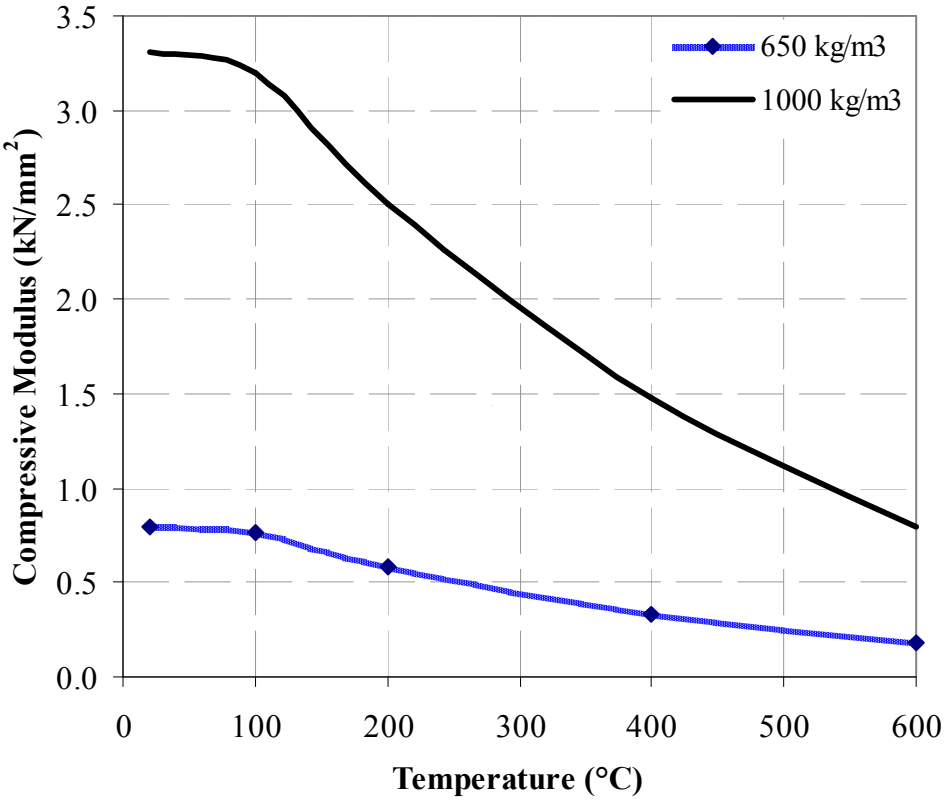

Figure 11 Compressive modulus of LFC as a function of temperature

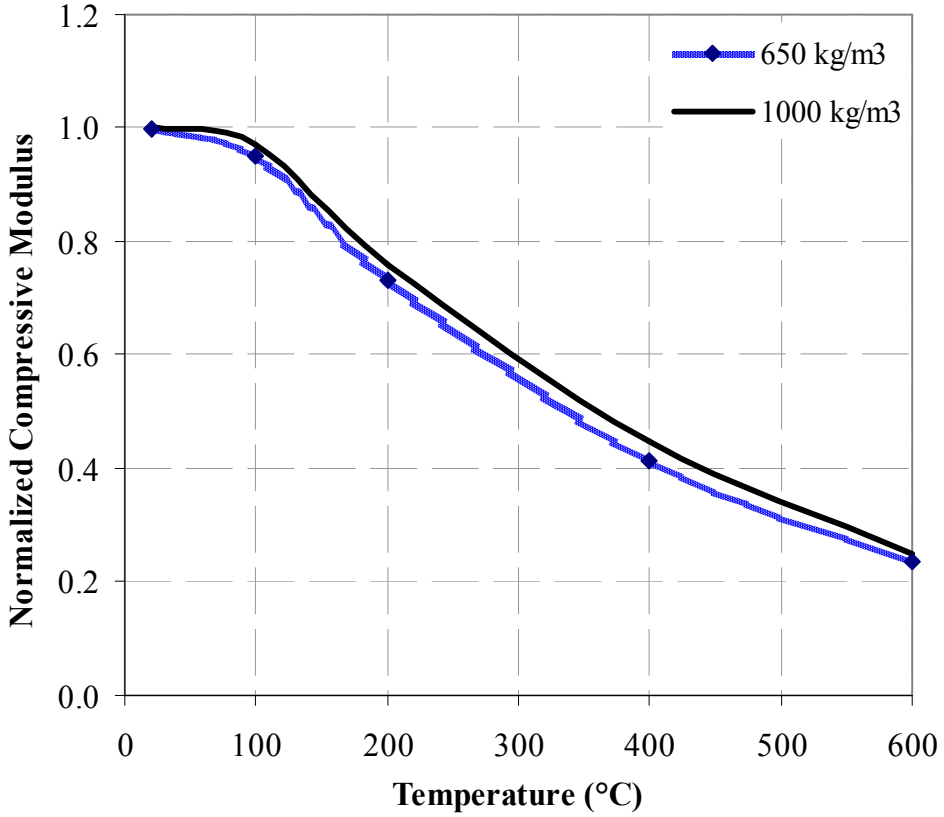

Figure 12 Normalized compressive modulus of LFC as a function of temperature

5.5 Flexural tensile strength of LFC

Since LFC is a brittle material, the bending test was intended to give a measure of the flexural tensile strength of the LFC. Figures 13 and 14 present the variation in flexural tensile strength of LFC as a function of temperature. The reduction in flexural tensile strength of LFC occurred predominantly after 90°C, regardless of the density of LFC. Consistent with changes in the aforementioned mechanical properties of LFC, which indicates that the primary mechanism causing degradation is micro cracking, which occurs as the free water and chemically bound water evaporates from the porous body. When the chemical constitution of LFC started to break down between 200°C and 300°C due to decomposition of the C-S-H and sulfoaluminate phases ($3CaO.Al_2O_3.CaSO_4.12H_2O$ and $3CaO.Al_2O_3.3CaSO_4.31H$), cracks formed followed by a significant drop in tensile strength. At 400°C, the tensile strength was about 60% of the initial value for both densities. At 600°C, the flexural tensile strength was only about 40% and 45% for 650 kg/m^3 and 1000 kg/m^3 densities respectively.

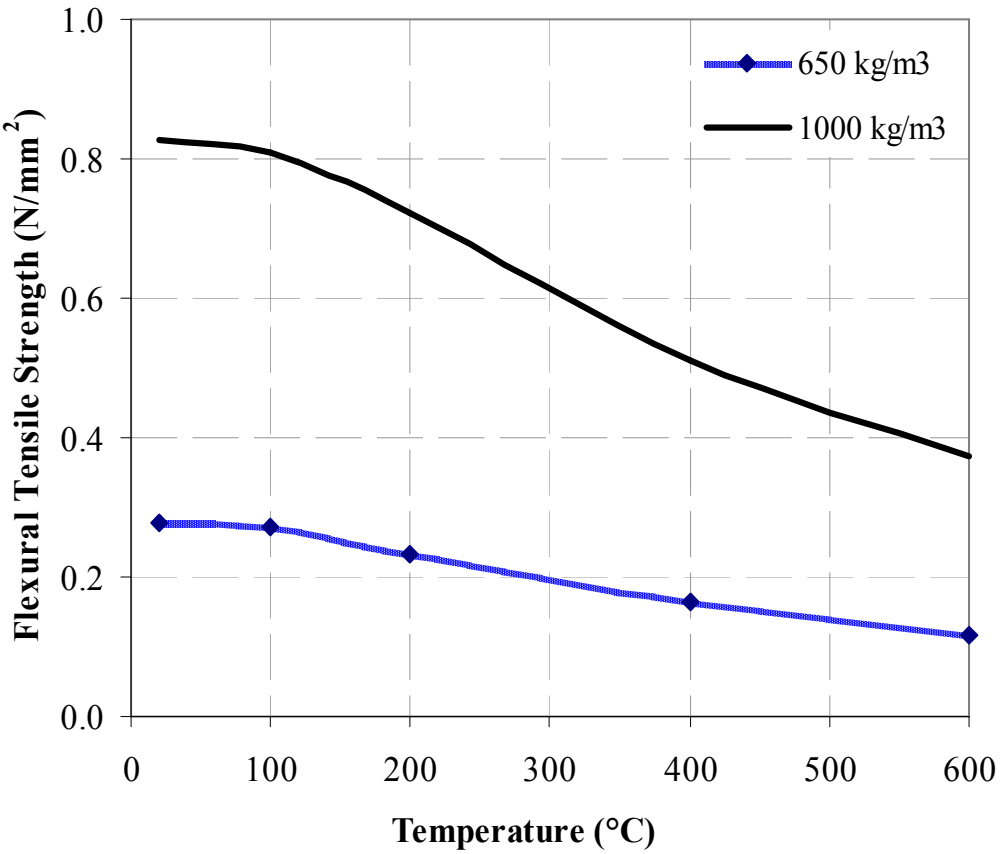

Figure 13 Flexural tensile strength of LFC as a function of temperature

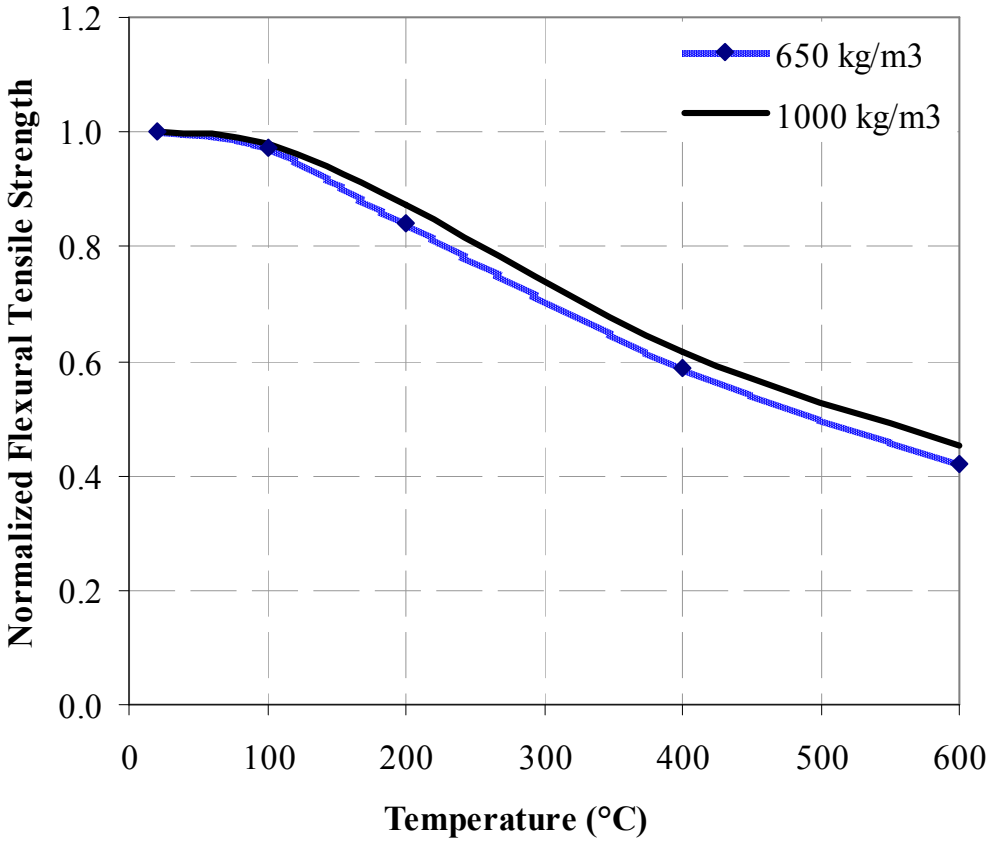

Figure 14 Normalized flexural tensile strength of LFC as a function of temperature

5.6 Flexural tensile modulus of LFC

Figures 15 and 16 illustrate the changes in flexural modulus of LFC as a function of temperature and comparison of the normalized flexural modulus with the normalized compressive modulus obtained from the cylinder tests. Although there are some differences, the variation of the normalized compressive modulus and normalized flexural modulus values are very similar for both densities at various temperatures.

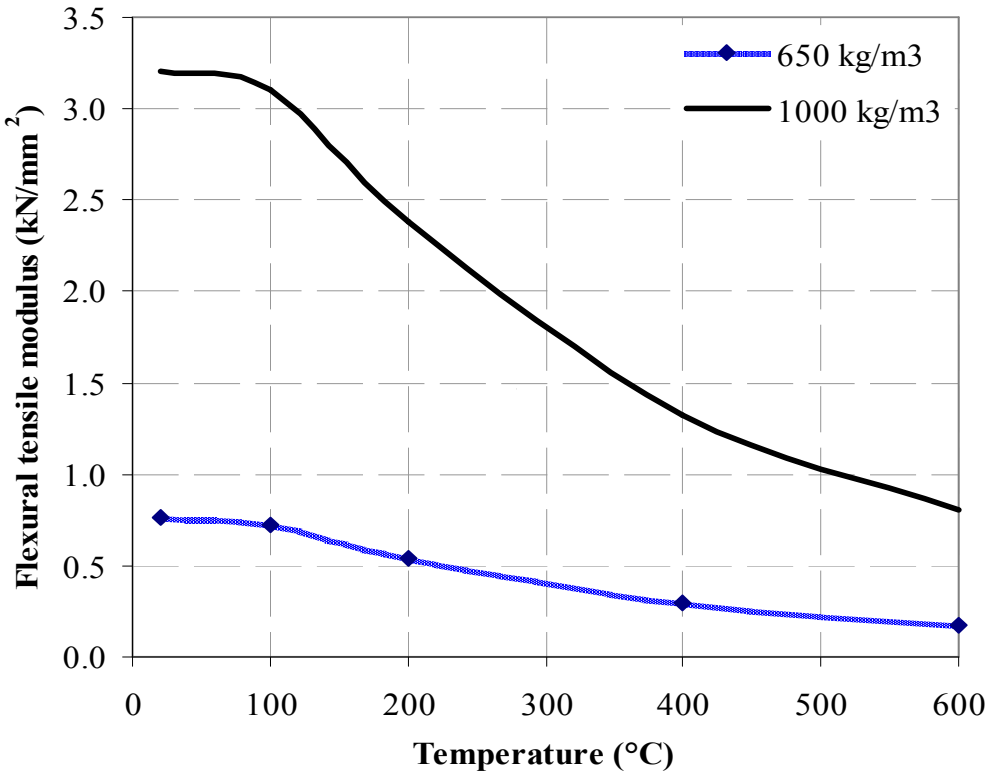

Figure 15 Flexural tensile modulus of LFC as a function of temperature

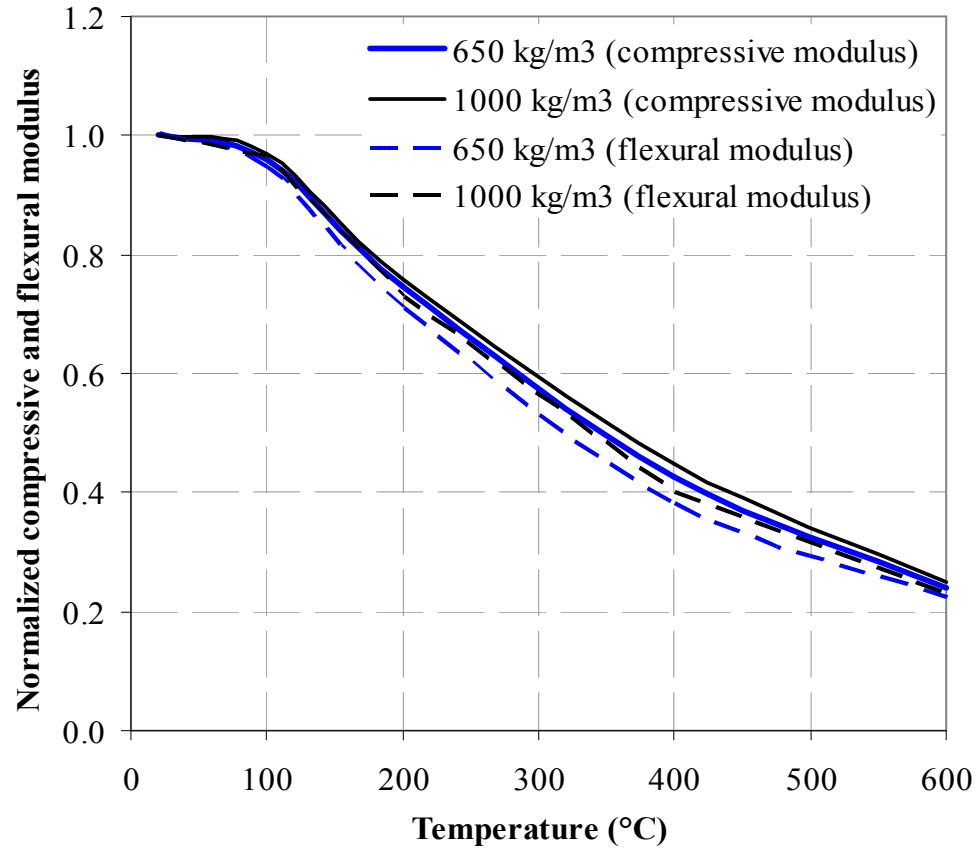

Figure 16 Comparison of normalized compressive modulus and flexural tensile modulus of LFC as a function of temperature

6.0 Conclusions

This paper has presented the results of a series of experimental studies to study the mechanical properties of LFC at elevated temperatures. Compressive cylinder tests and three point bending tests were carried out for two different LFC densities at various temperatures from ambient up to 600^{o}C. The mechanical properties included compressive cylinder strength, compressive modulus of elasticity, compressive stress-strain relationship, strain at the maximum compressive stress, porosity, flexural bending strength and modulus of elasticity.

The experimental results consistently demonstrate that the loss in stiffness for cement based material such as LFC at elevated temperatures occurs predominantly after about 90°C, regardless of density. This indicates that the primary mechanism causing stiffness degradation is microcracking, which occurs as water expands and evaporates from the porous body. As expected, reducing the density of LFC reduces its strength and stiffness. However, for LFC of different densities, the normalised strength and stiffness (ratio of elevated temperature value to ambient temperature value) –temperature relationships are very similar.

Acknowledgments

Acknowledgement is made to the funding bodies of author PhD studies, University Science Malaysia and Ministry of Higher Education Malaysia. The author would also acknowledge the assistance rendered by academic members and staff of the School of Mechanical, Aerospace and Civil Engineering with particular thanks goes to the technical staff members Mr. Jim Gee, Mr. John Mason, Mr. Bill Storey, Mr. Paul Townsend and Mr. Paul Nedwell for their invaluable.

References

1. Van Deijk, S. *Foamed Concrete*. A Dutch View, BRE, 1992, pp. 2-8.
2. Kearsley, E. P., and Mostert, H. F., *Opportunities for expanding the use of foamed concrete in the construction industry*. In: Dhir, R. K., Newlands, M. D., McCarthy, A., Editors; Use of foamed concrete in construction, Thomas, London, 2005, p. 29-36.
3. Dransfield, J. M., *Foamed concrete: Introduction to the product and its properties*. One day awareness seminar on 'Foamed concrete: properties, applications and potential' held at University of Dundee, Scotland, 2000, p. 1-11.
4. Giannakou, A., and Jones, M. R., Potentials of foamed concrete to enhance the thermal performance of low rise dwellings. In: Dhir, R. K., Hewelett, P. C., Csetenyi, L. J., Editors; Innovations and development in concrete materials and construction, Thomas Telford, United Kingdom, 2002, p. 533-544.
5. Hamidah, M. S,, Azmi, I., Ruslan, M. R. A., Kartini, K., and Fadhil, N. M., *Optimisation of foamed concrete mix of different sand-cement ratio and curing conditions*. In: Dhir, R. K., Newlands, M. D., McCarthy, A., Editors; Use of foamed concrete in construction, Thomas, London, 2005, p. 37-44.
6. Jones, M. R., *Foamed concrete for structural use*. In: Proceedings of one day seminar on foamed concrete: properties, applications and latest technological developments, Loughborough University, 2001, p. 27-60.
7. Jones, M. R., and McCarthy, A., Behaviour and assessment of foamed concrete for construction applications. In: Dhir, R. K., Newlands, M. D., McCarthy, A., Editors; Use of foamed concrete in construction, Thomas, London, 2005, p. 61-88.
8. Nambiar, E. K. K., and Ramamurthy, K., *Air-void characterization of foam concrete*. J. Cement Concr. Res., 2007. **37**(2): p. 221-230.
9. Lin, W. M., Lina, T. D., and Powers-Couche, L. J., *Microstructures of fire-damaged concrete*. Journal of American Concrete Institute Materials, 1996. **93**(3): p. 199-205.

10. Schneider, U., and Herbst, H. *Permeability and porosity of concrete at high temperature*. Technical report 403, Deutscher Ausschuss für Stahlbeton, Berlin, In German, 1989.
11. Khoury, G. A., Majorana, C. E., Pesavento, F., and Schrefler, B. A. *Modelling of heated concrete.* Mag. Concr. Res., 2002. **54**(2): p 77–101.
12. Hertz, K. D. *Concrete strength for fire safety design*. Mag. Concr. Res., 2005. **57**(8): p. 445-453.
13. Taylor, H. F. W. *Cement Chemistry*. London: Academic Press, 1992.
14. Md Azree, O. M. *Effect of using additives to the compressive strength of lightweight foamed concrete*. Master Dissertation, School of Housing, Building and Planning, University of Science Malaysia, Penang, 2004.
15. BS EN 197-1. *Cement: Composition, Specifications and conformity criteria for low heat common cements*. British Standards Institution, London, 2000.
16. BS EN 12620. *Aggregates for Concrete*. British Standards Institution, London, 2002.
17. Phan, L. T., and Carino N. J. *Code provisions for high strength concrete strength temperature relationship at elevated temperatures*. J. of Mater. Struct., 2003. 36(2): p. 91-98.
18. Cabrera, J. G., and Lynsdale, C. J. *A new gas permeameter for measuring the permeability of mortar and concrete.* Mag. Concr. Res., 1998. **40**(144): p. 177-182.
19. Khoury, G. A., *Compressive strength of concrete at high temperatures: A reassessment.* Mag. Concr. Res., 1992. **44**(161): p. 291-309.
20. Ai, H., Young, J.F., and Scherer, G. W. *Thermal expansion kinetics: Method to measure permeability of cementitious materials: II, application to hardened cement pastes*. J. Am. Ceram. Soc., 2001. **84**(2): 385-391.

Thin-Walled Structures ▮ (▮▮▮▮) ▮▮▮–▮▮▮

Contents lists available at ScienceDirect

Thin-Walled Structures

journal homepage: www.elsevier.com/locate/tws

Structural performance of lightweight steel-foamed concrete–steel composite walling system under compression

Md Azree Othuman Mydin, Y.C. Wang*

School of Mechanical, Aerospace and Civil Engineering, The University of Manchester, PO Box 88, Manchester M60 1QD, UK

ARTICLE INFO

Article history:
Received 25 May 2010
Accepted 17 August 2010

Keywords:
Composite walling
Sandwich panel
Thin-walled
Foamed concrete
Structural performance
Loadbearing wall

ABSTRACT

This paper presents the results of an experimental and analytical investigation on the structural behaviour of a composite panel system consisting of two outer skins of profiled thin-walled steel plates with lightweight foamed concrete (LFC) core under axial compression. The gross dimensions of the test specimens were 400 mm × 400 mm × 100 mm. A total of 12 tests were carried out, composed of two duplicates of 6 variants which were distinguished by two steel sheeting thicknesses (0.4 mm and 0.8 mm) and three edge conditions of the sheeting. The density of LFC was 1000 kg/m^3. Experimental results include failure modes, maximum loads and load-vertical strain responses. In analysis, full bond between the steel sheets and the concrete core was assumed and the LFC was considered effective in restraining inward buckling of the steel sheets. Using the effective width method for the steel sheets, the load carrying capacities of the test specimens were calculated and compared with the experimental results. It was found that a combination of the Uy and Bradford plate local buckling coefficients with the Liang and Uy effective width formulation produced calculation results in good agreement with the experimental results. Finally, a feasibility study was undertaken to demonstrate the applicability and limit of this new composite walling system in low rise construction.

1. Introduction

Lightweight foamed concrete (LFC) is a cellular material composed of cement–sand matrix enclosing a large number of small pores roughly 0.1–1.0 mm size, uniformly distributed in either a matrix of aggregate and cement paste or cement paste alone. The essential advantage of LFC to the field of concrete technology is the capability to control its density over a wide range. LFC densities of 400–1600 kg/m^3 can be attained by appropriate control in dosage of foam for application as structural, partition and insulation material. Although LFC has primarily been utilized as a void filling and insulation material, it is possible to use LFC as structural loadbearing material in low loadbearing systems such as walls in low-rise residential buildings. LFC construction would be particularly attractive if precast LFC members can be made to be carried by manual workers on site without the use of machinery.

The authors have recently conducted research studies to obtain data of thermal and mechanical properties of LFC [1,2]. We have found that due to its porous internal structure, LFC has very low thermal conductivity, making it a suitable material for building use as insulating or fire resisting material. LFC can also be made to have a reliable amount of compressive resistance, making it possible to use LFC as loadbearing material. However, the authors' research on compressive properties of LFC indicated that LFC suffered from brittle failure. Therefore, a suitable method of using LFC in loadbearing construction would be to use it in composite action with steel, which has high ductility. This research explores the use of LFC in composite action with steel sheeting in lightweight composite walling construction. Should LFC be cast in-situ, the thin steel sheeting can be used as formwork during construction. Because of the low density of LFC, the pressure on the steel sheeting during construction would be much lower than using normal strength concrete, allowing thin steel sheeting to be used.

Before such a system can be used in practice, it is necessary to carry out fundamental research to thoroughly investigate its behaviour. This paper will present the results of an experimental and analytical study of the compressive behaviour of short composite panel made of profiled thin steel sheeting as the facing and LFC as the core material.

2. Experiments

The experiments were designed to provide information on the load deformation response and failure modes of the specimens. The objective of the experiments was to enable development of a calculation method.

* Corresponding author. Tel.: +44 161 3068968; fax: +44 161 306 4646.
E-mail address: yong.wang@manchester.ac.uk (Y.C. Wang).

0263-8231/$ - see front matter © 2010 Elsevier Ltd. All rights reserved.
doi:10.1016/j.tws.2010.08.007

2.1. Geometrical descriptions of specimen

The dimensions of the test specimens were 400 mm high × 400 mm wide × 100 mm thick. The short height of the specimens would mean that failure of the specimens would be governed by cross-sectional capacity. A total of 12 prototype specimens were tested under axial compression. These 12 specimens consisted of two duplicates of 6 types, being two steel thicknesses (0.4 and 0.8 mm) in combination with three edge conditions of the steel sheeting. Fig. 1 shows details of the prototype specimen. The profiled steel sheeting was made in-house from plain sheeting of 0.4 or 0.8 mm thickness by fly press. The two profiled steel facings were connected using 6 mm × 10 mm bolts and nuts. Referring to Fig. 2, the steel sheeting could have one of the three edge conditions: (a) the steel sheets do not cover the LFC panel thickness (referred to as no stopping edge), (b) the steel sheets cover the LFC panel thickness but are not joined (referred to as with stopping edges), (c) the steel sheets cover the LFC panel thickness and are joined by welding (referred to as welded stopping edge). These three steel sheeting edge conditions were investigated to assess the influence of the steel sheeting in restraining the LFC to improve its ductility.

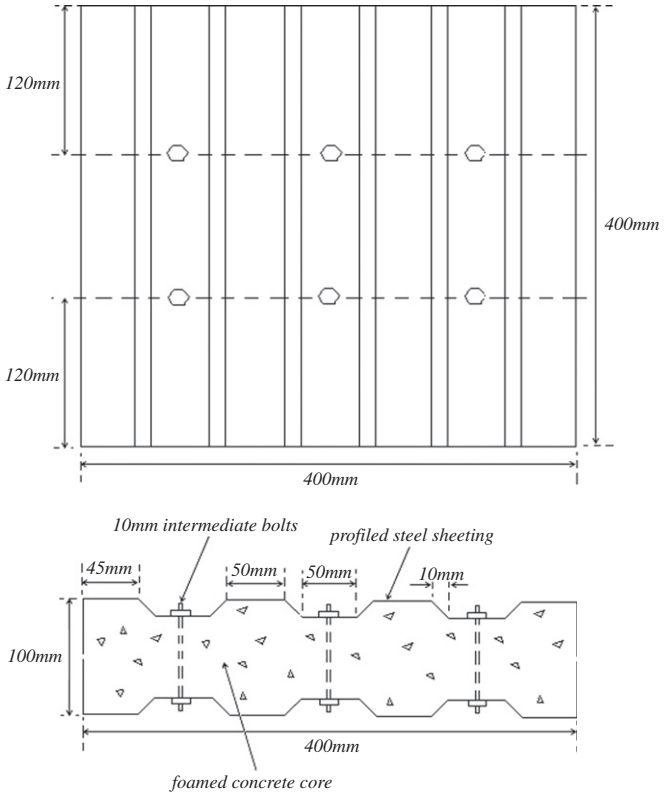

Fig. 1. Details of prototype composite walling.

2.2. Casting, curing and instrumentation

All twelve specimens (Fig. 3) were cast in house on the same day so that the LFC core would have the same design strength. The LFC used in this study was made from ordinary Portland cement, fine sand, water and stable foam [3,4]. Table 1 lists details of the constituent materials. The cement–sand ratio was 2:1 and the water–cement ratio was maintained at 0.5.

The stable foam was produced using foam generator Porta-foam TM2 System, obtained from a Malaysian manufacturer (www.portafoam.com). This system runs from an air compressor and consists of a main generating unit, a foaming unit and a lance unit. The foaming agent used was Noraite PA-1 (protein based), which is suitable for LFC densities ranging from 600 to 1600 kg/m^3. Noraite PA-1 comes from natural sources and has a weight of around 80 g/litre and expands about 12.5 times when used with the Portafoam foam generator.

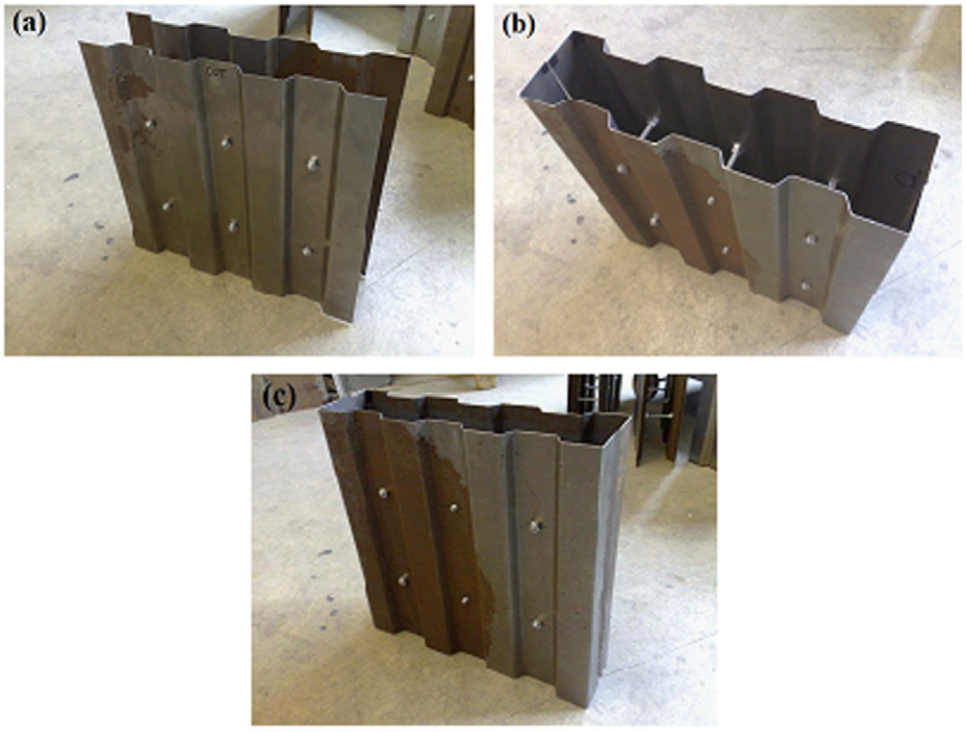

Fig. 2. Steel sheeting edge conditions: (a) no stopping edge, (b) with stopping edge and (c) with welded stopping edge.

LFC with density of 1000 kg/m^3 was chosen as it was found to have a useful amount of mechanical properties to construct a lightweight loadbearing walling system when in composite action with the profiled cold-formed thin-walled steel sheeting. Three LFC cubes and three cylinders were also cast on the day the composite panels were made. Additional two sets of three identical tests were also conducted to determine the strength of LFC core alone without any steel plate. Fig. 4 shows the shapes of these two additional sets. These tests were carried out to establish the LFC core strength contribution factor when in composite action with the steel sheeting. These two shapes were used to determine the effects of profiling on compressive strength of the core, as observed by Wright [5]. LFC was poured vertically similar to the direction of loading and the test samples were naturally cured in the indoor climate of the concrete lab. The composite panel was tested at the 28th day after casting.

A number of strain gauges were placed on the specimens and Fig. 5 shows their locations on a sample. In all cases, the strain gauges were at mid-height (h/2) of the specimen.

Fig. 3. LFC filled profiled cold-formed thin-walled steel.

Table 1
Constituent materials used to produce LFC.

Constituents	Type
Cement	Ordinary Portland cement conforming to BSEN 197–1 [1]
Sand	Fine sand conforming to BS EN 12620, with additional sieving to eradicate particles greater than 2.36 mm, to improve the LFC flow characteristics and stability [2]
Stable foam	Noraite PA-1 (protein based) foaming agent with weight of around 80 g/litre produce from Portafoam TM2 System.

2.3. Test set-up

The specimens were loaded in axial compression and the test was carried out in a universal compression testing machine with a maximum capacity of 2500 kN after 28 days of casting (Fig. 6). The tests were displacement controlled. The top and bottom of the specimens were ground flat prior to testing so as to ensure equal load distribution. In addition to the strain gauges on the

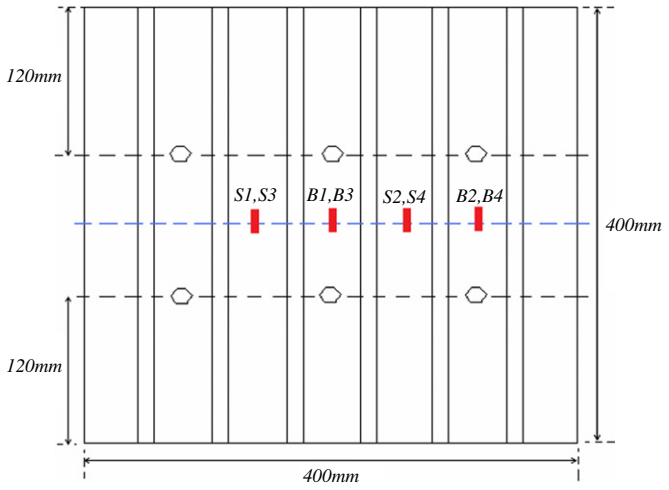

Fig. 5. Strain gauge arrangement.

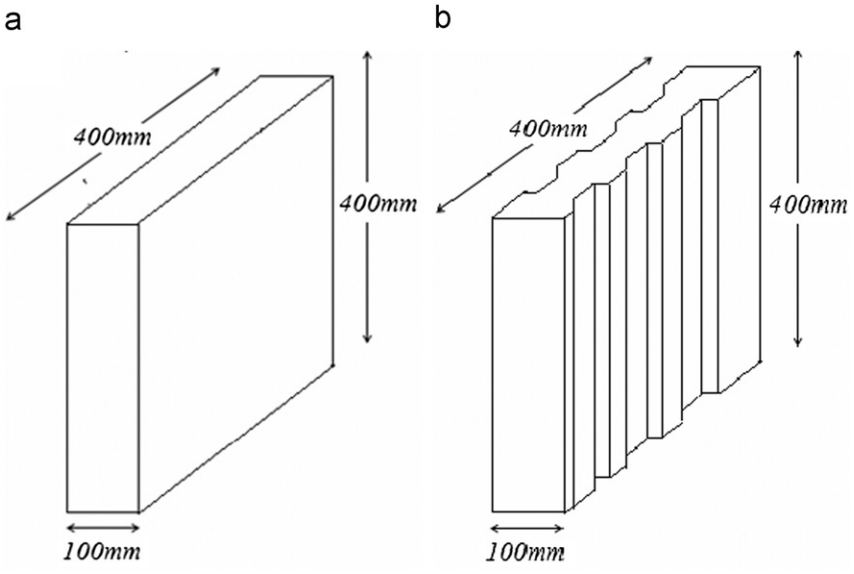

Fig. 4. Dimensions of the two additional LFC core samples: (a) rectangular LFC panel and (b) profiled LFC panel.

sample, the displacement of the loading platen was also recorded to measure axial deformation of the specimen. Observations were made on general behaviour including cracking of concrete, buckling of sheeting and failure mode.

2.4. Material properties

Three concrete cubes and 3 cylinders were cast and tested on the same days as the composite walling specimens. The cube tests after 28 days gave an average strength of 5.9 N/mm^2 and the cylinder tests provided an average strength of 5.1 N/mm^2. The test results are given in Table 2 and they are quite consistent. Table 2 also gives the results of the additional tests on the LFC panels. Data from the steel sheeting supplier gave yield strength of 280 N/mm^2 and a modulus of elasticity of 200,000 N/mm^2.

The strength ratio given in Table 2 indicates that the compressive strength of LFC was influenced by the shape and size of the specimens, which conforms to the observed behaviour of the normal strength of the concrete. The average cylinder strength and solid panel strength were 15% and 30% lower than the cube strength, respectively. The strength of the profiled panel was slightly smaller than the strength of the solid panel as found by Wright [5].

3. Test results and observations

Table 3 lists the ultimate strength (maximum load) of each specimen. Except for tests 9 and 10 which show a difference of about 10%, other duplicate tests reached very similar ultimate strengths. Figs. 7–12 present the load versus mid-height vertical strain relationships for the six types of specimens. The different strain gauges (S1–S4 and B1–B4) recorded very similar data so only data from one of each sets are considered (S1 on the steel surface without any mechanical connectors, B1 on the steel surface between the mechanical fasteners).

Figs. 7–12 indicate that in all cases, the strain gauge S1 recorded more elastic strains than B1, indicating participation of the mechanical fasteners. In all cases, the test sample was able to sustain the maximum applied load for a considerable axial deformation. The descending branch of all the load–strain curves was gradual, indicating good ductility of the test specimen.

Table 3 shows that the ultimate strength of the specimens with stopping edge was about 10% higher than those without any stopping edge for both steel thicknesses. Panels with welded steel edges sustained on average 17% more load than those without stopping edge. In Section 4, it will be shown that the increase in the strength can be attributed to the increase in the effective width of the steel sheeting.

Table 3
Summary of test results.

Test no.	Reference	Steel thickness (mm)	Ultimate strength (kN)
1	NSE1	0.4	161
2	NSE2		169
3	NSE3	0.8	240
4	NSE4		247
5	WSE1	0.4	175
6	WSE2		187
7	WSE3	0.8	263
8	WSE4		272
9	WE1	0.4	189
10	WE2		207
11	WE3	0.8	285
12	WE4		302

NSE=no stopping edge; WSE=with stopping edge; WE=welded edge

Fig. 6. Axial compression test set-up.

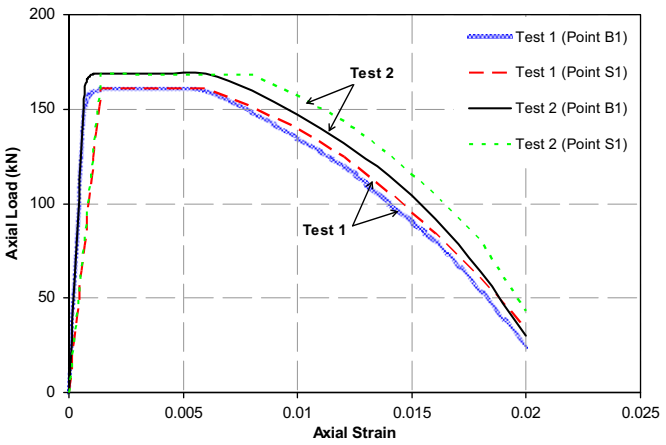

Fig. 7. Load versus mid-height strain relationships for the panel with 0.4 mm steel thickness and no stopping edge.

Table 2
Variation of compressive strength of LFC core for different shapes and dimensions.

Shapes	Dimension (mm)	Compressive strength (N/mm^2)			Average strength (N/mm^2)	Ratio of strength to cube strength
		Test 1	Test 2	Test 3		
Cube	100 × 100 × 100	5.7	6.2	5.9	5.9	1.00
Cylinder	100ø × 200	4.9	5.1	5.3	5.1	0.86
Solid panel	400 × 400 × 100	4.1	4.0	4.3	4.1	0.69
Profiled panel	400 × 400 × 100	3.8	3.7	3.5	3.7	0.63

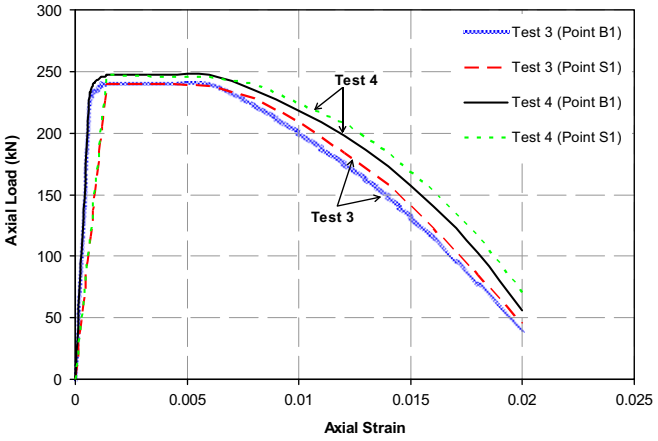

Fig. 8. Load versus mid-height strain relationships for the panel with 0.8 mm steel thickness and no stopping edge.

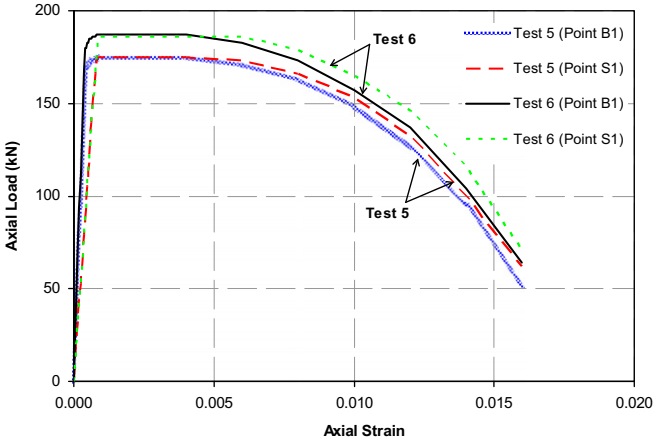

Fig. 9. Load versus mid-height strain relationships for the panel with 0.4 mm steel thickness and with stopping edge.

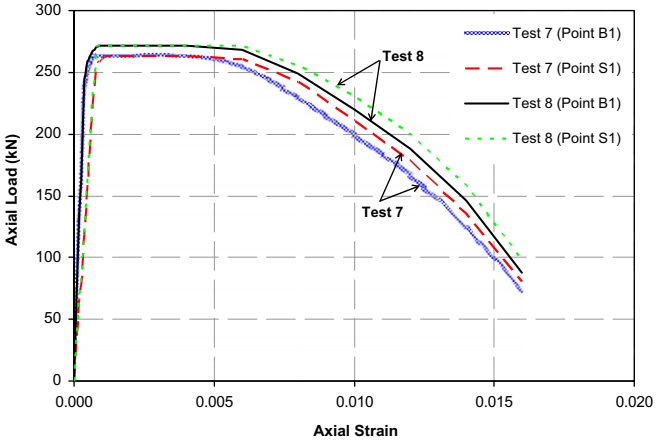

Fig. 10. Load versus mid-height strain relationships for the panel with 0.8 mm steel thickness and with stopping edge.

Fig. 13 compares the load versus mid-height strain (point B1) relationships of the two steel sheeting thicknesses and three edge conditions, and also with profiled panels without steel sheeting. As expected, the ultimate load and axial stiffness of the composite panel increases with increase in the steel thickness and improved edge condition. The most striking feature of Fig. 13 is that the use

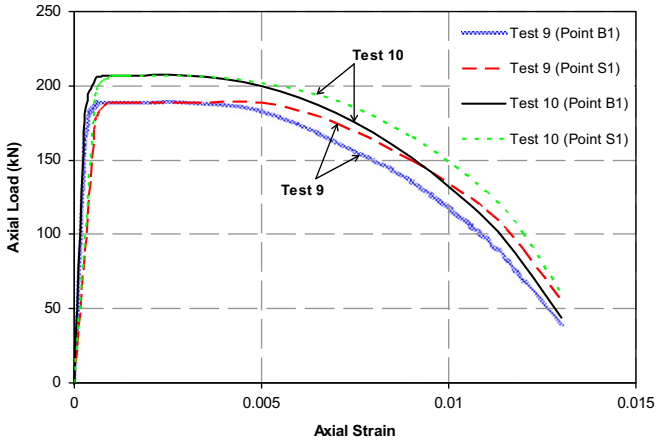

Fig. 11. Load versus mid-height strain relationships for the panel with 0.4 mm steel thickness and with welded edge.

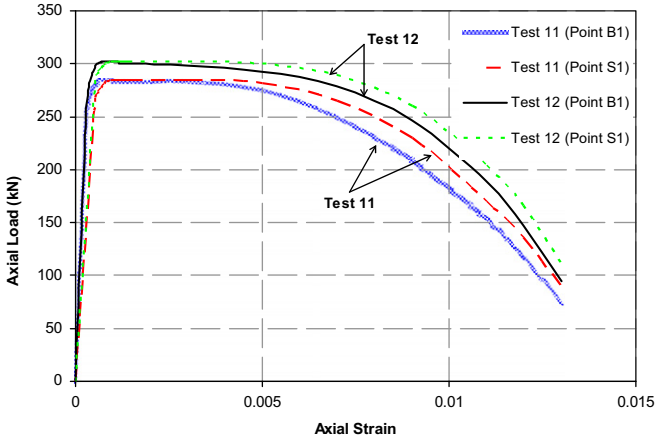

Fig. 12. Load versus mid-height strain relationships for the panel with 0.8 mm steel thickness and with welded edge.

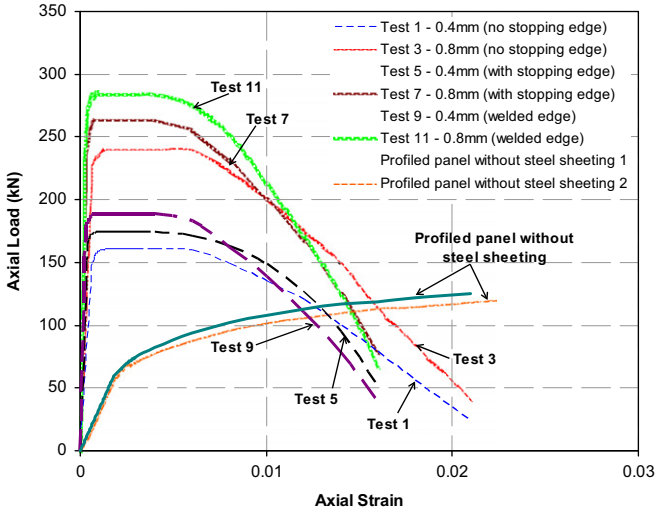

Fig. 13. Comparison of load versus mid-height strain (point B1) relationships of the two steel sheeting thicknesses and three edge conditions and also with profiled panels without steel sheeting.

of steel sheeting on both faces of the profiled LFC panel considerably increased the ductility of the panel for all the edge conditions and steel thicknesses. The introduction of steel sheeting enables the panel to sustain a high proportion of its peak load at increasing deformations. In contrast, for the profiled panel without steel sheeting, both specimens failed in a brittle manner after reaching the peak load and it was not possible to attain the descending branch of the load–strain relationship.

Fig. 14 shows a failed sample for all three edge conditions: (a) without stopping edge, (b) with stopping edge and (c) with welded edge. The steel sheeting experienced local buckling before failure, but the LFC core of 1000 kg/m^3 density was capable of preventing the panel from inward buckling. In all cases, failure of the panel was initiated by local buckling of the steel sheeting, followed by crushing of the LFC core. Although the steel sheeting provided some ductility to the panel, the welded steel edges were not able to provide much confinement effect to the LFC panel. There was no separation of the steel sheeting from the LFC core until near failure, indicating that the mechanical fasteners were able to hold the steel sheeting and the LFC core together to enable them to resist the applied load in composite action. Clearly, if composite walling system using LFC is to be used in real projects, bond between the profiled steel sheeting and the LFC infill should be considered. However, it is expected that because LFC would be less demanding owing to its lower strength than normal strength concrete, the steel sheeting used in composite walling systems using normal strength concrete would still be suitable.

4. Analytical results

As previously described, the panels can be considered to be in composite action and the LFC core was able to prevent the steel sheeting from inward local buckling. Therefore, the test specimens will be analysed as a conventional composite walling system.

Since the test panels were short (height to thickness ratio=4), no global buckling was observed and the panel strength reached the cross-sectional resistance. Also experimental observation

Fig. 14. Failure mode for composite panel without stopping edge: (a) failure mode of panel without stopping edge with outward buckling of steel, (b) failure mode of specimen with stopping edge and (c) failure mode of specimen with welded edge.

indicates that there was little evidence (e.g. bulging of the steel sheeting) of any confinement effect on the LFC core provided by the steel sheeting. Therefore, the ultimate resistance of the panel, N_u, may be calculated from

$$N_u = N_s + N_c \quad (1)$$

where N_s is the resistance of the steel sheeting and N_c the resistance of the LFC core. The following sections will discuss how N_s and N_c may be obtained.

4.1. Steel sheeting resistance

4.1.1. Critical local buckling stress

The local buckling stress of the steel plate in concrete-filled steel section is influenced by the width to thickness ratio, boundary condition, initial geometric imperfection and residual stresses induced by welding or cold-formed process [6]. For ideal steel plates, the critical elastic buckling stress can be determined by the following equation [7]:

$$\sigma_{cr} = \frac{k\pi^2 E_s}{12(1-\nu^2)(b/t)^2} \quad (2)$$

where σ_{cr} is the local buckling stress, k is the elastic buckling coefficient, which accounts for the effect of the plate aspect ratio and boundary condition on the critical buckling stress, E_s is the modulus of elasticity of the steel, ν is the Poisson's ratio, b is the width of the plate and t is the thickness of the plate.

4.1.2. Plate buckling coefficient

The plate buckling coefficient of the steel section depends on the boundary condition. Therefore, the buckling coefficient is a function of the boundary condition along the longitudinal edges and the type of loading. The k values for various common boundary conditions and loading cases are given by a few authors [8,9]. Gerard and Becker [8] summarized the buckling coefficient, k, as a function of plate boundary condition and aspect ratio (a/b). Gerard and Becker's results are based on steel plates in contact with rigid medium. Uy and Bradford [9] recently proposed a slightly different set of plate buckling coefficients for steel plates in contact with elastic medium, which would be more suitable to the current problem. For the current research which has uniform distribution of compressive stress, the buckling coefficients are compared in Table 4.

Table 4
Buckling coefficient of steel plates under compression.

Boundary condition	Buckling coefficient, k	
	Gerard and Becker [8]	Uy and Bradford [9]
S–F	0.425	0.8
S–S	4	5.6

S-F: simply supported–free, S–S: simply supported-simply supported.

4.1.3. Effective width

For thin-walled structures, the current design method is to use an effective width to account for local buckling. According to Winter [10], the effective width (b_{eff}) of a plate of width b can be calculated using the following equation:

$$\frac{b_{eff}}{b} = \sqrt{\left(\frac{\sigma_{cr}}{f_y}\right)}\left[1-0.22\sqrt{\left(\frac{\sigma_{cr}}{f_y}\right)}\right] \quad (3)$$

where b_{eff} is the effective width, b is the original width, σ_{cr} is the local buckling stress and f_y is the yield stress. The yield stress f_y, multiplied by the effective width gives the ultimate strength of the plate approximately.

Liang and Uy [6] conducted a theoretical study on the post-local buckling behaviour of steel plates in steel box columns filled with concrete, by using the finite element method. They found that the post-local buckling characteristics of steel plates in concrete filled thin-walled box columns have not been adequately studied theoretically and there is also lack of an efficient method for evaluating the initial local buckling loads of steel plates. They examined the effective width methods for the ultimate strength design of steel plates restrained by concrete and of short concrete-filled welded box columns in compression and proposed the following two effective width equations:

$$\frac{b_{eff}}{b} = 0.675\left(\frac{\sigma_{cr}}{f_y}\right)^{1/3} \quad \text{for } \sigma_{cr} \le f_y \quad (4)$$

$$\frac{b_{eff}}{b} = 0.915\left(\frac{\sigma_{cr}}{\sigma_{cr}+f_y}\right)^{1/3} \quad \text{for } \sigma_c > f_y \quad (5)$$

The resistance of the steel sheeting can be calculated as

$$N_s = b_{eff} t f_y \quad (6)$$

4.2. Strength of LFC core

A study conducted by Wright [5] established that there was a reduction in load carrying capacity in profiled concrete panel when compared to solid panel. He found that the extreme edges

Table 5
Effective width of steel plates in composite panel.

Steel Thickness (mm)	Total effective width (b_e/b)			
	Uy and Bradford k value		Gerard and Becker k value	
	Winter [10] (1)	Liang and Uy [6] (2)	Winter [10] (3)	Liang and Uy [6] (4)
No stopping edges				
0.4	0.51	0.47	0.44	0.43
0.8	0.74	0.65	0.67	0.60
With stopping edges				
0.4	0.49	0.46	0.43	0.41
0.8	0.74	0.66	0.67	0.59
Welded edges				
0.4	0.54	0.49	0.47	0.45
0.8	0.82	0.71	0.74	0.66

of the profiled panel did not present a solid mass of concrete and the extra bending stresses (due to any loading eccentricity or material non-uniformity) must be carried by only that concrete in the ribs of the profile. This reduces the load carrying capacity of the rib to resist the applied axial load.

Wright [5] then derived an empirical correction to calculate the reduced concrete strength for uniform axial compression, where the reduction in concrete strength is assumed to be directly proportional to the extent of void created by profiling the compressed edge of the panel. A reduction factor, α, which is applied to the concrete strength is given as follows:

$$\alpha = 1 - \frac{A_{vf}}{A_c} \tag{7}$$

where A_{vf} is the area of the profile voids on one face and A_c is the area of concrete. For the tested samples, the calculated α value is 0.91.

The test results in Table 2 appear to confirm the findings by Wright [5] where the compressive strength of the profiled LFC panel was found to be lower than the concrete strength of the solid panel. Therefore, an experimental correction (α reduction factor in Eq. (6)) must be included when calculating the resistance of the LFC core in the composite walling system.

Based on this result, the resistance of the LFC core in the proposed composite walling system can be determined as follows:

$$N_c = 0.69 A_c f_{cu} \alpha \tag{8}$$

The factor of 0.69 (see Table 2) takes into account the reduced strength of LFC in a panel construction compared to the cube strength of LFC, and it was determined by dividing the average solid panel strength (4.1 N/mm^2) by the cube strength (5.9 N/mm^2). With the introduction of α calculated using Eq. 7 (0.91), Eq. (8) gives a final factor of 0.63 which is the same as the experimental result in Table 2, obtained by dividing the LFC strength in the profiled panel by the LFC cube strength.

4.3. Load carrying capacity of composite wall panels

Based on the discussion in the last section, the load carrying capacity of the composite wall panel in axial compression, taking into consideration the effective width and concrete strength reduction factor for profiled shape, can be calculated by using the following equation:

$$N_s = 0.63 A_c f_{cu} + b_{eff} t f_y \tag{9}$$

Table 5 presents the total effective width of steel sheeting for the two different thicknesses and the three different edge conditions, using the aforementioned two different methods of calculating the plate buckling coefficient and two methods of

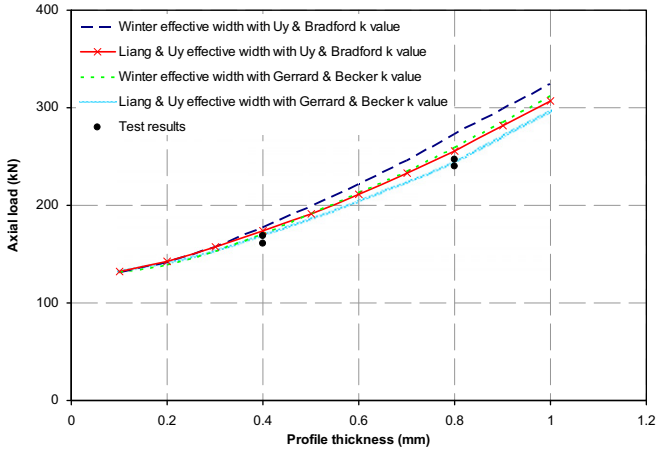

Fig. 15. Comparisons between predicted strengths and test results for composite panel with no stopping edge.

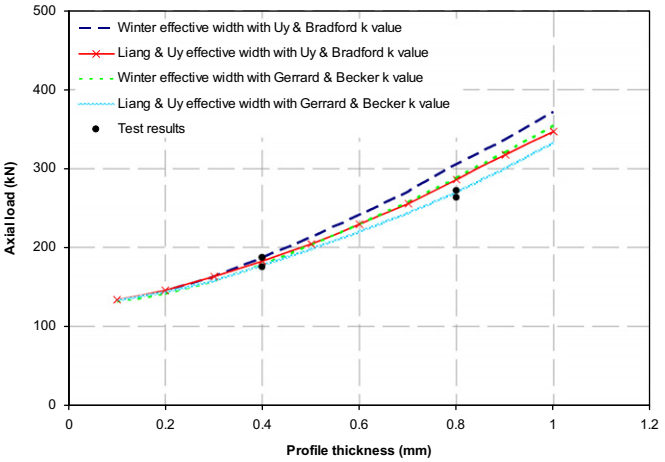

Fig. 16. Comparisons between predicted strengths and test results for composite panel with stopping edge.

Table 6
Comparisons between predicted composite panel strengths and test results.

Ref. No.	Predicted Strength (kN)				Ratio predicted/experiment			
	Gerard and Becker *k* value		Uy and Bradford *k* value		Gerard and Becker *k* value		Uy and Bradford *k* value	
	Liang and Uy	Winter	Liang and Uy	Winter	Liang and Uy	Winter	Liang and Uy	Winter
NSE1	169	171	174	177	1.05	1.06	1.08	1.10
NSE2					1.00	1.01	1.03	1.05
NSE3	245	259	256	273	1.02	1.08	1.07	1.14
NSE4					0.99	1.05	1.04	1.11
WSE1	177	179	182	187	1.01	1.02	1.04	1.07
WSE2					0.95	0.96	0.98	1.00
WSE3	270	288	286	306	1.03	1.09	1.09	1.16
WSE4					0.99	1.06	1.05	1.12
WE1	182	184	187	192	0.96	0.97	0.99	1.02
WE2					0.88	0.89	0.90	0.93
WE3	287	307	300	325	1.01	1.08	1.05	1.14
WE4					0.95	1.02	0.99	1.07
Mean, *x*					0.9867	1.0242	1.0258	1.0758
Standard deviation, *s*					0.0458	0.0596	0.0532	0.0674

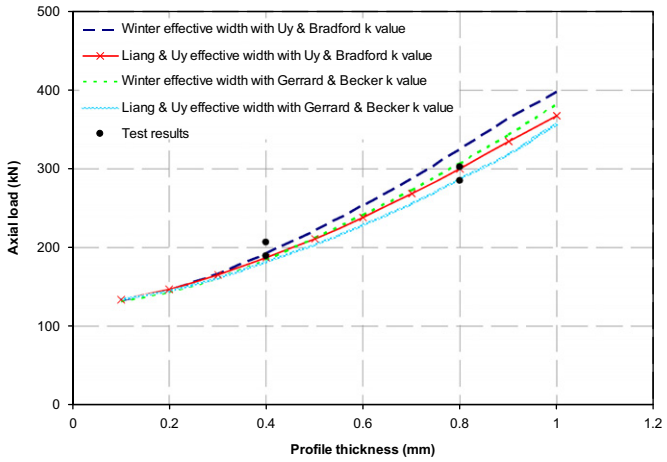

Fig. 17. Comparisons between predicted strengths and test results for composite panel with welded edge.

calculating the plate effective width. The total effective width coefficient is obtained as the sum of effective widths of all the segments of the profiled steel sheeting divided by the total width of the steel sheeting.

It is interesting to notice that if the same plate buckling coefficient is used, the two different effective width methods (compare (1) with (2) or (3) with (4)) give substantial differences in the total effective width of the steel sheeting, with the Liang and Uy [6] method (Eqs. (4) and (5)) of calculating the effective width giving results about 10% lower than the Winter [10] method (Eq. (3)). Likewise, when the same effective width method is used, the two different methods of calculating the plate buckling coefficient (compare (1) with (3) or (2) with (4)) results in large differences in the total effective width of the steel sheeting, with the Uy and Bradford [9] method giving values about 10% higher than the Gerard and Becker [8] method. However, when the traditional Gerard and Becker [8] plate buckling coefficient is combined with the traditional Winter effective width formula (column 3 in Table 5), the results are very similar to those obtained by combining the more recent plate buckling coefficient method of Uy and Bradford [9] with the more recent effective method of Liang and Uy [6] (column 2 in Table 5).

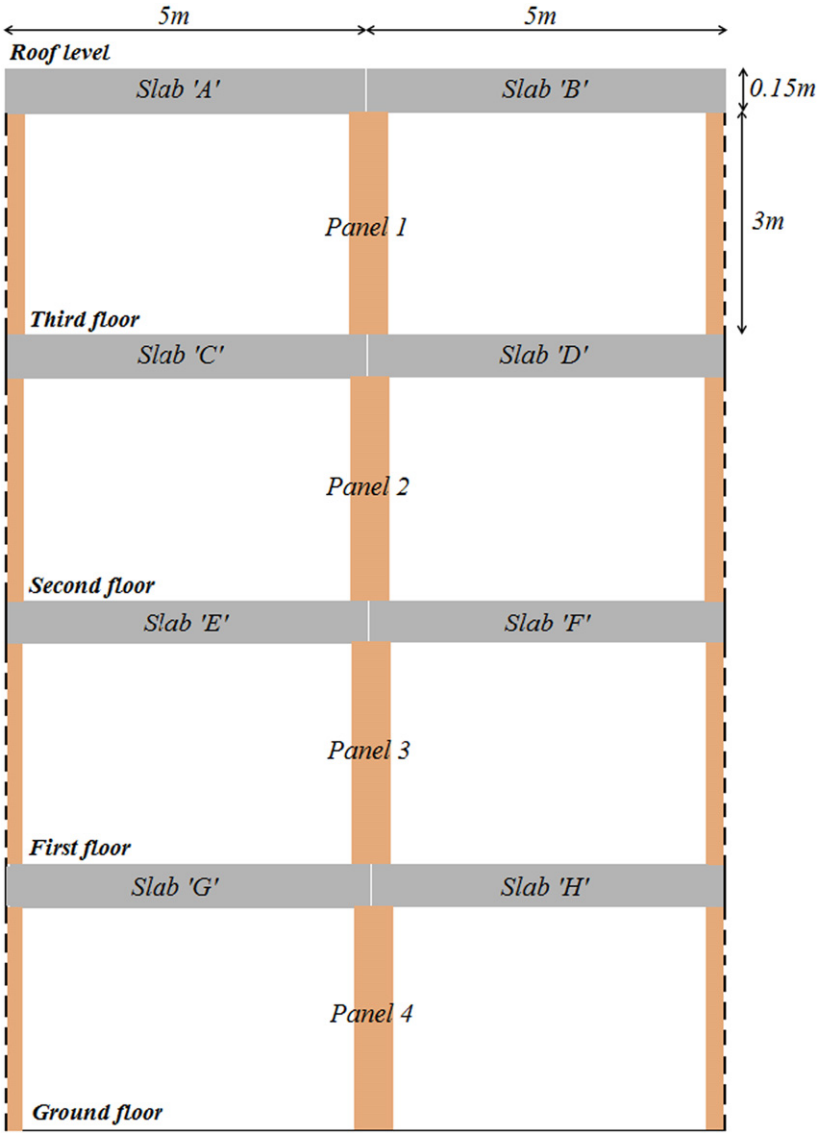

Fig. 18. Arrangement of LFC composite wall panels for a four-storey residential building section.

Table 6 compares the calculated and measured wall panel strengths for all the 12 tests using the different effective widths of Table 5. Due to the relatively low contribution by the steel sheeting to the strength of the panels, all four methods produced similar panel strengths. To verify the homogeneity and, hence, the reliability of the predicted strength over experimental results obtained from the proposed equation (Eq. (9)), a statistical analysis was carried out. The mean x and standard deviation s were calculated for each combination of design method as shown in Table 6. Overall, the ratio of predicted strength-experiment results using all the four methods indicates that the specimens were relatively homogeneous. Among these four methods, both the effective widths (2) and (3) in Table 5 give good estimation of panel strength. Among these two methods, method (2) appears to give slightly more accurate predictions. The results in Table 6 are also presented in Figs. 15–17. It should be pointed out that the buckling coefficient for plates from Uy and Bradford [9] and effective width formulation proposed by Liang and Uy [6] were derived for composite column design. From the results in Table 6, these models are also acceptable for design use for composite panel using LFC.

5. Feasibility study

This paper has so far concentrated on experimental and analytical studies of the structural behaviour and ultimate load carrying capacity of a composite walling system using LFC under axial compression. The potential market for this system is low-rise residential construction. To demonstrate the feasibility of this proposal, this section presents a preliminary feasibility study to check whether the composite walling system has sufficient load carrying capacity.

It is proposed to construct the interior load bearing walls by using 100 mm thick composite walls with 0.4 mm steel sheeting, as tested in this research. Fig. 18 shows the elevation section of a four-storey residential building and the floor span is 5 m. Table 7 summarizes the applied loads on the interior walls (panels 1–4) supporting different floors.

Table 8 compares the applied loads (per 0.4 m) on the different panels with the available panel strengths (per 0.4 m) based on the experimental results in Table 3. It is expected that the 3 m wall panel as proposed in Fig. 18 will have a lower strength than the 400 mm high test panels due to buckling. However, the results in Table 8 clearly indicate even the 100 mm thick panel with 0.4 mm steel sheeting has sufficient load carrying capacity for four floors.

6. Conclusions

This paper has described two series of tests on a new composite wall panel system consisting of two outer skins of profiled thin-walled steel sheeting with lightweight foamed concrete (LFC) core under axial compression, for steel sheeting thicknesses of 0.4 and 0.8 mm, respectively. Each series of tests had three edge conditions for the sheeting. These tests provided information on the behaviour and failure mode of these panels. An analytical model has been developed to calculate the maximum load bearing capacity of this type of wall system. The following conclusions may be drawn:

1) Failure of the panel system was initiated by outward local buckling of the steel sheeting, which was followed by concrete crushing of the LFC core. The LFC core of 1000 kg/m^3 density was sufficient to prevent the steel sheeting from inward buckling.
2) All the specimens showed good ductility, giving gradual reduction in load carrying capacity at increasing deformation. In contrast, without using steel sheeting, the core LFC panels experienced brittle failure after reaching the peak load.

Table 7
Design of prototype composite panel.

Description	Unit	Value
Slab thickness	mm	150
Dead load (partitions & finishes)	kN/m^2	1.5
Imposed loads (floor)	kN/m^2	2.5
Self weight of slab (with normal strength concrete)	kN/m	$=0.15\times24\times5=18.0$
Partition & finishes	kN/m	$=5\times1.5=7.5$
Characteristic dead load, G_k	kN/m	$=18+7.5=25.5$
Characteristic imposed load, Q_k	kN/m	$=5\times2.5=12.5$
Design load, F	kN/m	$=(1.4\times25.5)+(1.6\times12.5)=55.7$
Self weight of the panel (100 mm thick wall of 1000 kg/m^3)	kN/m	3.2
Load carried by Panel 1	kN/m	55.7
Load carried by Panel 2	kN/m	114.6
Load carried by Panel 3	kN/m	173.5
Load carried by Panel 4	kN/m	232.4

Table 8
Assessment of adequacy of 100 mm thick wall with 0.4 mm thick steel sheeting.

Description	Required load carrying capacity per 0.4 m wide (kN)	Wall adequate based on average experimental results in Table 3		
		no stopping edge (165 kN)	with stopping edge (181 kN)	with welded stopping edge (198 kN)
Panel 1	$=0.4\times55.7=23$	√	√	√
Panel 2	$=0.4\times114.6=46$	√	√	√
Panel 3	$=0.4\times173.5=70$	√	√	√
Panel 4	$=0.4\times232.4=93$	√	√	√

3) The increase in load carrying capacities of the panels with stopping edge and welded edge can be attributed to the increased effective width of the steel sheeting. The load carrying capacities of panels with stopping edge and with welded edge were about 10% and 17% higher than those without any stopping edge for both steel sheeting thicknesses.
4) The proposed panel strength calculation model takes into consideration the effect of profiling on concrete strength according to Wright. This model is able to predict the axial capacity of the proposed panel very well. To calculate the steel sheeting effective width, the combination of Uy and Bradford plate local buckling coefficients with the Liang and Uy effective width formulation appears to give the best agreement with the experimental results. Nevertheless, the traditional effective width method proposed by Winter in conjunction with the traditional plate local buckling coefficients of Gerard and Becker also gives close results compared to the experiments.
5) The proposed panel system, using 100 mm LFC core and 0.4 mm steel sheeting, has sufficient load carrying capacity to be used in low-rise residential construction of 4 floors.

Acknowledgements

The first author would like to thank the Ministry of Higher Education Malaysia and the University of Science Malaysia for their financial support of his PhD study at the University of Manchester. The technical assistance by the laboratory staff at the University of Manchester is greatly appreciated.

References

[1] Md Azree Othuman Mydin, Wang YC. Elevated-temperature thermal properties of lightweight foamed concrete. J Constr Building Mater, in press, doi:10.1016/j.conbuildmat.2010.07.016.
[2] Md Azree Othuman Mydin, Wang YC. Mechanical properties of unstressed lightweight foamed concrete exposed to high temperatures. J Cement Concr Compos, submitted for publication.
[3] BSI. BS EN 197-1: Cement. Composition, specifications and conformity criteria for low heat common cements. London: British Standards Institution; 2000.
[4] BSI. BS EN 12620: aggregates for concrete. London: British Standards Institution; 2002.
[5] Wright H. The axial load behaviour of composite walling. J Constr Steel Res 1998;45:353–75.
[6] Liang QQ, Uy B. Theoretical study on the post-local buckling of steel plates in concrete-filled box columns. Comput Struct 2000;75:479–90.
[7] Bulson PS. The stability of flat plates. London: Chatto and Windus; 1970.
[8] Gerard G, Becker M. Handbook of structural stability: Part I—buckling of flat plates. NACA TN 1957;3781.
[9] Uy B, Bradford MA. Elastic local buckling of steel plates in composite steel–concrete members. Eng Struct 1996;18:193–200.
[10] Winter G. Strength of thin steel compression flanges. Trans ASCE 1947;112:527–54.